Investigation of Fuel Chemistry and Bed Performance in a Fluidized Bed Black Liquor Steam Reformer

FINAL REPORT

Reporting Period Start Date: 09/30/2002
Reporting Period End Date: 06/30/2007

Kevin Whitty
University of Utah

Issue Date: September 2007

DOE Cooperative Agreement DE-FC26-02NT41490

Prime (submitting) Organization:
University of Utah
1471 East Federal Way
Salt Lake City, UT 84102

Project Subcontractors:

Brigham Young University
A-261 ASB
Provo, UT 84602

Reaction Engineering International
77 West 200 South, Suite 210
Salt Lake City, UT 84101

University of Maine
5717 Corbett Hall
Orono, ME 04469

Georgia Tech Research Corp
505 Tenth Street, NW
Atlanta, GA 30318

DISCLAIMER

EXECUTIVE SUMMARY

The University of Utah project "Investigation of Fuel Chemistry and Bed Performance in a Fluidized Bed Black Liquor Steam Reformer" (DOE award number DE-FC26-02NT41490) was developed in response to a solicitation for projects to provide technical support for black liquor and biomass gasification. The primary focus of the project is to provide support for a DOE-sponsored demonstration of MTCI's black liquor steam reforming technology at Georgia-Pacific's paper mill in Big Island, Virginia. A more overarching goal is to improve the understanding of phenomena that take place during low temperature black liquor gasification. This is achieved through five complementary technical tasks: (1) construction of a fluidized bed black liquor gasification test system, (2) investigation of bed performance, (3) evaluation of product gas quality, (4) black liquor conversion analysis and modeling and (5) computational modeling of the Big Island gasifier.

Several experimental devices have been constructed under this program. The largest of these is a 10-inch diameter pressurized fluidized bed steam reformer having four bundles of 20 heaters and designed to simulate conditions within a full-scale reformer. This system is housed at the University of Utah's off-campus Industrial Combustion and Gasification Research Facility, and includes all necessary auxiliary equipment (steam generating boiler and feedwater conditioning system, steam superheater, syngas afterburner, flue gas cooler and computerized control system). A smaller nitrogen-fed fluidized bed system has been constructed at Brigham Young University for the purpose of studying bed agglomeration behavior and conditions that cause such agglomeration. An even smaller 2-inch nitrogen fluidized bed in the laboratories at the University of Utah allows investigation of mechanisms of particle growth, particularly coating and particle clustering by black liquor. Other experimental devices include a single-droplet reactor for study of liquor pyrolysis behavior and a Plexiglas cold flow model of the University of Utah steam reformer that allows visualization and measurement of gas and solid flow characteristics.

Several computational models have been developed under this program. One, developed at the University of Utah is a relatively simple, Microsoft Excel-based model that predicts gas velocities and compositions and local gasification rates throughout the reactor. In addition, the model predicts the overall gasification rate and steady state carbon content of the bed. The value of this model lies in its simple interface, portability and ease of modification. A more advanced model developed by Reaction Engineering International considers three phases within the bed (dense, bubble and wake) and takes backmixing of solids into account. Bubble hydrodynamics (size, velocity, splitting and coalescence) are also taken into consideration. The model calculates mass and energy balances of the system and uses drying and devolatilization rates and reaction kinetics to determine the local chemistry of the system, overall conversion and gas composition throughout the bed and freeboard. A third model focuses specifically on heat transfer and associated temperatures in and around the tube bundles of a full-scale reformer. This model takes as input results from 3-D hydrodynamics simulations created at NETL using MFIX, and can predict particle temperatures as well as heater tube internal and surface temperatures. Yet another model predicts how particle size distribution changes over time based on relative contributions from various mechanisms responsible for particle growth and shrinkage.

Conversion of black liquor in a steam reformer occurs in stages: drying, pyrolysis and heterogeneous steam reforming. The product gas leaving the reformer is primarily a mixture of steam, H_2, CO_2, CO and methane. The water-gas shift reaction is strongly catalyzed by alkali species in the bed solids, resulting in high concentrations of hydrogen as carbon monoxide reacts with steam to form hydrogen and carbon dioxide. Condensable hydrocarbons ("tars") are produced as the liquor pyrolyzes. Formation of tars increases as the flow of black liquor to the system increases, but decreases as the temperature of the reformer increases. The tars comprise primarily un-, mono- and di-substituted, mostly methyl phenols. The composition of the condensed material does not vary significantly with changes in operating conditions.

As liquor is fed to the fluidized bed, it coats the particles and the organic material reacts away. As a particle is repeatedly coated and reacted, thin layers, or "shells," build up on the particle and it becomes larger. Other mechanisms responsible for particle growth are agglomeration, sintering and "clustering," whereby several small particles are captured within a droplet of liquor, which binds them together. Agglomeration tends to occur in regions of the reactor that have low gas flow, or that are particularly hot. The heater bundles are therefore usually where agglomeration initiates. As agglomerated material builds up on the heater tubes, heat transfer decreases and the spacing between tubes becomes less. This restricts the flow of gas, creating more stagnation and heat, thereby causing further agglomeration. The mechanism of agglomeration seems to start with bridging between edges of particles. Potassium chloride may also play a role.

Addition of titanium dioxide to the black liquor changes the chemistry of the bed. Sodium titanate complexes are formed, which provides two benefits. The titanate-containing bed has a much higher melting temperature than a bed formed solely from inorganics of black liquor. This allows operation several hundred degrees hotter than without titanate. This results in nearly 100% conversion of carbon in the liquor. The sodium titanate complexes form sodium hydroxide when mixed with water, thereby decreasing the causticizing load in a mill. Based on results from tests with kraft liquor performed under this program, it is conceivable that the need for causticizing could become dramatically less when fluidized bed steam reforming is combined with titanate addition.

The heterogeneous reaction between steam and bed solids controls the overall rate of carbon conversion. This reaction is inhibited by hydrogen and carbon monoxide. In a commercial system, hydrogen formed during pyrolysis and steam reforming is estimated to average roughly 0.5 atmospheres. With this much hydrogen, the rate of conversion by heterogeneous reaction with steam is 5-10 times slower than in a steam-only environment. As such, a full-scale system can be expected to have lower carbon conversion than a small-scale, atmospheric-pressure reformer having a lower fuel/steam ratio. Lower overall carbon conversion of large-scale systems is also predicted by the computational models developed under this program.

The computational models indicate that bubbles do travel upwards through the tubes of the heater bundles, particularly in the center. Downflow of solids near the walls hinders bubble flow in those regions. As particle size increases, bubble density within the tube bundles decreases, suggesting that the bubbles instead prefer to flow around the heaters. This has been shown to be the case for the Utah gasifier. A commercial gasifier likely experiences similar behavior. As part of a project de-scope and decommissioning of the Georgia-Pacific demonstration system during the period of performance of this project, the models were not systematically compared to a full-scale system refined to improve accuracy and predictive ability.

TABLE OF CONTENTS

TABLE OF FIGURES

INVESTIGATION OF FUEL CHEMISTRY AND BED PERFORMANCE IN A FLUIDIZED BED BLACK LIQUOR STEAM REFORMER

1. INTRODUCTION

University of Utah's project entitled "Investigation of Fuel Chemistry and Bed Performance in a Fluidized Bed Black Liquor Steam Reformer" (DOE Cooperative Agreement DE-FC26-02NT41490) was developed in response to a solicitation released by the U.S. Department of Energy in December 2001, requesting proposals for projects targeted towards black liquor/biomass gasification technology support research and development. Specifically, the solicitation was seeking projects that would provide technical support for Department of Energy supported black liquor and biomass gasification demonstration projects under development at the time.

1.1 Background

Gasification of black liquor has long been recognized as a promising alternative to the conventional recovery boiler, and has the potential to achieve improvements in terms of energy efficiency, safety and environmental performance. Over the past three decades, over 20 companies have worked on development of black liquor gasification technology [1]. Most of these development efforts were abandoned, however, due to technical challenges or lack of funding. Currently, development is focused on two technologies, high temperature entrained-flow gasification and low temperature fluidized bed gasification.

Manufacturing Technology and Conversion International (MTCI) has been developing fluidized bed black liquor steam reforming technology for more than 20 years. The technology is currently being marketed by ThermoChem Recovery International (TRI).

In the MTCI/TRI steam reforming system (Figure 1), steam is fed through a bubbling fluidized bed of small (~250 micron) particles composed mainly of alkali salts (mostly carbonates). Black liquor is injected into the lower half of the bed, where it “paints” the bed particles, dries and reacts. Most of the organic portion of the liquor is converted to gaseous species, primarily H_2, CO, CO_2, methane and other hydrocarbons. The final product gas is rich in hydrogen, 59-70% on a dry basis [2-4]. The inorganic portion of the liquor adds to the bed inventory, necessitating occasional removal of bed solids, usually through a lock hopper. The solids are dissolved to form green liquor.

Steam reforming is an endothermic process, so the bed is indirectly heated by several bundles of horizontal tubes placed within the bed and heated either electrically (small scale systems) or by pulsing combustion exhaust gases (commercial scale systems). Typical operating temperatures are in the range 605-615°C (1120-1140°F).

The solids residence time in the fluidized bed is quite long, 40-50 hours, so the reactors are relatively large. The bed in a commercial system is roughly 3.5 meters (11 feet) diameter and 10 meters (33 feet) high. The deep bed creates a pressure drop over the bed of roughly 2.2 atm (33 psi).

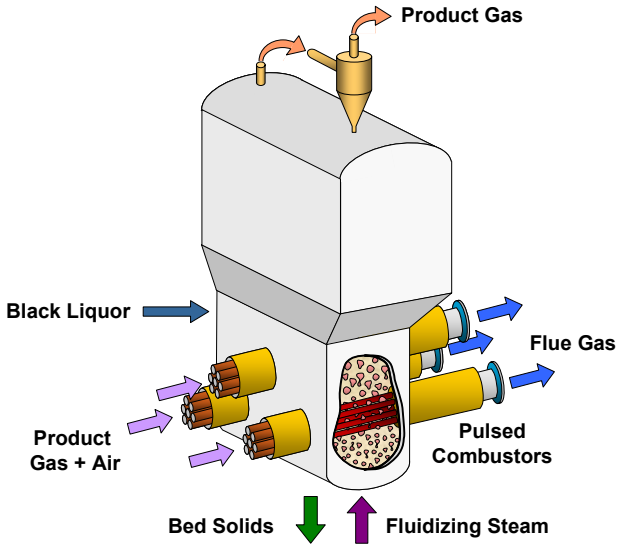

Figure 1. Schematic of the MTCI fluidized bed black liquor steam reformer. Adapted from [2].

In 2001, Georgia Pacific Corporation was awarded a contract from the U.S. Department of Energy for demonstration of the MTCI fluidized bed steam reforming technology at its Big Island, Virginia paper mill. Over the next several years, a 200 ton/day system with two parallel reformers was designed and constructed. The system was started up in early 2004.

1.2 Project Objectives and Scope

The primary objective of the project reported here was to provide technical support for the demonstration of MTCI's black liquor steam reforming process at Georgia-Pacific's paper mill in Big Island, Virginia. A more overarching goal is to increase the understanding of and acquire relevant data on conversion of black liquor in low temperature gasification systems. The project achieves these goals through the following technical tasks:

1. Construction of a fluidized bed black liquor gasification test system
2. Investigation of bed performance
   - 2.1 Mapping of bed properties and chemistry
   - 2.2 Evaluation of bed agglomeration propensity
   - 2.3 Evaluation of titanate addition
3. Evaluation of product gas quality
   - 3.1 Speciation of gaseous products
   - 3.2 Characterization and destruction of tars
4. Black liquor conversion analysis and modeling
5. Modeling of the Big Island gasifier
   - 5.1 1½-D model of entire reactor
   - 5.2 3-D modeling of specific parts of the reactor

The project includes four subcontracts to groups that possess expertise in technical areas relevant to the project. These subcontractors and their corresponding roles within the project are:

1. Brigham Young University (Prof. Larry Baxter): bed agglomeration studies
2. University of Maine (Prof. Adriaan van Heiningen): conversion analysis and titanate addition
3. Georgia Institute of Technology (Prof. Pradeep Agrawal): catalytic destruction of tars
4. Reaction Engineering International (Dr. Adel Sarofim): gasifier modeling

In addition to these official project members, the University of Utah worked closely with Georgia-Pacific Corporation, MTCI and ThermoChem Recovery International in execution of the project.

This report describes the technical achievements throughout the project, describes the experimental equipment and computational modeling associated with the project and presents results and conclusions of the work.

2. EXPERIMENTAL

Several experimental systems of varying size and complexity were built under this project. The largest of these, the black fluidized bed black liquor gasification research system, is the heart of the research in the project. Other systems include a bed agglomeration test reactor, a 2-inch fluidized bed for particulate studies, a single particle reactor, a tar sampling system and a cold flow fluidized bed model. These systems are described in the sections that follow.

2.1 Fluidized Bed Black Liquor Gasification Research System

The University of Utah's pressurized fluidized bed black liquor gasification research system was designed to simulate conditions in a full-scale fluidized bed steam reformer such as Georgia-Pacific's Big Island demonstration system. This design of the reactor for the Georgia-Pacific demonstration system is almost identical to fluidized bed steam reformer installed at Norampac's Trenton, Ontario paper mill. Design specifications for the University of Utah system are listed in Table 1.

A schematic diagram of the gasifier system is presented in Figure 2. A 3-D rendering and photograph showing the major components and their configuration is shown in Figure 3 and Figure 4. P&ID diagrams (process and instrumentation diagrams) are shown in Appendix A. The gasifier system includes five primary subsystems: (1) steam feed system, (2) black liquor feed system, (3) fluidized bed reactor, (4) solids removal system and (5) product gas (syngas) handling system. All these subsystems are necessary for the gasifier to operate. The whole system is driven by an integrated control system that monitors and controls critical process variables. The subsystems are described in detail in the sections that follow.

TABLE 1. BLACK LIQUOR GASIFIER SPECIFICATIONS

Specification	Typical		Maximum	
Reactor operating pressure (bottom of bed)	300 kPa	44.0 psia	689 kPa	100.0 psia
Reactor operating temperature	604 °C	1120 °F	718 °C	1325 °F
Black liquor feed rate (as solids)	68 kg/d	150 lb/d	218 kg/d	480 lb/d
Steam feed rate	42.2 kg/h	93.0 lb/h	90.7 kg/h	200.0 lb/h
Superficial gas velocity (bottom of bed)	0.396 m/s	1.30 ft/s	1.52 m/s	5.00 ft/s
Bed diameter	0.254 m	10.0 inch	0.254 m	10.0 inch
Bed height	1.27 m	50.0 inch	1.52 m	60.0 inch
Solids residence time	90 h	90 h	200 h	200 h

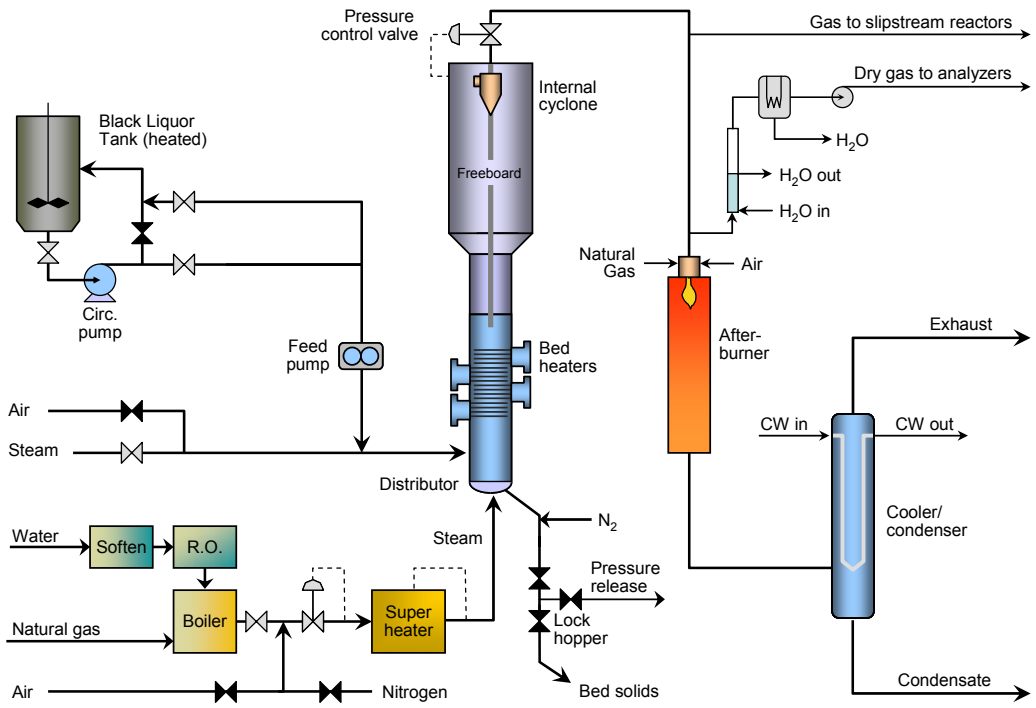

Figure 2. Schematic diagram of black liquor gasifier system.

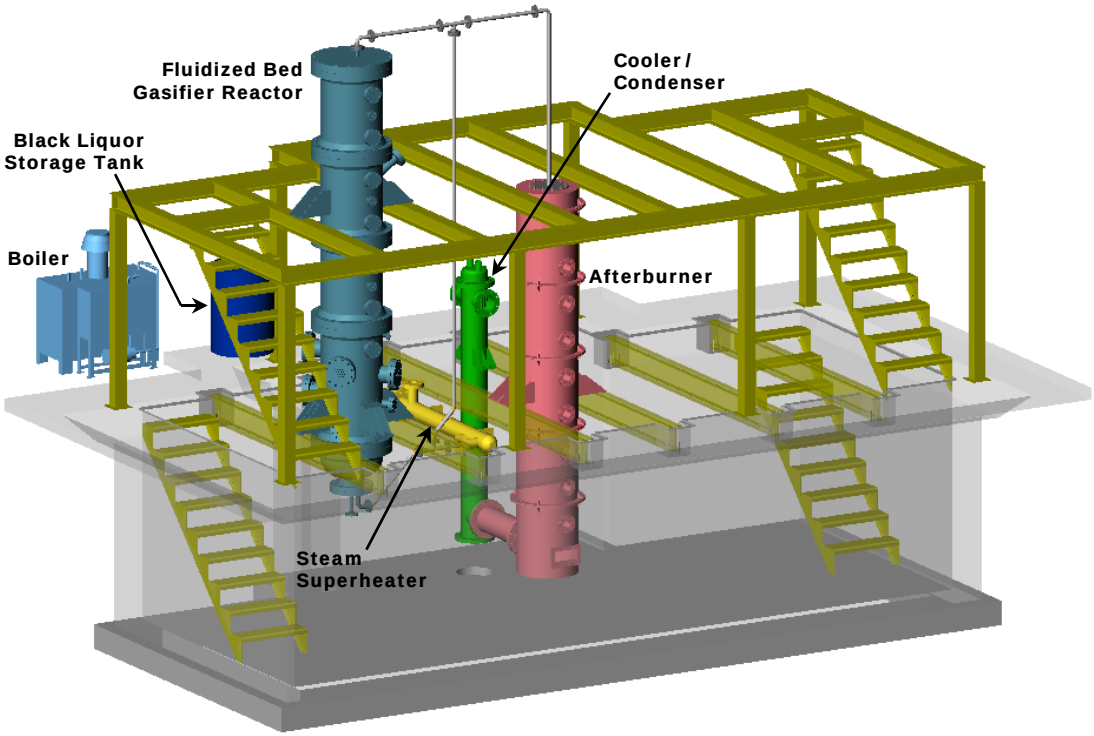

Figure 3. 3-D CAD rendering of the University of Utah black liquor gasification test system showing major components.

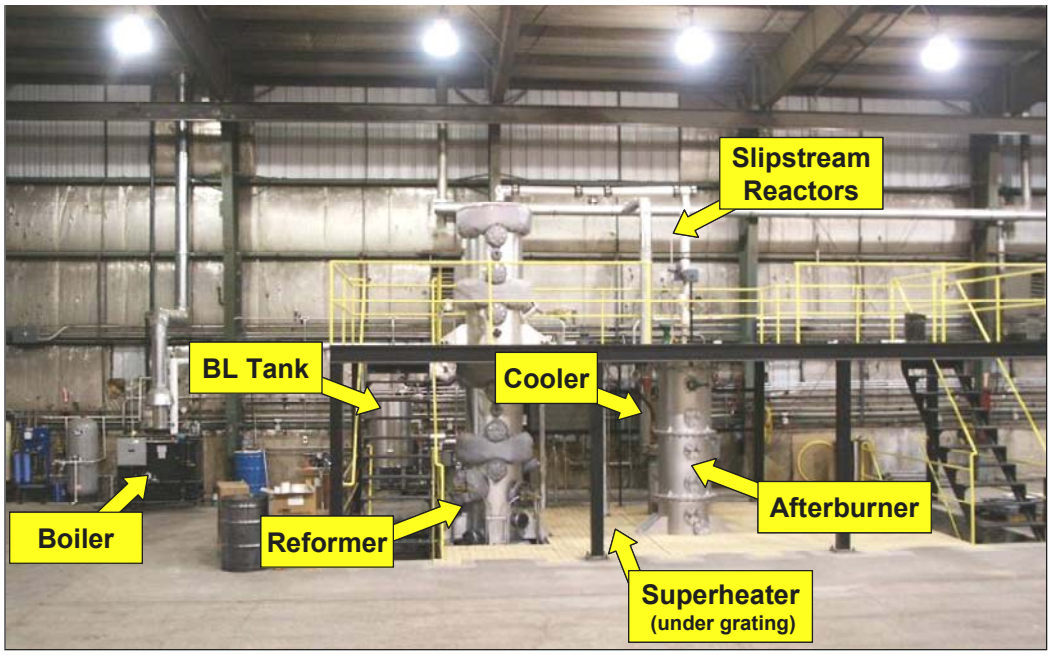

Figure 4. Photograph of the black liquor gasification test system.

2.1.1 Steam Feed System

There are three main process units in the steam feed system: feedwater conditioner, steam generator (boiler) and steam superheater.

Feedwater conditioning. City water is brought into a water conditioning system comprising a twin-tank water softener, reverse osmosis filtration system and activated carbon filter. The conditioning system removes particulates and dissolved minerals in the water, which ensures high quality steam, minimizes blowdown requirements and extends the life of the superheater. Chemicals to maintain boiler life are added to the water exiting the RO unit, which is pumped to a 50 gallon bladder tank for storage. The feedwater conditioning system and boiler are shown in Figure 5.

Boiler. The clean water passes to the boiler system, a Parker Boiler model 103-9.5 natural gas-fired drum boiler. The boiler is rated at 1034 kPa (150 psi), and at Salt Lake City's elevation can deliver up to 120 kg/hr (265 lb/hr) steam. The boiler package includes a feedwater storage tank, pump and chemicals addition system. The boiler has a blowdown valve for purging dissolved solids from the system.

Immediately after generation, the steam passes through a condensate knockout drum to an adjustable pressure regulator which lowers the steam pressure to a pressure closer to the reactor pressure. This improves controllability of the steam flow rate and raises the level of superheat in the steam. The steam runs through a control valve and v-cone flowmeter, which are coupled to the control system and used to control the steam flow rate. All steam lines to between the boiler and superheater are electrically heat traced to minimize heat losses and associated condensation.

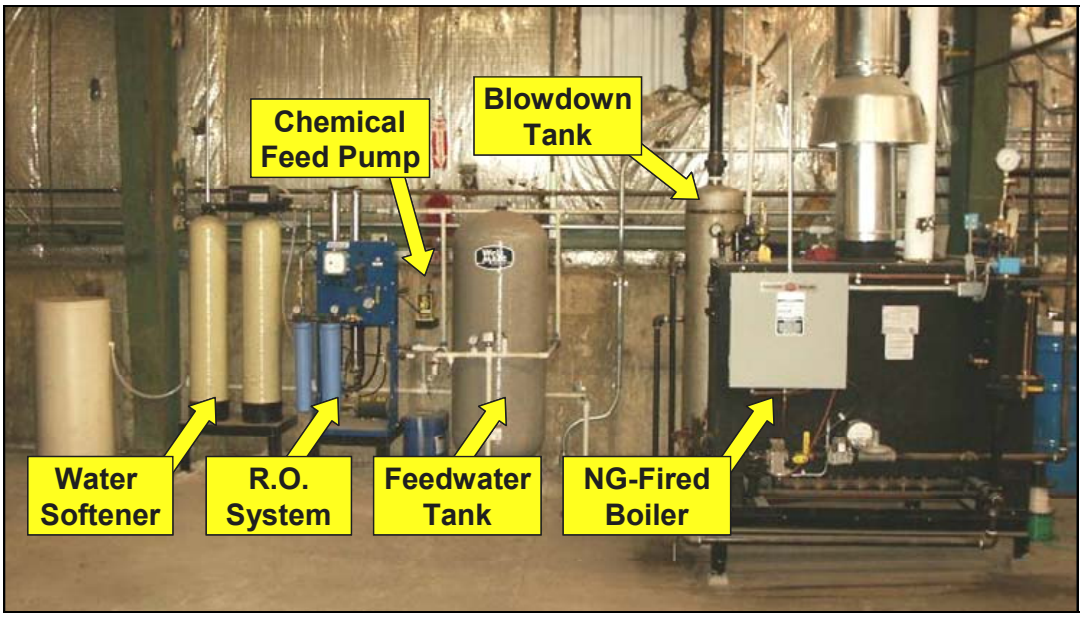

Figure 5. Steam generation system.

Superheater. Before entering the reactor, the steam passes through the superheater to increase the temperature to as much as 620°C (1150°F). The superheater is a 35 kW circulation heater built by AccuTherm, housing 24 Incoloy 840 sheathed elements in a stainless steel pressure vessel (Figure 6). The pressure vessel is rated for 2070 kPa (300 psi) at 621°C (1150°F), which matches the design pressure of the reactor itself. The superheater's power is enough to heat up to 90 kg/hr (200 lb/hr) steam at 1034 kPa (150 psi) to 620°C (1150°F).

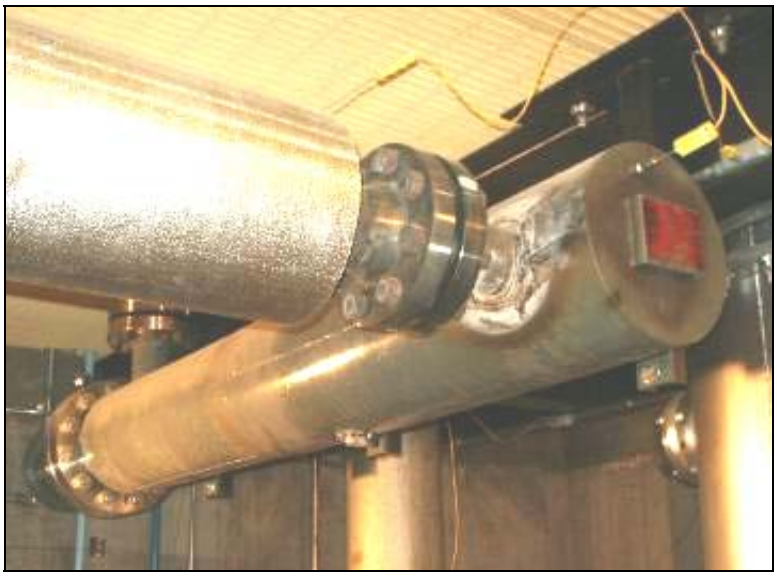

Figure 6. 35-kW steam superheater. Steam flows downwards into the heater on the left side and exits from the port in the foreground.

The system was designed to be able to accommodate a product gas recycle line. Steam exiting the superheater would be the motive gas to entrain product gas taken from the exit of the reformer. The recycle line has not yet been installed.

2.1.2 Black Liquor Feed System

The black liquor feed system comprises a liquor storage tank, recirculation pump, metering pump injector. Black liquor is loaded from drums into a heated storage tank. The tank holds approximately 570 liters (150 gallons) of liquor, or enough for roughly 3 days of continuous testing at standard conditions. The exterior of the tank is electrically heated and insulated. A centrifugal pump circulates black liquor from the tank outlet on the bottom back to the top of tank, and provides a means of mixing the liquor. Both the pump and recirculation line are electrically heat traced. The tank, pump and recirculation line are mounted on a platform secured to four load cells, thus allowing the weight of liquor in the tank to be determined. The flow rate can be confirmed by following the weight loss of the tank over several hours.

In the original design, a high pressure metering pump (FMI model QV-Q1CSC) near the tank pumped liquor through a 0.5-inch heated line to the reactor. This system frequently plugged, however, so a recirculation line was added to bring liquor near the injector. The FMI pump was replaced with a peristaltic pump that uses high pressure neoprene tubing. This rebuild solved the pluggage problem. The liquor is fed to an injector near the bottom of the reactor. The injector has a steam-purged annulus around the barrel through which the liquor is fed. A second steam flow, also metered through a high temperature rotameter, is mixed and fed with the black liquor through the barrel.

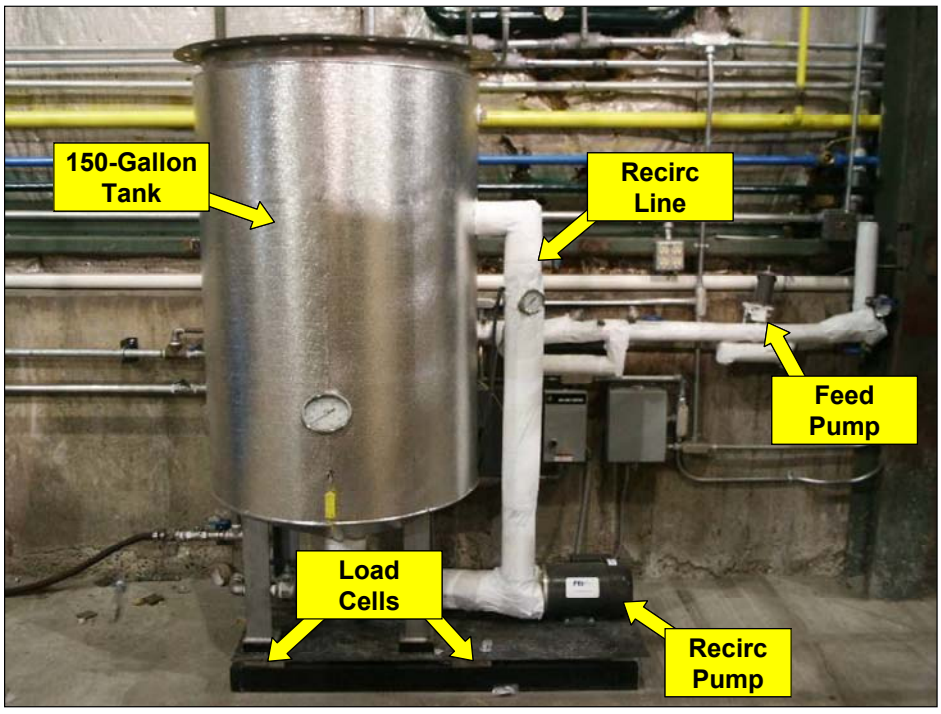

Figure 7. Black liquor feed system.

2.1.3 Fluidized Bed Reactor

The fluidized bed reactor is built in five sections, and consists of a gas distributor, bed section and freeboard. The reactor shell is 0.75 meter (30 inches) diameter, and the total height of the reactor is approximately 5.2 meters (17 feet). The bed section is 0.25 meters (10 in.) diameter, 1.4 meters (55 in.) tall. Design drawings for the reactor are presented in Appendix B. The reactor is an ASME-certified pressure vessel rated at 800°F and 300 psi, with 300-class flanges. In order to minimize heat losses and avoid condensation against the inside of the shell, the entire vessel is insulated.

Distributor section. The distributor section is the lowest section of the reactor, and is made up of a plenum and distributor for gas introduction and distribution. The distributor has twenty evenly-spaced bubble caps, which have an orifice in the bottom to create high enough pressure drop to ensure even gas distribution. A pipe for solids removal runs from the center of the distributor plate through the plenum and out to the solids removal lock hopper system. A parallel pipe for steam enters the bottom of the system and runs to the plenum below the distributor plate. The space between the plenum and reactor shell is filled with castable insulating refractory.

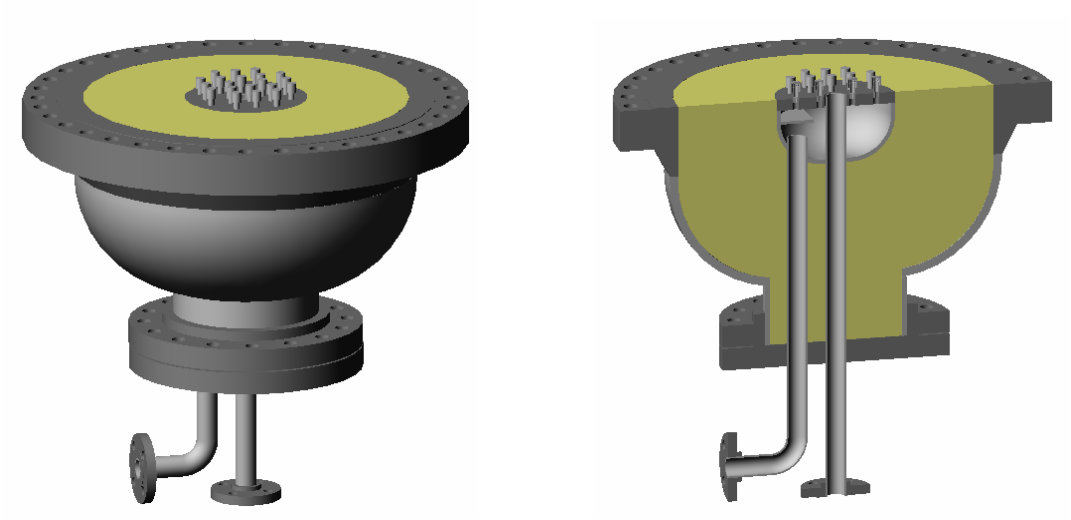

Figure 8. Distributor section and split view of same. Steam enters from the left. Solids exit through the central pipe.

Bed section. The bed section (Figure 9) is the heart of the system. It is 1.5 meters (60 inches) tall, with the bed itself occupying the lower 1.4 meters (55 inches). Two layers of refractory are cast such that a 0.25 meter (10 inch) diameter bed cavity results.

Five 8-inch nozzles are welded to the shell, above one another and offset 90 degrees for insertion of the four in-bed heater bundles. (The top nozzle allows addition of a fifth heater bundle if desired. Alternately, the bottom bundle can be moved to the top position if, for example, it is observed that black liquor is contacting the bottom heater bundle before the liquor is fully dry.) Each bundle contains 20 half-inch ID thermowells in a 4x5 staggered configuration, welded to a an 8-inch blind flange. A refractory plug cast around the thermowells fits into the nozzle and a corresponding hole in the refractory of the bed section. A 0.5-inch diameter cartridge heater is inserted into each thermowell. The cartridge heater is as long as the thermowell, but only 165 mm (6.5 inches) at the

end, where the thermowell is in the bed, is heated. In total, 32 kW of energy can be input to the bed through the heater bundles.

The eighty heaters each have an internal thermocouple that measures temperature in the core of the heated section. These are connected to the system's digital control system and used as feedback for the bed heating system. The tube bundle sections each have an additional, smaller thermowell extending into the bed for measurement of bed temperature. A fifth thermocouple above the heater bundles also monitors bed temperature. Comparison of the five thermocouples in the bed provides an indication of how well the bed is fluidized. When the bed is fluidized well, the thermocouples all read within five degrees of one another. The bed temperature control system calculates an average temperature from these five thermocouples and periodically adjusts the setpoint average temperature of the heaters in the bundles up or down by the same number of degrees as the bed setpoint and measured average temperature differ.

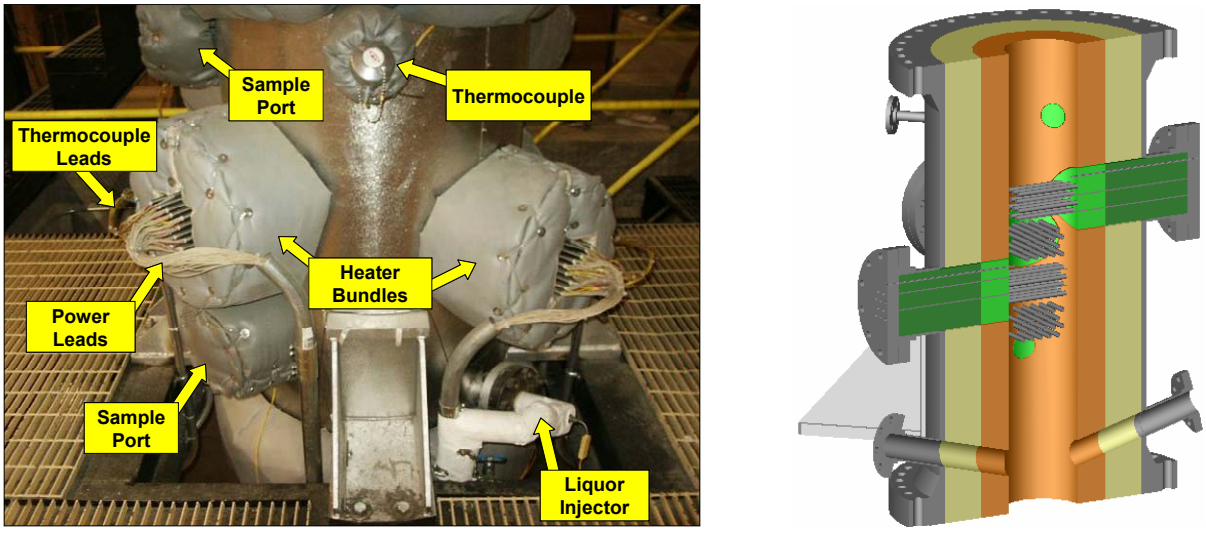

Figure 9. Photograph of the bed section of reactor and rendering showing a split view. The four bundles of heaters can be clearly seen, as can the two angled liquor injection ports at the bottom, sample ports and thermocouple ports.

Two 3-inch nozzles are welded at a 15-degree downwards angle near the bottom of the bed section. One of these is dedicated for liquor injection. The other can either be used for liquor injection, sampling or measurement of temperature and pressure. The liquor is injected approximately 3 inches above the distributor. Two 3-inch ports just above and just below the heater bundles allow for sampling or insertion of coupons for material testing. An additional 1-inch port near the top of the bed section allows temperature or pressure measurement.

The height of the bed is continuously monitored by measuring the differential pressure across the bed. This pressure is input into a formula for bed height, determined base on calibration with a known quantity of bed material. The high side of the dP transmitter is connected to the nitrogen purge line entering the tube connecting the reactor to the lock hopper. The low side is in the freeboard. The bed height is used to determine when the lock hopper needs to be cycled.

Freeboard section. The freeboard section (Figure 10) occupies the top three shell sections, and is approximately 3 meters (10 feet) tall. The bottom half has the same diameter as the bed, 0.25 meters (10 inches). This expands to 0.36 meters (14 inches) about halfway up the freeboard to reduce the gas velocity and limit particle entrainment. An internal cyclone is installed in the top of the reactor, and a dipleg from the cyclone into the bed returns captured particulate matter to the system.

Pairs of diametrically opposed 3-inch sample ports are located approximately every half meter (20 inches) along the length of the freeboard section. Diametrically opposed 1-inch ports for temperature and pressure measurement are located approximately every meter (40 inches). A 2-inch nozzle for product gas outlet is located in the top of the unit. This nozzle connects to a flange on the inside of the vessel, to which the internal cyclone is mounted. A downwards-angled 4-inch port located halfway up the freeboard section allows loading of bed solids into the reactor.

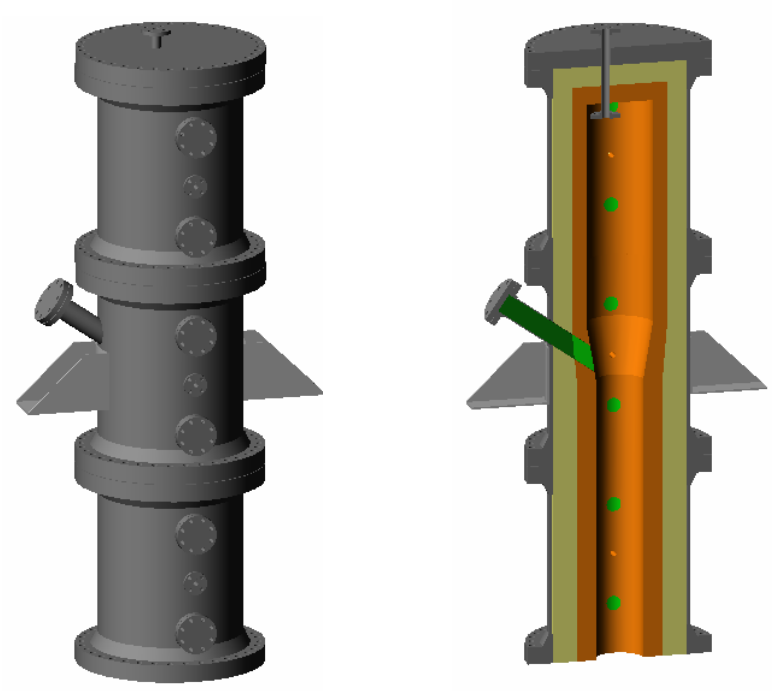

Figure 10. Freeboard section of reactor, and split view of same. The port for loading bed solids is on the left.

2.1.4 Solids Removal System

The solids removal system is located below the reactor and is made up of a lock hopper and nitrogen purge system. The lock hopper comprises a section of pipe between two valves, plus a purge valve for pressure relief. During operation, the upper valve, an lens-disc sliding valve for solids handling (Everlasting Process Valves), opens momentarily to allow solids to fall from the reactor via a 1½-inch pipe running through the distributor into the hopper. The top valve is then closed and the hopper purge valve is opened to depressurize the lock hopper. Once depressurized, the bottom valve, a metal-seated double-actuated ball valve, opens to release the solids into a receiving receptacle. Each cycle of the lock hopper releases about 2.5 pounds of bed material.

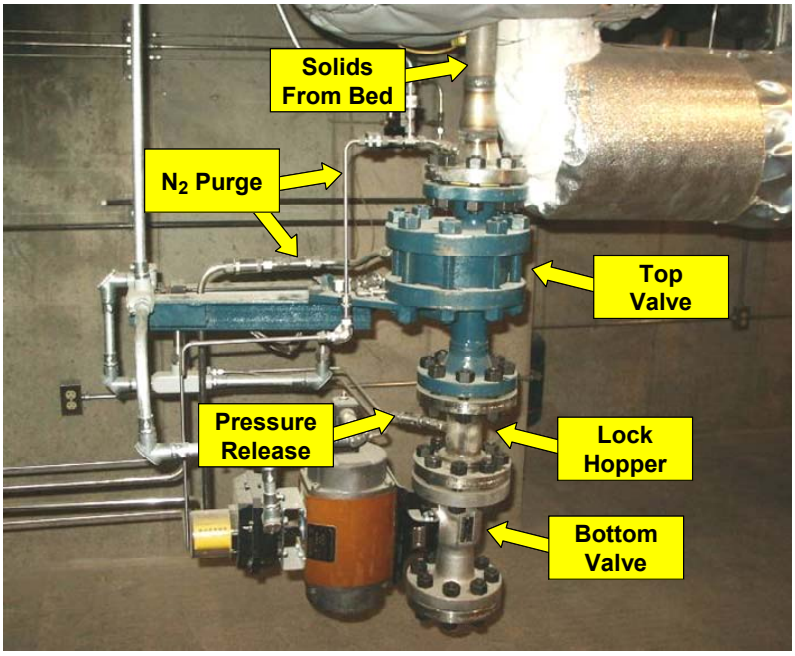

Figure 11. Lock hopper system for solids removal.

The section of pipe above the lock hopper is continuously purged with nitrogen so the solids and surrounding gas are cool and non-reactive when they are removed from the system. The purge also removes any steam from the solids removal pipe, so that there is no risk of condensation and associated pluggage in the lock hopper.

2.1.5 Product Gas Handling System

The product gas handling system safely disposes of the synthesis gas produced in the gasifier. After passing through the internal cyclone in the reactor, the gas runs through a control valve, coupled to a pressure transmitter in the reactor freeboard, that sets the pressure of the system. Downstream of this valve the gas is at atmospheric pressure. A sample line from this atmospheric, pre-combustion section of the system feeds the product gas to the on-line analyzers. Sampling and return ports are also installed to allow installation of slipstream reactors around the pressure control valve. The pressure difference upstream and downstream of the pressure control valve can be used to flow gas through slipstream reactors.

Afterburner. The product gas must be combusted before being exhausted, so it is fed to a downwards-flowing natural gas-fired afterburner (Figure 12). The afterburner is a 4.6 meter (15 foot) tall vessel lined with two layers of refractory to make a 14-inch diameter reaction chamber. Gas enters the top of the vessel and is combusted by two opposing natural gas burners in the top two ports. The gas is burned at a minimum temperature of 1000°C (1830°F) for at least two seconds to ensure efficient destruction of any tars remaining in the gas at this point. Additional ports downstream are provided for sampling or viewing. The afterburner is operated under slightly negative pressure, provided by the facility's induced-draft fan.

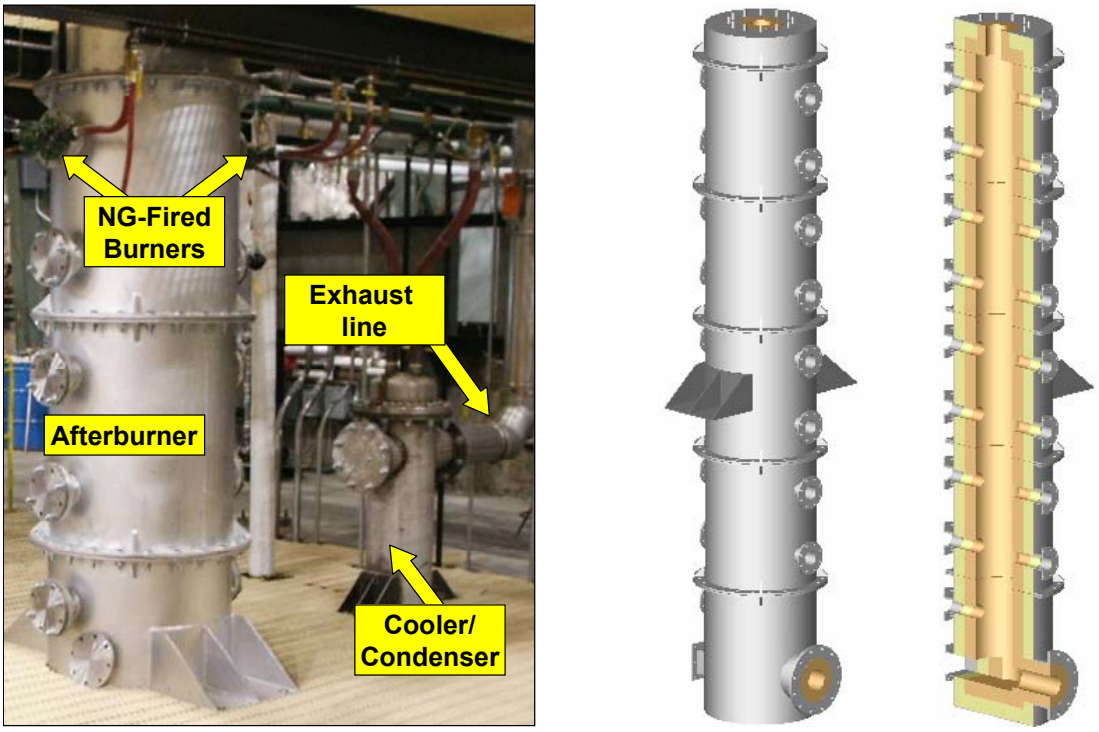

Figure 12. Photograph of afterburner and cooler, plus rendering and split view of afterburner. The bottom sections of the afterburner and cooler aren't seen in the photo.

The syngas is not cooled before being fired in the afterburner, but is kept hot to avoid tar condensation and to avoid risks associated with hydrogen sulfide in a concentrated syngas that would result if the gas were first cooled and condensed. Because the gasifier product gas is primarily steam, this results in a relatively large afterburner and natural gas requirement. This was determined to be preferable to potential operating problems and safety risks associated with cooling the gas first.

Cooler/condenser. The hot product gas from the afterburner is fed to a water-cooled heat exchanger (Figure 13) to cool the gas and condense out water. The cooler is approximately 3.3 meters (11 feet) tall an 0.3 meters (12 inches) diameter. It contains forty ¾" heat exchange tubes, and is designed to condense the whole load of superheater product gas, condensing out the steam, when the gasifier is running under pressure with 90 kg/hr (200 lb/hr) steam feed. Gas from the afterburner travels upwards through the cooler. Condensed water flows down the outside of the heat exchange tubes and drops out the bottom of the vessel into a sump drain in the floor. The cooling water is on a closed loop, and runs through a cooling tower outside the building.

The cooled gas from the heat exchanger runs to the facility's flue gas handling system. An ID fan draws the exhaust to the stack. Various dampers in the exhaust system are used to control the pressure. These are adjusted such that the afterburner runs slightly negative.

2.1.6 Process Control System

The entire gasification test system is controlled by an OPTO-22 based computerized process control system. The control system logs critical process variables and has control loops to control temperatures, pressures and flow rates. The control system includes several safety subsystems that will safely shut down the system in case of a system trip or unexpected event such as a power outage. The operator interfaces with the control system through a PC having a multi-screen customized graphical interface. A common control interface is used for operation of the gasification system and all auxiliary systems (e.g. cooling tower, exhaust gas handling system). The interface for control of the gasification system is shown in Figure 14. The operator can adjust values by clicking on the appropriate reading.

2.1.7 Sampling and Analysis Systems

The gasification system has sampling systems for bed solids, product gas and tars. Bed solids can be sampled from a sample port located 14 inches above the distributor. Alternately, solids can be sampled from the lock hopper discharge.

2.1.7.1 Gas sampling and analysis

Product gas is sampled downstream of the pressure control valve, just before the gas enters the afterburner. At this point the gas is still mostly steam and contains tars. Cleaning and drying the gas for the analyzers creates a challenge. The gas is fed into a directly-cooled impinger, into which fresh water is constantly fed. The steam and tars condense and exit through an overflow line with a vapor lock. The gas is then cooled to roughly 2 °C to condense out as much water as possible, after which it is pumped to the control room where the analyzers are located.

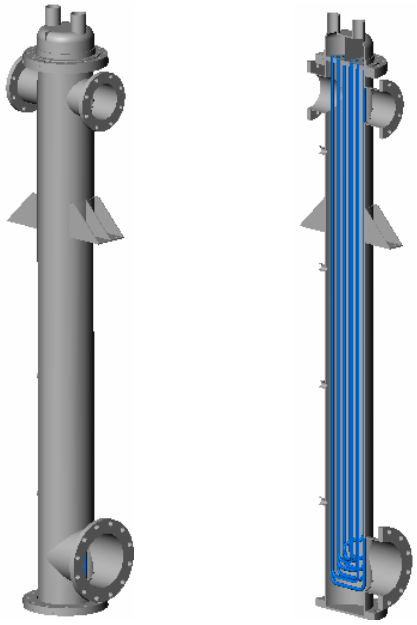

Figure 13. Rendering of the cooler/condenser and split view of same. Gas enters through the side port in the bottom and exits through the top. Condensate drains out the bottom.

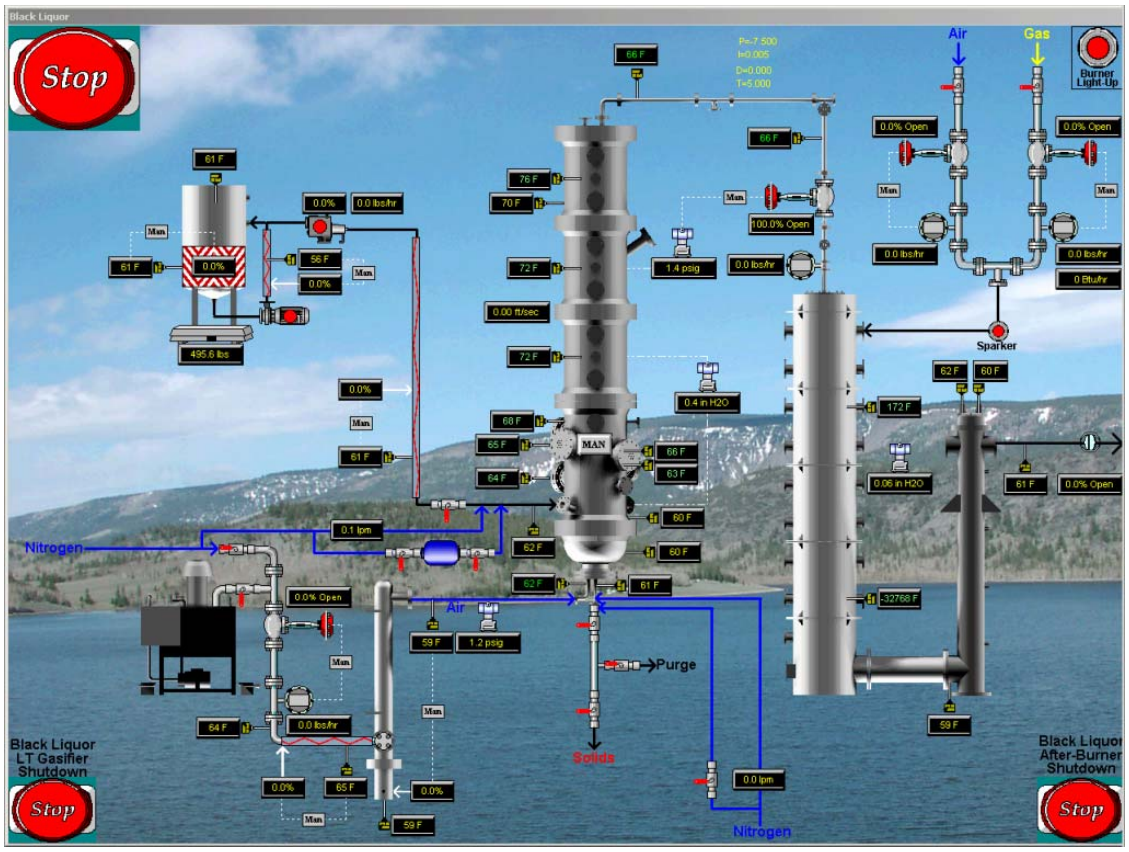

Figure 14. Graphical operator interface for gasification system.

Two analyzers are used for gas analysis. One is a continuous monitor for hydrogen, carbon monoxide, carbon dioxide and methane (Figure 15). Hydrogen is measured by thermal conductivity. Other gases are measured via infrared and a correction for hydrogen is made to reflect the thermal conductivity of the other gases. This analyzer is used primarily for process control. Concentrations of these gases are logged through the process control system.

The other analyzer is a micro-gas chromatograph, a Varian CP-4900. This system has four different columns to cover a wide range of molecular species, and is able to detect major gas components as well as hydrocarbons to C_6 and sulfur species. Micro-GC technology is relatively new, and allows complete analysis of the gas in less than three minutes. The GC is calibrated for the following gases:

- hydrogen
- carbon monoxide
- carbon dioxide
- nitrogen
- oxygen
- methane
- ethane
- propane
- n-butane
- iso-butane
- pentane
- hexane
- acetylene
- ethylene
- propylene
- benzene
- hydrogen sulfide
- methyl mercaptan

Figure 15. Continuous analyzer for H_2, CO, CO_2 and CH_4.

2.1.7.2 Tar sampling and analysis

Analysis of tars is a significant component of this program. Because tars condense over a very wide temperature range, including below the condensation temperature of steam, obtaining samples of tars is quite challenging. Several groups have developed and published protocols for tar sampling. The most robust aspects of these were combined for the sampling system for the Utah gasifier. There are six components to the sampling system: (1) 30x100 mm quartz thimble filter, (2) three impingers containing water in a cold (approx. 20°C) water bath, (3) three impingers containing solvent in an ethylene glycol bath at –20°C, (4) a backup filter to protect downstream equipment, (5) centrifugal vane pump and (6) gas volume totalizer. A diagram of the sampling system is presented in Figure 16, and a photograph of the system as installed is shown in Figure 17.

Tars were captured in the impinger train and mixed with the condensed steam and impinger solvent. For nearly all tests, the solvent was dichloromethane, which is immiscible with water. The hydrophobic tars would remain in the dichloromethane, and the two phases were separated using a separatory funnel. The dichloromethane was then removed from the mixture by evaporation at 40°C, slightly above the boiling point of dichloromethane. Evaporation was continued until dichloromethane was condensing at a rate of less than one drop per minute, and then an additional 30 minutes beyond that. The result was a concentrated mixture of tars. The mass of this was considered the mass of the tars in the sample. The volume of dry gas sampled was recorded (typically 200 liters) so it was possible to compute the tar loading in the dry gas in units of e.g., grams per standard cubic meter. Because the amount of steam condensed in the impinger train could be measured, it was also possible to calculate the tar loading in the raw (non-dry) gas. Photographs of the separation and tar isolation procedure are shown in Figure 18.

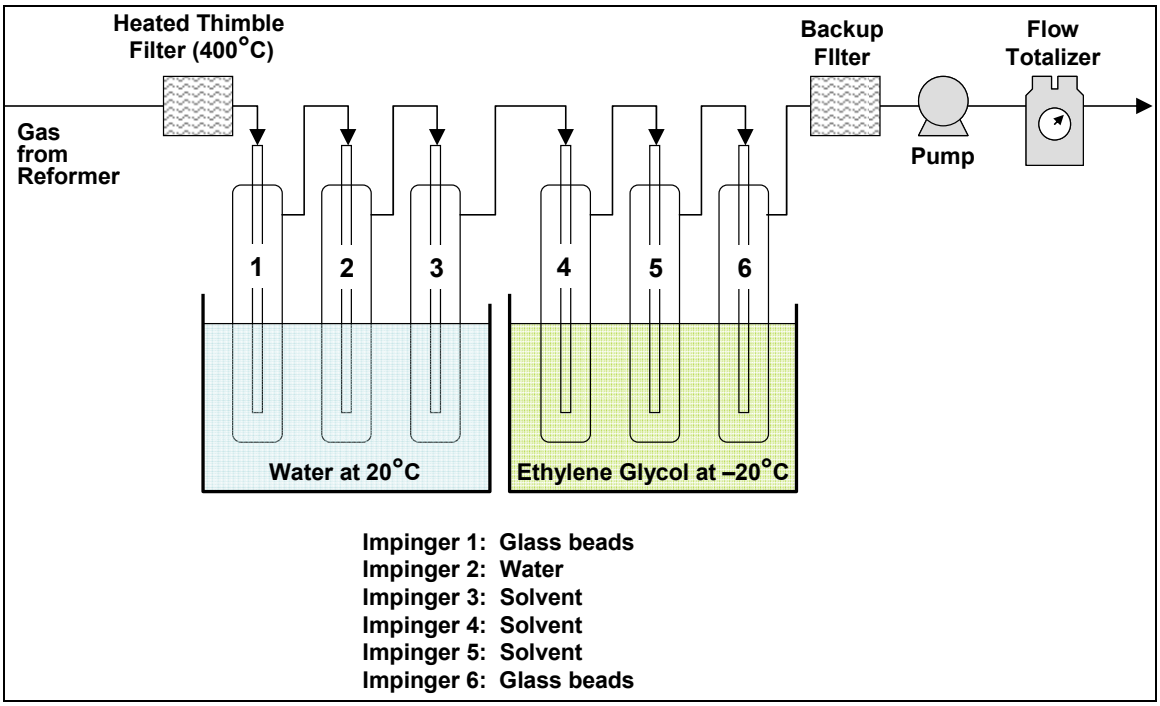

Figure 16. Schematic diagram of tar sampling system.

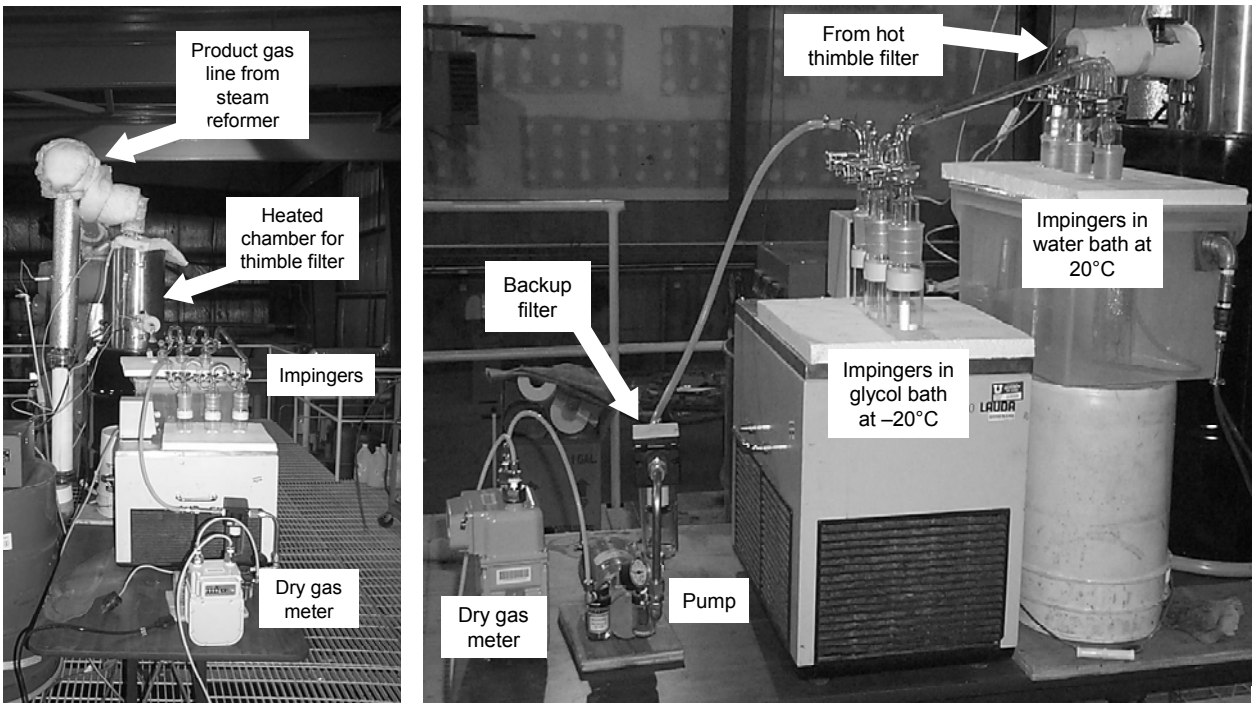

Figure 17. Tar sampling system. View from west (left) and south (right).

Figure 18. Isolation of tars. Extraction (left), solvent removal (middle, right).

Over the course of the program, it was discovered that using dichloromethane as a solvent and evaporating it as described above was not fully effective if the goal was to measure the total mass of tars sampled. The reason for this is that despite that the evaporation temperature of 40°C is higher than the boiling point of methane, some dichloromethane remained in the sample and was thus considered part of the mass of the sample. The total tar loadings computed were thus higher than they should have been. Efforts were made to correct these erroneous measurements by analyzing the tar samples for chlorine. This would determine the fraction of the sample that was dichloromethane. This turned out not to be effective, however, due to the volatility of the dichloromethane in the sample and variations in sample handling between evaporation and chlorine analysis. Follow-up analysis of the tar samples does indicate that on average approximately 40% of the sample mass was dichloromethane. As such, the measured weights, which include dichloromethane, are 65-70% high.

Despite the unrepresentatively high gravimetric tar values resulting from this procedure, trends observed are considered to be valid. Evaporation was conducted in the same manner and to the same degree of intensity for all tests, as determined by the dichloromethane evaporation (and condensation) rate. It is assumed that the concentration of dichloromethane in the various samples is thus the same. The fact that gravimetric tar measurements by this technique were very reproducible indicates that this is a reasonable assumption. As such, trends are valid, but the magnitude of the trends and the absolute tar concentrations associated based on these measurements are high.

As a result of the unrepresentatively high tar values given with dichloromethane, as well as health concerns associated with this particular solvent, the tar sampling method was modified to use isopropyl alcohol (IPA) as a solvent. This is the solvent suggested in the tar sampling protocol developed under a program by the International Energy Agency [5]. A few tests were performed near the end of the program with this technique. Because IPA is miscible with both water and heavy organics (tars), the resulting solution was a single phase. As such, it was not necessary to perform multiple extractions and separations as was necessary with dichloromethane. Rather, the entire mixture was evaporated as per the method outlined in the IEA protocol [5]. A vacuum was applied until the total pressure was 100 torr, and the mixture was evaporated in a rotary evaporator at 55°C.

The intention was to evaporate both the isopropyl alcohol and the water in the sample. Because IPA is more volatile than water, it evaporated more readily. In order to ensure that water was removed, pure ethyl alcohol was added to the mixture near the end of the evaporation stage. Ethyl alcohol forms an azeotrope with water, so this would enhance evaporation of water. This stage was repeated until no water was remaining, as observed by its immiscibility with the organic tars. The remaining material was the concentrated tar sample.

This new procedure was much simpler, quicker and safer than the approach of using dichloromethane. The resulting tar concentrations were much less, as well. This method is known to give an unrepresentatively low concentration of tars, since IPA is not as good of a solvent as dichloromethane and many of the lighter compounds are lost during the higher temperature, lower pressure evaporation stage. Nonetheless, the reproducibility of this method is good, and it is recommended for future such tar sampling.

In addition to the impinger train system described above, a single-component system for sampling tars from a fluidized bed steam reformer was developed. This system comprises a few different components: an impinger column, a sample pump and a dry gas meter. The impinger column is a special design, a so-called "Petersen column" that was suggested in the IEA Bioenergy Tar Protocol [5] as an alternative to the classic series of impingers commonly used in this type of sampling. This type of sampler is much more fieldable than a normal impinger train. A photograph of the University of Utah's Petersen column is presented in Figure 19.

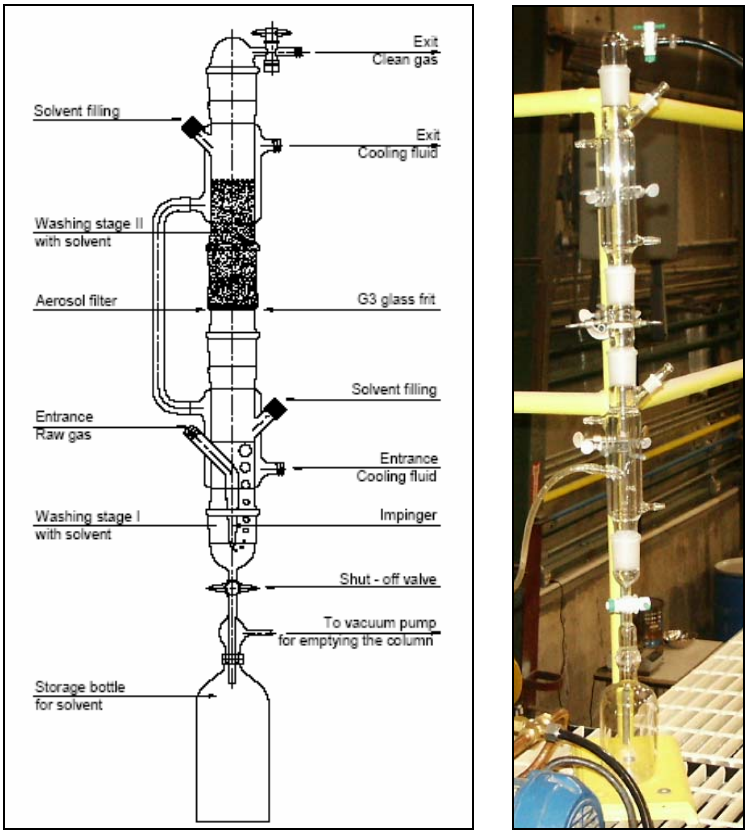

Figure 19. Schematic [5] and photograph of the "Petersen column" used for tar sampling.

The sampling column has two stages. In the first, gas flows through an impinger containing an organic solvent. The gas flows upwards from this first stage to the second, where it flows through a glass frit at the bottom of another level of solvent. The fine bubbles create a large surface area that enhances transfer of condensable organics to the solvent. Both stages are surrounded by cooling jackets to minimize vaporization of solvent. Once sampling is complete, the solvent can easily be drawn into a bottle attached to the bottom of the column by applying a vacuum to the bottle. This system allows the user to quickly prepare for another round of sampling.

This system was tested early during the program. However, there were problems with leakage and introducing the hot gas into the cooled system without damaging the glass. The impinger-based system shown in Figure 17 was more developed, so subsequent testing was conducted with this system. The column system (Figure 19) does seem promising, however, and with more attention could prove to be superior.

2.2 Bed Agglomeration Test Reactor

As part of their experimental study on agglomeration of bed material in a low temperature black liquor gasifier, Brigham Young University developed a small-scale experimental fluidized bed reactor capable of determining fluidization characteristics. The reactor (Figure 20) is square, six inches on a side, and 45 inches tall. It is constructed of 316L stainless steel L-channel frame with 316L stainless steel panels on two sides and three panes of high temperature glass on each of the remaining two sides. The glass, Neosurround made by Jones Paint and Glass, can withstand temperatures up to 800ºC (1470°F). The panels and glass are sealed with 0.125-inch high-temperature graphite gasket.

The distributor for the reactor has an air straightener to minimize any non-congruencies in the reactor's air inlet. The distributor plate itself comprises a stainless steel plate with many small (~1/16 inch) holes separated by about 0.5 inches, covered by a fine screen to keep particles from falling through.

The bed is fluidized with nitrogen. The gas is metered with a flowmeter, after which it passes through a 1.65 kW electric preheater, which can heat the gas to 250°C (480°F). The rest of the heat for the bed is provided by sixteen 0.5-inch cartridge heaters oriented in four perpendicular levels of four heaters each. Some heaters have internal thermocouples to measure their core temperature. In addition, several of the heaters have an external thermocouple glued to the surface with a high-temperature, thermally conductive adhesive. Four more thermocouples within the bed section monitor the temperature of the bed solids.

Bed agglomeration reactor cold-flow model. Prior to building the actual test unit, Brigham Young University built a cold flow model of the test reactor to assist in design of the real system. The cold flow fluidized bed is four feet tall, constructed of an axially-cut section of ABS pipe with a Plexiglas window secured by mechanical straps and sealed using flexible tubing, thus allowing for a greater pressure at the distributor. Photographs of the cold flow model are presented in Figure 21.

Compressed air is fed to the cold flow model through a rotameter to adjust the flow rate. A series of six pressure transducers, attached to the back of the reactor, show pressure at varying locations vertically along the bed. An analog pressure gauge is attached to the upstream air supply to determine the total pressure necessary for fluidization.

Figure 20. Photographs of the fluidized bed reactor for bed agglomeration studies, with close-ups of the sixteen cartridge heaters and the air straightener/plenum section.

Preliminary experiments with 300 micron sand indicated that modifications were needed for the stainless steel high-temperature reactor. It was determined that the original design of a hemi-cylindrical reactor generated an unevenly distributed flow profile and create zones of low fluidization. The design for the full-scale reactor was therefore modified to the square design described above.

2.3 Single Droplet Reactor

The University of Utah constructed a laboratory reactor for studying pyrolysis and gasification behavior of single droplets or particles of black liquor. The design is based on a similar reactor that has been successfully used for black liquor studies at Åbo Akademi University in Finland. The Utah reactor is constructed from two concentric quartz tubes positioned in a vertical tube furnace. The inner tube is approximately 1 meter (40 inches) long, 38 millimeters (1.5 inches) diameter. The outer tube is approximately 0.7 meter (28 inches) long and 63 millimeters (2.5 inches) in diameter. The outer tube is centered around the inner tube and sealed on the top and bottom. Gas is fed through a flowmeter, enters the bottom of the outer tube and flows upwards between the outer and inner tubes, where it is heated. The heated gas then enters the inner tube through a series of small holes, flows downwards through the hot part of the reactor and is exhausted through a port in the bottom of the reactor. A photograph of the top part of the reactor is presented in Figure 22.

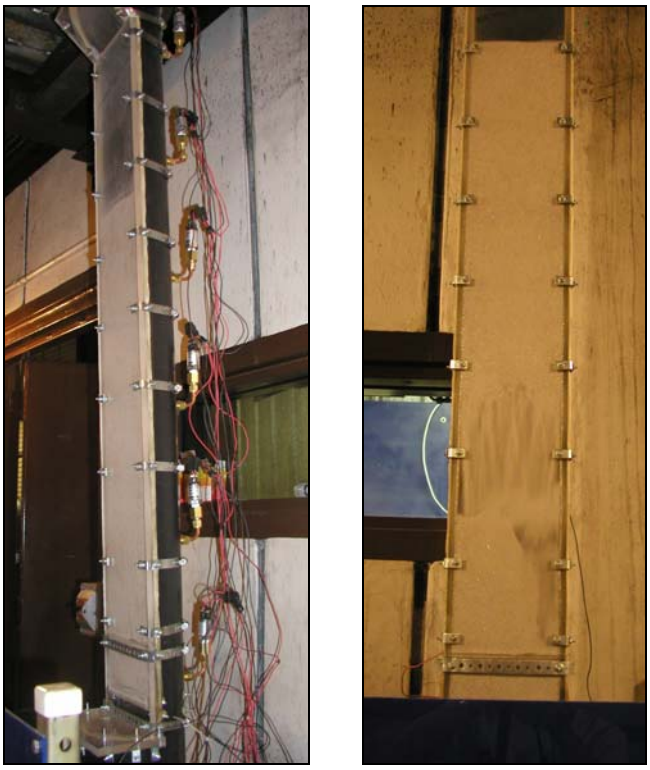

Figure 21. Brigham Young University's cold flow model: side view (left) and operating (right).

Figure 22. Single-droplet reactor.

A purge chamber at the top of the reactor provides a cool, inert environment for sample preparation and cooling after an experiment. A small flow of nitrogen (approximately 20% of the total flow) is fed into this chamber and flows downwards through the inner tube. It meets and mixes with the preheated primary gas just inside the heated section of the furnace. This design produces a sharp temperature transition, thereby maximizing heating rate. The top section of the reactor containing the purge chamber can be removed from the main body by removing a ground glass fitting, thereby facilitating sample loading and unloading.

In a typical pyrolysis experiment, approximately 10 mg of concentrated black liquor is attached to a coil of fine wire. The wire is attached to a glass ring on the bottom of the glass rod, and is pulled into position in the purge chamber. The top section of the reactor is put into place and purge and reactor gas are set to the desired setpoints. The rod is then quickly lowered into the hot zone of the furnace and kept there for the desired amount of time, after which the sample is pulled back up into the purge zone. The sample is allowed to cool and stabilize in this zone, after which it is removed and carefully weighed to determine pyrolysis yield. The resulting char is saved for possible further analysis.

2.4 2-inch Fluidized Bed Reactor

The University of Utah constructed a 2-inch fluidized bed reactor to study growth particles and variations in particle size distribution when liquor is injected into a hot fluidized bed (Figure 23). The reactor is essentially a 2-inch piece of either quartz tubing or stainless steel pipe secured to a specially machined base. The base comprises the distributor, nitrogen feed inlet port, a thermocouple port for measuring the plenum temperature and a port to allow injection of black liquor. The distributor is simply a plate of porous stainless steel attached to the reactor base. A second thermocouple for measuring the bed temperature extends from the top of the reactor into the bed.

Nitrogen is used as a fluidizing medium. The flow rate is controlled by a variable area flowmeter, and the gas is preheated prior to feeding to the reactor. Preheating is achieved through a combination 1.1 kW rod heater and 1.9 kW tube furnace housing a stainless steel heating chamber. This is the sole source of heat to the system, i.e., there are no in-bed heaters or shell heaters. The fluidized bed is therefore installed right on the outlet from the tube furnace and nitrogen preheater. The system is well insulated and able to operate at temperatures representative of those in a full-scale system, up to 605°C (1120°F).

Two methods of introducing black liquor into the bed have been developed. The first involves injecting liquor into the bed near the distributor. The injector is made of two concentric tubes, with liquor flowing through the center tube and cooling nitrogen flowing through the outer tube to shield the liquor from the heat of the bed. The other method simply involves feeding liquor into the top of the reactor and allowing droplets to fall on the bed. For both types of injection preheated, relatively dilute liquor is fed through a peristaltic pump and then through tubing to the reactor.

Samples of bed material can be taken during operation by essentially vacuuming out a bit of the bed through the top plate of the reactor and capturing the particles on a stainless steel filter.

Figure 23. 2-inch fluidized bed. Thermocouples in the plenum and extending from the top into the bed can be seen. The liquor injector is located just above the lower yellow thermocouple.

2.5 Fluidized Bed Gasifier Cold-Flow Model

A cold flow model of the University of Utah fluidized bed gasifier was built as an aid in system design, visualization of reactor flows and interpretation of data. The cold flow model is also useful as a validation tool for the program's modeling efforts.

In order to ensure that the cold flow model accurately simulates the behavior of the bed in the true gasifier system, it is important that four dimensionless scaling parameters are kept the same between the two systems [6]:

$\frac{d_p u \rho_g}{\mu}$	$\frac{\rho_s}{\rho_g}$	$\frac{u}{(g d_p)^{0.5}}$	$\frac{L}{d_p}$
Reynolds number	Density ratio	Froude number	Geometric similarity of distributor, bed, particle

The cold flow model was designed to keep these scaling parameters equal between the systems when the gasifier is operating at standard conditions. The final cold flow model design calls for a bed diameter of 6.5 inches, fluidizing 200 micron soda lime glass beads with a 50/50 mixture of helium and air at room temperature. A comparison of specifications for the true gasifier and the cold flow model is presented in Table 2. No visually discernable difference can be detected when fluidizing with pure air as opposed to the 50/50 helium/air mix, so most of the tests are run with pure air.

TABLE 2. COLD FLOW MODEL DESIGN SPECIFICATIONS

Characteristic	Gasifier		Model	
Average pressure in bed	290 kPa	42 psia	103 kPa	15 psia
Operating temperature	604 °C	1120 °F	20 °C	68 °F
Bed diameter	0.254 m	10.0 in	0.164 m	6.5 in.
Expanded bed height	1.27 m	50.0 in	0.864 m	34.0 in.
Heating tube diameter	0.0173 m	0.680 in	0.0109 m	0.433 in.
Particle diameter	300 μm	0.0118 in	200 μm	0.00787 in
Particle density	2,275 kg/m^3	142 lb/ft^3	2,500 kg/m^3	156 lb/ft^3
Superficial gas velocity	0.396 m/s	1.30 ft/s	0.326 m/s	1.07 ft/s
Gas density	0.633 kg/m^3	0.0395 lb/ft^3	0.700 kg/m^3	0.0437 lb/ft^3
Gas viscosity (x 10^5)	3.08 kg/m-s	2.07 lb/ft-s	1.89 kg/m-s	1.27 lb/ft-s
Reynolds number	2.44		2.36	
Froude number	7.30		7.36	
Density ratio	3,595		3,641	
Geometric similarity (bed/particle)	10,160		9,906	

As seen by the nearly identical values for the critical dimensionless scaling parameters, one can be confident that the behavior of the cold flow model is representative of the real system. It is of interest to note that the time scale factor for the cold flow model is 0.82, meaning that processes that occur in 1 second in the real system require only 0.82 seconds in the cold flow model. Hence, videos of the cold flow model must be played back at 82% of their recorded speed to give an accurate representation of the speed at which the real system is fluidizing.

Pictures of the cold flow model are shown in Figure 24. The body is fabricated in sections from cast acrylic (Plexiglas) tube (0.164 m, 6.5 in ID) with grooves machined into the ends to allow the individual pieces to be stacked on top of one another. The "heating tubes" in the tube bundle sections are glass tubes (11 mm OD). Two sets of four tube bank sections were constructed, one with staggered tubes and one with parallel tubes. Several pieces of different lengths were constructed for the bottom section below the tube bundles. The modular design allows different arrangements to be constructed, and permits individual sections to be independently rotated. The tube bank sections can be oriented parallel or perpendicular to one another, and the height below the tube banks can be changed by using different length pieces.

The distributor (Figure 25) is made of two plates with forty-two 9/16" holes evenly distributed over the area. Two layers of tight-weave fabric are sandwiched between these plates to create high pressure drop across the distributor to ensure even distribution of the fluidizing gas. As in the real system, a solids removal port runs through the center of the distributor. This connects to a pipe running through the plenum, and to a ball valve below the reactor to allow easy drainage of bed solids.

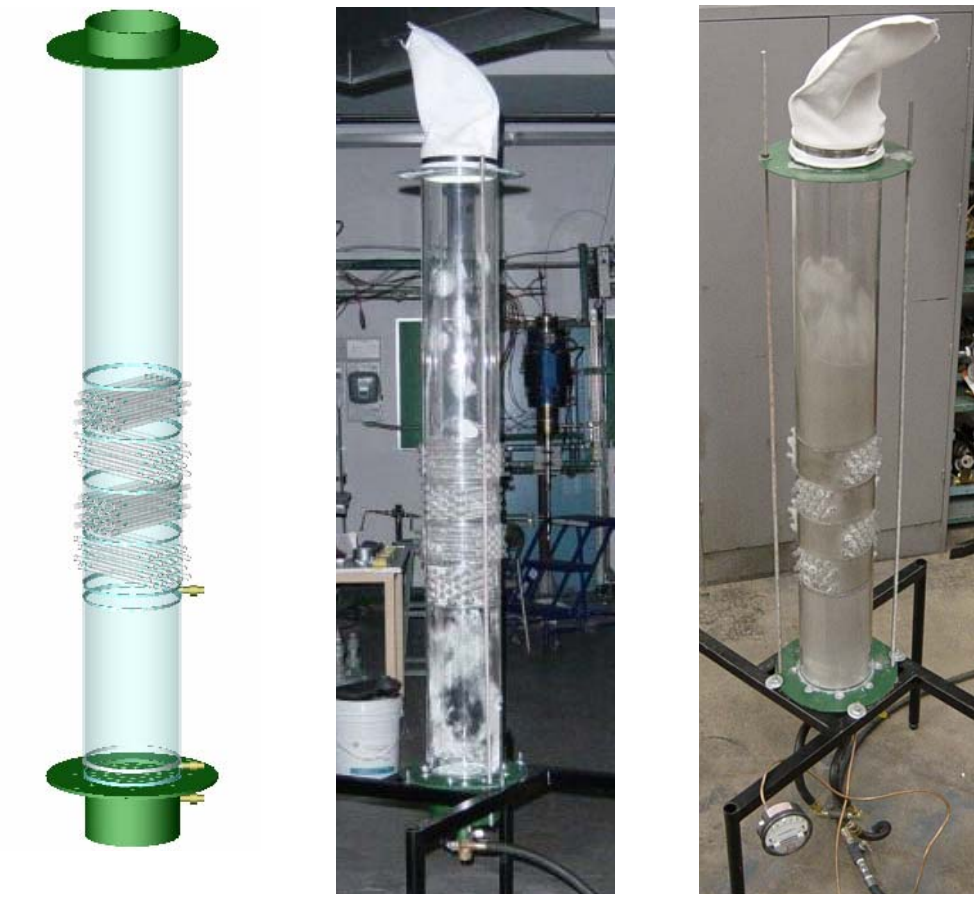

Figure 24. Rendering and photographs of the cold flow model of the University of Utah fluidized bed gasifier. The photo on the right shows the system during operation.

Figure 25. Cold flow model distributor.

During operation, compressed air and helium are fed through variable area flowmeters to the plenum of the fluidized bed, below the distributor, and flow evenly through the distributor. At standard operating conditions (14.8 scfm total flow, 26" slumped bed height), pressure drop across the distributor accounts for approximately 40% of the total pressure drop across the system.

The cold flow model has a number of uses. Generally speaking, it provides visual insight into the behavior of the fluidized bed gasifier. The bed can be videotaped during operation and played back at slower speed to identify flow patterns of solids and gas. The cold flow model is a useful tool for developing and validating computerized models of the fluidized bed gasification system, particularly with regard to flow of gas and solids around and through the horizontal heat exchange tubes. One such application is shown in Figure 26, where two probes are inserted into adjacent glass tubes. One probe has a light source, either visible or infrared. The other probe has a photodetector. As bubbles pass between the tubes, light from the source is seen by the detector. By coupling the detector to a computerized data acquisition system, variations in light intensity, corresponding to bubble size and frequency, can be tracked. By setting zero and full scale intensities for a packed bed and empty bed, respectively, the average bed density between tubes can be determined and mapped for the entire tube bundle region.

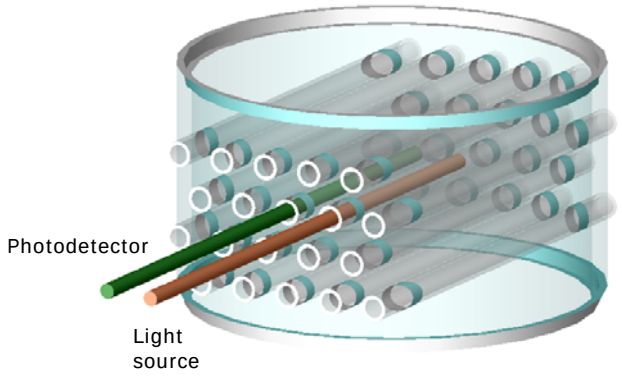

Figure 26. Tube section of cold flow model showing light source and detector probes inserted into "heater" tubes.

3. COMPUTATIONAL MODELS

Several computational models of fluidized bed steam reformers were developed under this project. The first, developed at the University of Utah, is a general, idealized model for any fluidized bed black liquor steam reformer that maps the gas compositions and flow rates throughout the reactor. The second model, developed by Reaction Engineering International, is a "1½-D" model of the entire Big Island reactor that predicts bubble development and rise, liquor conversion, temperature distributions and gas compositions. A third model developed specifically for heat transfer predictions is described in Section 3.3 and a fourth for modeling particle size distribution development is presented in Section 3.4. As part of a project de-scope and decommissioning of the Georgia-Pacific demonstration system during the period of performance of this project, the models were not systematically compared to a full-scale system refined to improve accuracy and predictive ability.

3.1 General Steam Reformer Model (UU Model)

3.1.1 General Description

Initially, this model was developed as an aid for designing the University of Utah black liquor gasification test system. The first version was essentially a glorified mass balance for the steam reformer, and one had to specify a carbon conversion rate. Over the course of the project, as data was gathered from the experimental systems, the model was improved and expanded to predict overall carbon conversion based on fundamental rate expression for black liquor conversion. The entire model is contained as one Microsoft Excel file, has a user-friendly interface, is portable and can easily be modified. A screen shot of the model interface is shown in Figure 27.

In designing the University of Utah test gasifier, the model was first set up to simulate the Big Island steam reformer. A copy of that model was made and the reactor geometry, conditions and flows were manipulated to create a system that would simulate conditions in the bottom section of a full-scale steam reformer to the extent possible, and that would be reasonably sized with regard to space available, construction and operating costs, and operator demand.

To set up the model, the user inputs the following variables:

- Reactor geometry
  - bed height and diameter
  - freeboard height and diameter
  - liquor injection height
- Black liquor properties (solids content, composition, heating value)
- Steam flow rate
- Fraction of product gas recycled and fed with steam into bed
- Freeboard pressure
- System temperature
- Assumed time for 99% liquor drying
- Assumed time for 99% liquor pyrolysis
- Kinetic expression for carbon conversion based on gas composition and pressure
- Activation energy for the steam-carbon gasification reaction

Based on these input values, the model predicts the following:

- Pressure profile throughout the bed
- Gas composition throughout the bed
- Supercritical and actual bed velocities throughout the bed
- Gas and solid residence time
- Local gasification rates
- Overall carbon conversion
- Solid product production rate and composition

The model makes the following assumptions:

- The entire bed, both gas and solid phase, is isothermal. This assumption is reasonable given the excellent mixing in fluidized beds and observations of temperature at different locations in operating steam reformers.

- Solids are perfectly mixed in the reactor (i.e., it can be treated as a CSTR). Again, this assumption is reasonable considering the excellent mixing in fluidized beds. Specifically, the time for complete particle mixing, on the order of a few minutes, is much less than the many hours required for particle conversion.

- Gas flows uniformly upwards through the bed (plug flow). Zero backmixing is assumed. In actual fluidized bed reformers the gas is well in excess of the minimum fluidization velocity. Minor local backmixing may occur, but is considered negligible.

- Liquor is introduced evenly over a horizontal cross-section of the bed. This assumption is reasonable for systems that have many liquor injectors that uniformly distribute the liquor. If a system has few injectors, there will be zones with relatively high and low concentrations of black liquor. This affects the impact of pyrolysis products on gas composition in those zones. Interestingly, near-injector zones that have high relatively high concentrations of pyrolysis gases would also have more local steam production resulting from liquor drying. For a typical liquor under these conditions the amount of steam generated by drying is roughly twice the amount of gas created during pyrolysis on a volumetric basis. The result is local dilution of the pyrolysis gases. Additionally, the volume expansion resulting from vaporization of water in the liquor would enhance radial dispersion of the liquor and pyrolysis gases.

- The gas composition at all positions within the bed are at equilibrium with regard to the water-gas shift reaction. This has been observed in operating black liquor steam reformers, and is a consequence of the highly catalytic nature of the large amount of alkali in the liquor. (See Section 4.2.1.1.)

- Carryover of fines is negligible. Experience does indicate that fines exit with the gas stream, but the quantity is small relative to the amount of liquor being introduced. The model does consider solid material leaving the bed through the lock hopper. Assuming the composition of the fines is similar to that of the bed material, one can consider the material loss by carryover is accounted for in the solid removal through the lock hopper.

- The system is at steady state.

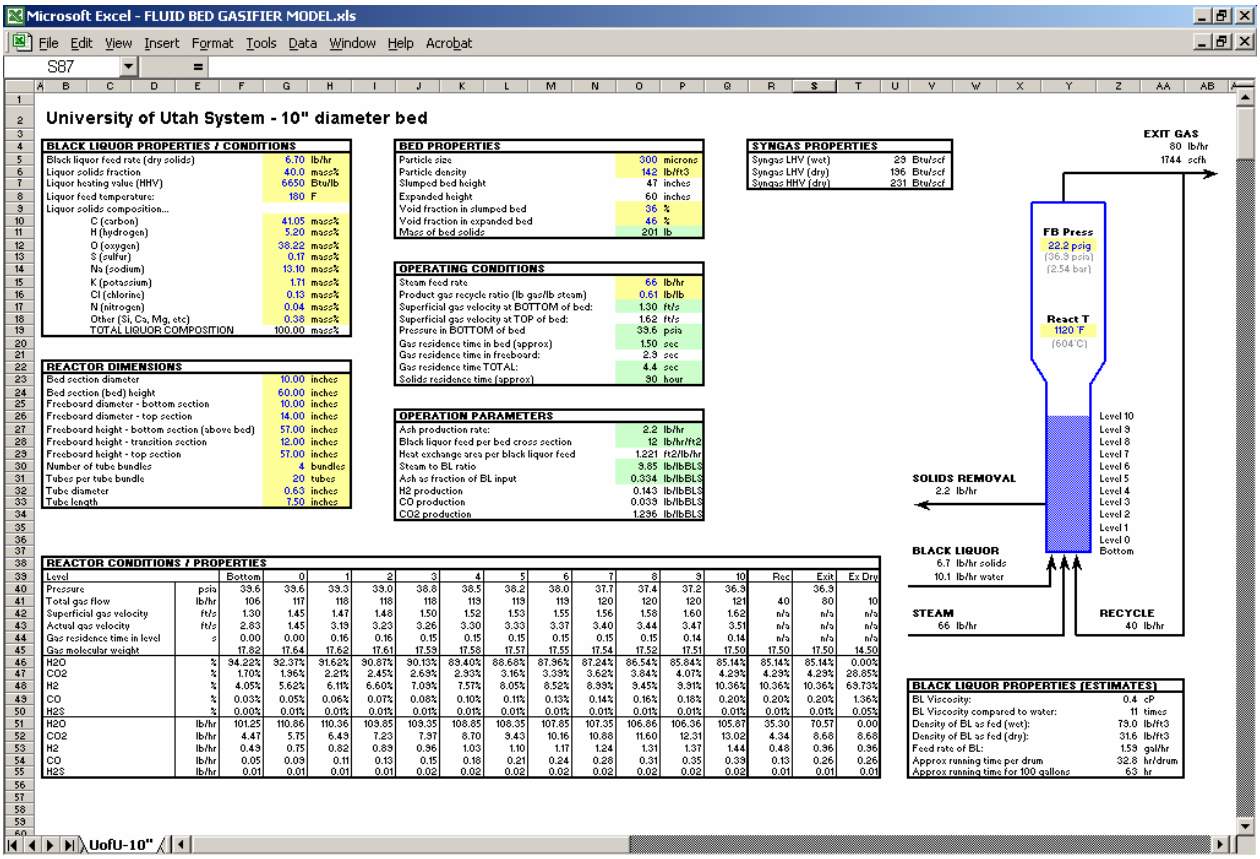

Figure 27. Screen shot of UU model interface.

All gas phase equilibrium calculations are performed by the following procedure:

1. The C, H, O and S atoms entering the system or level are totaled.
2. All S atoms and 2xS hydrogen atoms are removed from the system.
3. The equilibrium composition of H_2O, CO_2, H_2 and CO for the remaining atoms is calculated.
4. The H_2S removed in step 2 is returned to the mixture.

In step 3, the composition is calculated by determining the equilibrium constant for the water-gas shift reaction at the specified temperature, manipulating gas species concentrations into a quadratic equation with one real root and identifying this root. The solution can thus be found directly, eliminating the need for iteration or a solver. Through this approach, the model solution updates immediately when a change is made to the inputs.

The model considers gas flow through the bed from the bottom up. The bed is divided into 100 sections of equal volume, and the compositions and flows into and out of each section (labeled Levels 1, 2, 3, etc.) are determined. In addition, there is a "bottom" level below Level 1 that considers only the incoming steam and recycled syngas, if any. Descriptions of the different sections and processes that take place in these sections are described in the sections that follow.

3.1.2 Treatment of Chemistry and Liquor Conversion

The user inputs the height at which black liquor is injected. Below this height, carbon conversion occurs only through heterogeneous reaction of the liquor-coated bed material and the surrounding gas. At the point of liquor injection and upwards, contribution to the gas phase results from drying and pyrolysis of the liquor as well as heterogeneous reaction.

3.1.2.1 Bottom Level: Steam and Recycled Syngas Feed

The user can input the steam feed rate as well as the recycle ratio, defined as mass of recycled syngas to mass of steam introduced into the reactor. The model first performs an initial mass balance for the total system to determine the final product gas composition. The appropriate flow of this product gas (based on recycle ratio) is combined with the incoming steam flow and the equilibrium composition of this mixture is determined. This mixture is passed on to Section 0.

3.1.2.2 Black Liquor Drying

Drying is assumed to progress extremely rapidly in a fluidized bed gasifier as a result of the relatively fine atomization of the liquor and excellent heat transfer and large particle surface area of the bed. The time for 99% drying is input and water release during drying is assumed to decrease exponentially with time from the point of liquor injection. Typically, it is assumed that drying was 99% complete in less than one second. This is consistent with experimental work on liquor conversion with particles this size.

3.1.2.3 Black Liquor Pyrolysis

Pyrolysis was assumed to initiate when drying was 99% complete. As with drying, the user inputs the time to 99% devolatilization and release of components during pyrolysis is assumed to decrease exponentially with time. The total amount of each component released during pyrolysis is determined as described below.

Carbon: Frederick and Hupa [7] investigated black liquor pyrolysis, and offer a relation to determine the percentage of carbon retained in the char as a function of temperature:

$$\textit{Percentage of carbon retained in char} = 645 \exp(-0.00332T) \qquad \text{(Eq. 1)}$$

where T is in °C.

Hydrogen: There has not been much interest in studying hydrogen release during pyrolysis, and no published results on this issue are available. Elemental compositions of liquor and chars are available, however. Hydrogen contents in black liquor solids are on the order of 3.5%. Reported hydrogen contents of chars are in the range 2 wt%. Char yield during formation of such chars is roughly 65%. An estimate of hydrogen released can thus be calculated: (3.5 – (2.0 x 0.65)) / 3.5 = 63%. The release is undoubtedly affected by temperature, but until data to model this are available, a constant 63% H loss is assumed.

Oxygen: Like hydrogen, there is essentially no data on oxygen release during pyrolysis. Data on component release versus temperature are available for carbon, sodium and sulfur, and the total volatiles yield versus temperature are also available. Using this information, a relation for oxygen

release as a function of temperature was back-calculated such that the total volatiles yield agrees with that estimated from Frederick and Hupa [7]:

$$\textit{Volatiles yield}\ (\%) = -39.7 + 0.1T \qquad \text{(Eq. 2)}$$

Data between 700 and 900°C were fit, and the relation can comfortably be extrapolated to 600°C. The resulting relation for the percent oxygen volatilized is:

$$\textit{Percent oxygen release} = 3.77 \exp(0.00292T) \qquad \text{(Eq. 3)}$$

where T is in °C.

Sulfur: Frederick et al. [8] offer a correlation for sulfur release during black liquor devolatilization. The correlation depends only on temperature. For temperatures between 250 and 1018°C,

$$\textit{Percent sulfur released} = -163.27 + 0.9717T - 1.15e^{-3}T^2 + 4.283e^{-7}T^3 \qquad \text{(Eq. 4)}$$

Sodium and potassium. Expressions describing the amount of sodium release during pyrolysis are available. In this model, zero release of both sodium and potassium is assumed. It is expected that such release would be very small at the low temperatures used in steam reformers. Also, the model focuses primarily on carbon conversion and loss of sodium during devolatilization is not expected to impact carbon conversion.

Other components. Release of other components in the black liquor (e.g. Cl, N, Ca) are ignored, since their concentrations are low and they do not directly impact conversion of carbon. These components are assumed to exit with the solid product.

3.1.2.4 Heterogeneous Char Gasification

Once the liquor has devolatilized, a char remains. This char is slowly gasified until an inorganic residue (ash) remains. Char gasification, or removal of organic carbon from the bed solids, is by far the slowest stage of liquor conversion. Considering the well-mixed nature of the bed, gasification is assumed to occur throughout the bed, both below and above the point of liquor injection. Local gasification rates do depend on gas composition.

Not all hydrogen, sulfur and non-inorganic oxygen is released in the pyrolysis stage. The small amounts that remain are assumed to be released uniformly over the bed volume, i.e., they are considered to be independent of gas environment and carbon conversion. Release of these components during the gasification stage is very small relative to overall conversion of the liquor.

The local rate of carbon conversion is calculated from one or a combination of expressions resulting from experimental studies of black liquor conversion in gasification environments. For these expressions, the rate is a function of temperature, partial pressures of the primary gases (H_2O, CO_2, H_2 and CO) and the concentration of carbon in bed solids. The rate of conversion is not uniform within the bed. Instead, it is most reactive at the bottom, where the gas comprises only steam. As H_2 and CO are produced, these decrease the local gasification rate higher in the bed. This effect is correctly simulated by the model.

Several laboratory-scale studies have investigated the rate of black liquor char gasification by both steam and carbon dioxide [9-16]. These studies are summarized below.

Steam gasification rates. Li and van Heiningen [12] studied the rate of char gasification in steam at atmospheric pressure using a thermogravimetric analyzer and developed the following generalized expression to describe the influence of gas environment on the gasification rate.

$$rate = -\frac{k_1[\mathrm{H_2O}]}{[\mathrm{H_2O}] + k_2[\mathrm{H_2}]} \qquad \text{(Eq. 5)}$$

As seen in the above expression, increasing the hydrogen concentration slows the rate of reaction. More recently, van Heiningen applied this expression to available data acquired at low pressure and developed numbers for the constants k_1 and k_2 [17]:

$$rate\left(\frac{\text{moles C}}{\text{m}^3 \cdot \text{s}}\right) = 3 \times 10^9 \, \frac{k_1[\mathrm{H_2O}]e^{-25{,}200/T(K)}}{[\mathrm{H_2O}] + 1.42[\mathrm{H_2}]} \qquad \text{(Eq. 6)}$$

where the gas concentrations have units moles/m^3 and the value of k_1 equals [Na] (moles/m^3) when [C] > [Na] and k_1 equals [C] when [Na] > [C]. This expression does not include the influence of carbon monoxide on the rate. Carbon monoxide is a product of the steam-carbon reaction and its presence has been shown to strongly inhibit the gasification rate [10].

Whitty, et al. [10] investigated steam gasification of black liquor char over the pressure range 1–30 atm and focused on the influence of product gas species, H_2 and CO, on the gasification rate. As was observed in the Li and van Heiningen studies, increasing hydrogen partial pressures decreased the gasification rate. Carbon monoxide was found to be an even stronger inhibitor. It was found that the rates could be well-described in terms of gas partial pressures by a Langmuir-Hinshelwood form expression:

$$rate\left(\frac{\text{mg}}{\text{mg} \cdot \text{s}}\right) = 10^{-4} \cdot \exp\left[28000\left(\frac{1}{923} - \frac{1}{T}\right)\right] \cdot \frac{9.01}{1 + \dfrac{p_{\mathrm{H_2}}}{0.449\, p_{\mathrm{H_2O}}} + 7.09\, p_{\mathrm{CO}}} \qquad \text{(Eq. 7)}$$

where the partial pressures of the gases have units of bar (absolute) and T is in Kelvin. This expression does reflect the inhibiting effect of carbon monoxide.

Carbon dioxide gasification rates. The product gas from operating reformers contains appreciable quantities of carbon dioxide, roughly 22-33%, formed primarily as a result of the water-gas shift reaction [18,19]. Carbon dioxide can gasify carbon in black liquor char or fluidized bed reformer particles to form carbon monoxide:

$$\mathrm{C(s)} + \mathrm{CO_2(g)} \rightarrow 2\,\mathrm{CO(g)} \qquad \text{(Eq. 8)}$$

The rate of this reaction is roughly one-third as fast as gasification with steam [10], but it does contribute to carbon conversion. Li and van Heiningen studied this reaction under atmospheric conditions and propose the following rate expression for fast pyrolysis black liquor char:

$$rate = -\frac{k_3[CO_2]}{[CO_2] + k_4[CO]} \qquad \text{(Eq. 9)}$$

Van Heiningen subsequently applied this expression to data obtained in a later experimental study [13] and developed values for k_3 and k_4 [17]:

$$rate\left(\frac{\text{moles C}}{\text{m}^3 \cdot \text{s}}\right) = 7 \times 10^{10} \frac{k_3[CO_2]e^{-30{,}070/T(K)}}{[CO_2] + 3.4[CO]} \qquad \text{(Eq. 10)}$$

where the gas concentrations have units moles/m^3 and the value of k_3 equals [Na] (moles/m^3) when [C] > [Na] and k_3 equals [C] when [Na] > [C]. This expression does not include the influence of carbon monoxide on the rate.

Frederick, et al. [14,15] measured rates of gasification of kraft black liquor char with CO_2 at elevated pressures and proposed the following form for the rate as a function of temperature and gas composition:

$$rate\left(\frac{\text{gram C}}{\text{gram C}_{\text{init}} \cdot \text{s}}\right) = \frac{p_{CO_2} - p_{CO}^2 / K_{eq}}{\frac{k' p_{CO_2}}{Y_{C,0}} + \frac{k'' p_{CO}}{Y_{C,0} N_{Na+K}}} \qquad \text{(Eq. 11)}$$

Gasification in mixtures of H_2O, CO_2, H_2 and CO. Clearly, the concentrations of all major species, H_2O, CO_2, H_2 and CO, influence the local rate of gasification in a fluidized bed steam reformer. The relative contributions of steam and carbon dioxide gasification may not be additive, and adding the rates of gasification by the individual reactions is complicated by the fact the gas composition adjusts towards water-gas shift reaction equilibrium.

Whitty, et al. [16] considered an environment in which the four major gases are present simultaneously, and performed a statistically designed series of thirty experiments with varying concentrations of H_2O, CO_2, H_2 and CO over the pressure range 1-30 atm. An empirical expression was developed to calculate the gasification rate as a function of the partial pressures of these gases:

$$rate\left(\times 10^4 \frac{\text{gram C}}{\text{gram C}_{\text{init}} \cdot \text{s}}\right) = 3.312 + 1.157 p_{H_2O} - 2.943 p_{H_2} - 3.869 p_{CO} + 0.6595\left(\frac{1}{p_{CO}}\right) \qquad \text{(Eq. 12)}$$

The model is set up so that any of the expressions above can be used to determine the local rate of carbon gasification.

3.1.2.5 Residue remaining after gasification

It is assumed that the final solid product is pure sodium carbonate, Na_2CO_3, plus residual unreacted organic carbon. The concentration of carbon depends on the efficiency of gasification. All sulfur and hydrogen are assumed to exit in the gas phase. The production rate of sodium carbonate is calculated based on the amount of incoming sodium (and potassium, which was treated in the same manner as sodium). The associated carbon and oxygen in the carbonate are then calculated. The amounts of carbon and oxygen released during gasification are determined by subtracting the amounts released during pyrolysis and exiting with the solid from the amount input with the black liquor solids.

3.1.3 Level-by-Level Calculations

Conditions at each level are calculated as follows:

Lower Levels (below liquor injection): At lower levels, variations in gas phase result from component release as the bed material undergoes heterogeneous gasification. At any particular level, the local gasification rate is calculated using the given kinetic expression as a function of gas composition and carbon concentration in the bed solids. The carbon released as a result of this reaction, as well as the appropriate quantity of hydrogen, sulfur and non-inorganic oxygen not released during pyrolysis (uniformly released during heterogeneous gasification as described above) is added to the gas phase. The equilibrium composition is calculated, as is the pressure at this point based on the given freeboard pressure, bed height and bed density. Since the temperature, pressure, volumetric gas flow rate, reactor geometry and bed void fraction are known, the superficial and actual gas velocities (after drying/devolatilization) are calculated.

Upper Levels (including and above liquor injection): There are several contributions to the gas phase at and above the point of liquor injection. As described above, drying of the liquor released water to the gas phase, with the degree of water release assumed to decrease exponentially. The rate of water release is input by the user (as time to 99% drying, from which the model back-calculates the appropriate exponential factor). The model uses actual gas velocity to track residence time for levels above the point of liquor injection and contributes the appropriate amount of water for a given level based on the drying rate, level residence time and time since liquor injection. A similar approach is taken for pyrolysis, except that individual species (C, H, O, S) are added to the gas phase based on the rate of pyrolysis (again, calculated based on the user's input of time to 99% pyrolysis), the time since the end of the drying phase (assuming that pyrolysis begins after drying is 99% complete) and the residence time of the level. The gas composition is updated and brought to equilibrium, then pressure, gas velocity and residence time are calculated. The final gas exiting the top of the bed (highest bed level) is taken to be the product gas from the reactor.

Freeboard: The geometry of the freeboard, including the expansion section at the top of the reactor, is input and the freeboard volume is calculated. The gas velocity and residence time in this section is subsequently calculated. It is assumed that no chemical reactions occur in the freeboard. It is also assumed that the loading of particles in the freeboard is low enough to not affect the overall gas velocity in that region.

The UofU model thus offers a relatively simple, portable tool useful for quick checks on approximate conditions in fluidized bed black liquor reformers. Comparison of predicted gas compositions to measured compositions from commercial units show good agreement. The model also provides a

tool for comparing one set of operating conditions against another, or to predict the influence of changes in operating parameters on overall performance of the system, particularly carbon conversion efficiency and corresponding carbon content in the bed material.

3.2 Advanced Model of Entire Reactor (REI Model)

Reaction Engineering International (REI) developed a "1½-D" three-phase countercurrent backmixing model based on an existing fluidized bed model that REI developed under a DOE-sponsored Vision 21 program. The model takes into account vertical temperature and concentration gradients and downflow near the wall. The model for a full-scale reactor, similar to that installed at Georgia-Pacific's Big Island mill, describes the fluid dynamics, chemistry and heat transfer in the reactor. Details of the system, such as interaction between bubbles and the pulsed heater tube bundles, are estimated from the correlations for heat exchange tubes in fluidized bed combustors.

The model assumes that the fluidized bed consists of three distinct phases:

- A particle-free bubble phase where the gas moves upward in plug flow
- A wake phase where the gas and the solids move upward with the bubbles
- A dense phase in which the solids move downward. The voidage in the dense phase is assumed to be the same as that in the wake phase and is assumed to be the voidage at minimum fluidization.

The bubble sizes are calculated allowing for bubble growth by coalescence with increasing height in the bed and decrease in bubble size as a result of bubble intersection with tubes. Different bubble sizes are calculated for the bubbles in the heater tube banks, the voids between the tube banks and the confining cylindrical walls, and the bubbles that flow through the open wedges between the overlap of tube banks. In the model the bubble sizes are averaged across a cylindrical cross section. Details of the model are given in the following sections.

3.2.1 Bubble hydrodynamics

3.2.1.1 Bubble size.

Bubble hydrodynamics in the tube banks differ from that outside the tube banks. With the presence of tube bundles, bubbles interact with the tubes, leading to bubble splitting thereby counteracting the tendency of bubble growth by coalescence. Thus, it is necessary to estimate bubble sizes using different approaches for the regions with and without tube bundles.

Regions below and above the tube bundles of the pulse combustors. For three-dimensional fluidized beds, the Darton correlation [20] has been widely used to predict bubble growth

$$d_b = 0.54(u_0 - u_{mf})^{2/5}(h + 4\sqrt{A_0})^{4/5} / g^{1/5} \qquad \text{(Eq. 13)}$$

where A_0 is the catchment area at the distributor plate. For the a full-scale system, this is calculated to be 0.0355 m^2.

Tube bundle regions of the pulse combustors. When bubbles strike tubes, the interaction between the tubes and bubbles may cause bubbles to break up. The size of the daughter bubbles can be predicted using a probabilistic approach developed by Hull et al. [21]. This approach may be summarized briefly as follows.

Assume that the parent bubble has a size, d_b, less than the horizontal spacing between the tubes, L. The probability of the parent bubble striking the tube and splitting to form daughter bubbles is $p = (d_t + d_b)/(d_t + L)$. The probability of the parent bubble slipping through the horizontal spacing between the tubes without splitting is then (1 − p). Assume also that on encounter with the tube, the parent bubble of size $d_b < L$ breaks up at most into two daughter bubbles of equal size. Therefore, for a three-dimensional bubble, $d_b^3 = 2d_{b,d}^3$, where $d_{b,d}$ is the size of the daughter bubbles. The average size of the bubbles leaving the tube banks, $d_{b,e}$, can now be estimated as $d_{b,e} = pd_{b,d} + (1-p)d_b$:

$$\frac{d_{b,e}}{d_b} = 1 - \left(1 - \frac{1}{\sqrt[3]{2}}\right)\left(\frac{d_t + d_b}{d_t + L}\right) \qquad \text{for} \quad d_b < L \tag{Eq. 14}$$

If $L \le d_b < d_t + 2L$, the probability of a bubble encountering two tubes simultaneously is $p = (d_b - L)/(d_t + L)$. It is assumed that such an encounter leads to the parent bubble breaking up into three daughter bubbles, one with diameter L, and the other two daughter bubbles being of equal size. Then, $d_{b,e}^3 = L^3 + 2d_{b,d}^3$ for three-dimensional bubbles. The probability of the parent bubble striking only one tube is (1 − p). In this case, the parent bubble splits into two bubbles with equal diameters, thus, $d_{b,e}^3 = 2d_{b,d}^3$. Using these relationships, the average daughter bubble size is given by

$$d_{b,e} = \frac{d_b}{\sqrt[3]{2}}\left(\frac{d_t + 2L - d_b}{d_t + L}\right) + \frac{L + 2\sqrt[3]{\frac{d_b^3 - L^3}{2}}}{3}\left(\frac{d_b - L}{d_t + L}\right) \tag{Eq. 15}$$

For $d_t + 2L \le d_b < 2d_t + 3L$, this approach yields

$$d_{b,e} = \frac{L + 2\sqrt[3]{\frac{d_b^3 - L^3}{2}}}{3}\left(\frac{2d_t + 3L - d_b}{d_t + L}\right) + \frac{L + \sqrt[3]{\frac{d_b^3 - 2L^3}{2}}}{2}\left(\frac{d_b - d_t - 2L}{d_t + L}\right) \tag{Eq. 16}$$

Similarly, for $d_t + 2L \le d_b < 2d_t + 3L$, the daughter bubble size is

$$d_{b,e} = \frac{L + \sqrt[3]{\frac{d_b^3 - 2L^3}{2}}}{2}\left(\frac{3d_t + 4L - d_b}{d_t + L}\right) + \frac{3L + 2\sqrt[3]{\frac{d_b^3 - 3L^3}{2}}}{5}\left(\frac{d_b - 2d_t - 3L}{d_t + L}\right) \tag{Eq. 17}$$

For $d_{b,e} \ge 2d_t + 3L$, equations similar to Equation 17 can be derived. This model has been validated through comparison of model predictions with measurements taken from a thin fluidized bed using a CCD video camera. The applicability of the model to three-dimensional bubbles was also examined. Yates and co-workers [22,23] reported measurements that relate the parent bubble size with the

average size of daughter bubbles resulting from encounter with horizontal rows of tubes. Calculations using the above model compared favorably with their experimental data [21].

3.2.1.2 Bubble Rise Velocity

The most frequently adopted two-phase theory shows that bubble rise velocity is the sum of the excess gas velocity and the isolated bubble rise velocity [24]:

$$u_b = u_0 - u_{mf} + 0.71\sqrt{gd_b} \quad \text{(Eq. 18)}$$

The excess gas velocity represents the visible bubble flow according to the two-phase theory. Several experimental investigations, however, indicate that the visible bubble flow is somewhat smaller than that predicted by the two-phase theory [25,26]. For simplicity, Equation 18 is used in this work.

3.2.1.3 Bubble Wake Fraction

Bubble wake fraction varies in a wide range as the operating conditions change. Measurements suggest that wake fraction depends on both particle and bubble sizes [27]. The scatter in the existing experimental data, however, makes it difficult to use an unequivocal correlation for bubble wake fraction. In the modeling of fluidized beds, it is generally assumed that wake fraction is constant [28]; in this work, that wake fraction is assumed to be 0.30.

3.2.1.4 *Bubble Fraction*

Based on the assumption that the fluidized bed consists of the bubble phase, wake and dense phases, the overall gas balance can be written as

$$u_0 = f_b u_b + f_b f_w \varepsilon_{mf} u_b + [1 - f_b(1 + f_w)]\varepsilon_{mf} u_{g,d} \quad \text{(Eq. 19)}$$

where u_0 is the local superficial gas velocity and $u_{g,d}$ is the gas velocity in the dense phase. Since there is no net particle flow in the vertical direction, particles moving upward in the wake phase must be balanced by the downward motion of particles in the dense phase, hence,

$$-f_b u_b f_w = [1 - f_b(1 + f_w)]u_{p,d} \quad \text{(Eq. 20)}$$

where $u_{p,d}$ is the particle velocity in the dense phase. The slip velocity between the gas and the particles in the dense phase is assumed to be the ratio of the minimum fluidization velocity to the bed voidage at minimum fluidization. Hence, the absolute gas velocity in the dense phase is given by

$$u_{g,d} = u_{p,d} + u_{mf} / \varepsilon_{mf} \quad \text{(Eq. 21)}$$

Equations 19 to 21 can then be employed to determine bubble fraction as a function of bed height. Note that when the superficial gas velocity is sufficiently high, $u_{g,d}$ may become negative indicating gas in the dense phase moving downward.

3.2.2 Overall Gas Balances

Since the total gas mass flow rate may change along the bed height as drying, devolatilization and gasification of black liquor proceed, the superficial gas velocity also changes; it can be written as

$$u_0 = \frac{m_g}{A\rho_g}; \quad m_{g,j} = m_{g,j-1} + \sum_{i=1}^{n} fR_i M_i Ah \qquad \text{(Eq. 22)}$$

where j is the computational cell index starting from the bottom of the bed; f is the phase fraction and R_i, M_i, and h are gas species formation rate (kmol/m^{3}s), species molecular weight and the cell height, respectively.

3.2.3 Species Mass Balances

For steady state conditions, species mass balance equations in different phases can be written as follows:

3.2.3.1 *Bubble phase*

$$\frac{d(u_b f_b A C_{i,b})}{dz} - (\lambda_1 C_{i,b} + \lambda_2 C_{i,w}) \frac{d(u_b f_b A)}{dz} + f_b A K_{bw} (C_{i,b} - C_{i,w}) + A f_b R_{i,b} = 0 \qquad \text{(Eq. 23)}$$

where $C_{i,b}$ denotes the concentration of species i. Subscripts b, w represent the bubble and wake phases, respectively. A is the cross-sectional area of the bed; it changes along the bed height in the regions of the tube bundles and the freeboard. The first term in the above equation is the convection due to the finite velocity of the bubble phase. The second term represents the cross-flow that accounts for the variation of bubble properties along the bed height above the gas distributor. λ_1 and λ_2 are constant; if $d(u_b f_b A)/dz \geq 0$, $\lambda_1 = 0$ and $\lambda_2 = 1$; if $d(u_b f_b A)/dz < 0$, $\lambda_1 = 1$ and $\lambda_2 = 0$. The third term is the exchange of gas between the bubble phase and the wake phase. The last term represents the consumption rate of species i in the bubble phase.

3.2.3.2 *Wake phase*

Similarly, for the wake phase, the gas species mass balance can be written as

$$\begin{aligned} &\frac{d(u_b f_b f_w A \varepsilon_{mf} C_{i,w})}{dz} + (\lambda_1 C_{i,b} + \lambda_2 C_{i,w}) \frac{d(u_b f_b A)}{dz} \\ &+ (\lambda_3 C_{i,d} + \lambda_4 C_{i,w}) \frac{d\{[1 - f_b(1+f_w)] A \varepsilon_{mf} u_{g,d}\}}{dz} + f_b K_{bw} A (C_{i,w} - C_{i,b}) \\ &+ f_b K_{wd} A (C_{i,w} - C_{i,d}) + f_b f_w \varepsilon_{mf} A R_{i,w,g} + f_b f_w (1 - \varepsilon_{mf}) A R_{i,w,p} = 0 \end{aligned} \qquad \text{(Eq. 24)}$$

The first term in the above equation is the convection term. The second and third terms are the cross-flow. The two parameters λ_3 and λ_4 are constant; if $d\{[1 - f_b(1+f_w)] A \varepsilon_{mf} u_{g,d}\}/dz \geq 0$, $\lambda_3 = 0$ and $\lambda_4 = 1$; if $d\{[1 - f_b(1+f_w)] A \varepsilon_{mf} u_{g,d}\}/dz < 0$, $\lambda_3 = 1$ and $\lambda_4 = 0$. The fourth and fifth terms are the exchange of gas between the bubble and wake phases and between the wake and dense phases, respectively. The last two terms represent species consumption rates due to homogeneous and heterogeneous reactions, respectively.

3.2.3.3 *Dense phase*

For the dense phase, the mass balance equation can be derived as

$$\frac{d\{[1-f_b(1+f_w)]A\varepsilon_{mf}u_{g,d}C_{i,d}\}}{dz}-(\lambda_3 C_{i,d}+\lambda_4 C_{i,w})\frac{d\{[1-f_b(1+f_w)]A\varepsilon_{mf}u_{g,d}\}}{dz} + f_b K_{wd}A(C_{i,d}-C_{i,w})+[1-f_b(1+f_w)]A\varepsilon_{mf}R_{i,d,g}+\{1-f_b(1+f_w)\}A(1-\varepsilon_{mf})R_{i,d,p}=0 \quad \text{(Eq. 25)}$$

The terms in the above equation represent convection, cross-flow, exchange of gas between the dense and wake phases, species consumption rates due to homogeneous and heterogeneous reactions, respectively.

3.2.3.4 *Freeboard region*

In the freeboard, homogeneous reactions, especially the water-gas shift reaction and the methane-steam reforming reaction, continue. The mass balance equation must account for these reactions. The species mass balance equation is

$$u_0\frac{dC_{i,f}}{dz}+R_{i,f}=0 \quad \text{(Eq. 26)}$$

3.2.4 Exchange Coefficients

The mass exchange coefficients have been adopted from Kunii and Levenspiel [6]. The mass transfer coefficient between the bubble phase and the wake phase is

$$K_{bw}=5.85(D_g^{0.5}g^{0.25}/d_b^{1.25})+4.5u_{mf}/d_b \quad \text{(Eq. 27)}$$

where D_g is the gas diffusivity and d_b is the bubble diameter. The mass exchange coefficient between the wake and emulsion phases is taken as

$$K_{wd}=6.77(0.71\sqrt{gd_b}D_g\varepsilon_{mf}/d_b^3)^{1/2} \quad \text{(Eq. 28)}$$

3.2.5 Energy Balance

Assume the gas in the bubble phase, the wake phase and the dense phase has the same temperature. An energy balance for the gas phase can be written as

$$\begin{aligned}&C_{pg}\rho_g u_0\frac{dT_g}{dz}+\frac{6h_w}{d_p}f_b f_w(1-\varepsilon_{mf})(T_g-T_{p,w})+\frac{6h_d}{d_p}[1-f_b(1+f_w)](1-\varepsilon_{mf})(T_g-T_{p,d})\\&+f_b\sum_{i=1}^{n}(-\Delta H_{i,b})R_{i,b}+f_b f_w\varepsilon_{mf}\sum_{i=1}^{n}(-\Delta H_{i,w,g})R_{i,w,g}\\&+[1-f_b(1+f_w)]\varepsilon_{mf}\sum_{i=1}^{n}(-\Delta H_{i,d,g})R_{i,d,g}+Q_t=0\end{aligned} \quad \text{(Eq. 29)}$$

where d_p is the particle diameter; h_w and h_d are the heat transfer coefficients between the gas and the particles in the wake phase, and between the gas and the particles in the dense phase, respectively,

and can be readily estimated using correlations given in Kunii and Levenspiel [6]. The first term in the above equation arises due to particle motion. The second term represents the convective heat transfer between the gas in the wake phase and the solids in the wake phase. Similarly, the third term accounts for the convective transfer between the gas in the dense phase and the solids in the dense phase. The fourth, fifth and sixth terms represent the gas phase reactions in the bubble phase, the wake phase and the dense phase, respectively. The last term is the heat transferred to the bed from the pulse combustors. Similarly, for the particles in the wake phase, the energy balance equation can be derived as

$$\begin{aligned} &C_{pp}\rho_p(1-\varepsilon_{mf})\frac{d(u_b f_b f_w A T_{p,w})}{dz}+C_{pp}\rho_p f_b f_w(1-\varepsilon_{mf})AK_{wd,p}(T_{p,w}-T_{p,d}) \\ &-C_{pp}\rho_p(1-\varepsilon_{mf})(\lambda_5 T_{p,w}+\lambda_6 T_{p,d})\frac{d(u_b f_b f_w A)}{dz} \\ &+f_b f_w A(1-\varepsilon_{mf})\left\{\frac{6h_w}{d_p}(T_{p,w}-T_g)+\sum_{i=1}^{n}(-\Delta H_{i,w,s})R_{i,w,p}\right\}+AQ_{vap}=0 \end{aligned} \qquad \text{(Eq. 30)}$$

where Q_{vap} is the energy required to vaporize the water in the black liquor. The second term accounts for the heat transfer due to the solids exchange between the wake phase and the dense phase. The fourth term represents heat exchange between the solids and the gas in the wake phase and the energy consumption due to the heterogeneous reactions in the wake phase. Other terms are similar to those in the previous equations. A similar energy balance equation can be written for the particles in the dense phase,

$$\begin{aligned} &C_{pp}\rho_p\frac{d\{u_{p,d}[1-f_b(1+f_w)]AT_{p,d}\}}{dz}+C_{pp}\rho_p f_b f_w AK_{wd,p}(T_{p,d}-T_{p,w}) \\ &+C_{pp}\rho_p(\lambda_5 T_{p,w}+\lambda_6 T_{p,d})\frac{d(u_b f_b f_w A)}{dz} \\ &+[1-f_b(1+f_w)]A\left\{\frac{6h_d}{d_p}(T_{p,d}-T_g)+\sum_{i=1}^{n}(-\Delta H_{i,d,p})R_{i,d,p}\right\}=0 \end{aligned} \qquad \text{(Eq. 31)}$$

Assume that there is not heat exchange between the gas phase and the reactor wall in the freeboard, the energy balance for the freeboard is then given by

$$u_0 C_{pg}\rho_g\frac{dT_g}{dz}+\sum_{i=1}^{n}(-\Delta H_{i,f})R_{i,f}=0 \qquad \text{(Eq. 32)}$$

The second term represents heat of reactions due to the homogeneous reactions.

3.2.6 Boundary Conditions

The boundary conditions for the energy balance equations are: at the bottom of the bed,

$$T_g=T_{g,inlet};\ T_{p,w}=\frac{m_p T_{p0}-[1-f_b(1+f_w)](1-\varepsilon_{mf})u_{p,d}A\rho_p T_{p,d}}{f_b f_w u_b(1-\varepsilon_{mf})A\rho_p} \qquad \text{at } z=0 \qquad \text{(Eq. 33)}$$

at the top surface of the fluidized bed,

$$T_{p,d} = T_{p,w} \qquad \text{at } z = H_t \qquad \text{(Eq. 34)}$$

The boundary conditions for the mass balance equations depend on the direction of the gas flow in the dense phase. If $u_{g,e} > 0$ at $z = 0$, then, at the gas distributor,

$$C_{i,b} = C_{i,w} = C_{i,d} = C_{i,inlet} \qquad \text{at } z = 0 \qquad \text{(Eq. 35)}$$

However, if $u_{g,d} < 0$ at $z = 0$, then, at the bottom of the bed,

$$C_{i,b} = C_{i,inlet};\ C_{i,w} = \frac{(u_0 - f_b u_b)C_{i,inlet} - [1 - f_b(1 + f_w)]\varepsilon_{mf} u_{g,e} C_{i,e}}{f_b f_w \varepsilon_{mf} u_b} \qquad \text{at } z = 0 \qquad \text{(Eq. 36)}$$

and at the top of the bed,

$$C_{i,d} = C_{i,w} \qquad \text{at } z = H_t \qquad \text{(Eq. 37)}$$

3.2.7 Drying and Devolatilization of Black Liquor

Experimental data show that drying and devolatilization of black liquor are heat transfer controlled processes under recovery furnace conditions [29]. Experiments and model simulations also indicate that, under these conditions, drying and devolatilization take place simultaneously as black liquor droplets are heated [30,31]. However, under the conditions considered here, it is expected that drying and devolatilization occur consecutively. It is assumed that devolatilization takes place only after the droplets are completely dry. The energy balance for a single black liquor droplet can be written as

$$C_{pp}\rho_p \frac{dT_p}{dt} = \frac{6h_w}{d_p}(T_g - T_p) - m_{vap}\lambda_{vap} \qquad \text{(Eq. 38)}$$

where m_{vap} is the volumetric evaporation rate (kg/m^{3}s) of black liquor water and λ_{vap} is the latent heat of evaporation. If drying is a heat transfer controlled process, black liquor droplets can then be assumed to be at pseudo-steady state, thus,

$$m_{vap} = \frac{6h_w}{d_p \lambda_{vap}}(T_g - T_p) \qquad \text{(Eq. 39)}$$

where T_g is the local gas temperature. Droplet temperature, T_p, can be assumed to be the temperature of the boiling point of water at the local pressure. Drying begins once black liquor enters the fluidized bed and is complete when all the water in black liquor vaporizes.

For simplicity, it is assumed that devolatilization time is the same as that of drying. The fraction of each component in black liquor released into the gas phase depends on the environmental temperature to which the black liquor subjects. Reported correlations [7,8] are used to determine C, H, O and S

release rates. Volatiles are assumed to consist of CH_4, CO, H_2O and H_2S. The amount of each gas species released can be determined from an elemental mass balance.

3.2.8 Gasification Kinetics

Global reaction mechanisms are used to describe black liquor gasification. The reactions considered in the model include:

Steam gasification (Li and van Heiningen, 1991 [12])

$$C + H_2O = CO + H_2 \qquad \Delta H = +1.3556\times10^{8}\ \text{J/kmol}$$

$$\text{Rate} = 2.56\times10^{9}\exp\left(-\frac{25300}{T_p}\right)\frac{p_{H_2O}}{p_{H_2O}+1.42p_{H2}}C_c \qquad \text{kmol/m}^3\text{s} \qquad \text{(Eq. 40)}$$

CO_2 gasification (Li and van Heiningen, 1990 [11])

$$C + CO_2 = 2CO \qquad \Delta H = +1.7174\times10^{8}\ \text{J/kmol}$$

$$\text{Rate} = 6.30\times10^{10}\exp\left(-\frac{30070}{T_p}\right)\frac{p_{CO_2}}{p_{CO_2}+3.4p_{CO}}C_c \qquad \text{kmol/m}^3\text{s} \qquad \text{(Eq. 41)}$$

Methane-steam reforming reaction (Jones and Lindstedt, 1988 [32])

$$CH_4 + H_2O = CO + 3H_2 \qquad \Delta H = +2.0616\times10^{8}\ \text{J/kmol}$$

$$\text{Rate} = 3.00\times10^{8}\exp\left(-\frac{15105}{T_g}\right)C_{CH_4}C_{H_2O} \qquad \text{kmol/m}^3\text{s} \qquad \text{(Eq. 42)}$$

Kinetics for other reactions have been adopted from MFIX (Guenther et al. [33]), which is a modified version of the reaction scheme used in Syamlal and Bissett [34], and is based on gasification kinetics proposed by Wen et al. [35].

Methanation (Wen et al. [35], Syamlal and Bissett [34])

$$C + 2H_2 = CH_4 \qquad \Delta H = -7.485\times10^{7}\ \text{J/kmol}$$

$$\text{Rate} = 9.87\times10^{-6}\exp\left(-7.087-\frac{8078}{T_p}\right)(p_{H_2}-p^{*}_{H_2})C_c \qquad \text{kmol/m}^3\text{s} \qquad \text{(Eq. 43)}$$

where

$$p^{*}_{H_2} = \sqrt{\frac{1.01325\times10^{5}\,p_{CH_4}}{\exp(-13.43+10999/T_p)}} \qquad \text{(Eq. 44)}$$

Carbon combustion (Wen et al. [35], Syamlal and Bissett [34])

$$C + \tfrac{1}{2}O_2 = CO \qquad \Delta H = -1.1129\times10^{8}\ \mathrm{J/kmol}$$

$$\mathrm{Rate} = \frac{5.9215\times10^{-4}\ p_{O_2}}{d_p\left(\frac{1}{k_f}+\frac{1}{k_r}\right)} \qquad \mathrm{kmol/m^3 s} \qquad \text{(Eq. 45)}$$

where the film resistance is given by

$$k_f = \frac{100 D_{O_2}\ \mathrm{Sh}}{d_p\ R_{O_2}\ T_f} \qquad \text{(Eq. 46)}$$

where R_{O_2} is the gas constant for oxygen, $R_{O2} = 0.25982\ \mathrm{m^3\cdot Pa/g\cdot K}$; T_f is the film temperature and can be calculated as

$$T_f = (T_g + T_p)/2 \qquad \text{(Eq. 47)}$$

The Sherwood number is given by (Gunn [36])

$$\mathrm{Sh} = (7 - 10\varepsilon_g + 5\varepsilon_g^2)\ (1 + 0.7\,\mathrm{Re}^{0.2}\mathrm{Sc}^{1/3}) + (1.33 - 2.4\varepsilon_g + 1.2\varepsilon_g^2)\,\mathrm{Re}^{0.7}\mathrm{Sc}^{1/3} \qquad \text{(Eq. 48)}$$

The surface reaction rate is given by (Desai and Wen [37])

$$k_r = 860\ \exp\left(-\frac{13587}{T_p}\right) \qquad \mathrm{g/Pa\cdot m^2\cdot s} \qquad \text{(Eq. 49)}$$

CO combustion (Westbrook and Dryer [38])

$$CO + \tfrac{1}{2}O_2 = CO_2 \qquad \Delta H = -2.8303\times10^{8}\ \mathrm{J/kmol}$$

$$\mathrm{Rate} = 2.238\times10^{12}\ \exp\left(\frac{-20130}{T_g}\right) C_{O_2}^{0.25} C_{CO} C_{H_2O}^{0.5} \qquad \mathrm{kmol/m^3 s} \qquad \text{(Eq. 50)}$$

CH_4 combustion (Westbrook and Dryer [38])

$$CH_4 + 2O_2 = CO_2 + 2H_2O \qquad \Delta H = -8.005\times10^{8}\ \mathrm{J/kmol}$$

$$\mathrm{Rate} = 2.12\times10^{11}\ \exp\left(\frac{-24356}{T_g}\right) C_{O_2}^{1.3} C_{CH_4}^{0.2} \qquad \mathrm{kmol/m^3 s} \qquad \text{(Eq. 51)}$$

H_2 combustion (Peters [39])

$$H_2 + \tfrac{1}{2}O_2 = H_2O \qquad \Delta H = -2.4686\times10^{8}\ \text{J/kmol}$$

$$\text{Rate} = 1.08\times10^{3}\ \exp\left(\frac{-15100}{T_g}\right)C_{O_2}C_{H_2} \qquad \text{kmol/m}^3\text{s} \qquad \text{(Eq. 52)}$$

Water-gas shift reaction (Wen et al. [35])

$$CO + H_2O = H_2 + CO_2 \qquad \Delta H = -4.115\times10^{7}\ \text{J/kmol}$$

$$\text{Rate} = 1.956\times10^{6} f_3 \left(\frac{P}{1.01325\times10^{5}}\right)^{\left(0.5-\frac{P}{250\times1.01325\times10^{5}}\right)} \exp\left(\frac{-13969}{T_g}\right)\left(C_{CO}C_{H_2O} - C_{CO_2}C_{H_2}/K_3\right) \qquad \text{kmol/m}^3\text{s} \qquad \text{(Eq. 53)}$$

where

$$f_3 = 10^{-3}\exp(-8.91 + 5553/T_g)C_{ash} \qquad \text{(Eq. 54)}$$

and the equilibrium constant is given by

$$K_3 = \exp(-3.63061 + 3955.71/T_g) \qquad \text{(Eq. 55)}$$

The reactions involving oxygen are insignificant since for the system considered here, there is not oxygen in the inlet streams or oxygen formed in the bed. However, these reactions are included so that the computer code developed may also be used for combustion of black liquor. The above mechanisms only account for gasification and combustion of carbon in black liquor. Since black liquor contains significant amount of oxygen and considerable amount of hydrogen, it is important to also consider the release of elemental oxygen and hydrogen from black liquor during gasification. It is assumed that ash consists of sodium carbonate and potassium carbonate. The release rates of elemental oxygen and hydrogen are assumed to be proportional to the carbon gasification/combustion rate and the ratio of the amount of elemental oxygen or hydrogen available for release to the amount of carbon available for gasification. Elemental oxygen and elemental hydrogen are assumed to release as water vapor and hydrogen or carbon monoxide depending on the relative release rates of elemental oxygen and hydrogen.

3.3 Heat Transfer Model for Heater Bundles

A computational model to predict heater bundle tube surface temperatures and particle temperatures in the tube bundle region was developed by Reaction Engineering International. The hydrodynamics for the model are MFIX simulation results, provided by the Department of Energy's National Energy Technology Laboratory through a collaborative effort. REI used these models to calculate the heat

transfer and temperatures in the heater bundles, either in a full-scale system, in the University of Utah system, or in the cold-flow model. The heat transfer model consists of three components.

Heat transfer from the combustion gases to the heater tubes. The energy balance for a single tube at a certain axial location (cell i) of the tube can be written as

$$q_{g2t,i} = A_i h_{g2t} (T_g - T_{in}) \quad \text{(Eq. 56)}$$

where A_i is the inner surface area of the tube for cell i and T_{in} is the local inner surface temperature of the tube; $q_{g2t,i}$ is the heat transfer for the particular tube cell. The heat transfer coefficient from the pulse combustor gases to the heater tube has been found to be significantly enhanced with the use of resonance tubes. The enhancement can be explained using the quasi-steady-state theory [40]. Measurements of the heat transfer in the MTCI PulseEnhanced combustor indicate that the quasi-steady-state theory correlates well with the measured data [41], but attempts to duplicate the results in the report raise some questions. Further work by Arpaci et al. [42] takes into account the effect of frequency of the velocity oscillations and shows that the heat transfer coefficient can be estimated using

$$Nu = 0.028\overline{Re}^{3/4}\left[1 + 0.21\frac{U_0}{\overline{U}}\left(1 + 7.36\frac{(\omega - 46)D}{\overline{U}}\right)\right]^{3/4} \quad \text{(Eq. 57)}$$

where Nu denotes the Nusselt number based on the hydraulic diameter D of the heater tube, $\overline{Re}$ is the Reynolds number based on the mean velocity $\overline{U}$ and U_0 is the amplitude of velocity oscillations with a frequency of ω. Equation 57 has been found to be in very good agreement with experimental data (Arpaci et al., 1993). For the present simulation conditions, calculation using Equation 57 indicates a heat transfer coefficient of 63 W/m^2·K, much lower than 170 W/ m^2·K reported in the design qualification test of the pulse combustor [41]; the latter is used in the simulation reported here.

Gas temperature inside the tube changes along the tube length. Assuming that the gas inside the tube is in plug flow, the energy balance for the gas can be derived as

$$\overline{U}\rho_g C_{pg}\frac{dT_g}{dL} + \frac{4h_{g2t}}{d_t}\left(T_g - T_{in}\right) = 0 \quad \text{(Eq. 58)}$$

where d_t is the tube inner diameter and L is the coordinate along the length of the tube. Boundary condition for the preceding equation is $T_g = T_{g,in}$ at L = 0. $T_{g,in}$ can be assumed to be the adiabatic flame temperature of the pulse combustor.

Total heat transfer from the combustion gases to a single tube is given by

$$Q_{g2t} = \sum_{i=1}^{n} q_{g2t,i} \quad \text{(Eq. 59)}$$

where n is the number of cells along the tube.

Heat transfer distribution along the tubes. Conduction heat transfer from the inner surface to the outer surface of the tube metal or glass tube can be calculated for the pulsed combustion conditions used in the full-scale unit or for the applicable heater configuration of the University of Utah unit. The temperature profile on the outer surface of the heater tubes may then be calculated. The energy balance can be written as

$$\frac{1}{r}\frac{d}{dr}\left(-r\frac{dT}{dr}\right)=0 \qquad \text{(Eq. 60)}$$

with a boundary condition of $T = T_{in}$ at $r = r_{in}$ and $T = T_{out}$ at $r = r_{out}$. Integration of the above equation leads to

$$T=\frac{T_{out}-T_{in}}{\ln\left(\frac{r_{out}}{r_{in}}\right)}\ln\left(\frac{r}{r_{in}}\right)+T_{in} \qquad \text{(Eq. 61)}$$

Heat transfer from the inner surface to the outer surface for cell i of length ΔL is given by

$$q_{i2o,i}=\frac{2\pi k_t \Delta L(T_{in}-T_{out})}{\ln\left(\frac{r_{out}}{r_{in}}\right)} \qquad \text{(Eq. 62)}$$

In the above equation, k_t is thermal conductivity of the tube metal. Total conduction heat transfer for a single tube is

$$Q_{i2o}=\sum_{i=1}^{n} q_{i2o,i} \qquad \text{(Eq. 63)}$$

Heat transfer from the tubes to the dense phase. Heat transfer between the bed solids and submerged horizontal tubes has been studied by many investigators. Many empirical correlations in the form of power relationships in terms of Re, Nu and Pr numbers have been developed. Glicksman et al. [43] compared the predictions of the heat transfer coefficients from six correlations with a large common experimental data base and found that the resulting RMS ranged from 38.5% to 94.0%. The possible reason for the poor agreement is that the original correlations were developed from a limited data base, with narrow ranges of pertinent variables. It was found that the modified Vreedenberg correlation, developed by Andeen and Glicksman [44], was relatively more successful on an overall basis. The modified Vreedenberg correlation can be written as

$$\frac{h_{t2p}D_t}{k_g}=900(1-\varepsilon)\left(\frac{uD_t\rho_p}{\mu}\frac{\mu^2}{d_p^3\rho_p^2 g}\right)^{0.326}\left(\frac{C_{pg}\mu}{k_g}\right)^{0.3} \qquad \text{(Eq. 64)}$$

where h_{t2p} = heat transfer coefficient, $W/(m^2\cdot K)$
C_{pg} = specific heat of gas, $J/(kg\cdot K)$

d_p = particle size, m
D_t = tube outer diameter, m
g = acceleration of gravity, m/s^2
k_g = thermal conductivity of gas, W/(m·K)
u = superficial gas velocity, m/s
ε = bed voidage
μ = gas viscosity, Pa·s
ρ_p = particle density, kg/m^3
ρ_g = gas density, kg/m^3

The above correlation is applicable for particles with mean diameters less than 1 mm. Since the modified Vreedenberg correlation excludes terms which account for fluid inertia effects, an upper limit on its applicability is that fluid inertia terms are of the same order of magnitude as viscous terms. This limit can be approximated as

$$\frac{u d_p \rho_p}{\mu} < 10 \qquad \text{(Eq. 65)}$$

Bed void fraction inside the tube bundles is provided through MFIX simulations conducted at NETL. The temperature of the bed solids is calculated by coupling the heat transfer through the tube walls with a balance on the solids flowing through the tube bundle. The particle energy balance can be written as

$$\frac{\partial}{\partial x}\left(m_x C_{pp} T_p\right) + \frac{\partial}{\partial y}\left(m_y C_{pp} T_p\right) + \frac{\partial}{\partial z}\left(m_z C_{pp} T_p\right) = h_{t2p} A_t'''\left(T_{out} - T_p\right) - (1-\varepsilon)\sum\left(-\Delta H_{i,p}\right) R_{i,p} \qquad \text{(Eq. 66)}$$

where
A_t''' = tube outer surface area per unit bed volume, m^2/m^3
C_{pp} = specific heat of solids, J/(kg·K)
m = particle mass flux, $kg/(m^2 \cdot s)$
T_p = particle temperature, K
$-\Delta H_{i,p}$ = heat of heterogeneous reaction, J/kmol
$R_{i,p}$ = heterogeneous reaction rate, $kmol/m^3 \cdot s$

Assume C_{pp} is constant. Then, under steady state conditions, the above equation can be simplified as

$$m_x C_{pp} \frac{\partial T_p}{\partial x} + m_y C_{pp} \frac{\partial T_p}{\partial y} + m_z C_{pp} \frac{\partial T_p}{\partial z} = h_{t2p} A_t'''\left(T_{out} - T_p\right) - (1-\varepsilon)\sum\left(-\Delta H_{i,p}\right) R_{i,p} \qquad \text{(Eq. 67)}$$

Particle mass flux is obtained from MFIX simulation results. Boundary conditions for the above equation can be determined from the REI 1½-D described in Section 3.2; heat transfer to the gasifier wall is assumed to be negligible. Equations 58, 59, 63 and 67 have to be solved simultaneously.

Iteration is necessary and is performed until all energy balances are satisfied. Note that the following equation also holds

$$NQ_{g2t} = NQ_{i2o} = h_{t2p} A_t''' V(T_{out,avg} - T_{p,avg}) \quad \text{(Eq. 68)}$$

where N is the total number of the heat tubes and V is the bed volume in each pulse combustor section. $T_{out,avg}$ and $T_{p,avg}$ are the average temperature of the outer surface of the heater tubes and average particle temperature, respectively, in the pulse combustor sections.

3.4 Particle Size Development Model

A computational model was developed to track changes in particle size distribution over time as the various mechanisms described above take place. The model begins with a given population of particles and a specific particle size distribution. The user then provides input regarding the contribution of each mechanism. Individual mechanisms can be "turned off" or set to contribute significantly to particle size development.

3.4.1 Mechanism handlers

Particles in a fluidized bed black liquor reformer can grow and shrink due to various mechanisms, which are described in detail in Section 4.1.1.4 of this report. The approaches by which these mechanisms are treated in the model are described below.

Coating. The model takes as input the total size (mass) of the fluidized bed, the black liquor solids feed rate, the fraction of solids that forms inorganic (non-gas phase) material and the density of the particles. It is assumed that the bed is mixed well enough that over time all particles receive the same thickness of coating. The coating thickness is determined by calculating the total surface area of all particles being tracked and distributing the volume of liquor inorganics introduced into the bed over a given period of time evenly over that surface area.

Agglomeration. No distinction is made between sintering, melt-induced agglomeration or liquor-induced agglomeration. The user inputs the fraction of particles that undergo agglomeration per hour and the minimum and maximum number of particles per agglomerate. During each computational cycle (1 hour), a sub-population of particles corresponding to that fraction are randomly selected. Each particle in that sub-population is added to one or more other particles from the sub-population. The number of particles in a particular agglomerate is random, but is between the minimum and maximum limits set by the user. The new particle that forms is assumed to be spherical with a volume equal to the sum of the volumes of the particles that formed it.

Attrition. The user inputs the fraction of the total particle volume (without void spaces between particles) that is attritted per cycle. The size limits of the asperities that result are also input. Attrition is assumed to affect all particles uniformly, proportional to the available surface area of the particle. During each computational cycle, the diameter of each particle in the population being tracked is reduced by the same amount, such that the total volume attritted matches the fraction input. This volume attritted is then distributed among new ("child") particles randomly sized within the limits set by the user. No distinction is made between mechanical and reaction-induced attrition.

Fracturing. The user inputs the percentage of particles that are fractured per hour, plus a minimum and maximum number of child particles produced from each fractured particle. On each computational cycle, the program randomly chooses the given fraction of particles from the population being tracked. For each, a number of equally-sized child particles, randomly chosen between the input minimum and maximum, are created. The sum of the volumes of the child particles equals the volume of the parent particle. No distinction is made between mechanical and reaction-induced fracturing.

Carryover. The model removes the smallest fraction of particles from the population. The user inputs two limits, the size below which all particles are assumed to be lost due to carryover and the size above which all particles are assumed to remain in the bed. On each computational cycle, the program considers each particle in the population. If a given particle falls below the upper size limit—that is, if there is a chance that the particle may be elutriated from the bed—the program assigns a probability to its being carried over. Particles sized below the lower input limit are always removed. Between the lower and upper limits, the odds that a particle will be removed during that computational cycle is determined by linear interpolation. For example, if the lower limit is 10 microns and the upper limit is 60 microns, a 5 micron particle will be elutriated, a 65 micron particle will remain in the bed and a 30 micron particle has a 60% chance of being elutriated: (60-30)/(60-10) = 60%.

Bed drain. In order to maintain the total bed volume when black liquor is being fed, a random sampling of particles is removed from the population during each computational cycle. The mass of particles removed in this manner equals the mass of input inorganic material minus the mass lost due to carryover.

3.4.2 Computational procedure

The model is programmed in Microsoft Excel Visual Basic for Applications (VBA). The user interface is shown in Figure 28. Initially, the user inputs the number of particles in the population to be tracked, its distribution type, mechanism-specific values and the total number of cycles to be simulated. A computational object is created for each particle and contains information such as particle diameter, volume, mass and surface area. A separate subroutine exists for each mechanism described above. One computational cycle typically constitutes one hour of simulated bed operation. The program runs through each mechanism subroutine, adding, subtracting, growing and shrinking the particles in the population accordingly. The order of subroutine calls alternates between having the growth mechanisms run first, then having the shrinkage mechanisms run, and vice-versa. At the end of each cycle a "clean up" routine is called to remove objects associated with particles that have disappeared due to agglomeration with other particles or elutriation from the bed. A data file of particle size distributions can be output for each cycle, although this slows computing time significantly. At a minimum, the size distributions 10%, 20%, 50% and 100% of the way through the specified time are logged.

The more particles tracked, the better the resolution of the resulting particle size distributions. On a 1.8 GHz Pentium M machine, tracking 50,000 particles requires about 2 seconds per cycle (simulated hour) but gives reasonable resolution for scoping of conditions. It is possible to track more than one million particles, which corresponds to about 20 grams of particles having a mean initial diameter of 250 microns. This provides excellent resolution and reproducibility, but such simulations generally need to run overnight.

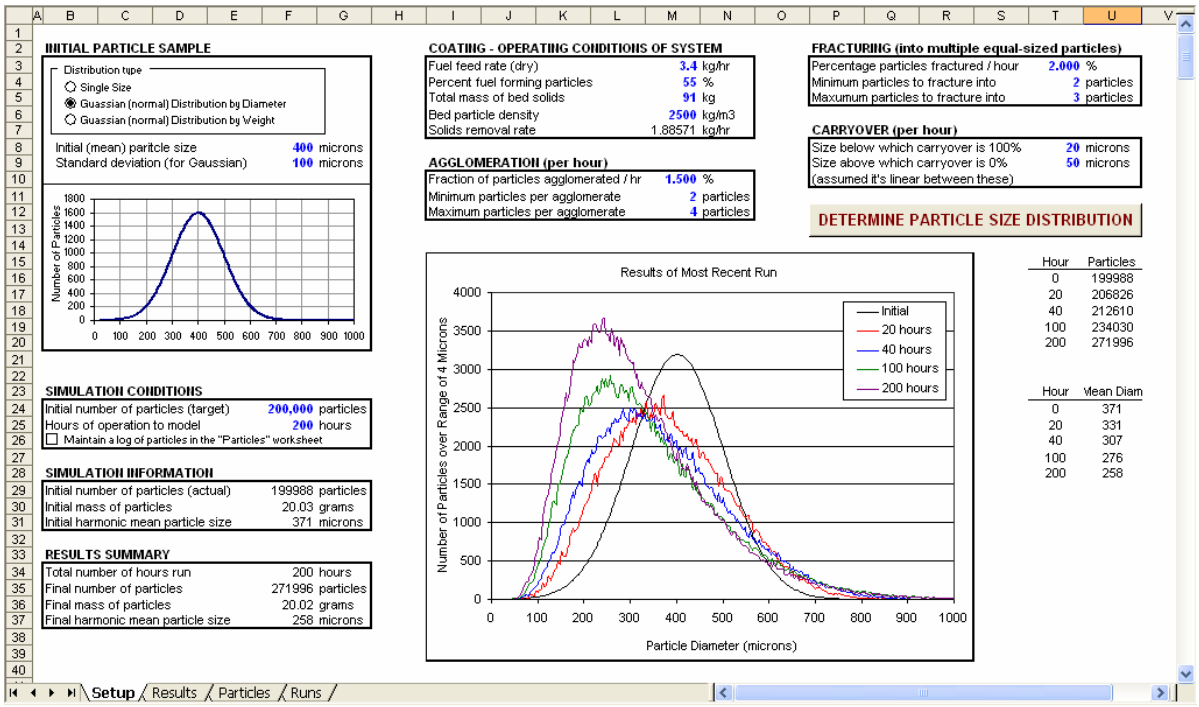

Figure 28. Interface for particle size distribution model.

4. RESULTS AND DISCUSSION

Select results from the project are presented in the sections below, ordered according to the four experimental and modeling tasks (Tasks 2-5) described in the Introduction.

4.1 Investigation of Bed Performance

Task 2, "Investigation of Bed Performance" includes three subtasks that involve (1) characterization of the bed solids and changes in the solid properties during conversion, (2) identification of factors contributing to bed agglomeration and (3) performance of the bed when titanate is added.

4.1.1 Bed Characterization

4.1.1.1 Optical Imaging of Particles

Samples of solids from commercial units as well as solids from the Utah steam reformer and the 2-inch fluidized bed were photographed through an optical microscope to gain a qualitative understanding of particle structure. In order to study the internal structure of the particles, and to get a sense of development of liquor coating on particles, some of the samples were captured in epoxy, then cross-sectioned and polished.

Evidence of particle growth through clustering is seen in Figure 29, which shows initial and final samples from experiments in the 2-inch fluidized bed with liquor injection. Particularly notable are the samples from Experiment 2 on the left. That starting material was glass beads, and the beads can clearly be seen to have been captured within the material. A theory about the specific mechanism of clustering could be that the wet liquor actually partly dissolves the edges of particles, and that the sticky edges fuse together. Unlike normal bed solids or sodium carbonate, however, the glass beads in Experiment 2 would not partly dissolve upon contact with the wet liquor. This indicates that the clustering mechanism, also known as droplet-induced agglomeration (Section 4.1.1.4) is in fact a direct result of the wet liquor capturing many smaller particles to make a large particle.

4.1.1.2 Scanning Electron Microscopy (SEM) Analysis

In addition to the optical microscopy studies described above, samples of bed material from full-scale systems, a process development unit (PDU), the Utah steam reformer and the 2-inch fluidized bed were analyzed by scanning electron microscopy to identify structural and compositional properties of the material. Samples of bed solids cast in epoxy, sectioned and polished were also analyzed to study internal structure and development of layers formed by liquor coating.

Images of several different particle size fractions for particles from both commercial and PDU systems are shown in Figure 30 to Figure 34. Figure 30 shows a series of bulk images of selected fractions for both bed materials. Below 212μm for the commercial material, particles are fairly uniform in shape, while over 212μm, there is a characteristic crack on a large fraction of the particles. This suggests that a type of fragmentation driven by either physical or chemical interactions exits. Cross-sectional images showed no presence of agglomerates on those fractions. Figure 31 presents a closer look at the particle surfaces. Although the surface of the larger particles appears smoother, this is a consequence of the lower magnification of these images.

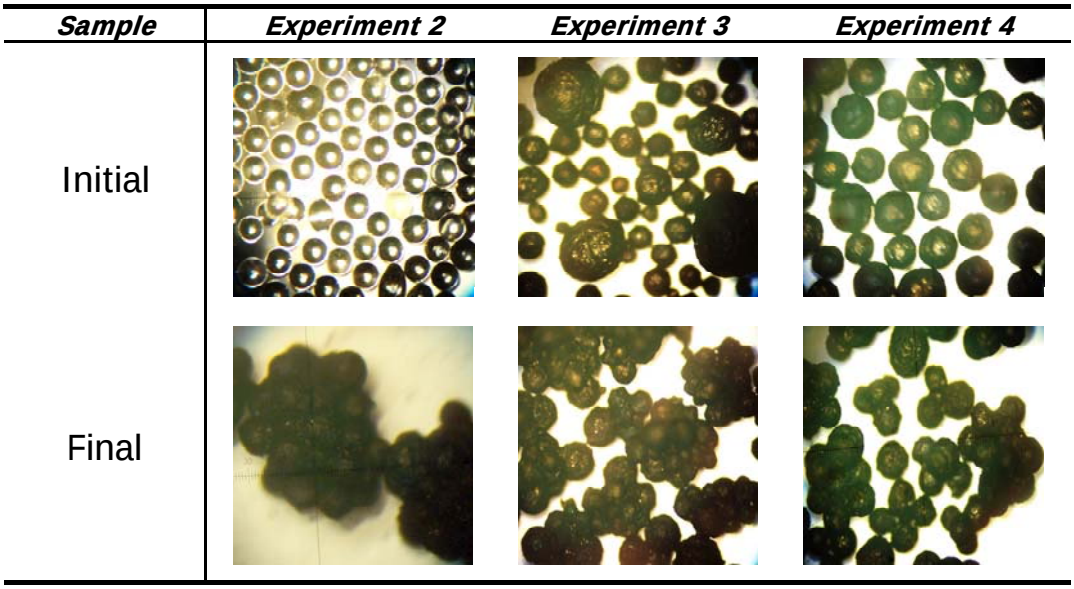

Figure 29. High magnification photographs of bed material from the 2-inch fluidized bed after operation under inert conditions with liquor injection. Initial bed materials for experiments 2, 3 and 4 were glass beads, unsieved sodium carbonate and pre-sieved sodium carbonate.

Figure 32 is a set of relatively low-magnification images showing 7 fractions varying from 75µm up to >600µm for both bed materials. Figure 33 is a set of higher magnification images of the same particles. The larger particles appear somewhat fragmentized. It is important to note that to avoid non-central cross sections, only the larger particles' cross-sectional areas were analyzed. No type of agglomerated or sintered material is observed, but it is clear that different types of regions are present in such areas. The larger particles of the PDU material clearly have a "core" and surrounding layers. Elemental analysis through EDX backscattering indicates that the core has much calcium and little sodium, while the layers have much sodium but little calcium. The buildup of liquor on the limestone core is apparent. This was not observed for the Big Island particles, since that bed has been turned over enough that there is very little limestone remaining. Other details seen during the SEM inspection on the cross-sectional areas are cracks and fissures which may result from: a) loss material derived from the sample preparation (polishing process), b) gas capturing due to its inward and/or outward flow, c) thermal shock or d) physical stress.

Evidence of liquor coating for all particles, including those from the full-scale reformer, can be seen in Figure 34. In general, the larger the particle the thicker the layer, as shown by the column of images of processed bed material. Comparing fractions 300 – 425µm and 425 – 600µm of the solids from the two reformers, it can be seen how similar those fractions are, even with slightly different layer thickness. The smaller particles (< 212µm) seem to have similar layering of ~20µm in thickness.

Fraction	Particles from full-scale system	Particles from PDU system
75 -106 micron	~	~
106 -150 micron 15kV x60	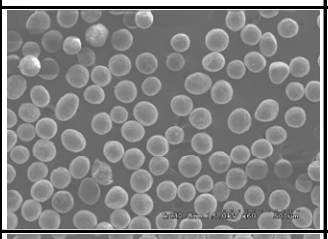	~
150 - 212 micron 15kV x50	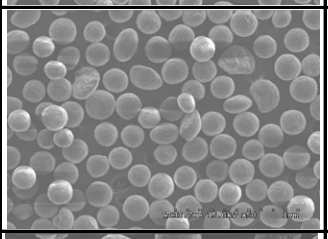	~
212 - 300 micron 15kV x60	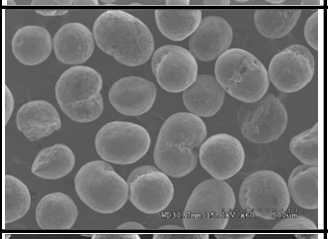	~
300 - 425 micron 15kV x50	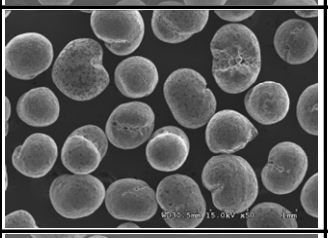	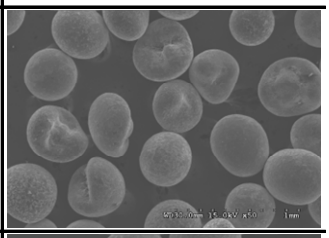
425 - 600 micron 15kV x500 (left) 15kV x50(right)	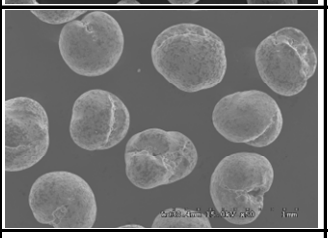	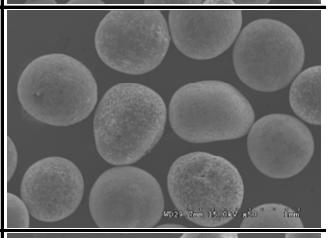
over 600 micron 15kV x30	~	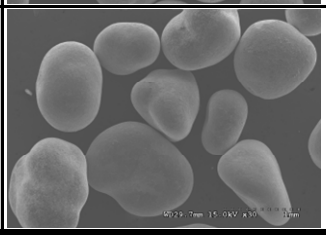

Figure 30. SEM images of particles from full-scale and PDU reformers.

Fraction	Particles from full-scale system	Particles from PDU system
75 -106 micron	~	~
106 -150 micron 15kV x900	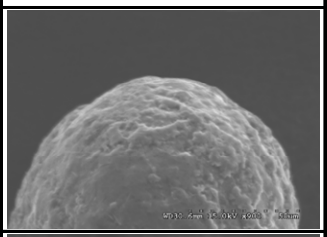	~
150 - 212 micron 15kV x1.0k	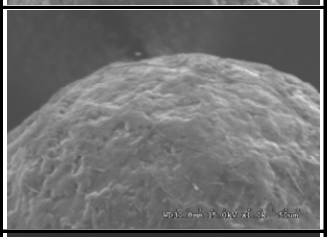	~
212 - 300 micron 15kV x800	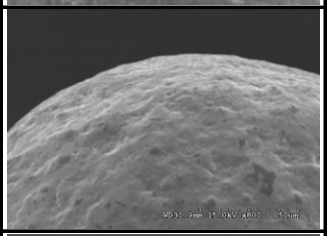	~
300 - 425 micron 15kV x600 (left) 15kV x800 (right)	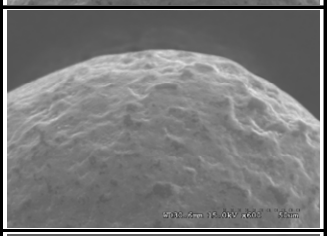	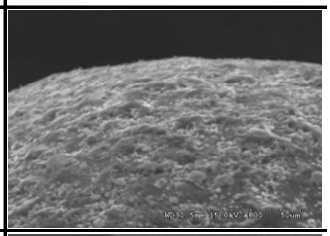
425 - 600 micron 15kV x500 (left) 15kV x450(right)	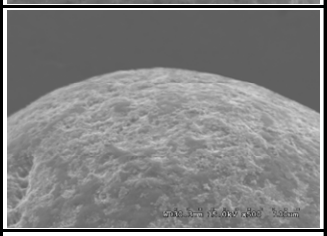	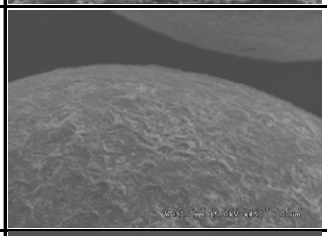
over 600 micron 15kV x450	~	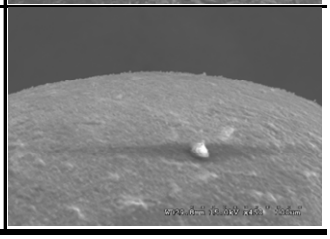

Figure 31. SEM images of the surface of particles from full-scale and PDU reformers.

In one series of experiments, limestone particles were fluidized in the 2-inch reactor while liquor was injected. Samples of the original limestone and particles removed after various exposure times were examined with the electron microscope. Results of these analyses as well as photos taken through an optical microscope are presented in Figure 35. As one would expect, the particles became darker over time due to deposition of liquor on the surface. This can be seen in the photos in the top row of the figure. At low magnification under the SEM, the surface of the particles appears to have become more textured over time, but higher magnification indicates that the microstructure became much more smooth, possibly resulting in less surface area. Surface area analyses were not performed on the limestone particles, but BET surface area measurements for glass bead starting material indicate that the surface area decreased as exposure time increased.

Evidence of liquor coating the particles is also clear from the SEM images. Figure 36 shows a cross-section of the edge of a limestone particle exposed to liquor injection in the 2-inch fluidized bed reactor for 8 hours. Layers of material on the edge of the particle are clearly visible. The combined thickness of these layers for this sample is about 15 microns. The images in (b) and (c) of Figure 36 show the same edge at lower magnification, and EDAX maps for calcium and sodium. Clearly, the liquor coats the particles and forms layers.

In some of the experiments, particles were observed to have bound together to form larger particles. A sample of this type of binding together is shown in Figure 37. Though the particles are held together by the coating, this type of structure is somewhat different than was observed for the clustered particles. The exact nature of this type of particle binding cannot be deciphered from these images.

4.1.1.3 Particle Size Distributions

The distribution of particle sizes (diameters) was determined for material from a steam reforming process development unit and a full-scale steam reformer by sieving samples from these units. For both types of samples, the particle size distributions were quite broad. For the commercial system, 90% of the particles were in the range 75-850 microns, with roughly half the particles in the range 150-300 microns. The harmonic mean diameter was roughly 250 microns.

Solids from a commercial unit having an initial organic carbon concentration of roughly 17 wt% was used as starting material for a "steam-out" test in the University of Utah steam reformer, during which no liquor was injected but carbon was gasified from the material. The progression of particle size distribution was followed as a function of conversion, and is shown in Figure 38. Clearly, there is very little change in particle size as the carbon is removed by gasification, suggesting that the inorganic matrix of the solids, which dictates the particles' size, remains relatively intact as the carbon is removed.

In addition to studying how particle size changes as carbon is reacted away, tests were performed in University of Utah's 2-inch fluidized bed to study how particle size develops when liquor is fed to the system but no heterogeneous reaction takes place. For these tests, reagent-grade sodium carbonate was used as initial bed material. Black liquor was injected into the freeboard of the reactor and allowed to fall onto the bed. The resulting mean particle diameter was tracked as a function of time, and the results of two such tests having different initial particle sizes and liquor injection rates can be seen in Figure 39.

Fraction	Particles from full-scale system	Particles from PDU system
75 -106 micron 15kV x35	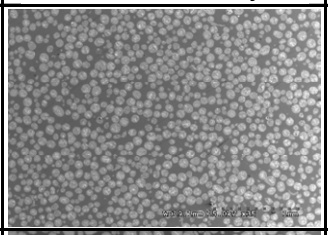	~
106 -150 micron 15kV x35	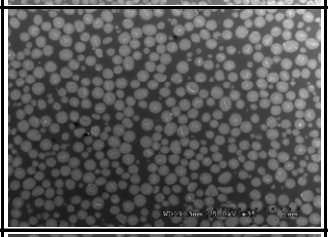	~
150 - 212 micron 15kV x35	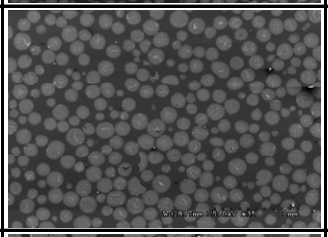	~
212 - 300 micron 15kV x35	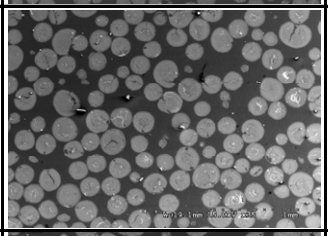	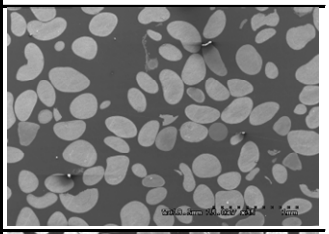
300 - 425 micron 15kV x35	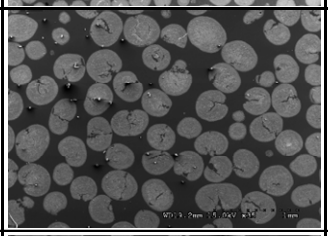	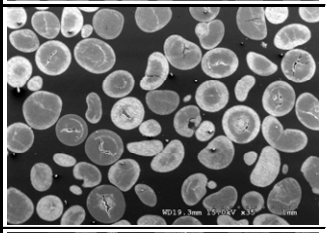
425 - 600 micron 15kV x35	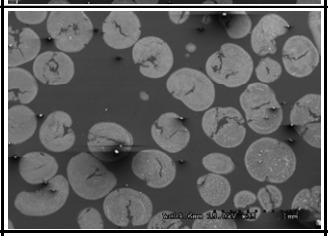	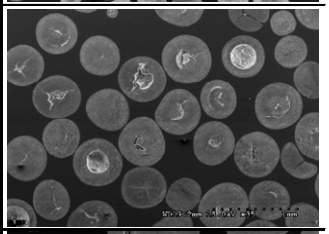
over 600 micron 15kV x35	~	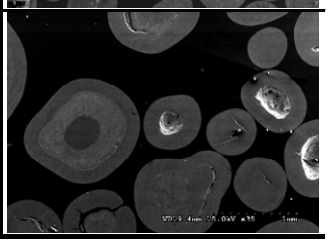

Figure 32. Low magnification SEM images of particles from full-scale and PDU reformers.

Fraction	Particles from full-scale system	Particles from PDU system
75 -106 micron 15kV x900	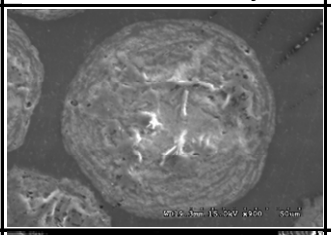	~
106 -150 micron 15kV x600	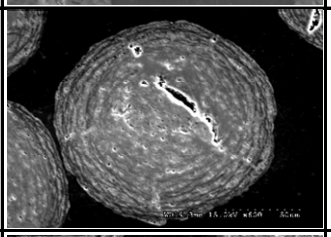	~
150 - 212 micron 15kV x400	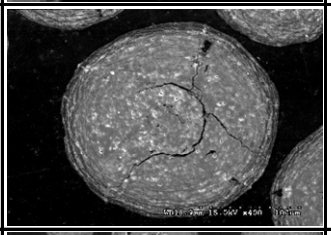	~
212 - 300 micron 15kV x300	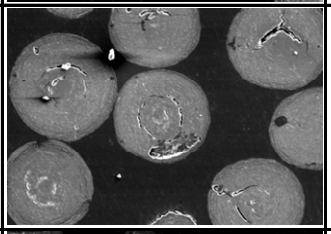	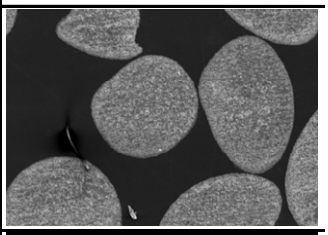
300 - 425 micron 15kV x200	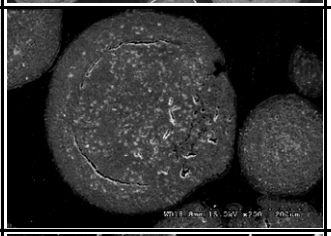	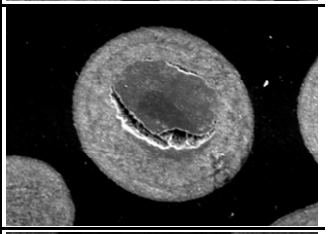
425 - 600 micron 15kV x90 (left) 15kV x150(right)		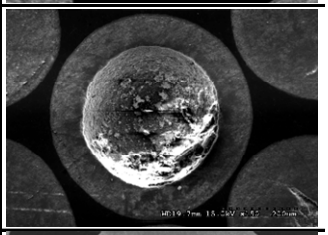
over 600 micron 15kV x90	~	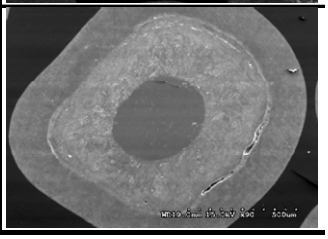

Figure 33. High magnification SEM images of particles from full-scale and PDU reformers.

Fraction	Particles from full-scale system		Particles from PDU system	
75 -106 micron 15kV x1.8k	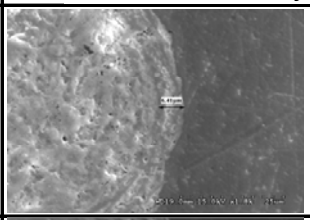	6.41µm	~	
106 -150 micron 15kV x1.2k	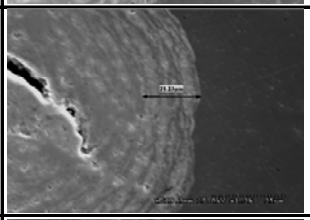	21.23µm	~	
150 - 212 micron 15kV x1.2k	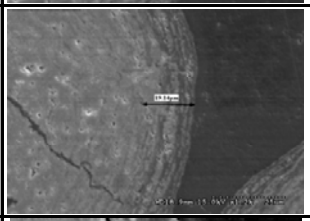	19.14µm	~	
212 - 300 micron 15kV x3.0k	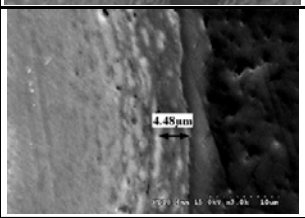	4.48µm	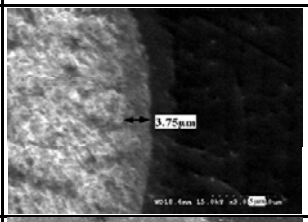	3.75µm
300 - 425 micron 15kV x200 (left) 15kV x700 (right)	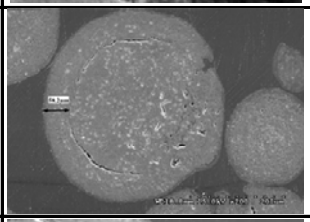	58.2µm	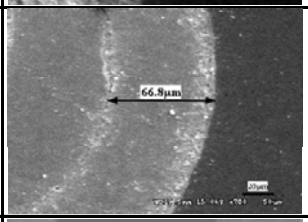	66.8µm
425 - 600 micron 15kV x450 (left) 15kV x150 (right)	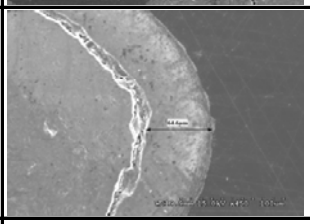	64.6µm	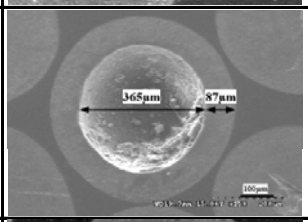	87µm 365µm
over 600 micron 15kV x90	~		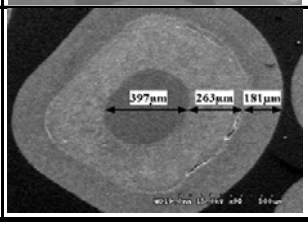	181µm 263µm 397µm

Figure 34. SEM images of cross-sections of particles from full-scale and PDU reformers. Layers of material, or "shells" are clearly visible for both types of particles. Approximate layer thicknesses are indicated.

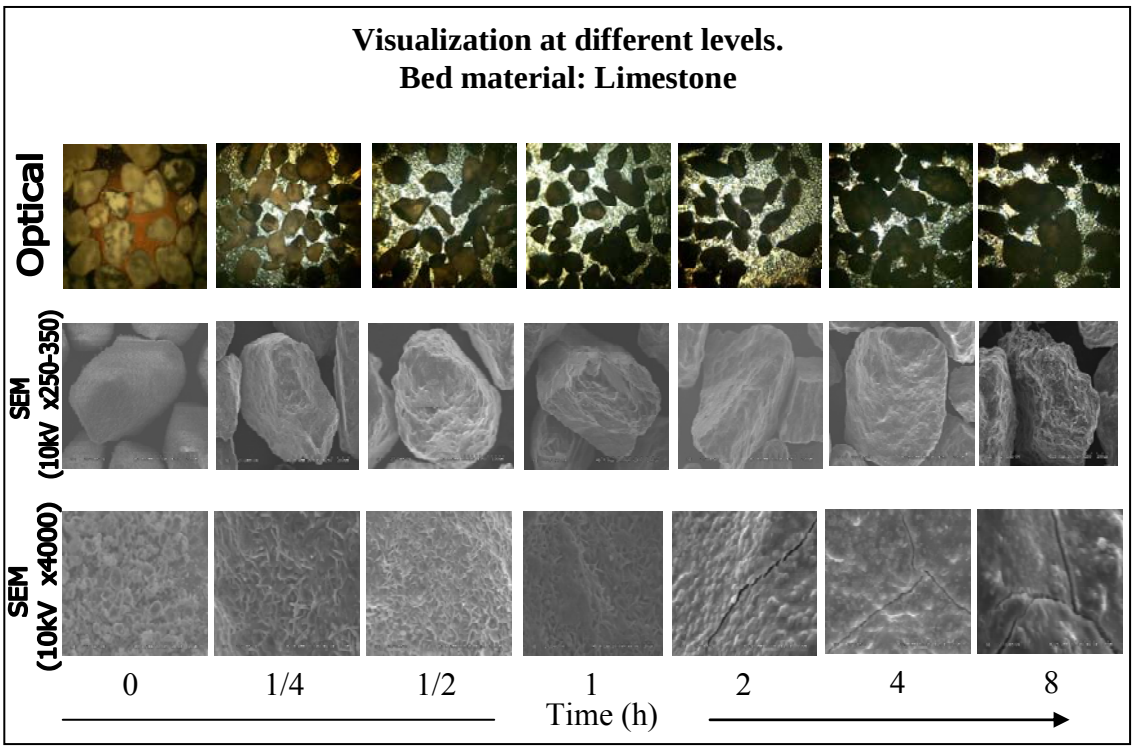

Figure 35. Optical and SEM images of particles sampled at various times after liquor injection began.

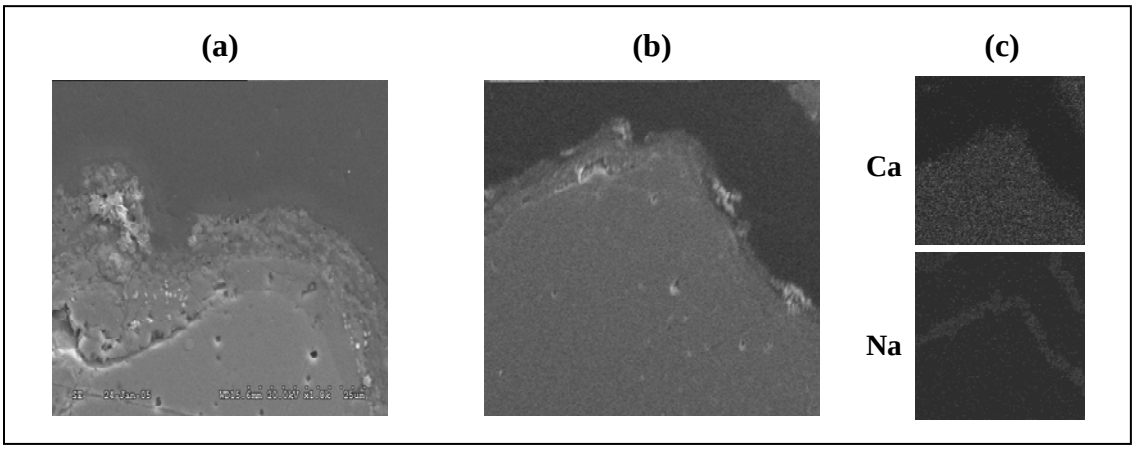

Figure 36. Photo (a) shows a close-up of the 8-hour sample, in which layers of material can clearly be seen. Photos (b) and (c) show the same particle at lower magnification with corresponding calcium and sodium maps. The strong presence of sodium in the coated layers is evident.

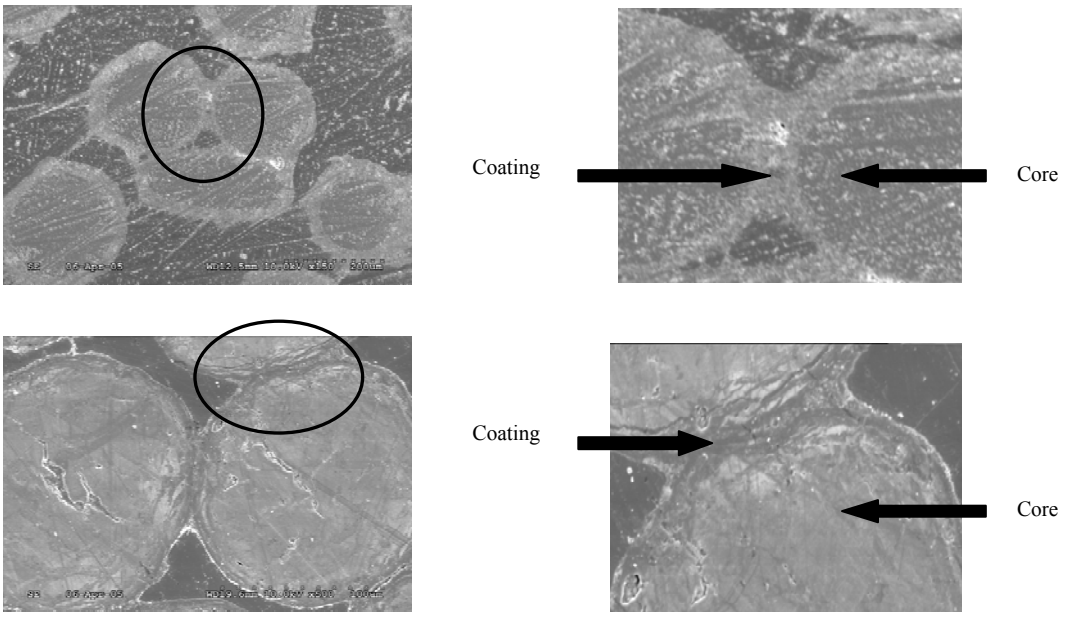

Figure 37. SEM images showing details of bridges formed between particles.

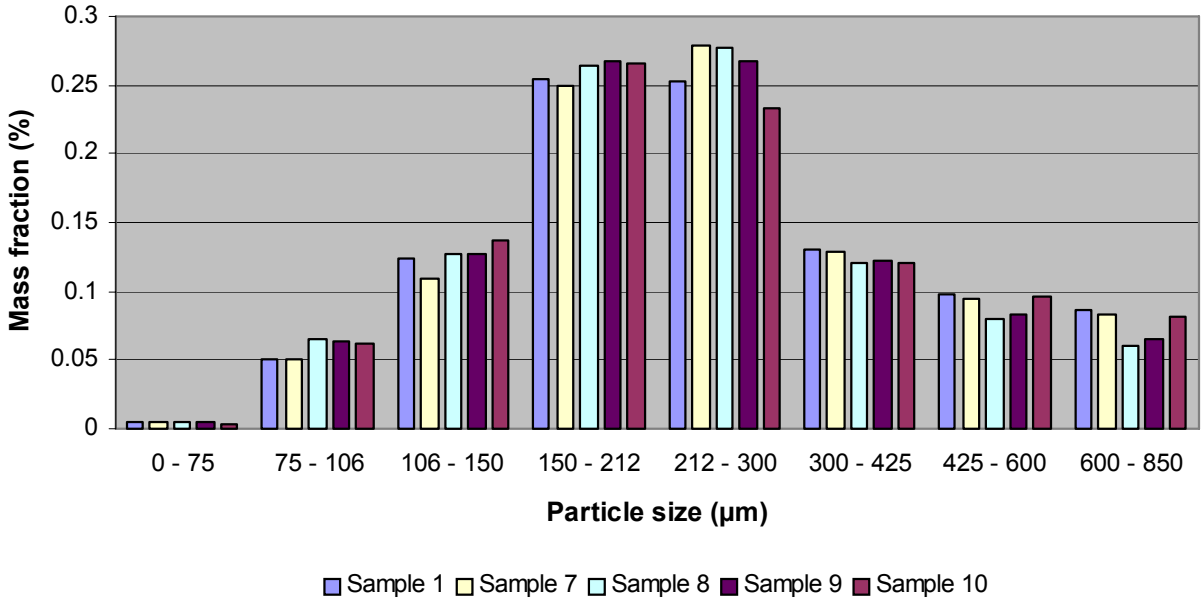

Figure 38. Progression of particle size distribution during a "steam out" run. Samples 1, 7 and 10 correspond to roughly 0%, 10% and 100% conversion, respectively.

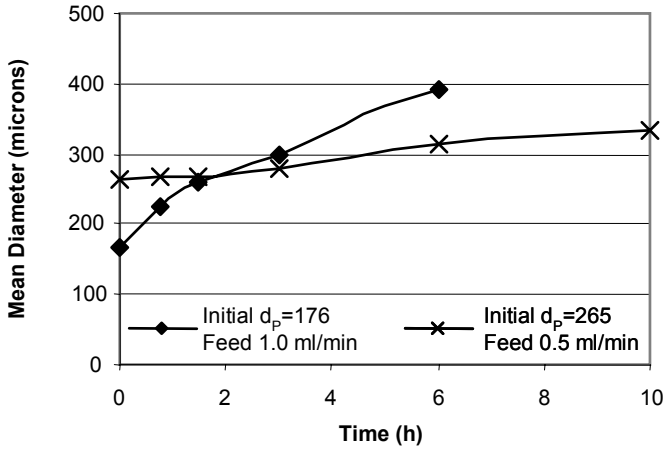

Figure 39. Development of mean particle diameter during an experiment in the 2-inch fluidized bed.

As seen in the figure, the mean particle diameter grew significantly over a relatively short period of time. Much of this can be attributed to the manner in which liquor was injected into the bed. As droplets fell onto the bed, they often captured several particles already in the bed and formed clusters of particles according to the droplet-induced agglomeration ("clustering") mechanism described below in Section 4.1.1.4. This was confirmed through microscopy, where large particles could be seen to be made up of several small particles held together by pyrolyzed liquor.

4.1.1.4 Particle Growth and Shrinkage Mechanisms

The overall particle size distribution can vary over time as a result of changing operating conditions and corresponding contributions of the different mechanisms responsible for particle growth and shrinkage. These mechanisms have been identified and are described below.

Growth mechanism: Coating. Coating involves "painting" of the particle by black liquor as it is injected into the gasifier. As the organic fraction of the liquor is removed through gasification, the inorganic fraction of the liquor creates a layer on the existing particle. This successive painting and shell formation increases particle size by creating an "onion" type structure of layers. A schematic of the coating mechanism is shown in Figure 40. In theory, a particle that remains in the bed for a very long time and is coated by liquor many times can grow to be very large.

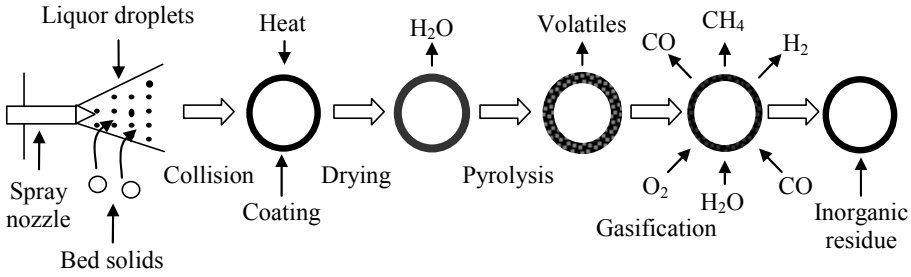

Figure 40. Schematic of coating mechanism.

Growth mechanism: Agglomeration. Agglomeration involves two or more particles adhering together by one of several mechanisms. *Sintering* occurs when particles adhere to each other below the particle melting point, and is a result of surface interactions of the particles. In *melt-induced agglomeration* the surfaces of one or more particles melt, partly or wholly, causing particles to stick together and form a larger cluster of particles. *Droplet-induced agglomeration* occurs when large droplets of black liquor capture several particles to create a "cluster" of individual particles bound by liquor. Such agglomerates nevertheless undergo drying, pyrolysis and steam reforming. The agglomeration mechanism is presented in Figure 41.

Shrinkage mechanism: Attrition. Attrition is defined as the particle size reduction mechanism in which abrasive wear between particles leads to the removal of asperities and fines from particle surfaces. Attrition includes two categories: (1) *mechanical attrition*, which involves the purely physical interaction between particles, and (2) *reaction-enhanced attrition*, which consists of the same abrasive wear, but is enhanced by surface weakening as solids react. Industrially, attrition is seen as a particle degradation phenomenon, usually associated with problems such as slight changes in particle size distribution (PSD) and the generation of fines. The former affects bed solids quality and/or operation, whereas the latter involves loss of material and particulate emissions.

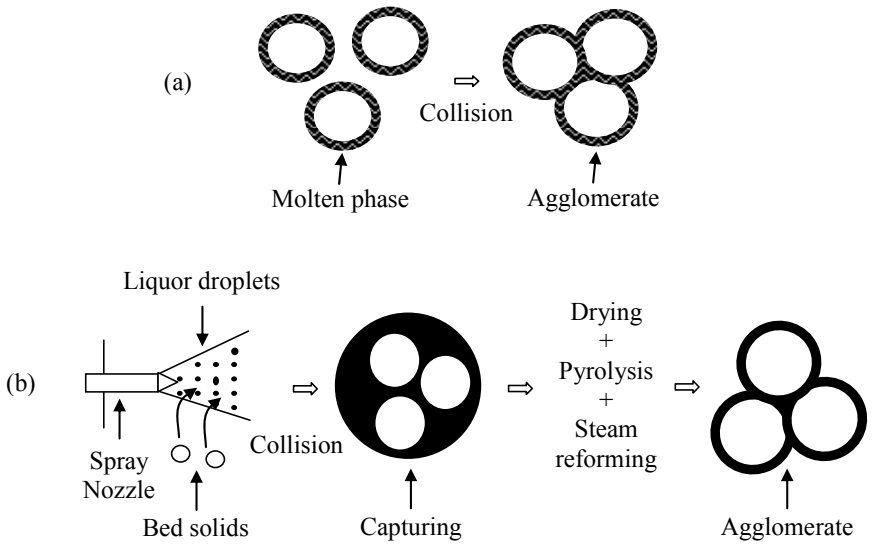

Figure 41. Agglomeration mechanisms: (a) agglomerate formation due to sintering or melting and (b) agglomerate formation due to droplet-particle collision.

Shrinkage mechanism: Fragmentation. Fragmentation is defined as the particle reduction mechanism in which a rapid fracturing of particles produces new particles that are all distinctly smaller than the original ones. Similar to attrition, fragmentation includes two categories: (1) *mechanical fragmentation*, which results from intense particle collisions, and (2) *reaction-enhanced fragmentation*, which consists of fracturing enhanced by particle structure weakening as solids react. This mechanism is also a particle degradation phenomenon but causes aggravated changes in particle size distribution. The attrition and fragmentation mechanisms are presented in Figure 42.

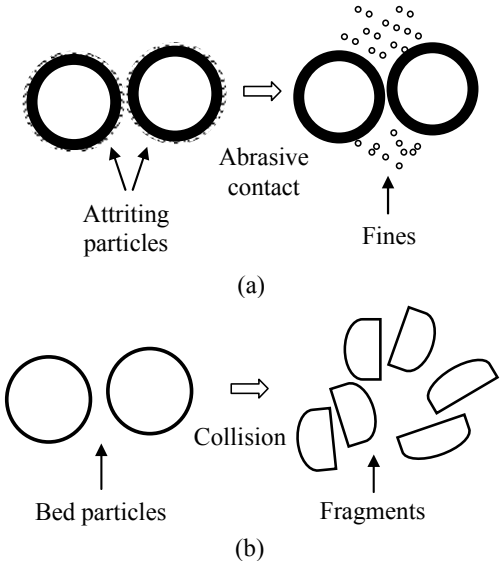

Figure 42. Particle size reduction mechanisms: (a) attrition and (b) fragmentation.

Shrinkage mechanism: Cluster-breaking. This mechanism involves releasing small particles that make up a droplet-induced agglomerate by reacting away the material that is holding the individual particles together. The bridges binding these particles become smaller and weaker as the organic fraction of the liquor reacts due to gasification. Eventually these can no longer withstand the forces in the bed and the individual particles are released. This mechanism is similar to fragmentation and is important for minimizing excessive growth of particles.

Particle carryover. Although not a physical mechanism that changes the size of individual particles, carryover, or elutriation of fine particles from a fluidized bed, does impact the particle size distribution by removing the smallest particles from the system.

Combining observations of particle structure, particle growth and particle-particle interactions described above with experience reported in literature of similar systems, a scheme describing mechanisms and pathways for particle growth has been postulated. This is presented schematically in Figure 43. The ultimate particle size distribution will be a function of the relative contributions of these mechanisms and the shrinkage mechanisms described above.

4.1.1.5 Particle Size Distribution Modeling

The computational model for particle size distribution development described in Section 3.4 was used to develop predictions of the particle size distribution of an initial Gaussian distribution of particles. A parametric study was conducted in which individual mechanisms were either "turned off" or adjusted to one of at most two sets of values. The objective was to see how strongly the different particle growth and shrinkage mechanisms affect the overall particle size distribution. For each simulation, an initial population of 200,000 particles having particle size distribution centered around 400 microns and having a Gaussian distribution was established. This population was simulated for 100 hours. The resulting particle size distribution when coating, agglomeration and fracturing dominate are shown in Figure 44, Figure 45 and Figure 46, respectively.

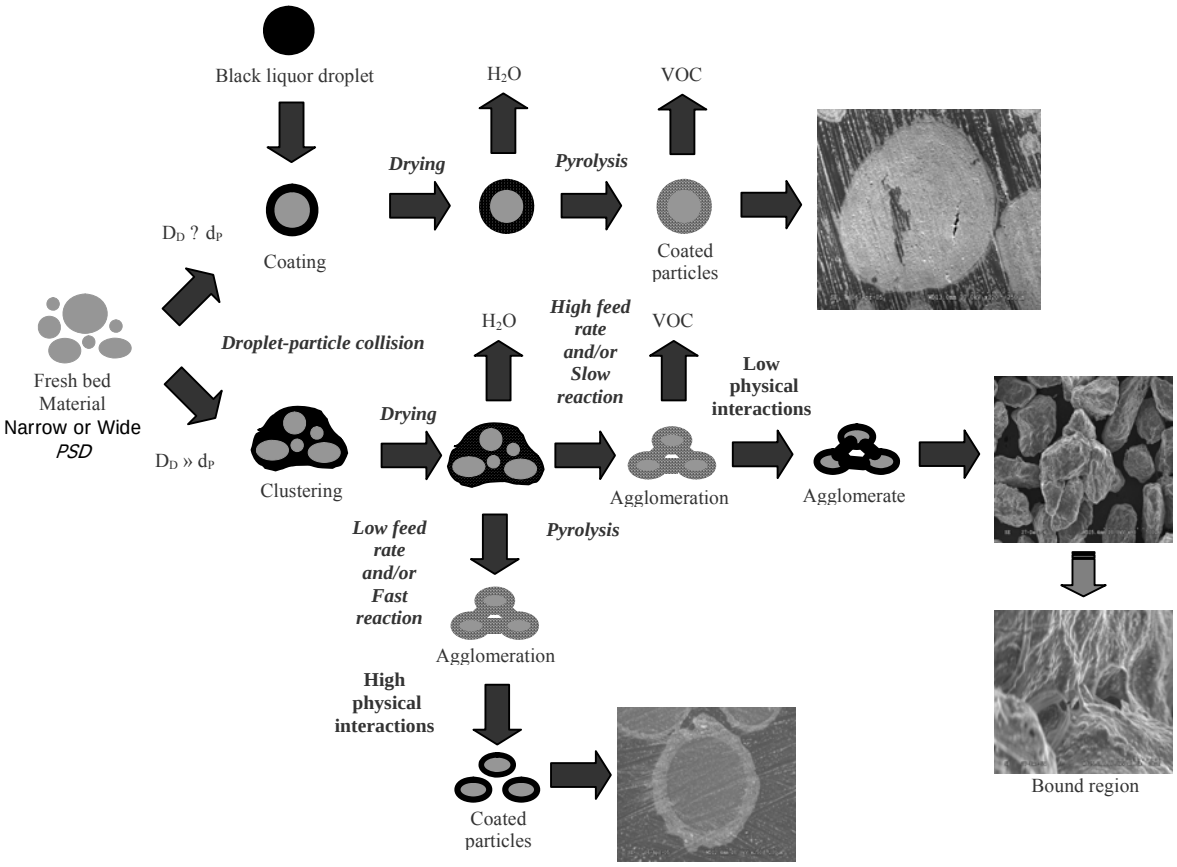

Figure 43. Pathways and mechanisms for particle growth.

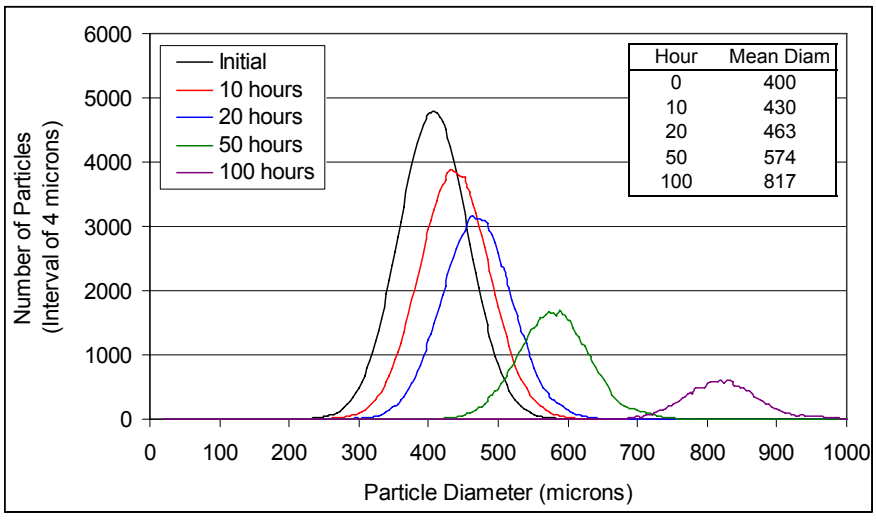

Figure 44. PSD development when coating dominates.

As one would expect, when only growth mechanisms are present, the average particle size increases. For the case when coating dominates, growth of particles is uniform, since the model assumes that liquor is coated evenly on all particles. In the simulation shown in Figure 45, when agglomeration dominates, particle growth is quite uniform, as well. In this particular simulation, it was assumed that 2 or 3 particles combine to form one larger particle. This even growth does not result if it is assumed that many particles (e.g., more than 6) combine to form a single agglomerate. In such a case, a population of large particles develops. For fracturing, the bimodal distribution resulting from fracturing to 2 or 3 particles is especially obvious for the 20 hour distribution in Figure 46.

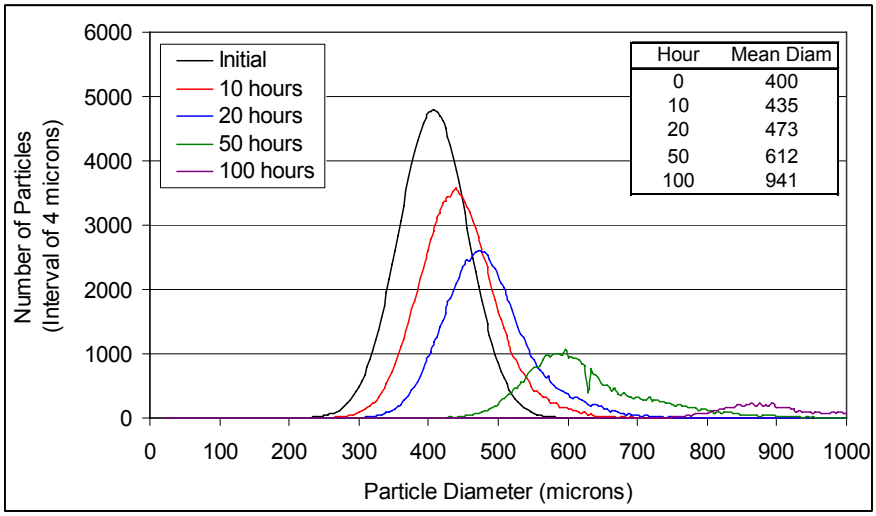

Figure 45. PSD development when agglomeration dominates. 1.5 percent of particles agglomerated per hour, forming one particle from either two or three other particles.

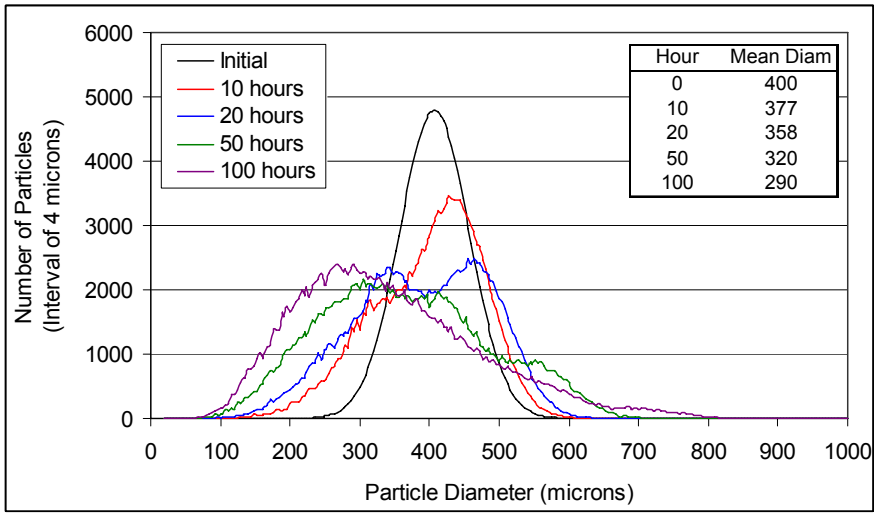

Figure 46. PSD development when fracturing dominates. 1.5 percent agglomerated to 2 or 3 particles per hour.

Figure 47 shows a typical result when all mechanisms are balanced. The mean particle size remains relatively constant. But, even under these conditions, the "tails" of the distribution increase over time.

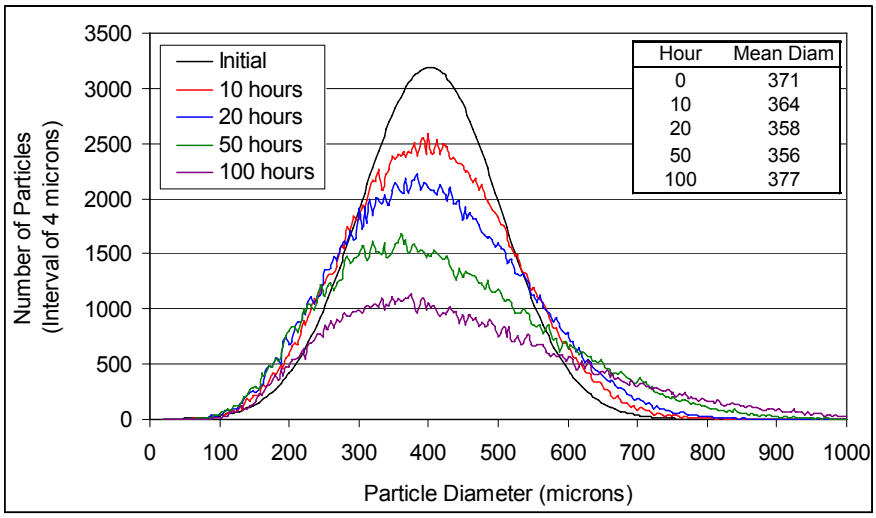

Figure 47. PSD development all mechanisms are participating and balanced.

The following conclusions resulted from this study:

- Coating results in uniform growth of all particles, as one would expect.
- Only a very small fraction (less than 2%, and more likely close to 0%) of the particles can undergo fracturing to break them into several equal-sized particles. If the fraction fractured was much more than 1-2%, the size distribution quickly shifted towards smaller particles. This effect was compounded if it was assumed that some of the particles were fracturing into more than two pieces.
- Very little particle-particle agglomeration must occur, since inclusion of much more than 1% agglomeration quickly shifted the mean size to larger diameters. This effect was only mildly dependent on the number of particles contributing to each agglomerated particle if the fraction of the total bed agglomerating was the same.
- Attempts to maintain average particle size or total number of particles by balancing fracturing and agglomeration were not very successful. The balance could be made if set up carefully, but the particle size distribution became wider over time for all cases. This does not correspond with what has been observed in operating steam reformers.
- The importance of fracturing likely increases as particle size increases, since the kinetic energy of such particles is higher. This may help keep particles from becoming excessively large, pushing the size distribution to smaller sizes.

- The mechanisms most responsible for particle size development appear to be coating and attrition. It was possible to maintain a reasonably narrow size distribution with a combination of these two mechanisms. This is not surprising, since they are in many regards opposites of one another.

- If the child particle sizes resulting from attrition were set to realistic values (based, in part, on SEM images of actual bed particles) they were all removed from the system through carryover.

The rate of carryover that resulted when attrition and coating were balanced to maintain a constant particle size distribution over several hours was much higher than what has been observed in actual operating systems. This suggests that perhaps they are returning to the bed through, for example, the cyclone catch and acting as new seed particles that eventually cycle enough that they grow to a size where they are no longer swept upwards with the gas.

The model does not have any mechanism for introduction of "seed" particles into the bed, for example from cyclone catch return or from rapid drying and devolatilization of small droplets that do not contact bed particles before they have become solid. Such a mechanism may also be important for maintaining a relatively small particle size distribution.

4.1.2 Bed Agglomeration Studies

Agglomeration of the bed is a significant concern for fluidized bed systems. In order to maximize conversion of black liquor in a fluidized bed steam reformer, it is desirable to operate the system at as high of temperature as practical while avoiding agglomeration. Under this program a variety of lab-scale studies were performed and combined with detailed particle analysis to shed light on agglomeration temperatures and mechanisms of agglomeration for various bed materials.

4.1.2.1 Agglomeration of Model Compounds

Black liquor and associated steam reformer bed particles are complex mixtures of compounds. In order to develop a fundamental understanding of how particle composition affects agglomeration, a testing campaign was carried out using pure compounds with or without impurities and with or without black liquor feeding. The test matrix included thirteen complete runs that were performed in the agglomeration test reactor described in Section 2.2: three with sodium sulfate (Na_2SO_4) bed material, eight runs using sodium carbonate (Na_2CO_3) bed material with varying levels of potassium chloride (KCl) impurity, and two runs using Na_2CO_3 bed material with KCl impurity and black liquor injected into the bed. Figure 48 shows the agglomeration temperatures for each experiment. For pure Na_2CO_3 bed material, the bed began to agglomerate at a bed temperature of 520 ºC. The agglomeration temperature rapidly decreased with the inclusion of KCl impurity in the bed. With 0.5% KCl impurity by weight added to the bed, the agglomeration temperature decreased by 40 ºC. Replicate experiments with impurity concentrations of 0.0% and 2.0% KCl establish the precision of the experiments (±5 ºC). The indicated agglomeration temperatures differed by 3 ºC and 5 ºC respectively. Because of the difficulty in determining an exact temperature at which agglomeration begins, a difference in temperature within 0.6% and 1.0% of the total temperature, respectively, represents an acceptable range for showing repeatability.

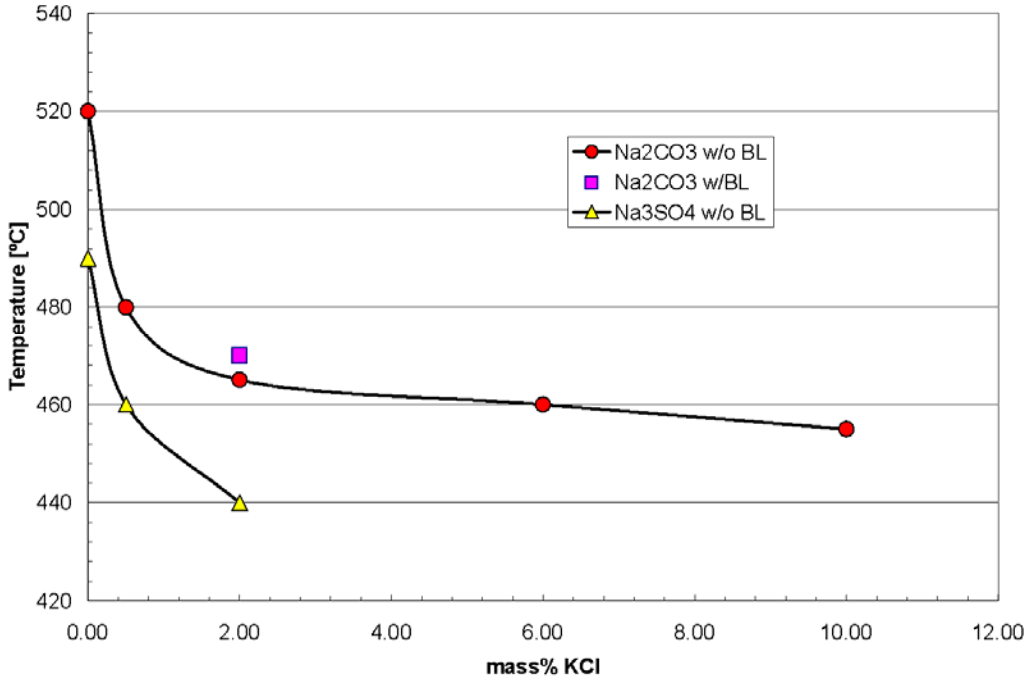

Figure 48. Agglomeration temperatures for various bed materials.

Results from the three runs performed with a Na_2SO_4 bed material indicate that agglomeration began at a bed temperature of approximately 490 ºC for pure Na_2SO_4 and 440 ºC for Na_2SO_4 containing a KCl impurity concentration of 2.0%.

The repeated test conducted with 2.0% KCl indicated two types of agglomeration. The first type was bed particles agglomerating to heater surfaces in partially stagnant regions of the reactor at approximately 465 ºC. The other type, described later, is agglomeration in the free-flowing particles away from the heaters. Figure 49 shows the bed material agglomerated to heater surfaces. As is evident from the picture, surface agglomeration occurred to a greater degree on the top of the heater surfaces (where flows are most stagnant). These data indicate that, with an increasing KCl concentration, the mass diffusion towards high-energy surface contact points increases and accordingly, the necessary contact time between particles for sintering to occur decreases.

A particularly useful analysis for this investigation involves generating elemental maps from SEM/XDS data based on these principles. Figure 50 shows a set of data that includes the secondary-electron image, the backscattered-electron image, and a series of images that show the spatially resolved concentrations of each element of interest.

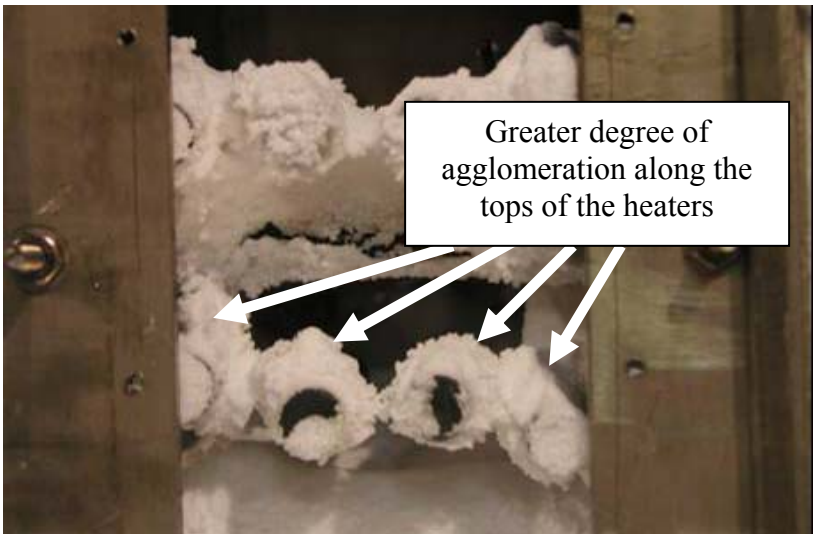

Figure 49. Agglomeration on heater surfaces

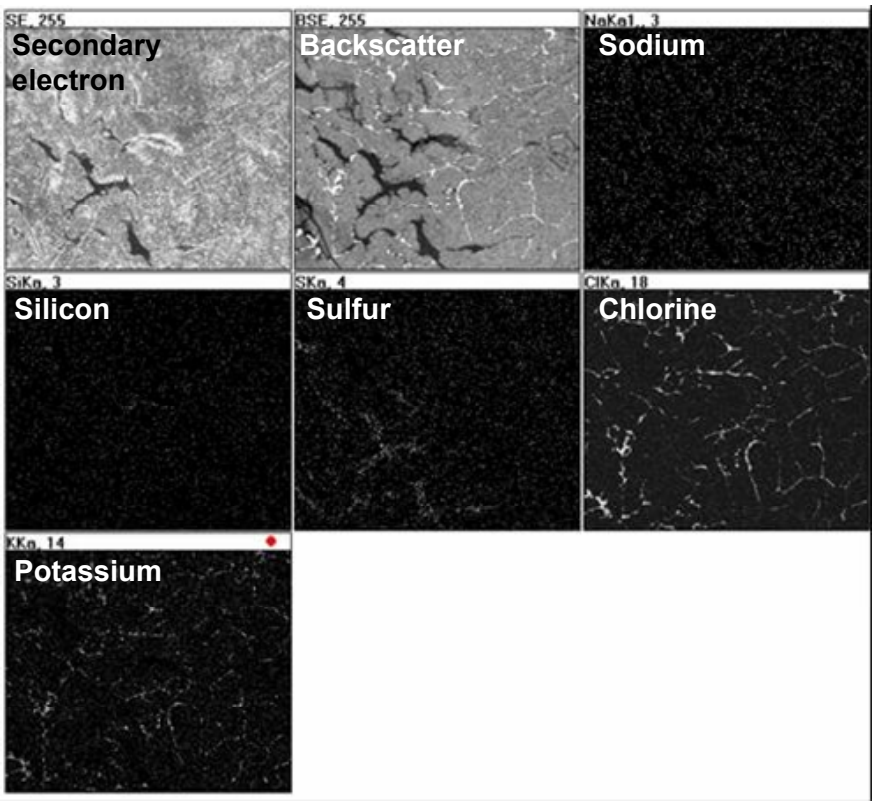

Figure 50. SEM elemental mapping of the agglomerate material from Figure 49, containing 2.0% KCl impurity. The KCl appears to bind the individual particles together. The first two images are the secondary electron and backscatter images, respectively. The remaining images are, in order of appearance from left to right and then top to bottom, Na, Si, S, Cl, and K.

The detector and window used in this analysis prevented detection of sodium. However, the chlorine and potassium plots strongly suggest that potassium chloride forms a thin coating on the particles that helps adhere them together. As demonstrated earlier, these particles are well below the melting points of either pure compound or any eutectic that normally forms from such compounds, indicating that there is no molten phase involved in this sintering. Nevertheless, the potassium chloride forms an apparent binding surface layer.

Figure 51 shows a backscatter SEM image of another sample taken from the same 2.0% KCl impurity test. The dark regions in the picture are voids while the gray regions are Na_2CO_3 and the white regions are KCl. The regional compositions were determined using x-ray diffraction. The Na_2CO_3 regions seem to be surrounded by a KCl boundary. This suggests a possible mass diffusion resulting from a concentration gradient between the KCl and Na_2CO_3. Diffusion from a difference in concentration in addition to mass diffusion from surface energy reduction could be one explanation for the decrease in sintering temperature with increasing KCl concentration.

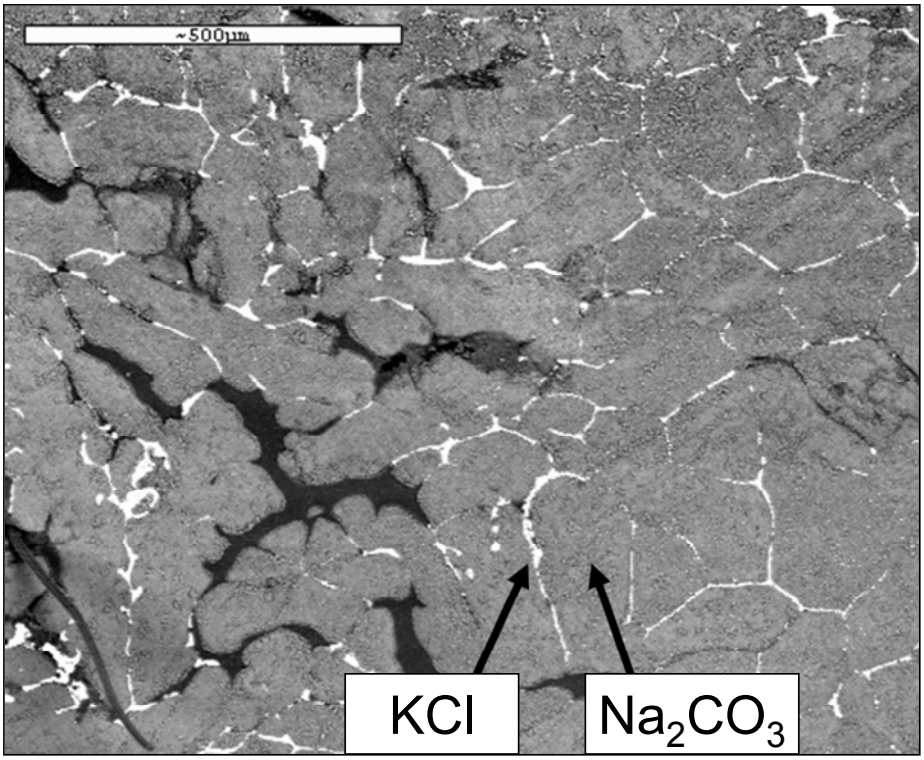

Figure 51. Backscatter image of an agglomerated particle at 6.0% impurity concentration

Experiments with no impurity in the bed material confirmed that agglomeration and sintering temperatures were difficult to distinguish because, unlike tests with impurity, the results did not show a spike in bed or heater surface temperature.

Particles removed from the reactor for the zero-impurity test were sized using varying sieves. Figure 52 shows the change in particle size before and after these tests. Note that the x-axis is the natural log of the particle diameter. The fraction of particles smaller than 100 µm was not included in both initial and final mass fraction calculations because these particles could easily have become entrained in the exiting gases instead of sintering. A factor of 5 increase in the weight fraction of particles larger than 500 µm, indicates that particle sintering occurred in the free bed material consistent with the increase in temperature between bed material and heater surface temperature. Figure 53 shows the enlargement of the particles before and after the agglomeration tests with excellent repeatability between the two post test measurements.

Figure 54 and Figure 55 show the sintering of pure Na_2CO_3 at 520 ºC occurring at the grain boundaries for particles that contact each other in the fluidized bed. The agglomerates in these figures came from the free bed and were not attached to the surface of the heaters, showing that agglomeration and sintering occurs even away from stagnant regions of the reactor. As is evident from these figures, sintering seems to have occurred at the edges of particles where the surface energy would be the highest. Thus, diffusion of material from regions of lower surface energy towards regions of higher surface energy is apparent.

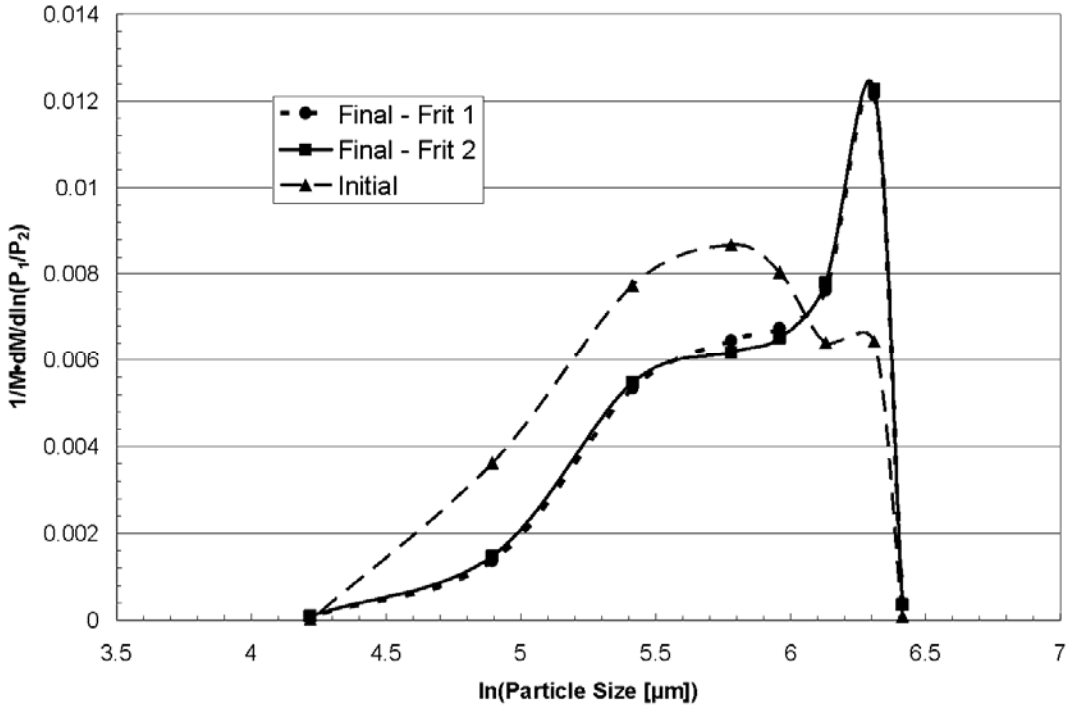

Figure 52. Particle size distributions for pure Na_2CO_3 bed material before and after agglomeration tests. Note that the x-axis is the natural log of the particle diameter.

Figure 53. Sodium Carbonate bed material before and after agglomeration tests

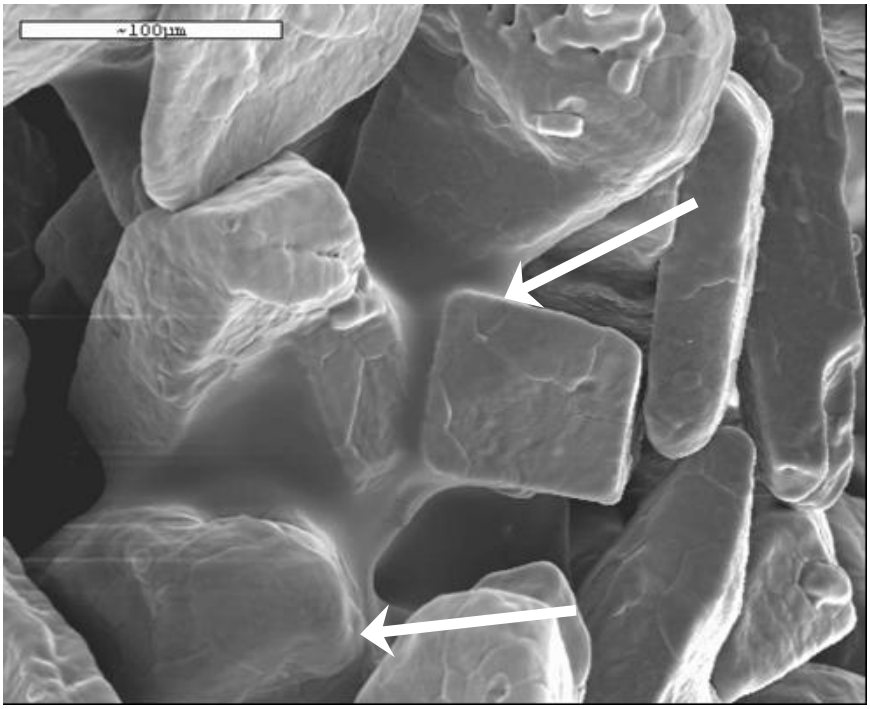

Figure 54. Bridging between particles at the onset of sintering at 520 ºC. Results from zero-impurity test.

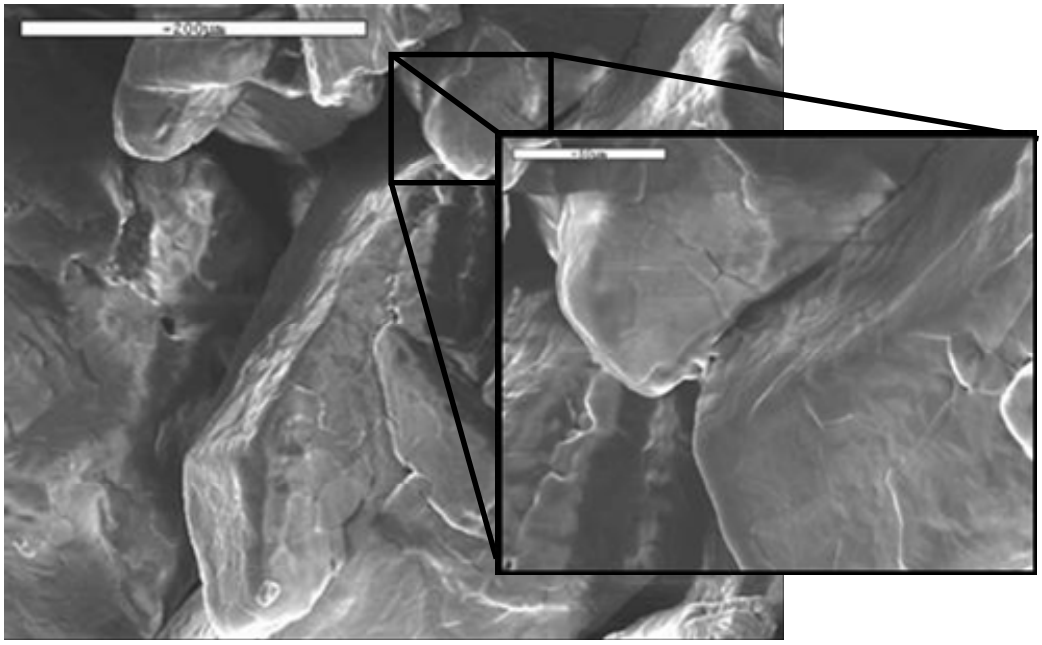

Figure 55. The onset of bridging between two particles at 520 ºC. Zero-impurity test.

Commercial gasification operation does not use pure bed materials but rather bed materials coated with residual char and inorganics from the liquor. Two types of experiments more closely simulated commercial systems. In the first, liquor was added to the laboratory reactor in small quantities, while ramping the temperature up, similar to the pure bed experiments. The feed rate and bed temperature range of liquor injection varied in these experiments. The second type of experiment involved using bed material from a commercial gasifier.

One of the runs with black liquor injection resulted in bed agglomeration in the same manner and at the same temperatures as those runs that did not involve black liquor injection. Water dilution lowered liquor viscosity to manageable levels (9.8% dry solids) in these liquor injection tests. In one of these runs, the black liquor was injected when the bed temperature reached 400 ºC. The large amount of water in the black liquor caused the bed temperature to decrease rapidly; the heater set point was still at 400 ºC and the heaters began heating up rapidly to compensate. Heater surface temperatures increased to over 550 ºC and the bed began to agglomerate to these surfaces. For the other run, the black liquor was injected at a lower bed temperature (300 ºC) and more slowly. The bed temperature did not drop as rapidly and agglomeration was avoided. After all of the black liquor was injected, the temperature was again incrementally increased. The bed began to agglomerate at a slightly higher temperature (470ºC vs. 465 ºC) as the run with the same amount of impurity (2.0%) but without the black liquor. However, this difference is within agglomeration temperature uncertainty of about 20 ºC to 25 ºC determined by a combination of bed to heater temperature difference, bed to heater set-point difference, and a visual assessment of fluidization quality in the reactor. The black liquor runs also contained agglomerated particles in the bed comprising bed particles coated with black liquor.

4.1.2.2 Agglomeration of Industrial Reformer Particles

The tests described above indicated that carbon content in the bed material has a significant effect on agglomeration and defluidization temperature and behavior. In order to gain a better understanding of this effect, high-carbon solids from a full-scale steam reformer were steam reformed at the University of Utah until the carbon concentrations were reduced to 17%, 2% and 0.3%. The 2% and 0.3% carbon materials were found to defluidize at relatively low temperatures, but after stopping the tests the material would not be agglomerated. Multiple tests were performed to determine and repeat the defluidization temperature and to produce agglomeration. The 0.3% carbon material was tested four times and the 2% carbon material was tested three times. The 17% carbon material was tested only once and did not defluidize or agglomerate up to a temperature of 652°C.

A summary of bed defluidization and bed agglomeration temperature of the materials tested is given in Table 3. The defluidization temperatures shown in the table were repeatable for the fixed reactor geometry, particle size distribution, particle shape, and fluidization velocity used in the test. It is possible that a change in any of these fixed variables could change the defluidization temperature. The agglomeration temperature is less certain. For each material, there was no agglomeration at the defluidization temperature. The material would "cake" together at the defluidization temperature but after cooling, was completely friable and returned to the original size distribution after the caked material was broken apart. It was also observed that after a material had reached the defluidization temperature it could be refluidized by cooling the bed material. A cycle of defluidization, refluidization, and defluidization could be achieved by heating, cooling, and then heating the material. Heating beyond the defluidization temperature created agglomeration on heater tubes. In each case, material that was not agglomerated on a heater tube had the same size distribution as the original material indicating that the agglomeration was a local phenomena near the tubes and that the tube surface temperature may be a better indicator of agglomeration temperature. Leaks in the reactor are another variable which may influence defluidization temperature. When significant leaks occurred, the defluidization temperature was lower. The data reported in Table 3 are for cases where leakage was negligible. Pietsch [45] stated that at about two-thirds of the melting temperature fluidization gets difficult due to partial melting and mass diffusion. This agrees with the sodium carbonate tests that have been run. Sodium carbonate has a melting temperature of 854°C and at two-thirds of the melting temperature (about 520°C) it becomes difficult to fluidize the bed material.

TABLE 3. AGGLOMERATION AND DEFLUIDIZATION TEMPERATURES.

Material	Defluidization Temp	Agglomeration Temp
Na_2CO_3	~520°C	Not available
Industrial bed material - 0.3% C	450°C	490°C
Industrial bed material - 2.0% C	460°C	530°C
Industrial bed material - 17% C	Not available (> 652°C)	> 652°C

After numerous repeatable tests similar to those outlined in the table above, it was concluded that particle growth does not occur in the bed material at the defluidization temperature. It is useful to think of the bed material which resides in two different zones within the reactor: (1) stagnant zones near heater surfaces, corners, and walls and (2) free bed material in areas where fluidization is normal. Bed material in stagnation zones near heaters will form agglomerates which sinter and form

hard deposits. Free bed material appears to defluidize at a repeatable temperature which is a weak function of the fluidization velocity. The cause of defluidization is not fully understood. If cooled under fluid flow, the particles refluidize. If cooled without flow, these free bed particles appear bound by very weak forces forming large agglomerates consisting of very weakly bound primary particles. When sieved or handled, the agglomerates break into primary particle size.

Two tests were performed at different target flow velocities to measure the dependence of defluidization temperature on velocity. Results are shown in Table 4. As expected, the higher flow velocity required a higher temperature to produce defluidization. It is expected that the momentum of colliding particles is greater at higher flow velocity causing a greater sintering force to be obtained in order for the particles to remain stuck together.

TABLE 4. EFFECT OF FLOW OF ON DEFLUIDIZATION TEMPERATURE.

Target Velocity	Defluidization Temp
1.0 ft/s	520 °C
1.6 ft/s	560 °C

Scanning electron microscopy (SEM) of industrial particles. SEM images were taken of the industrial bed particles after the experiments. Figure 56 below is a high quality backscattered electron (BSE) image of the x-ray elemental map for an particle containing 2% organic carbon which agglomerated after having been tested in the agglomeration test reactor. The same image indicating individual elements is shown in Figure 57. Figure 58 and Figure 59 are additional images of the sintering and agglomeration of coated particles. The backscatter and x-ray maps show a well defined layer of carbon, potassium and chlorine on the outside edge of each particle. This layer is present on all particles, as shown in the figures, except where the particles have become indistinguishable from each other, i.e. one solid mass. The oval in the top right of Figure 56 shows where it is difficult to determine where one particle starts and another ends.

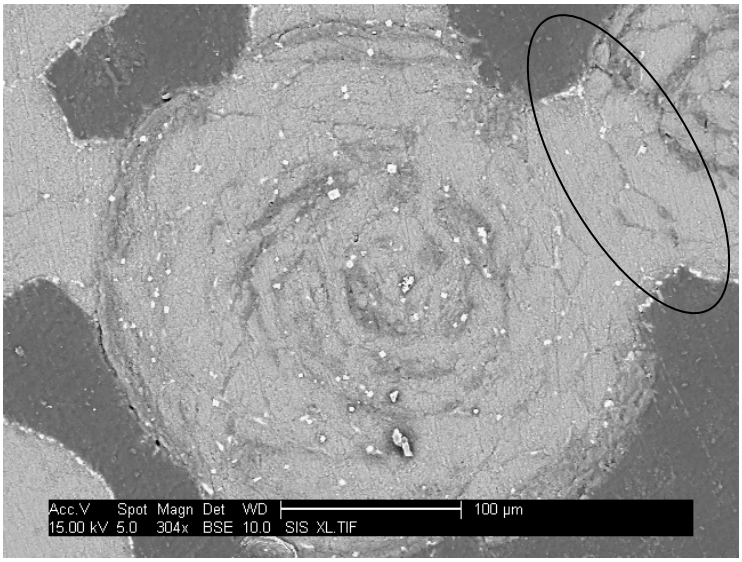

Figure 56. BSE image of a 2% Carbon content particle received from UofU.

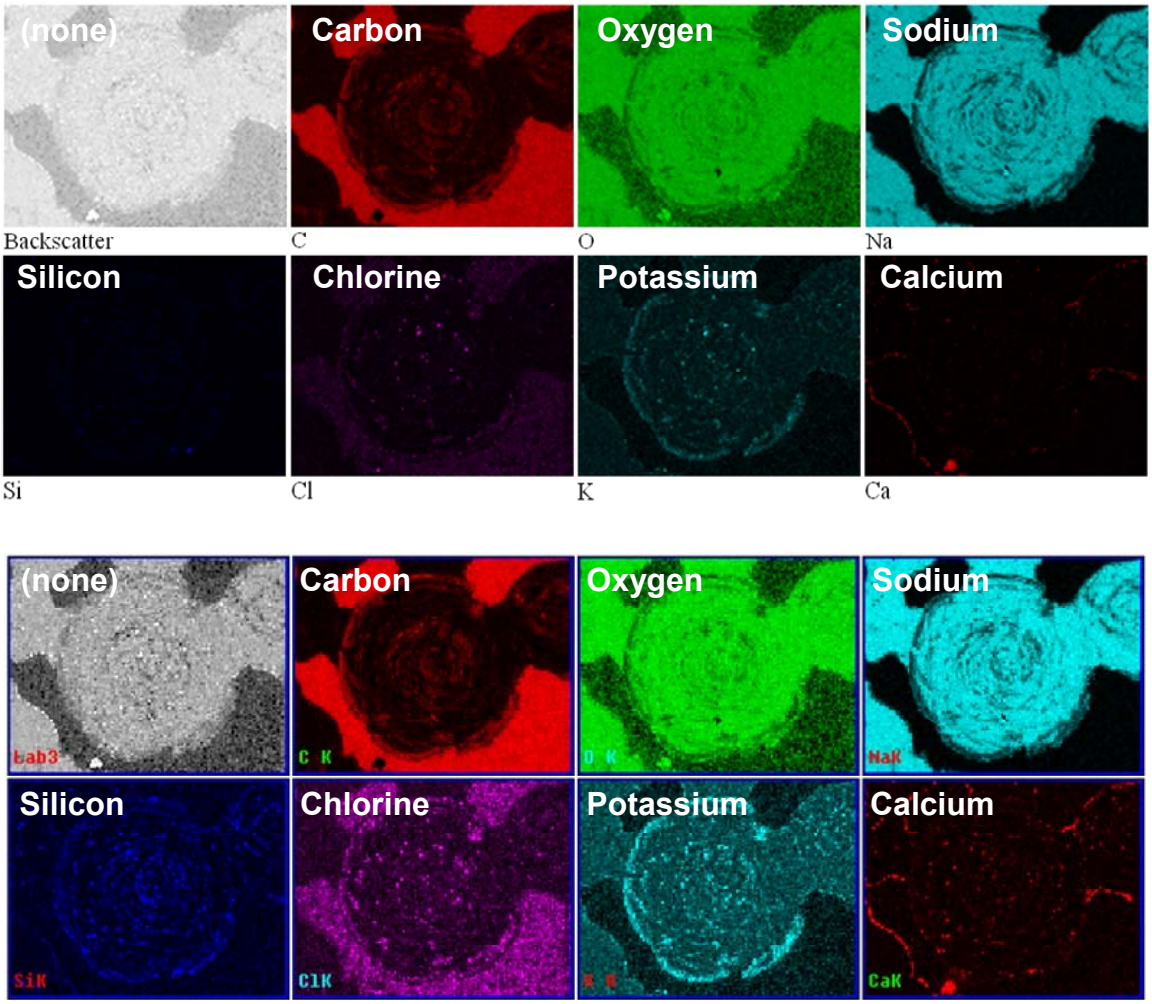

Figure 57. Elemental map created using X-ray analysis on an ESEM. In the upper image, no adjustments have been made and brightness corresponds to concentration (wt%). In the lower image, contrast has been enhanced so brightness does not reflect the concentration.

The images also suggest that layers of carbon are created as the particles are coated time and time again. This is evident by the circles of carbon, potassium, and chlorine that look like swirls in the middle of the particles. Another interesting observation is that the particles which have sintered and formed solid bonds (top right particle Figure 56) have lower concentrations of potassium and chlorine. Figure 58 below is another image to illustrate the outer layer on agglomerated particles.

It appears that the particles are joined first by the thin layer and then the layer dissipates leaving a solid bond between them. Figure 56 shows the solid bond in the top right corner and Figure 59 shows the mixture of the two bonding mechanisms where the larger particle bonds with the smaller particle in the top left corner.

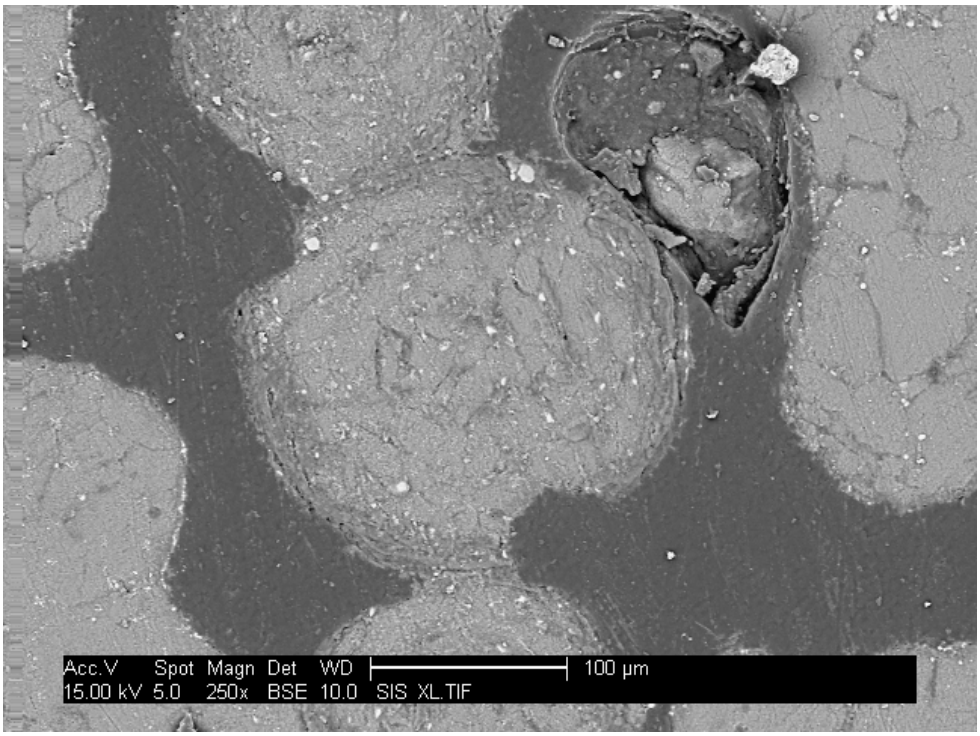

Figure 58. Backscatter image of 2% carbon agglomerated particles illustrating the thin outer layer.

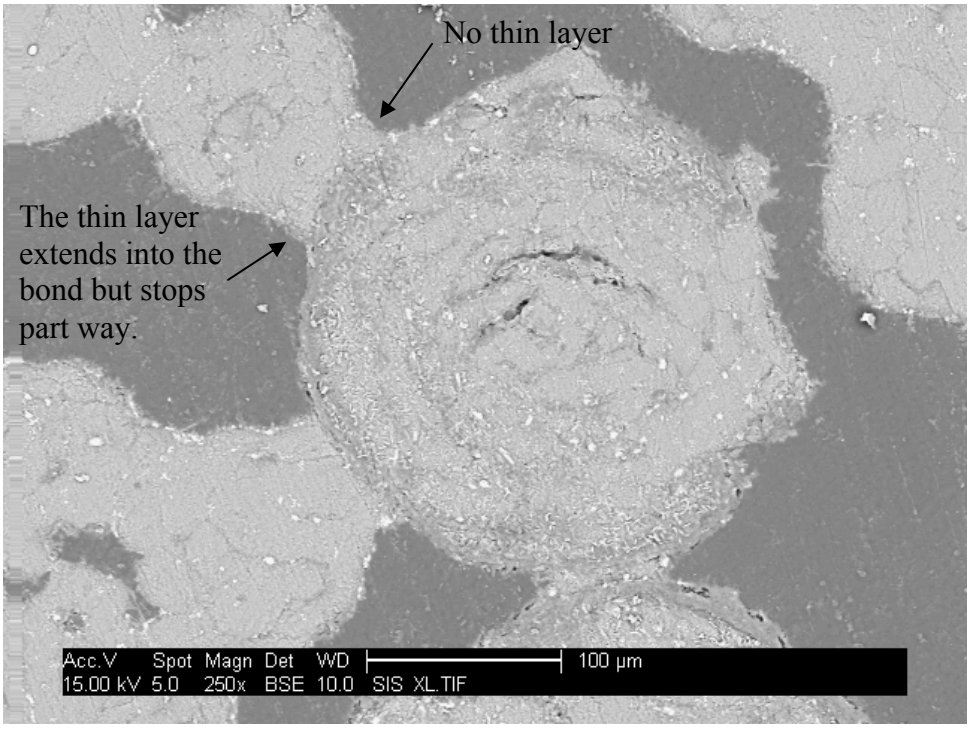

Figure 59. BSE image of 2% carbon agglomerated particles that are beginning to sinter.

A further observation is that the outer layer becomes thinner as the particles are gasified. It also appears that the carbon, potassium, and chlorine in the center of the particles diffuses or reacts away from the center. These two observations are illustrated in Figure 60 to Figure 62, which show backscattered SEM images for particles containing 17%, 2% and 0.3% organic carbon, respectively. The dark spots in Figure 62 are empty pockets and the light gray is small amounts of C, K, and Cl. The decrease in the difference between the contrast of the majority of the particle (white) and the circular swirls (gray) shows a decrease in C, K, and Cl concentrations.

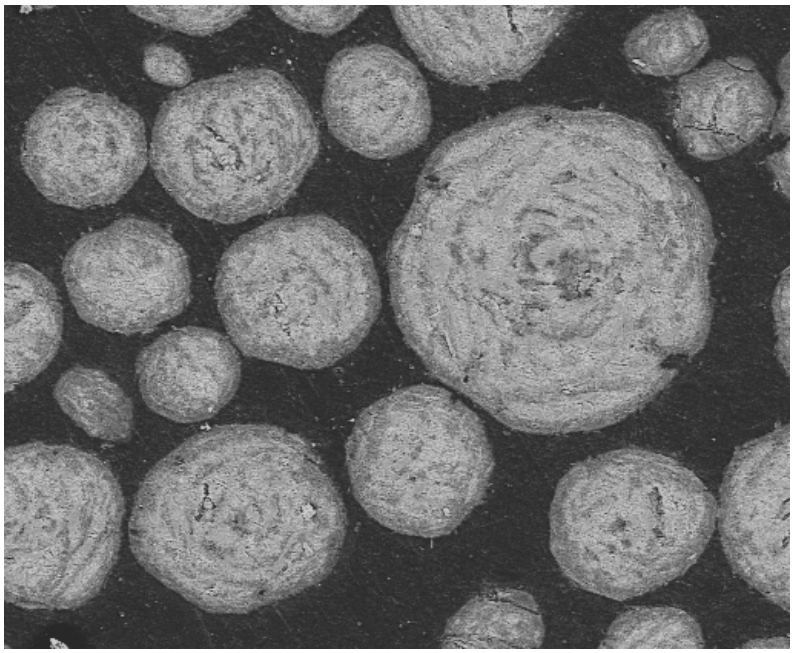

Figure 60. BSE image of 17% organic carbon content particles.

4.1.2.3 Sintering Model

An analytical model was developed to help understand the relationship between the measured heater surface and bed temperatures and the particle size of the bed material. For the entire reactor system at steady state, the energy inflow must equal energy flowing out of the reactor in the form of mass flow and heat transfer (convection and radiation). The energy balance for the reactor is given by Equation 69.

$$\dot{W}_{in,heaters} + \dot{m}_{out} h_{in} = \dot{m}_{out} h_{out} + \dot{Q}_{out,radiation} + \dot{Q}_{out,\,freeconvection} \qquad \text{(Eq. 69)}$$

where:

$\dot{W}$ = energy input to heaters, watts

Q = heat transfer from the system (by radiation or convection), watts

$\dot{m}$ = mass flow, kg/s

h = enthalpy, J/kg

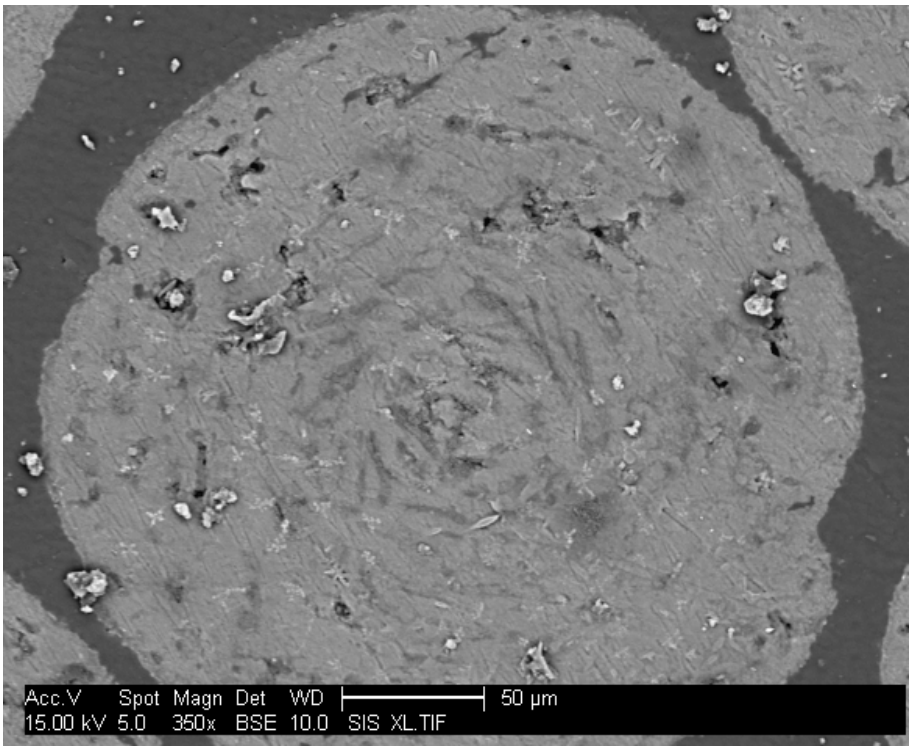

Figure 61. BSE image of 2% organic carbon content particles.

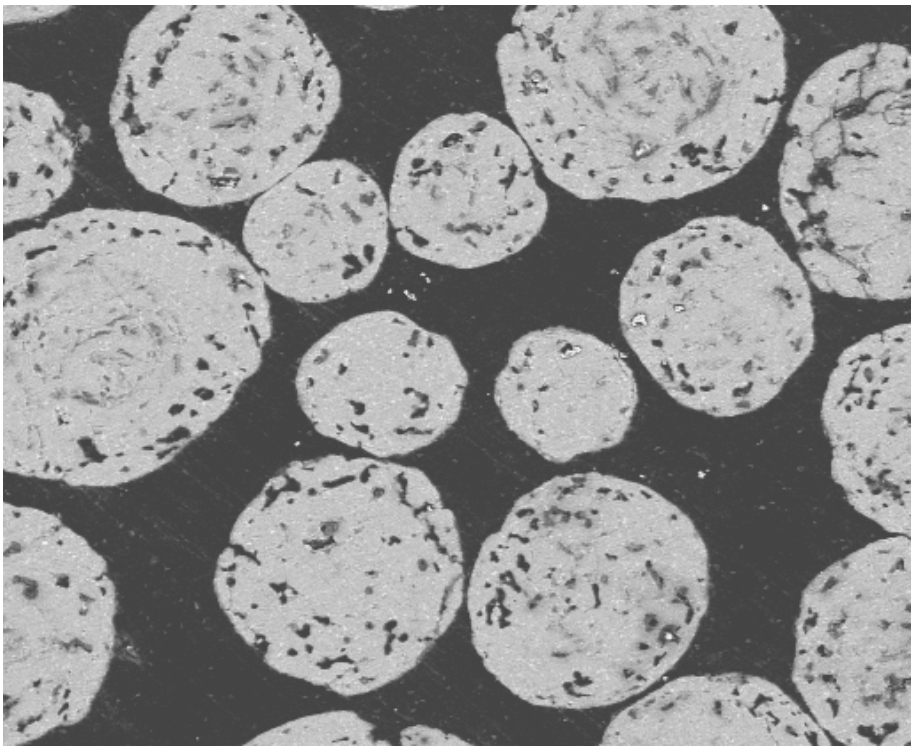

Figure 62. BSE image of 0.3% organic carbon content particles.

Insulating the reactor causes the heat transfer terms to be small in comparison to the remainder of terms in Equation 69. Dropping the heat transfer terms and substitution temperatures for the enthalpy terms gives Equation 70. For the reactor, the electrical work in is equal to the heat transfer from the surface of the heaters to the bed which can be calculated from a heat transfer coefficient and temperature difference as shown in Equation 71. Finally, it should be recognized that the fluidization velocity and not the mass flow was held constant as the bed was heated. Therefore the mass flow rate can be written in terms of velocity as shown in Equation 72.

$$\dot{W}_{in,heaters} = \dot{m} C_p (T_{out} - T_{in}) \quad \text{(Eq. 70)}$$

$$\dot{W}_{in,heaters} = VI = h_{heater} \cdot A_{heater} \cdot (T_{surface} - T_{bed}) \quad \text{(Eq. 71)}$$

$$m_{in} = \rho_{gas} A_r V_{gas} = \frac{P_{reactor}}{R_g T_{bed}} A_r V_{gas} \quad \text{(Eq. 72)}$$

where:

C_p = gas heat capacity, J/(kg·K)
$P_{reactor}$ = reactor absolute pressure, kPa
R_g = gas constant, kPa·m^3/(kmol·K)
h_{heater} = heater to bed heat transfer coefficient, W/(m^2·K)
A_{heater} = total heater surface area, m^2
T_{bed} = bed temperature, K
$T_{surface}$ = heater surface temperature, K
ρ_{gas} = gas density, kg/m^3
A_r = Cross sectional area of the reactor, m^2

Substituting Equations 71 and 72 into Equation 70 gives the final result showing the relationship between the surface and bed temperatures as shown in Equation 73. Equation 73 shows a weak dependence between the temperature in the bed and the difference between the surface and bed temperatures. As bed temperature increases, the temperature difference should approach a constant value for a given heat transfer coefficient (h_{heater}). The heat transfer coefficient is expected to be relatively constant for a given bed particle size, but will decrease as particle size increases. A continuously increasing temperature difference between the surface and bed temperatures is therefore an indication of a decreasing heat transfer coefficient or increasing particle size and sintering in the bed.

$$T_{surface} - T_{bed} = \frac{P_{reactor} A_r V_{gas} \cdot C_{p,g} \cdot (1 - \frac{T_{in}}{T_{bed}})}{R_g \cdot h_{heater} \cdot A_{heater}} = const \frac{(1 - \frac{T_{in}}{T_{bed}})}{h_{heater}} \quad \text{(Eq. 73)}$$

The difference between heater surface bed temperatures were plotted versus bed temperature for two test runs with pure Na_2CO_3 and industrial bed material. Figure 63 shows a comparison of the measured data (symbols) and modeled temperature data (lines) for several fixed particle sizes.

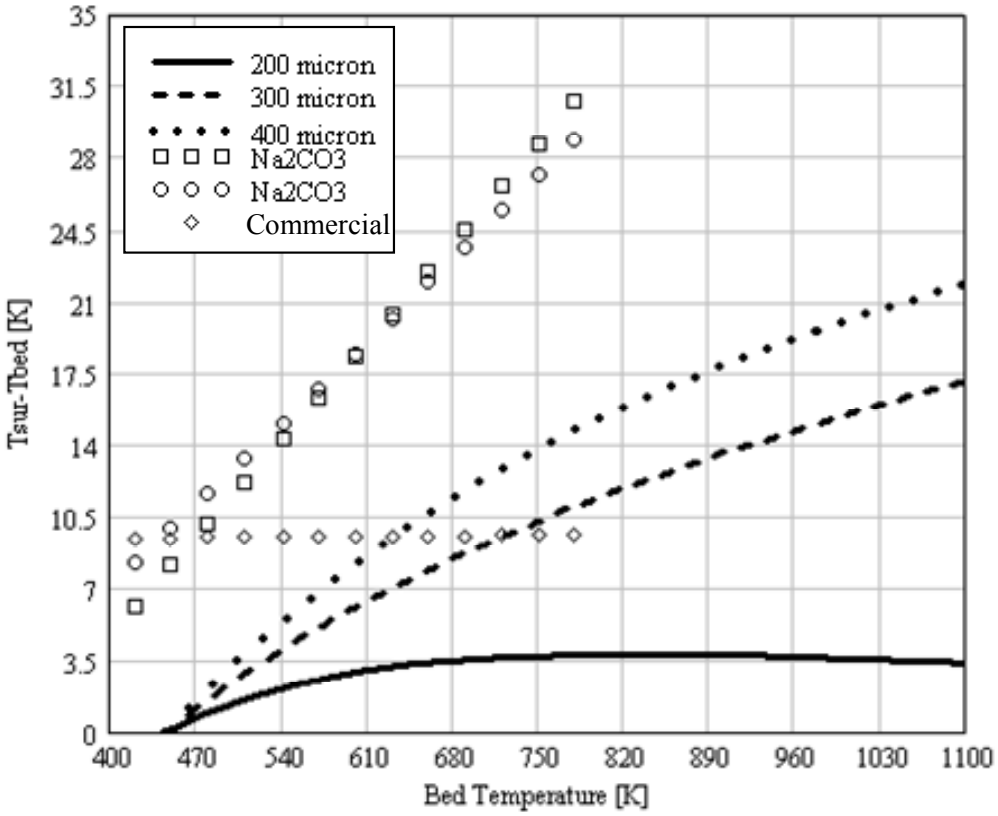

Figure 63. Model results compared to a linear regression of data from two tests with pure Na_2CO_3 and industrial bed material

From the particle size distribution after each run, no change in particle size was detected for the industrial bed material. The slope of the line for this material is flat matching the slope of modeling results for 200 micron particles. The slope of Na_2CO_3 bed material is constant and does not decrease with increasing bed temperature. This can be explained by an increasing particle size indicating that these bed materials were sintering.

4.1.3 Influence of Titanate Addition on Bed Performance

Addition of titanate during black liquor gasification offers many benefits with regard to system operability and pulp mill chemistry. Titanate forms complexes with sodium in the bed to form sodium titanates. The chemistry of titanate during black liquor gasification is detailed elsewhere [46]. One benefit of titanate addition is that, under appropriate conditions, it can effect in-situ causticization of the liquor so that sodium hydroxide is formed upon introduction of the bed material into water or weak wash. From an operational standpoint, titanate is of interest because it increases the melting point of the bed solids. This allows operation at higher temperature, which has positive impacts on both carbon conversion and formation of tars.

Near the end of the overall project, a testing campaign was carried out using the University of Utah reformer, to assess how the bed behaves when operated at high temperature with addition of titanate to the black liquor. Normally, starting bed material is either carbonate-based bed material from previous campaigns or material sent from commercial reformers. However, the melting point of such bed solids are too low for the temperatures targeted in this campaign, and the bed would undoubtedly agglomerate. For this campaign, the starting bed material was alumina (Al_2O_3) particles, sieved to less than 650 microns.

Kraft black liquor from a mill in the southeastern U.S. was used for the testing. The liquor had a solids content of 52% and contained 4.5% sulfur on a dry basis. To prepare the run, titanium dioxide (TiO_2) powder was mixed with the liquor at a ratio of 0.43 kg TiO_2 per kilogram black liquor solids. The resulting mixture had a solids content of approximately 61%.

The system was operated at 715°C (1320°F), which is much hotter than the normal operating temperature of 605°C (1120°F). The titanate-loaded black liquor fed easily. There were no problems either in the holding tank, the recirculation system, feed pump or injector. Liquor conversion was extremely high, in excess of 99%, due to the high temperature. The bed particles did not have the characteristic black color that they normally do, but were instead light tan in color.

In terms of operability, the alumina bed particles that were used for this test fluidized very poorly. While fluidizing velocities with the normal bed particles are on the order of 0.9 to 1.3 ft/sec, it was found that the alumina particles would not fluidize well below 2.5 ft/sec. A significant fraction of particles were carried over, out of the bed, as well. This is due to the high drag resistance associated with the non-sphericity of the particles. Carryover was so significant that alumina sand was found in the condensate drain line from the cooler/condenser downstream of the afterburner. Upon later cleaning and maintenance of the syngas combustion and flue gas cooling systems, in excess of 100 pounds of alumina sand was removed from the system. Figure 64 shows a comparison between the alumina particles used in this test and normal bed particles. From the picture, it is clear why the alumina particles did not fluidize well. Over the course of the test, the bed did seem to behave a little better, presumably as the particles become more rounded due to coating and attrition.

The system was operated with black liquor feed for a total of 24 hours, after which it had to be shut down due to excessive pressure in the afterburner snuffing the natural gas burners. The pressure buildup in the afterburner was caused by partial pluggage of the flue gas channel to the cooler/condenser by carried over titanate particles. Over the 24 hours, operation was reasonably stable.

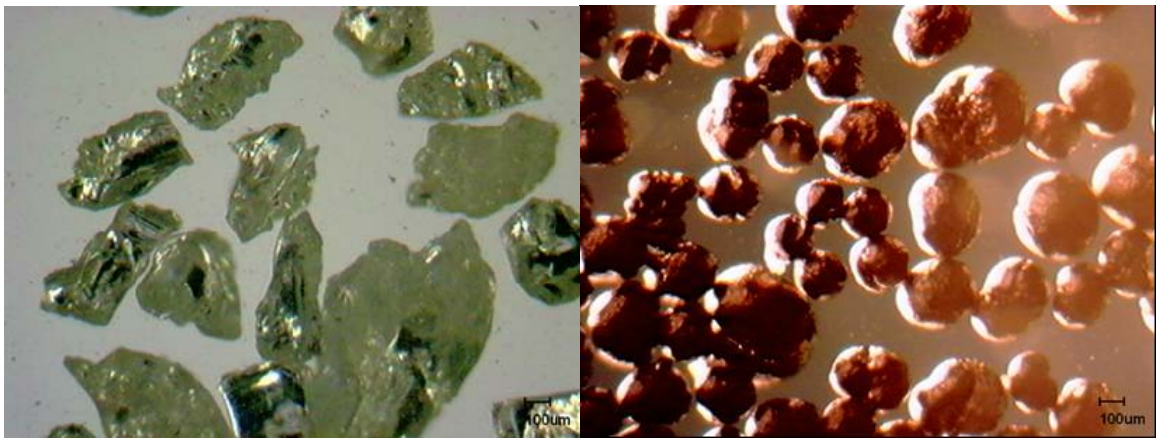

Figure 64. Optical micrographs of alumina (Al_2O_3) particles used in the titanate tests (left) and normal bed particles from a fluidized bed steam reformer (right).

The bed material from the reformer was analyzed to determine the effectiveness of the direct causticization reactions. Four samples of bed material were leached for 1 hour in boiling water. Leacheates were then titrated for NaOH, and Na_2CO_3 with HCl 0.1 N. Table 5 lists the insolubles, NaOH, and Na_2CO_3 of the four samples, as well as corresponding causticity. Overall, causticity values are acceptably large. Insolubles increased with time, which seems contrary to what would be expected as the insoluble alumina particles are coated with the soluble black liquor and associated salts. This may be due to variations in black liquor feed rate.

TABLE 5. CAUSTICITY OF BED SAMPLES FROM TITANATE RUNS

Sample	Insolubles	NaOH	Na_2CO_3	Causticity
Day 2, 11:30	79.8%	17.2%	7.8%	79.1%
Day 2, 15:00	80.9%	14.9%	5.2%	82.9%
Day 2, 17:00	86.4%	11.0%	6.4%	74.7%
Final bed	90.0%	9.6%	3.0%	84.7%

Overall, the titanate tests were considered to be a success. The time for operation was shorter than desired, and the bed was not given sufficient time to come to steady state. There were also operational problems, but those were related to the alumina bed material that was chosen. This was, however, the largest-scale test to date of titanate addition in a fluidized bed steam reformer. The high causticity, the very high carbon conversion and the fact that the bed could be operated at high temperature without agglomeration are encouraging. For future tests, it is recommended that round beads be used as particles. Round alumina beads are apparently difficult to create, and no source for affordable alumina beads has been found. But, perhaps another type of particle, such as zirconia oxide, could be considered.

4.2 Evaluation of Product Gas Quality

The aim of this task was to provide information about the composition and properties of the gas produced in the steam reformer. The first subtask focused on non-condensable species, particularly minor species, while the second subtask focused on condensable hydrocarbons ("tars").

4.2.1 Speciation of Gaseous Products

The product gas from a black liquor steam reformer contains many species in various concentrations. In addition to steam, the primary gases are hydrogen (H_2), carbon dioxide (CO_2), carbon monoxide (CO) and methane (CH_4). Minor species include other light hydrocarbons, hydrogen sulfide and possibly other reduced sulfur compounds, and condensable hydrocarbons ("tars").

4.2.1.1 Importance of water-gas shift reaction

The primary reaction responsible for consumption of bed carbon is that between steam and carbon in the bed material: $H_2O(g) + C(s) \rightarrow H_2(g) + CO(g)$. From this reaction alone, one would expect the gas to consist of steam, H_2 and CO, with H_2 and CO present in equal amounts. But, there are other heterogeneous reactions, as well as gas-phase reactions occurring that affect the final composition of the gas. The most important gas-phase reaction is the water-gas shift reaction: $H_2O(g) + CO(g) \rightarrow H_2(g) + CO_2(g)$.

Gas analysis of operating black liquor steam reformers both with and without liquor injection indicates that, throughout the bed, the gas is at equilibrium with regard to the water-gas shift reaction. At the operating temperature of the steam reformer, homogeneous gas-phase kinetics of the water-gas shift reaction are typically very slow and several hundred hours would be required to achieve equilibrium in a gas-only environment [47,48]. However, the water-gas shift reaction is strongly catalyzed by alkali species [49]. Given the extremely large surface area available in the fluidized bed and the fact that the product gas composition is at equilibrium with regard to the water-gas shift reaction, one can conclude that a fluidized bed black liquor steam reformer is very catalytically active and efficient at driving the water-gas shift reaction to equilibrium.

As a result of the catalyzed water-gas shift reaction, the relative concentrations of H_2, CO and CO_2 in the dry product gas are quite close to equilibrium concentrations, rather than the 1:1 H_2:CO ratio one would expect from the steam reforming reaction alone. The high partial pressure of water and the equilibrium ratio at steam reforming temperatures pushes the water-gas shift reaction shown above to the right, so there is relatively little carbon monoxide in the gas, and correspondingly high concentrations of CO_2. Results from tests in the Utah reformer, feeding pure steam and with no liquor injection (thus forcing the steam-carbon reaction to occur) indicate that the CO_2 to CO ratio is on the order of 10 to 1. This is also predicted by computational modeling.

4.2.1.2 Measured gas compositions

The gas conditioning and analysis procedure, including the gases that could be analyzed by gas chromatography, were described in Section 2.1.7.1. Most, but not all, of these species were detected in the gas. A typical gas analysis for operation under standard conditions is shown in Table 6. Closure was a bit high, with the sum of all gas species totaling 107%. The nitrogen concentration in the Utah reformer is significantly higher than in an full-scale system due to its relatively small size and need for nitrogen purge. Also, by the presence of oxygen it appears that there was an air leak into

the system. The normalized, nitrogen and oxygen-free gas composition is the most appropriate comparison to that expected from a full-scale system. Hydrogen content was high, 59% on a normalized basis. The carbon monoxide concentration is low, and the gas has clearly shifted as described in the previous section. For this set of conditions, the heating value (HHV) of the normalized nitrogen and oxygen-free gas is 299 Btu/scf (12.0 MJ/Nm^3).

TABLE 6. TYPICAL GAS CHROMATOGRAPH GAS ANALYSIS

Gas Species	Raw concentration (vol%)	Normalized, N_2 and O_2-free (vol%)
Hydrogen	42.40	59.10
Carbon monoxide	4.04	5.63
Carbon dioxide	19.70	27.46
Methane	4.44	6.18
Ethane	0.46	0.64
Ethylene	0.21	0.29
Propane	0.08	0.11
Propylene	0.36	0.51
n-Butane	0.013	0.019
Isobutane	0.003	0.003
n-Pentane	0.039	0.054
Nitrogen	31.08	—
Oxygen	4.17	—

Results of a second analysis of one of the tests is shown in Table 7. Overall, the composition is similar to that presented in Table 6. The raw analysis indicated a small quantity (0.96%) of oxygen, indicating a small air leak in the sampling system. The raw gas also contained roughly 20% nitrogen which came from purge streams and nitrogen in the air leak. The corrected gas concentrations, subtracting the contributions of nitrogen and oxygen and normalized to 100%, are also shown in the table. The gas is high in hydrogen, roughly 53% by volume, and contains hydrocarbons as high as C5 (pentane). The measured concentration of propylene is very suspect. The expected concentration of this molecule is on the order of 0.1%, since it is a somewhat large, double-bonded gas-phase molecule. It is possible that a gas species that was not calibrated for overlapped with propylene or was near that peak. The concentration of butane also seems high. Based on the normalized N_2 and O_2-free gas, the heating value (HHV) of the syngas is 264 Btu/scf (10.6 MJ/Nm^3).

GC analysis was performed during the tests with titanate addition, when kraft liquor containing 4.5% sulfur was run. The measured gas composition was similar to that shown in Table 6 and Table 7, except that the gas contained approximately 1.1 hydrogen sulfide (H_2S) on a nitrogen and oxygen-free basis.

Efforts were made to correlate product gas composition with operating conditions in the steam reformer. No clear trends could be identified, however, when nitrogen- and oxygen-free conditions were compared. Methane concentrations did seem to vary more than the other gases, but were still in a relatively narrow range of 4-7% by volume.

TABLE 7. SECOND TYPICAL GAS CHROMATOGRAPH GAS ANALYSIS

Gas Species	Raw concentration (vol%)	Normalized, N_2 and O_2-free (vol%)
Hydrogen	46.03	53.04
Carbon monoxide	3.86	4.45
Carbon dioxide	27.12	31.25
Methane	4.32	4.98
Ethane	0.42	0.48
Ethylene	0.31	0.36
Propane	0.58	0.67
Propylene	2.90	3.34
n-Butane	1.20	1.38
Isobutane	0.004	0.005
n-Pentane	0.045	0.052
Nitrogen	19.68	—
Oxygen	0.96	—

4.2.2 Characterization and Destruction of Tars

Much of the program focused on tars, since tars are known to be a significant operational problem in all biomass gasification systems. The University of Utah system was operated under a variety of conditions to identify operating variables that affect tar production. In addition, tars formed in a full-scale system were analyzed to determine their composition.

4.2.2.1 Measurement of Total Tars under Different Operating Conditions

Several testing campaigns were devoted to identifying the influence of operating conditions on tar formation. For these, tar was captured using a dichloromethane-based impinger system, then isolated by evaporation as described in Section 2.1.7.2. The volume of dry gas sampled during tar isolation was recorded, so the concentration of tars in the dry product gas (g/scm or lb/scf) could be calculated. The fraction of fuel or organic carbon that forms tars could also be calculated if the dry gas production rate and liquor solids feed rate were known. This was estimated for each of the tar measurements, but there is uncertainty since not enough data was available to close the carbon balance on the system. Also, in many cases several tar samples were collected at different conditions within one day and the reformer did not fully achieve steady state, particularly with regards to carbon content in the bed. The analysis to determine tar production as a function of organic carbon content forces a mass balance on sodium to get the solids removal rate and overall mass flows to get the product gas flow rate. The elemental hydrogen balance usually closed quite well (within ±10%) using this method and the product gas H_2 concentration measured by the CEM. Closure of the carbon balance was generally worse, ranging from 86% to 207%, with most values around 125% based on carbon in CO, CO_2 and estimated CH_4.

Reproducibility of Tar measurements. Three tar samples were taken under identical conditions over the course of one day. These were subsequently analyzed, and results are presented in Figure 65. The reproducibility of the tar measurements proved to be quite good. The calculated normalized

95% confidence interval (normalized by dividing by the average), expressed as a percent, is ±16% in terms of tar loading (lb/scf dry) and ±7% in terms of organic carbon to tars. These intervals are included as error bars in all subsequent results.

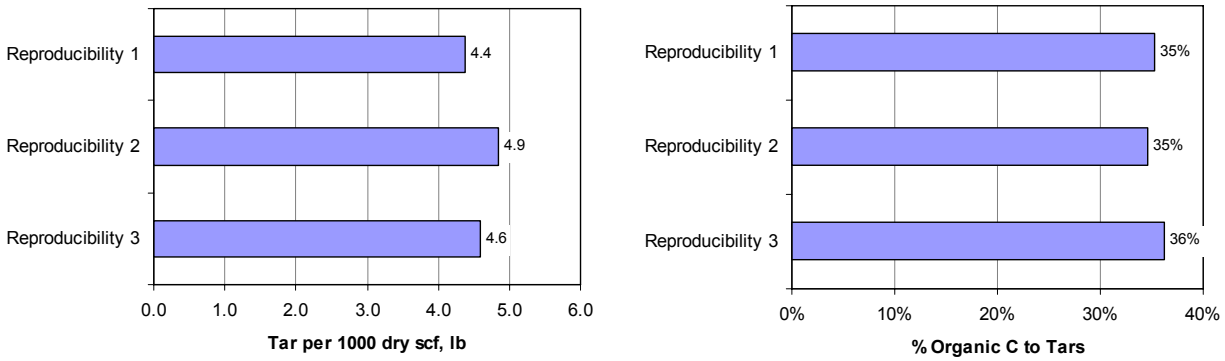

Figure 65. Reproducibility of tar measurements, shown in "raw" form as mass of tar condensed per dry standard gas volume (left) and calculated fraction of organic carbon forming tars (right). All runs conducted with 32 lb/hr steam, 11.4 lb BLS/hr liquor flow and 1120°F (604°C) bed temperature. Note that values are estimated to be 65-70% too high, as discussed in Section 2.1.7.2.

Influence of temperature on tar production. A series of tests was performed in which the fluidized bed was operated at three different temperatures: 566, 604 and 643°C (1050, 1120 and 1190°F). The resulting tar loading and calculated fraction of organic carbon converted to tars are shown in Figure 66. Clearly, less tar was produced at higher temperatures. This agrees with experience and lab-scale studies of biomass tar production. As temperature increases, the tars are thermally broken down to a larger extent.

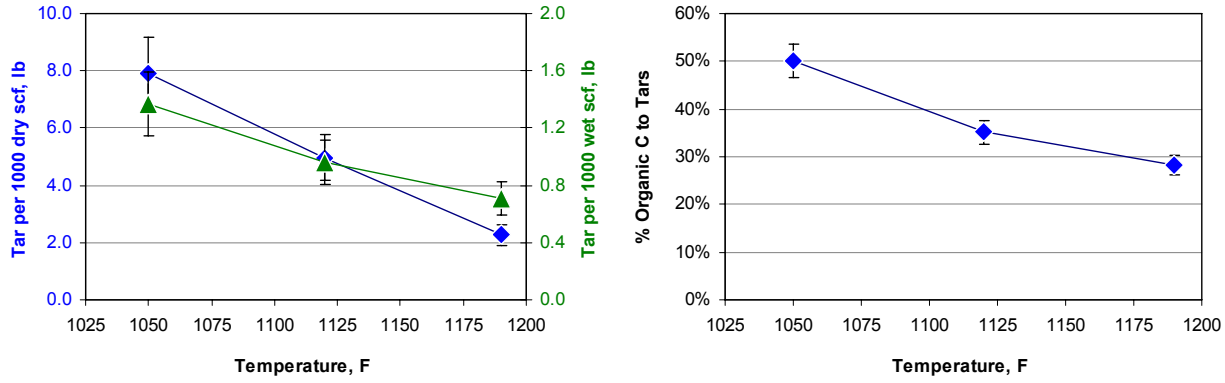

Figure 66. Tar production as a function of bed temperature. Mass of tar condensed per dry standard gas volume (left) and calculated fraction of organic carbon forming tars (right). All runs were conducted with 33 lb/hr steam flow and 8.3 lb BLS/hr liquor. Note that values are estimated to be 65-70% too high, as discussed in Section 2.1.7.2.

Influence of black liquor flow rate on tar production. Two campaigns were conducted to identify how black liquor flow rate affects tar production. In "Series 1," the fluidized bed was allowed to come to steady state over several days at a flow rate of roughly 25 lb/hr liquor (14 lb/hr dry solids). During the morning of the sampling day, the liquor flow rate was increased to 38 lb/hr (21 lb/hr solids) and maintained for only a short while (less than one hour) before tar sampling commenced. It took roughly 30 minutes to sample 200 liters of dry gas. Immediately after this, the flow rate was adjusted downwards to the base value of 25 lb/hr liquor (14 lb/hr solids). Sampling at this flow rate began 2.5 hours after the flow had been re-adjusted. At the conclusion of this "medium" flow rate sampling, the liquor flow rate was adjusted downwards to 13 lb/hr liquor (7 lb/hr solids). The final sampling commenced roughly 1.5 hours after the liquor flow rate had been turned down. For this first series, all runs were conducted with a steam flow of 33 lb/hr and a bed temperature of 1120°F.

In "Series 2," the system had been allowed to stabilize for several days at a liquor feed rate of roughly 18 lb/hr (10 lb/hr solids). The flow rate was turned down to 5.8 lb/hr (3.1 lb/hr solids), representative of the liquor flow/bed solids ratio used in the technology developer's PDU, during the morning. After about 1 hour at this flow rate, sampling commenced. When sampling was completed 30 minutes later, the flow rate was increased back to 18 lb/hr (10 lb/hr solids). The second measurement at the higher flow rate was begun about 3 hours after the flow had been increased again. For this second series, all runs were conducted with a steam flow of 33 lb/hr and a bed temperature of 1125°F.

Results from both series of tests are displayed in Figure 67. Clearly, both series of tests indicated the same behavior. Tar concentration in the gas increased with liquor flow rate, but was stable in terms of the amount of organic carbon in the liquor ending up in tars.

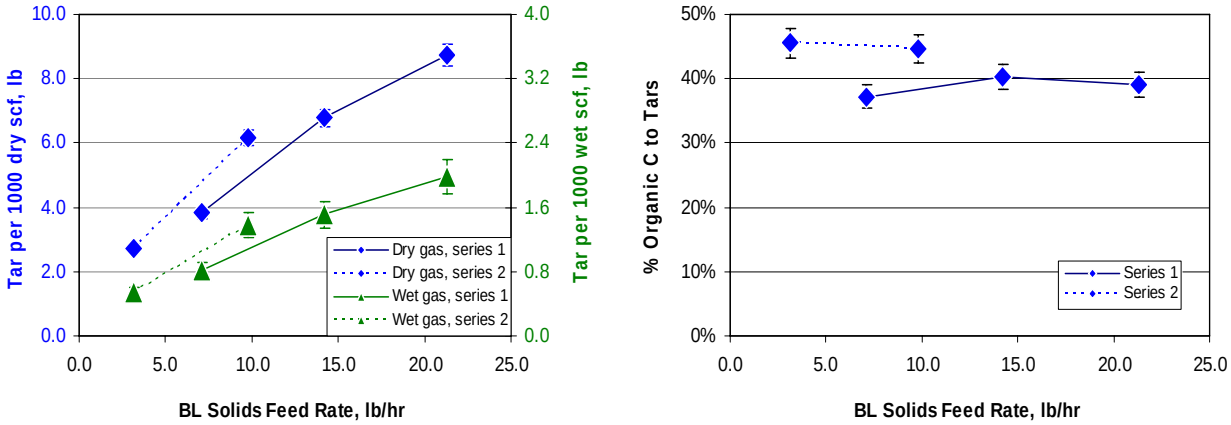

Figure 67. Influence of black liquor flow rate on tar production. Two different series of tests, performed during two different campaigns, are indicated. Left figure shows the measured concentrations of tars in the dry and wet gas. Right figure shows the calculated fraction of organic carbon in the black liquor that ends up as tars. All runs were conducted with a steam flow of 33 lb/hr and a bed temperature of 1120°F (604°C). The error bars in the figures represent a 90% confidence interval. Note that values are estimated to be 65-70% too high, as discussed in Section 2.1.7.2.

These results are not consistent. Specifically, there is discrepancy between the concentration in the dry gas and the fraction organic C resulting as tars. Dry gas production should be nearly proportional to liquor flow rate. (The total flow of purge nitrogen to the system accounts for roughly 10% of the dry gas flow.) If the same fraction of liquor organic carbon is forming tar, one would expect the blue lines in the left graph to be essentially flat, since the two increasing numbers (tar production and dry gas flow) would have basically the same ratio. This was not observed.

This inconsistency is thought to result from the fact that the system, specifically bed carbon, was not allowed to achieve steady state between measurements. Steady state carbon content in the bed is known to increase at higher liquor feed rates. When the liquor flow was increased for the measurement at high flow in Series 1, much of the additional carbon introduced to the system was staying in the bed to increase its carbon content to a higher value consistent with the high liquor flow. This carbon would have otherwise formed dry gas by heterogeneous reaction with steam, so the dry gas flow was unrepresentatively low and the corresponding tar concentration in the dry gas unrepresentatively high. As the liquor flow was successively lowered, the bed had a higher concentration of carbon than would exist at steady state at the given liquor flow. So, an unrepresentatively high amount of bed carbon was being converted to dry gas, resulting in unrepresentatively low tar production/dry gas flow ratios. A similar effect resulted in Series 2. This observation underscores the importance of allowing the system, particularly the bed carbon content, to stabilize before sampling tars.

The apparent lack of correlation between tar production and liquor flow rate in these tests is inconsistent with what has been observed in full-scale reformers. This could be a consequence of the very low liquor flow in the University of Utah system, and the fact that, on a volumetric basis, most of the flow through the injector is steam. This results in a disperse spray exiting the injector. Under a given set of conditions (temperature, heating rate, gas environment), a certain portion of the black liquor will form tars. With the relatively low fuel/steam ratio in the Utah system, all black liquor is seeing identical conditions, undergoing the same time-temperature history, within the range of flows tested. In the full scale system, where the majority of the flow through the injector is liquor, the liquor stream exiting the injector is much more concentrated. As more liquor is pushed through the injector, more water evaporates and there is less contact between the bed and the liquor, resulting in slower heating rates and a flatter temperature-time history. In addition, the local chemistry in the injection zone in the full scale system is much more hydrocarbon-rich than in the Utah development system, which could affect tar formation.

Influence of air addition on tar production. Two different campaigns were conducted to study the influence of air injection on tar formation in the gasifier. In the first campaign, air was injected through the fluidizing grid in one test and through the liquor injector in another test. Black liquor flow was 21 lb/hr (9 lb/hr solids for a weaker-than-normal 44% solids liquor). In the first test with air, the fluidizing steam flow rate was decreased by 12% and a corresponding amount of air (volumetric basis) was injected into the steam line immediately downstream of the superheater. The fluidizing velocity was thus maintained. This air dilution did cause the incoming steam (steam/air) temperature to drop slightly, from 1120°F to 1050°F. The system was allowed to operate under these conditions for 35 minutes before sampling began. After tar sampling was complete the system was restored to 100% steam for fluidizing. The second test involved feeding the same "12%" flow rate of air through the injector, which consisted of a tube feeding both liquor and steam. This "12% air" flow was approximately the same on a volumetric basis as the steam flow that had been running through

the injector. Steam flow through the grid was not adjusted, so the fluidizing velocity remained the same. In neither of these tests was the air pre-heated.

In the second campaign, the black liquor flow was slightly higher (24 lb/hr, or 13.4 lb/hr solids for a 56% solids liquor) and the amount of air injected was increased to 18%. In addition, the air was pre-heated to 1000°F when feeding through the distributor and 250°F when feeding through the liquor injector. Unfortunately, the air line was not insulated so it cooled significantly before being introduced to the distributor so the fluidizing gas temperature dropped to 978°F. Otherwise, the tests were conducted in the same manner as for the previous 12% air addition tests.

Results of both of these campaigns are shown in Figure 68. It does indeed appear that introducing air has a positive effect on tar production. However, the values in the left-hand graph are misleading because nitrogen in the air diluted the gas, particularly the dry gas, thereby resulting in exceptionally low tar concentrations. Corrected data are shown in Figure 69, where the incoming flow of nitrogen in the air was subtracted from the product gas. By the nature that the mass balance was performed, the calculated values for % organic C to tars do not need to be corrected. The tests where 12% air was injected show no statistically significant effect of air injection through the fluidizing grid, but there does seem to be a small positive effect of injecting air through the liquor injector. The tests with 18% air do show a positive, statistically significant influence on tar production.

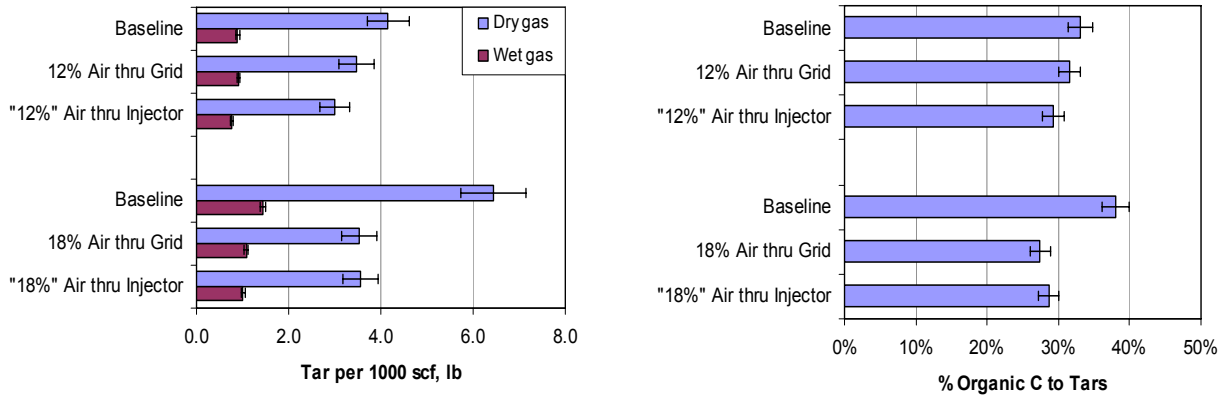

Figure 68. Uncorrected data showing the influence of introducing air into the system, either by displacing a portion of the fluidizing steam ("thru grid") or by substituting air for the injector steam. Left figure shows the uncorrected measured concentrations of tars in the dry and wet gas. Right figure shows the calculated fraction of organic carbon in the black liquor that ends up as tars. The error bars in the figures represent a 90% confidence interval. All runs conducted at 1120°F (604°C) fluidizing gas volumetric flow corresponding to 33 lb/hr steam and constant liquor flow rate for a given series. Note that values are estimated to be 65-70% too high, as discussed in Section 2.1.7.2.

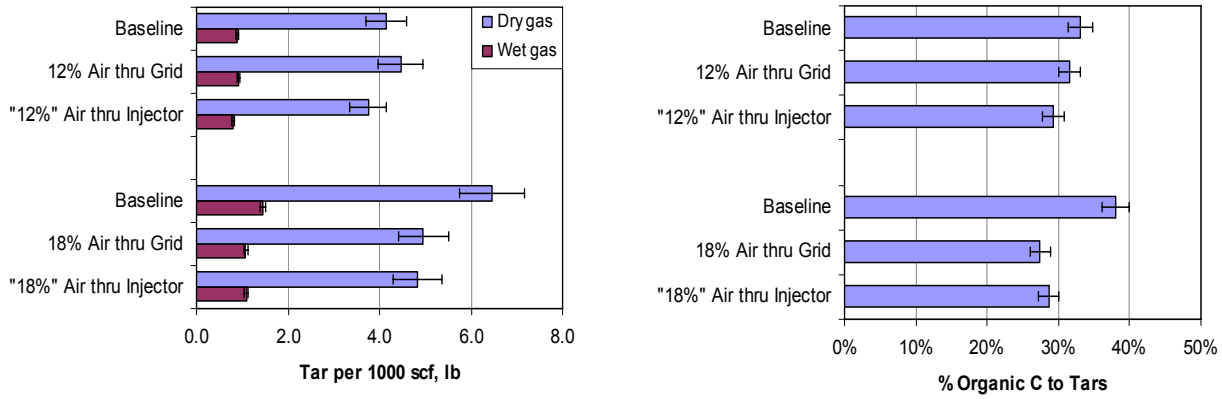

Figure 69. Corrected measurements indicating the influence of air addition. Corrected values in the left graph take into consideration dilution by nitrogen in the injected air. Note that values are estimated to be 65-70% too high, as discussed in Section 2.1.7.2.

Influence of fluidizing steam temperature on tar production. A series of measurements was taken which included operation with a low fluidizing steam temperature (895°F compared to normal fluidizing steam temperature of 1120°F). Results of these measurements are shown in Figure 70. The tar concentrations and fraction organic carbon to tar for the two tests do not fall outside the confidence intervals, so based on these data there is no statistically significant effect of fluidizing steam temperature on tar production. This is not surprising. Fluidized beds are very well mixed, uniform-temperature systems with excellent solid-gas heat transfer. So, the fluidizing steam is heated to the bed temperature almost immediately upon introduction. This was confirmed in this test by a thermocouple located 4 inches above the fluidizing grid, which showed the same temperature for both fluidizing steam temperatures.

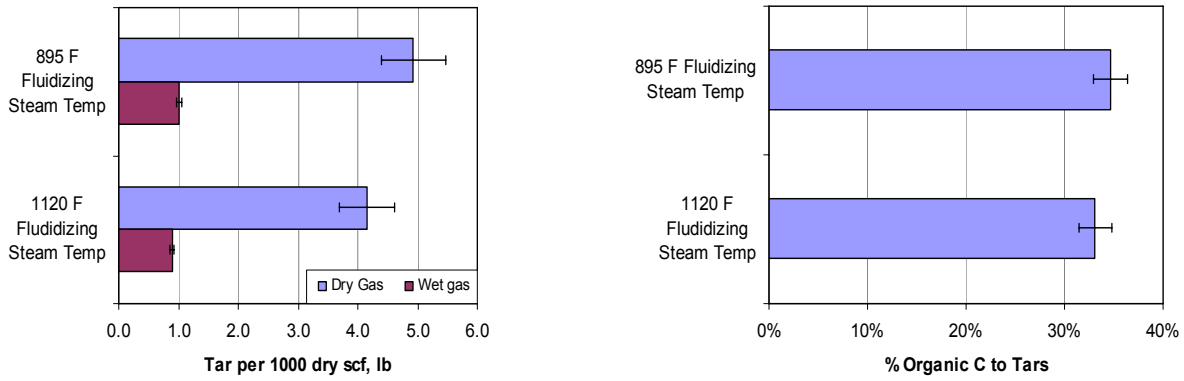

Figure 70. Influence of steam fluidizing temperature on tar formation. Left figure shows the measured concentrations of tars in the dry and wet gas. Right figure shows the calculated fraction of organic carbon in the black liquor that ends up as tars. The error bars in the figures represent a 90% confidence interval. All runs performed at a bed temperature of 1120°F (604°C). Note that values are estimated to be 65-70% too high, as discussed in Section 2.1.7.2.

Influence of fluidizing velocity on tar production. A test was performed to study how fluidizing velocity affects tar production. A baseline test was run at the standard fluidizing velocity of 0.95 ft/s. In a subsequent test, the fluidizing velocity (steam flow rate) was increased by 50% to yield a fluidizing velocity of 1.42 ft/s. Black liquor flow was 18 lb/hr (10 lb/hr solids). For these tests, there was no statistically significant influence on tar production, as seen in Figure 71.

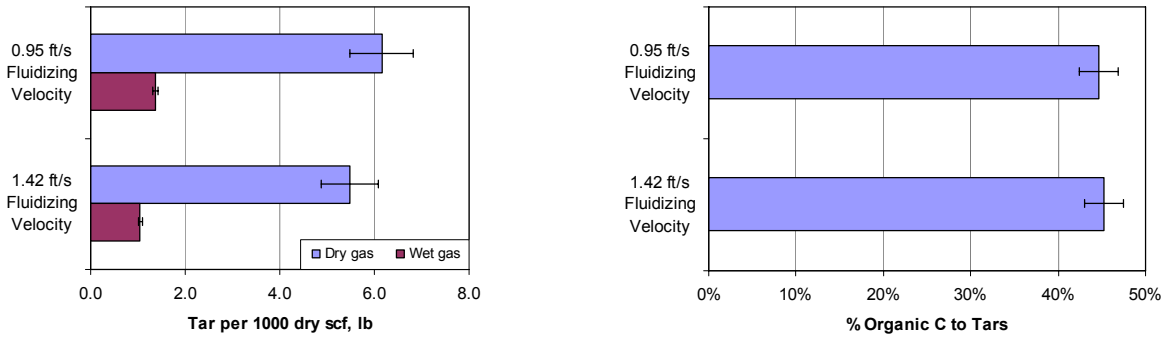

Figure 71. Influence of fluidizing velocity on tar production. Left figure shows the measured concentrations of tars in the dry and wet gas. Right figure shows the calculated fraction of organic carbon in the black liquor that ends up as tars. The error bars in the figures represent a 90% confidence interval. All runs performed at 1120°F (604°C) bed temperature and 9.8-10.0 lb/hr BLS flow. Note that values are estimated to be 65-70% too high, as discussed in Section 2.1.7.2.

Influence of potassium hydroxide addition on tar production. Potassium is known to catalyze tar destruction under certain conditions. It has been suggested that perhaps adding potassium to the steam reformer would catalyze tar destruction. A test was conducted in which potassium hydroxide was added to the black liquor to see if it could encourage catalytic tar cracking. For the final run of the day, concentrated potassium hydroxide was added to increase the concentration of potassium from roughly 6% K/(Na+K) to 15%. This liquor was allowed to run through the system for several hours before sampling was conducted. Results are shown in Figure 72. For these tests, there is no statistically significant effect of potassium hydroxide addition, particularly in terms of the fraction organic carbon in the liquor ending up as tars.

4.2.2.2 Characterization of Tars formed under Different Operating Conditions

Part of the focus of this project was on characterizing the tars that have been sampled and isolated, as described in the previous section. All concentrated tar samples from the University of Utah reformer were analyzed by gas chromatography (FID detector), and select samples were analyzed by gas chromatography-mass spectroscopy (GC-MS). A typical GC-MS analysis is presented in Figure 73, with several of the major peaks identified. The tars are primarily mono-, di- and tri-substituted one and two-ring phenolic compounds.

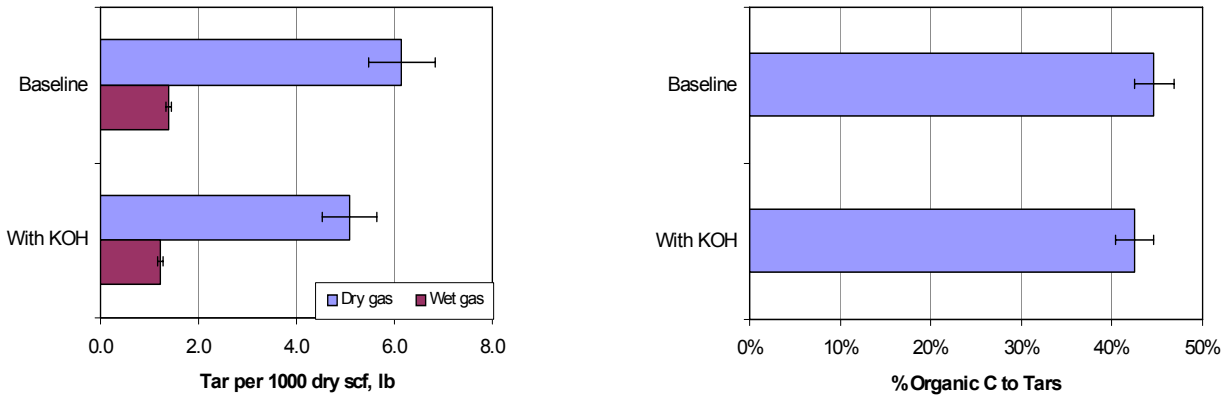

Figure 72. Influence of potassium hydroxide addition on tar production. Left figure shows the measured concentrations of tars in the dry and wet gas. Right figure shows the calculated fraction of organic carbon in the black liquor that ends up as tars. The error bars in the figures represent a 90% confidence interval. Note that values are estimated to be 65-70% too high, as discussed in Section 2.1.7.2.

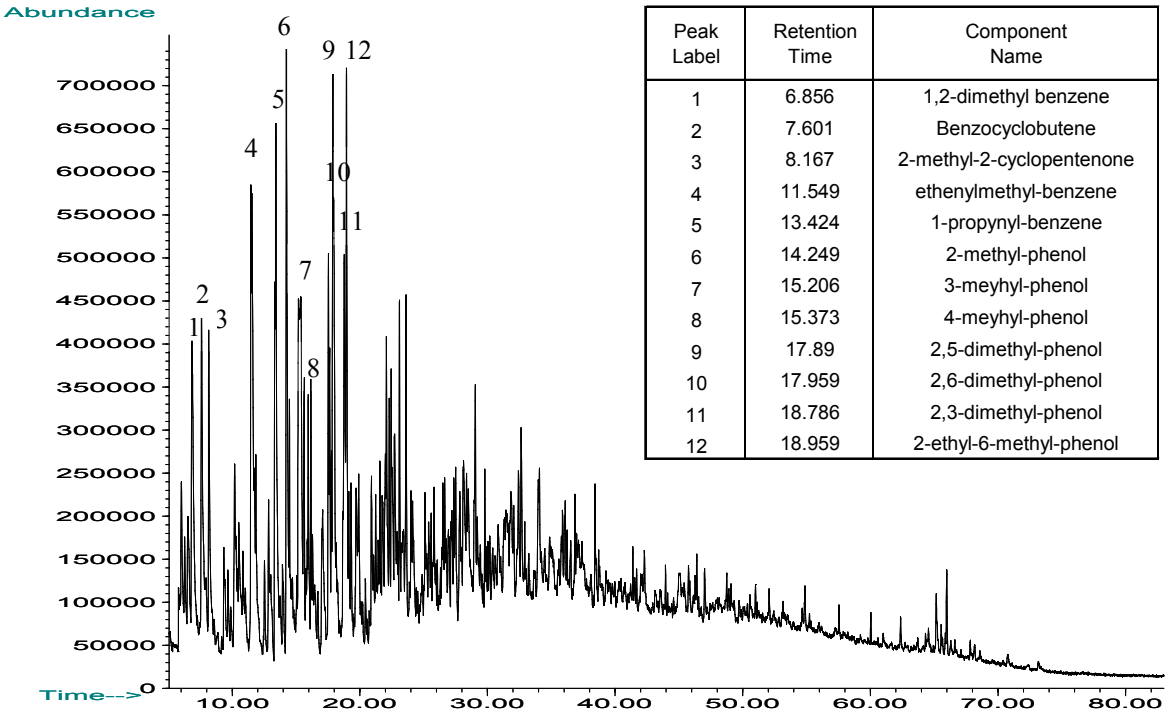

Peak Label	Retention Time	Component Name
1	6.856	1,2-dimethyl benzene
2	7.601	Benzocyclobutene
3	8.167	2-methyl-2-cyclopentenone
4	11.549	ethenylmethyl-benzene
5	13.424	1-propynyl-benzene
6	14.249	2-methyl-phenol
7	15.206	3-meyhyl-phenol
8	15.373	4-meyhyl-phenol
9	17.89	2,5-dimethyl-phenol
10	17.959	2,6-dimethyl-phenol
11	18.786	2,3-dimethyl-phenol
12	18.959	2-ethyl-6-methyl-phenol

Figure 73. GC-MS chromatogram of a typical tar sample from the small-scale steam reformer.

Variation with process conditions. It is useful to consider how the composition and physical nature of the concentrated tars varied as a function of operating conditions. The various tar samples were all subjected to analysis by gas chromatograph using a flame ionization detector (FID). Select samples were also analyzed by gas chromatograph-mass spectroscopy (GC-MS) to identify components in the tars. Figure 74 shows GC-FID chromatograms of twelve concentrated tar samples, taken during operation under a variety of conditions. Clearly, the chromatograms are all nearly identical, indicating that the composition of the tar material is relatively independent of the operating conditions tested.

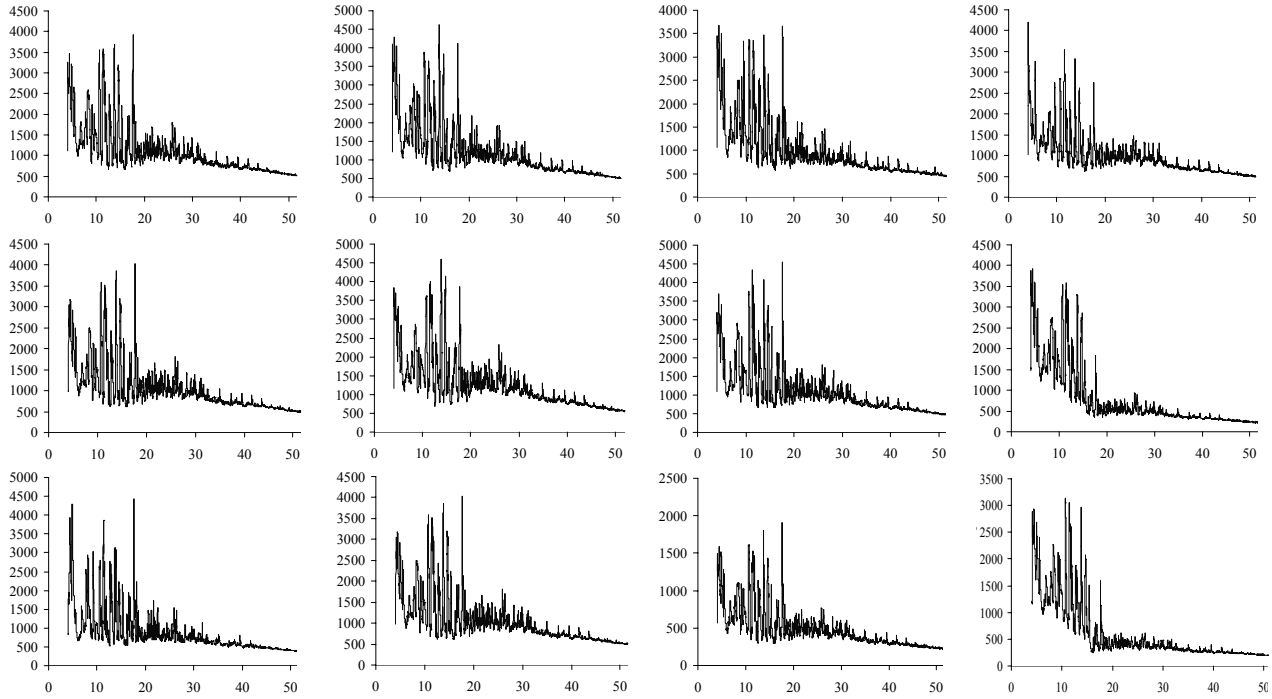

Figure 74. GC-FID analysis of several different tar samples, taken under different operating conditions.

The similarity of the tar "fingerprint" for samples from a full-scale reformer and the University of Utah reformer is also notable. Figure 75 shows such a comparison. The industrial sample was taken from the exit gas line of the Georgia-Pacific Big Island reformer by Georgia Institute of Technology, and analyzed in a manner similar to how samples from the Utah gasifier were analyzed. The two chromatograms from similar operating conditions are stretched such that phenol and phenanthrene line up. Clearly the compositions of the two samples are similar. This is consistent with the observation above that tar composition is relatively independent of operating conditions.

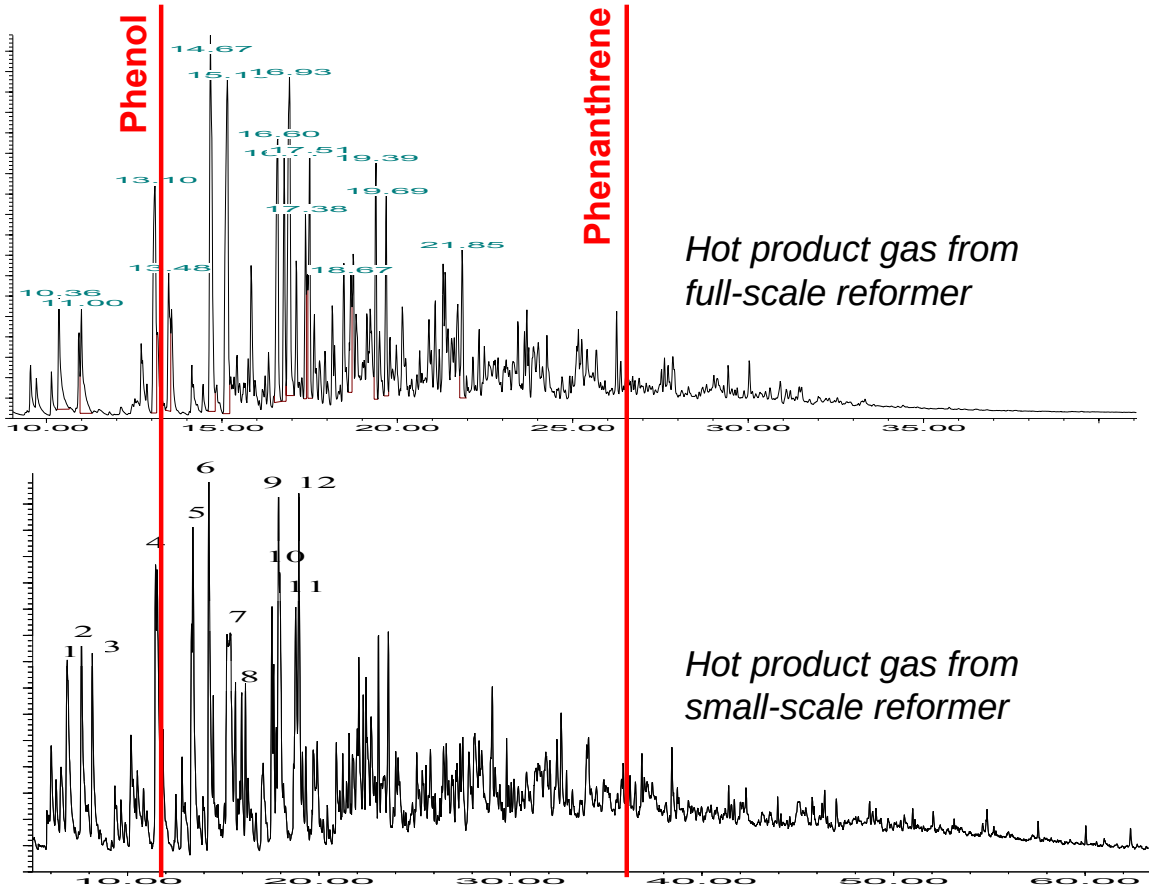

Figure 75. Comparison of "fingerprints" of tars in the product gas of a full-scale black liquor steam reformer and the University of Utah steam reformer, as measured by GC-MS. The chromatograms were stretched such that phenol and phenanthrene line up. Clearly, the samples are similar.

TGA analysis. An additional analysis that was performed involves measuring the volatility of tar samples as a function of temperature. This has been done for the tar samples that were isolated previously in the program by using a thermogravimetric analyzer (TGA), which tracks the weight of a sample as temperature changes. For these studies, the tar samples were slowly heated from room temperature to 1000°C in a pure nitrogen environment while the weight was monitored. Prior to the experiments, the samples were kept overnight at 50°C to remove dichloromethane, since it had come to our attention by this time that the samples did contain residual solvent. As tar components evaporated, the sample weight decreased. High volatile compounds were released first, followed by less-volatile, generally heavier compounds.

As with the GC analysis, little variation was observed in the volatilities of the various tar samples. Most of the curves differed from one another by a statistically insignificant amount, as determined by reproducibility runs with one of the samples. For tars collected while running the system at different temperatures, however, the volatilities did differ by a statistically significant amount. Figure 76 shows the mass loss curves for tars isolated when operating at different temperatures. Increasing the

bed temperature corresponds to increased tar volatility, suggesting that the components in the tar mixture are less complex. High temperatures promote most of the gasification reactions. However, heavy multiring tar formation is also aggravated from the repolymerization of broken aromatic rings. The results obtained suggest that even at the highest temperature tested these repolymerization reactions did not increase the molecular complexity of the tar mixture, implying that repolymerization reaction were not fast enough at these temperatures.

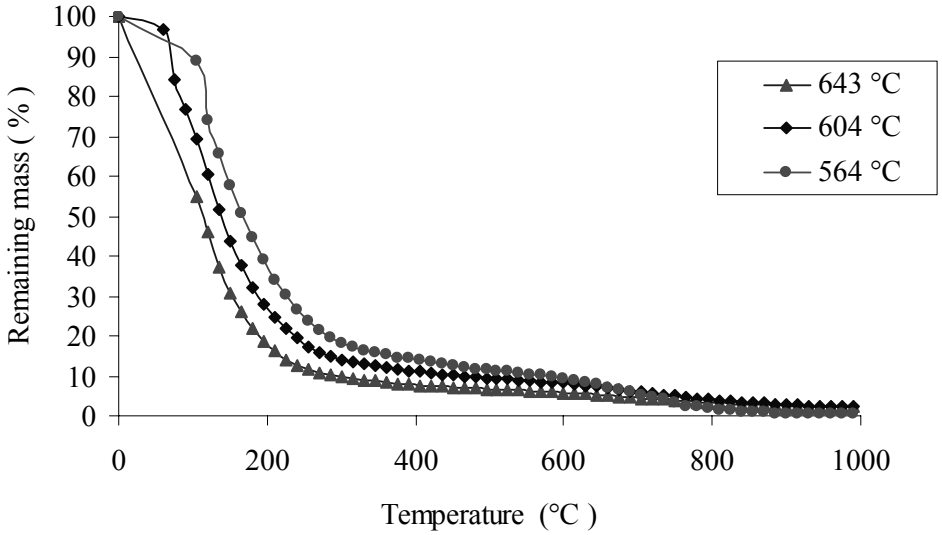

Figure 76. TGA curves for tars isolated during operation at different temperatures.

4.2.2.3 Characterization of Tars from an Industrial Reformer

As part of the technical support component of the project, the University of Utah analyzed samples of condensate from the gas conditioning system of Georgia-Pacific's Big Island demonstration system to identify tar species present. Organics were isolated by extracting the condensate with dichloromethane and analyzing the solvent by gas chromatography-mass spectroscopy (GC-MS).

A typical chromatogram from these analyses is shown in Figure 77. Over 70 different aromatic and polyaromatic species were identified in this particular sample. Of these, 24 were present in high enough concentrations that they could be quantified by integrating the area of the peak in the chromatogram. These 24 components are listed in Table 8, ordered by abundance in the sample. The majority of the tar compounds in the condensate are un-, mono- and di-substituted, mostly methyl phenols having molecular weights ranging from 94 to 178 and boiling points generally around 225°C. Such compounds make up more than 85% of the material found in the analyses.

Many other compounds were also identified in this sample, although their concentration was too low to allow quantification. These minor species are listed in Table 9, ordered by molecular weight. These compounds are generally somewhat heavier and have higher boiling points than those that

made up the majority of the sample. This is likely a consequence of the relatively low temperature of the condensate.

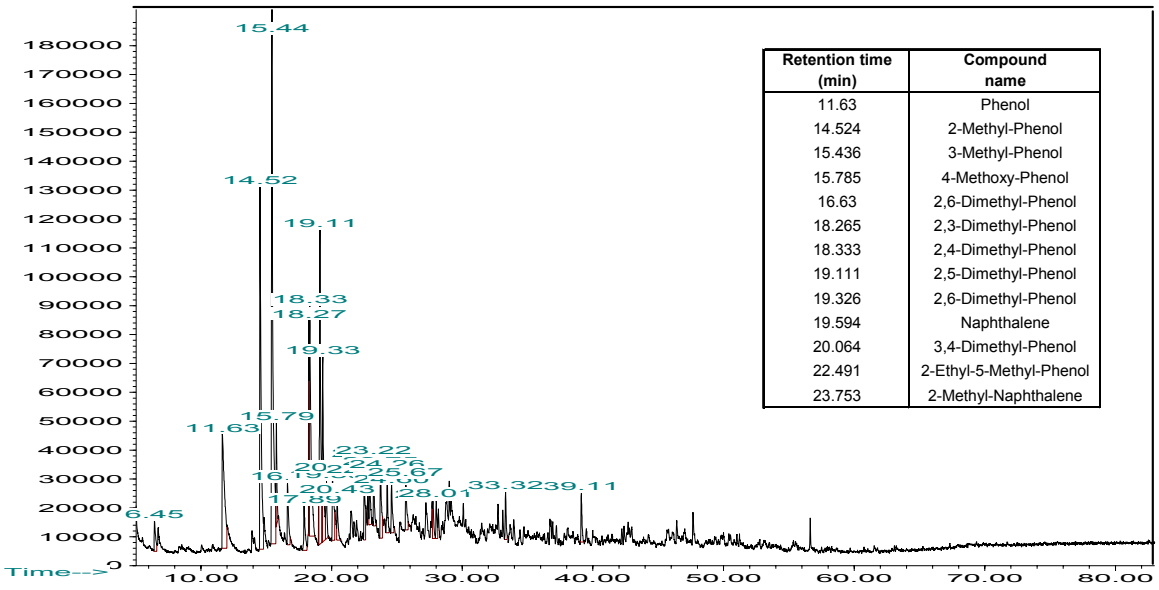

Retention time (min)	Compound name
11.63	Phenol
14.524	2-Methyl-Phenol
15.436	3-Methyl-Phenol
15.785	4-Methoxy-Phenol
16.63	2,6-Dimethyl-Phenol
18.265	2,3-Dimethyl-Phenol
18.333	2,4-Dimethyl-Phenol
19.111	2,5-Dimethyl-Phenol
19.326	2,6-Dimethyl-Phenol
19.594	Naphthalene
20.064	3,4-Dimethyl-Phenol
22.491	2-Ethyl-5-Methyl-Phenol
23.753	2-Methyl-Naphthalene

Figure 77. GC-MS chromatogram of tars in condensate from the Big Island steam reformer's syngas cleaning system.

TABLE 8. MAJOR TAR COMPONENTS IDENTIFIED IN CONDENSATE FROM GEORGIA-PACIFIC'S BIG ISLAND REFORMER GAS CLEANING SYSTEM.

Compound Name	Mol.Wt.	Boil Temp (°C)	Relative Concentration
3-Methyl-Phenol	108	202	100.0
2-Methyl-Phenol	108	191	65.2
2,5-Dimethyl-Phenol	122	211	54.8
2,4-Dimethyl-Phenol	122	211	47.7
Phenol	94	182	38.2
2,6-Dimethyl-Phenol	122	201	31.0
2,3-Dimethyl-Phenol	122	217	18.9
3,4-Dimethyl-Phenol	122	227	15.0
2-Methyl-Naphthalene	142	241	13.4
4-Methoxy-Phenol	108	202	11.5
2,6-Dimethyl-Phenol	122	201	10.9
2-Ethyl-5-Methyl-Phenol	136	224	10.2
Naphthalene	128	218	9.9
2,4,5-Trimethyl-Phenol	136	232	9.3
3-Ethyl-Phenol	122	216	9.0
2,3-Dihydro-1H-Indene-1-one	132	244	8.9
1-Methyl-Naphthalene	142	242	8.8
2,3-Dihydro-3-methyl-1H-Indene-1-one	132	244	8.4
Anthracene	178	340	7.0
2,3,5-Trimethyl-Phenol	136	234	6.7
9H-Fluorene	166	295	6.5
(1-Ethyl-2-Propenyl)-Benzene	146		6.3
1,4-Dimethyl-Naphthalene	156	265	6.1
2-Methyl-Cyclopentanone	98	140	5.9

TABLE 9. MINOR TAR COMPONENTS IDENTIFIED IN CONDENSATE FROM GEORGIA-PACIFIC'S BIG ISLAND REFORMER GAS CLEANING SYSTEM.

Compound Name	Mol.Wt.	Boil Temp (°C)
2-Methyl-Pyridine	93	128
2-Phenyl-1H-Indene	93	128
2-Methyl-Pyrene	108	191
1,2,4-Trimethyl-Benzene	120	169
1-Ethyl-4-methyl-Benzene	120	162
2-Ethyl-Phenol	122	205
[1-(2,4-cyclopentadien-1-yliden)ethyl]-Benzene	130	
2,3-Dimethyl-9H-Fluorene	132	244
4-Ethyl-3-Methyl-Phenol	136	229
3-Ethyl-5-methyl-Phenol	136	234
2,4,6-Trimethyl-Phenol	136	220
4-Ethyl-2-Methyl-Phenol	136	225
3,4,5-Trimethyl-Phenol	136	250
2,3,6-Trimethyl-Phenol	136	
Acenaphthylene	152	380
2,6-Dimethoxy-Phenol	154	261
1,1-Dimethyl-1H-Indene	154	254
Acenaphthene	154	279
1-Ethyl-Naphthalene	156	267
1,6-Dimethyl-Naphthalene	156	263
1,3-Dimethyl-Naphthalene	156	265
2,6-Dimethyl-Naphthalene	156	263
1,2-Dimethyl-Naphthalene	156	266
1H-Phenalene	166	
9H-Fluorene-9-carboxylic acid	166	295
9H-Phenalene	166	295
4-Methyl-1,1'-Biphenyl	168	268
4-Methyl-9H-Fluorene	168	268
1,4,5-Trimethyl-Naphthalene	170	
Phenantrene	178	340
2-Methyl-9H-Fluorene	180	318
1-Methyl-9H-Fluorene	180	
1-Methyl-Phenanthrene	192	
4-Methyl-Phenanthrene	192	
1-Methyl-Anthracene	192	363
Spiro[2.4]heptan-4-one	202	404
Fluoranthene	202	384
Pyrene	202	404
2-Phenylnaphthalene	204	346
2-Ethenyl-Naphthalene	206	
2,3-Dimethyl-Phenanthrene	206	
2,7-Dimethyl-Phenanthrene	206	
7-Methyl-Benzofuran	216	410
7-Methyl-Benzofuran	216	410
11H-Benzo[a]fluorine	216	412
11H-Benzo[b]fluorine	216	401
1-Methyl-Pyrene	216	
Ethenyl-Benzaldehyde	228	448

A second chromatogram of tar components found in the condensate on a different day, when operating the gas cleaning system under different (cooler) conditions, is shown in Figure 78. The overall profile is the same as the chromatogram in Figure 77. This sample contained somewhat fewer compounds, which is likely a result of the lower temperature operation forcing many of the heavier compounds to condense to solid form. Overall, the sample was again mostly composed of un-, mono- and di-substituted, mostly methyl phenols.

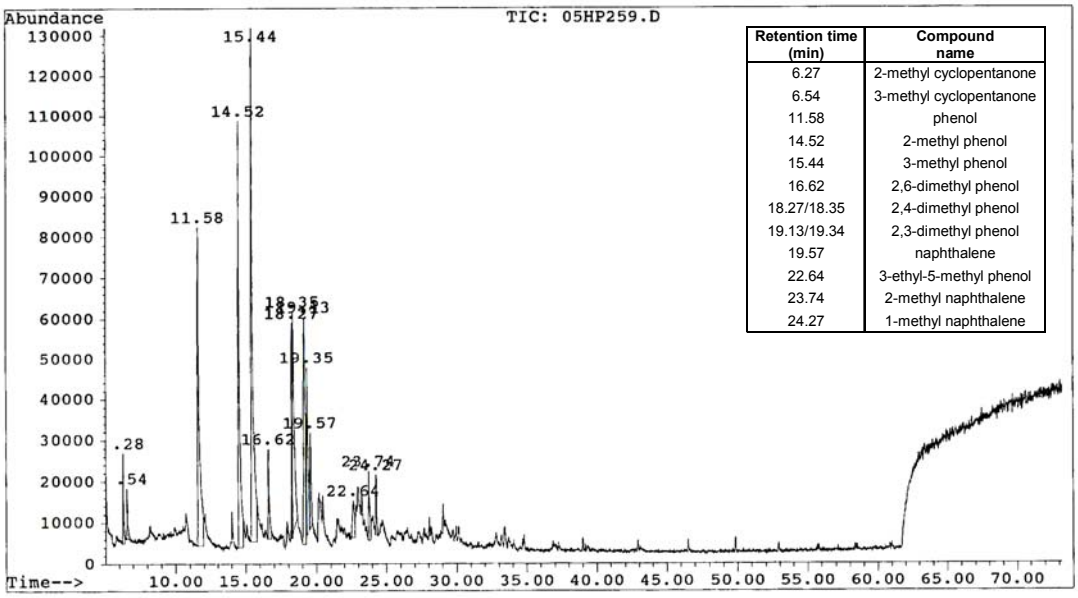

Retention time (min)	Compound name
6.27	2-methyl cyclopentanone
6.54	3-methyl cyclopentanone
11.58	phenol
14.52	2-methyl phenol
15.44	3-methyl phenol
16.62	2,6-dimethyl phenol
18.27/18.35	2,4-dimethyl phenol
19.13/19.34	2,3-dimethyl phenol
19.57	naphthalene
22.64	3-ethyl-5-methyl phenol
23.74	2-methyl naphthalene
24.27	1-methyl naphthalene

Figure 78. A second GC-MS chromatogram of tars in condensate from the Big Island steam reformer's syngas cleaning system.

It should be noted that many heavier compounds were also produced, but that the condensation temperature of these components is high enough that they did not remain in condensate, but rather formed solid deposits in the industrial system. A sample of such condensed tar material revealed a very large, complex mixture of hundreds of compounds. The complexity of the chromatogram for the sample of condensed deposit makes identification and quantification of components very challenging.

4.3 Black Liquor Conversion Analysis and Modeling

Conversion of black liquor in a low-temperature gasifier such as the fluidized bed steam reformer under investigation in this project occurs in three successive stages: (1) drying, (2) devolatilization (pyrolysis) and (3) heterogeneous gasification, or reaction of steam with the carbon in the bed material to form CO and H_2 according to reaction $H_2O(g) + C(s) \rightarrow H_2(g) + CO(g)$. Other components, such as sulfur, may also be gasified in this final stage, but the primary reaction is with carbon.

It is useful to consider these three processes individually when creating models that describe conversion. Drying rates have been shown to be dependent on heat transfer, so drying is not given any emphasis in this project. Devolatilization behavior accounts for a significant fraction of the

conversion. Release of "tar" compounds occurs during the devolatilization stage. Component release can be investigated under well-controlled conditions through fundamental, lab-scale experiments. Additionally, one can focus on liquor devolatilization during steam reforming in a more representative environment by operating the reformer with liquor injection, but at a temperature low enough that heterogeneous gasification rates are negligible.

The final stage of conversion, heterogeneous reaction of carbon in the bed solids and steam, can be investigated through fundamental lab-scale experiments such as TGA or pressurized TGA studies, where the weight loss of bed material can be studied when reacted with steam, with or without the presence of other gaseous components such as hydrogen and carbon monoxide. This final stage can also be focused on in a fluidized bed steam reformer by operating the steam reformer without liquor injection. That has been done in this project, and preliminary results are described below.

4.3.1 Steam Reforming Tests to Study Carbon Conversion

Several studies were performed to identify how the gas environment affects carbon conversion during the heterogeneous steam reforming stage of liquor conversion.

4.3.1.1 Measurement of Carbon Conversion in a Steam-only Environment

Experiments were run in which bed material from a commercial steam reformer containing roughly 17% carbon was gasified by feeding pure steam at 1120°F. The progression of carbon content versus time for one such experiment is shown in Figure 79. Nearly 24 hours were required to gasify essentially all carbon (from 13.3 wt%) out of the material. (The carbon content dropped from ~17% to 13.3% as the system was brought on line and heated to 1120°F.) The rate of conversion is linear relative to the amount of carbon remaining in the sample, indicating that the steam reforming reaction is first order relative to carbon concentration.

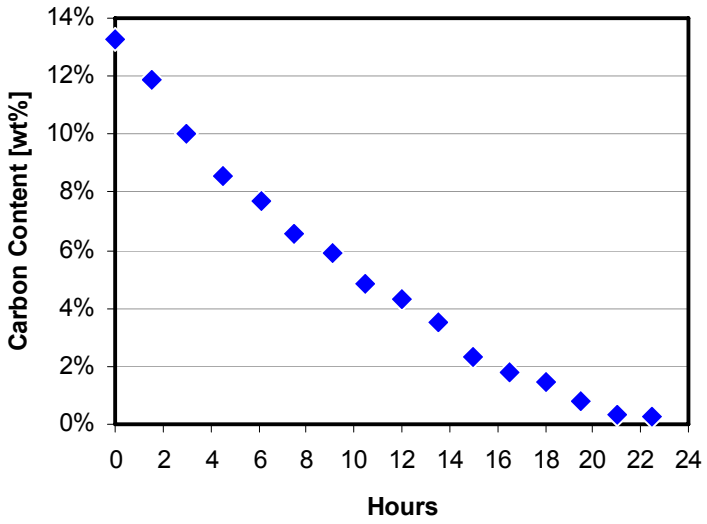

Figure 79. Carbon content in bed material versus time for a "steam-out" run with no liquor injection and pure steam, at 1120°F (604°C).

4.3.1.2 Influence of Hydrogen on Carbon Conversion Rate

Earlier investigations of steam gasification of black liquor have indicated that the presence of the product gases, hydrogen and carbon monoxide, decrease the rate of gasification [11,12,50-52]. In order to investigate the extent to which the heterogeneous gasification rate is reduced, experiments were performed in which hydrogen or carbon monoxide was fed into the steam line entering the reactor. The relatively large scale of the system required that many cylinders of compressed gas (H_2 or CO) be used. Due to the expense involved, only one or two different concentrations were tested for each gas.

Results from the UU model indicate that the partial pressure of hydrogen in a commercial steam reformer averages roughly 0.5 atm. It was decided to operate the Utah steam reformer such that the partial pressure of hydrogen would be roughly half this amount. An experiment was performed in which the steam flow was decreased by 25%, and enough hydrogen was added to result in a concentration of 25 vol% in the feed, thereby maintaining the fluidizing velocity. The first couple hours of the experiment, the reformer was operated with steam only in order to compare against the steam-only run shown in Figure 79. Hydrogen was then added to the gas for 6.5 hours, after which the gas was switched back to 100% steam.

The data for these two runs are shown in Figure 80. The initial carbon content at "time zero" was similar for both. The rate of gasification for the first two hours, in a steam-only environment, is comparable for the two experiments. Once hydrogen was added to the gas, however, the rate of gasification decreased dramatically. The two lines in the figure were fit by linear regression to the data points between 2 and 8.5 hours, when the hydrogen was being fed. The rate without hydrogen present was 0.75 %-units carbon per hour. The rate when the gas contained roughly 0.25 atm hydrogen was only about one-fifth that, or 0.16 %-units carbon per hour.

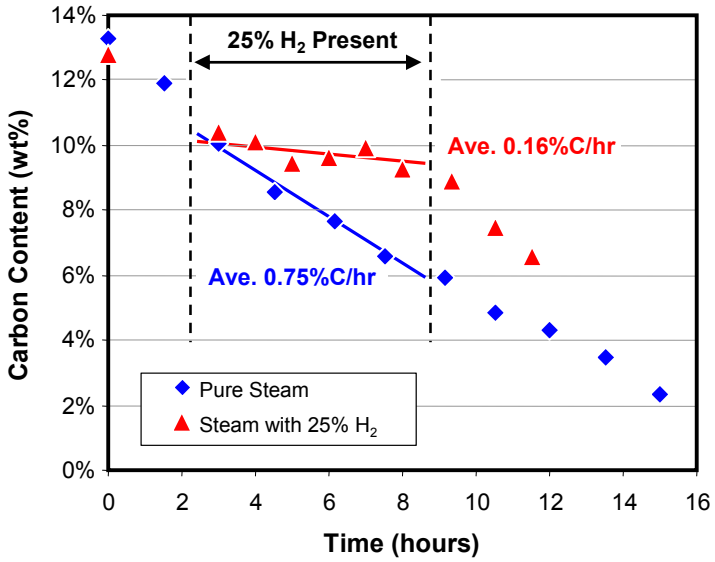

Figure 80. Influence of hydrogen on carbon conversion rate. In the red run, the gas composition was changed to 75% steam, 25% hydrogen, corresponding to a H_2 partial pressure of 0.25 atm, approximately 2 hours into the run, and kept at that composition for 6.5 hours, after which it was switched back to 100% steam.

Based on the initial result above, that 0.25 atm hydrogen decreases the rate by a factor of five, modeling estimates that a steam reformer that achieves 98% carbon conversion in a steam-only environment would achieve only 91% conversion with 0.25 atm hydrogen in the gas. If the effect of hydrogen on the rate were linear, such that 0.5 atm hydrogen decreased the rate by a factor of 10, the conversion in the same commercial unit with 0.5 atm hydrogen would be just 83%.

4.3.1.3 Influence of Carbon Monoxide on Carbon Conversion Rate

Earlier studies have indicated that, at equal partial pressures, carbon monoxide more strongly inhibits heterogeneous gasification of black liquor char than does hydrogen [50,51]. As noted in Section 4.2.1, however, the concentration of hydrogen is several times that of carbon monoxide. Based on the model described in Section 3.1, it is estimated that the partial pressure of carbon monoxide ranges from 0 to 0.06 atm in the full-scale steam reformers.

An experiment was therefore performed in the Utah steam reformer, similar to that described in the previous section, with no liquor injection, but with addition of carbon monoxide to the feed steam. In this experiment, two different concentrations of carbon monoxide were added. The first 1.5 hours of the run were with steam only. The steam feed was then decreased slightly and carbon monoxide was added such that its concentration was 6.4%, corresponding to roughly 0.06 atm partial pressure. The system was run under these conditions for 5.3 hours. The flow of carbon monoxide was subsequently decreased so that its concentration was 2.6% and the system was run under these conditions for an additional 8.3 hours.

The results of this test are shown in Figure 81, which displays the analyzed carbon content for the two runs versus time, with "time zero" for the steam-only run taken as that which had the same approximate carbon concentration as the first data point in the CO addition run. For the times during which 6.4% and 2.6% carbon monoxide were added, the approximate gasification rate was determined by using linear regression to fit a line to the data points over that period, and defining the slope of this line (%-units carbon/hr) as the carbon conversion rate during that period.

As seen in the figure, the presence of carbon monoxide in the reacting gas has little impact on the heterogeneous gasification rate. At the higher concentration (p_{CO} ~0.06 atm), the rate was roughly two-thirds that when pure steam was the reacting gas. At the lower concentration, the difference in rates with and without carbon monoxide addition was negligible.

4.3.2 Modeling of Carbon Conversion

The computational model described in Section 3.1 was used to identify how operating conditions affect carbon conversion. These results are presented in detail in the modeling results section. In summary, carbon conversion decreases with increasing liquor flow, decreasing system temperature, decreasing steam flow and increasing liquor solids content. The most significant factor affecting conversion, not surprisingly, is temperature. Liquor flow rate also has a significant influence.

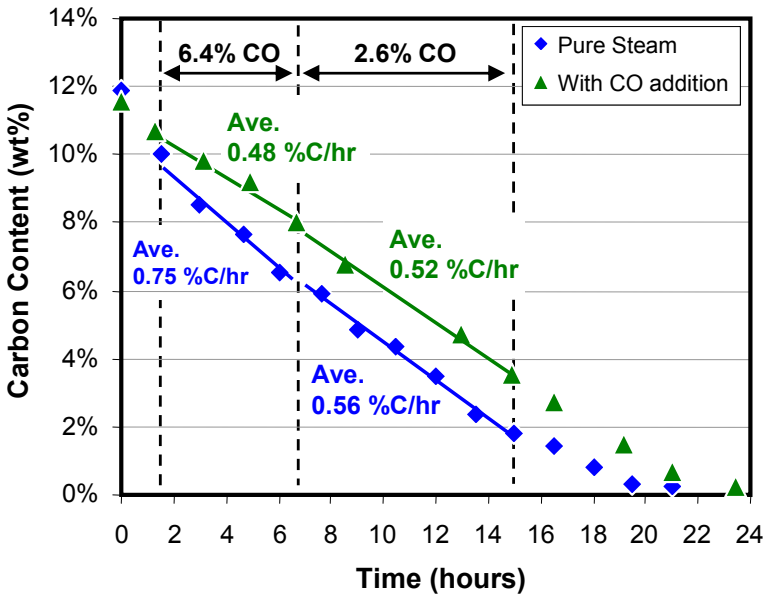

Figure 81. Influence of carbon monoxide on carbon conversion rate. In the green run, 6.4% carbon monoxide (~0.064 atm partial pressure) was added 1.5 hours into the run, and kept at that composition for 5.3 hours, after which it was lowered to 2.6% CO (p_{CO} ~0.026 atm) and kept at that composition for 8.3 more hours. It was then switched back to 100% steam.

4.4 Reactor Modeling Studies

4.4.1 Cold Flow Modeling Studies

The cold flow model described in Section 2.5 was used to gain a better understanding of gas and particle flow in the Utah steam reformer. As part of a collaborative modeling effort with the National Energy Technology Laboratory (NETL), the model was used to acquire quantitative data on bed performance. Specifically, the flow of bubbles through the heater bundles, the extent of particle segregation in the bed and heat transfer between heater tubes and the bed were studied. Results of these studies are presented in the sections that follow.

4.4.1.1 Bubble Voidage within Heater Bundles

A novel technique for identifying the presence of bubbles flowing between two adjacent tubes was developed. A two-probe system having a directional infrared light source and IR detector, shown conceptually in Figure 26 on page 27 and as a photo in Figure 82, was constructed and coupled to a data acquisition system that logged the received intensity of light 600 times per second. An example of the raw signal received from this system is shown in Figure 83. At this sampling rate, bubble frequency (bubbles per second), approximate bubble size and average voidage between the two probes could be determined.

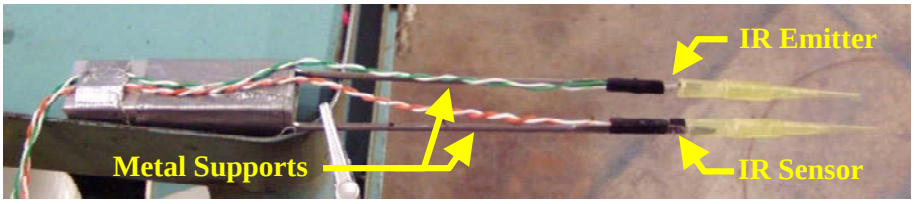

Figure 82. Probe for bubble detection.

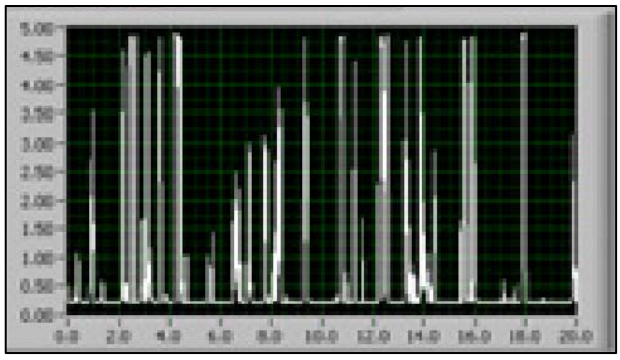

Figure 83. Signal from IR bubble detection system.

The signal was logged at each of the 16 levels in 16 locations at each level, which totals to 256 data logs per particle size. Because there are five tubes on each level, there are 4 spaces between tubes that can be measured. In each of these spaces, data was measured at 4 lengths along the tube: the center, two centimeters, four centimeters and six centimeters from the center of the tubes and symmetry was assumed for the opposite end of the tubes. At each of these points, data was taken at a rate of 600 Hz for 30 to 40 seconds.

Average bubble void fraction was calculated by first calculating the void fraction at each of the data points in the log. Then this calculated data was integrated with respect to time using the trapezoidal rule, and divided by the total time to get the average void fraction. A matrix for each level with both average void fraction and average bubble frequency was then developed. From these values a three dimensional surface could be plotted at each level to further visualize the data.

Three series of experiments were performed, each using a different average particle size, 90, 200 or 625 microns. Maps of bubble voidage within each of the sixteen levels of the tube banks were prepared for each particle size. Examples of bubble voidage plots for three layers, when fluidizing 200 micron particles, are presented in Figure 84. Level 1 is the bottom row of tubes. Level 4 is the top row of the bottom bundle. Level 5 is the bottom row of the second bundle and is oriented perpendicularly to Level 4. S1 to S4 correspond to the four spaces between the five tubes in that layer, and positions 1-7 are along the axial length of the tubes, with 4 being the center. Clearly, the voidage is highest in the center, or core of the bed. This suggests that bubbles prefer to travel through the tube bundles rather than near the walls. This corresponds with the visually observed downflow of solids near the walls.

It is of interest to know how particle size affects the behavior of the bed, particularly the propensity of particles to flow through the heater bundles. Figure 85 shows the measured bubble voidage profiles for the fourth level from the bottom (the top row of tubes of the bottom bundle) when running 90, 200 and 625 micron particles. Clearly, as particle size increases there is less tendency for bubbles to travel through the tube bundle; for the largest particles it appears that the center of the bundle was nearly stagnant.

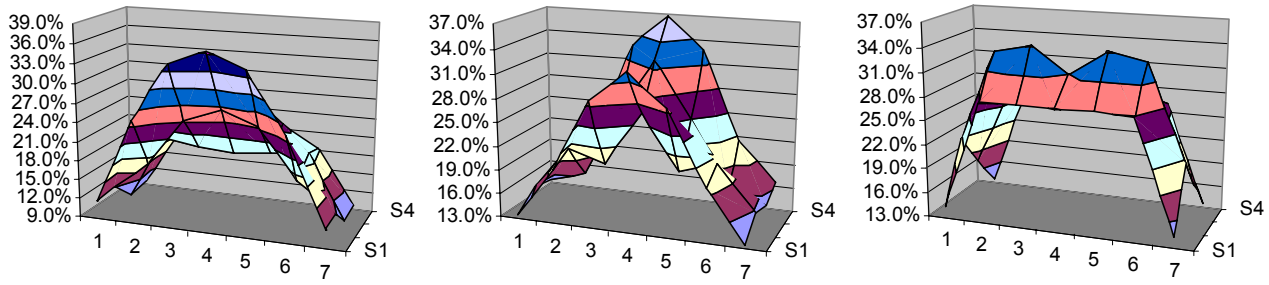

Figure 84. Measured bubble voidage profiles at Level 1 (bottom of the bed, left), Level 4 (middle) and Level 5 (right). S1-S4 represent the four spaces between the five tubes at that level. Positions 1-7 represent the length along the tube, with point 4 being the center of the tube.

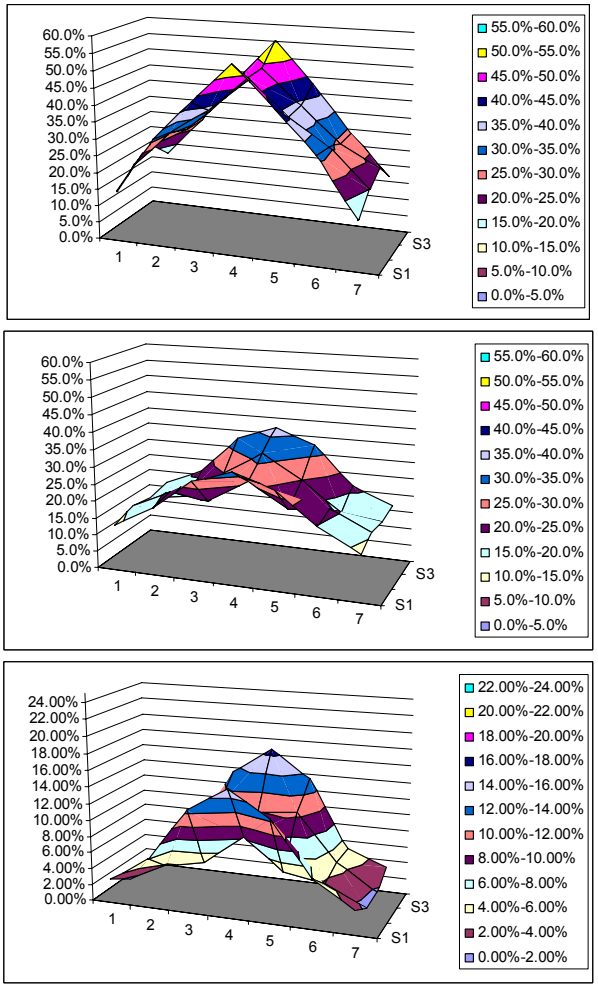

Figure 85. Bubble voidage profiles for average particle diameters of 90 (top), 200 (middle) and 625 (bottom) microns. Superficial velocity 1.07 ft/s in all cases (corresponds to 1.3 ft/s in the Utah gasifier).

4.4.1.2 Particle Segregation Studies

Studies were conducted to identify the degree of particle segregation in the bed. Soda lime glass beads with similar properties in two different sizes, 625 and 200 micron, were mixed 50/50 by bulk volume. The cold-flow model was run at a superficial velocity of 1.07 ft/sec for approximately 20 minutes to ensure that the particles had fully established their flow patterns and been given opportunity to segregate before any particle sampling was attempted.

A sampling device was designed to remove a small sample of bed particles from any location in the fluidized bed, except within the tube banks, while the bed was running. This probe was connected to a hose with vacuum on the other end. This hose was then attached to a trap that would collect the particles. A ball valve was placed in between the probe and the trap to stop the flow of particles when inserting the probe A sample of 100-400 grams was collected at each height and sieved using a 420 micron sieve. These separated portions were then weighed to get a ratio or percentage of each size. Data was collected at 10 heights in the bed, approximately 4 inches away from each other and

in between the tube banks. Three trials were performed at the center of the bed as well as against the walls of the bed. In between each trial, the particles that were removed earlier were remixed so the bed was at 26 inches and the bed was run for approximately 20 minutes again to assure proper mixing.

Results of the testing, showing the fraction of large particles in samples taken down the centerline of the bed and at the wall of the bed, are shown in Figure 86 and Figure 87, respectively. Overall, there is very little segregation of particles. The superficial velocity used in these studies, 1.07 ft/s, is higher than the minimum fluidization velocities of the particles, which were determined to be 0.13 ft/s for the 200 micron particles and 0.83 ft/s for the 625 micron particles. Generally, one can expect little segregation if the velocity is above the minimum fluidization velocities of all the particles.

As seen in the figures, there appears to be three different forms of behavior, particularly at the walls of the reactor. Below the tube banks, it seems there is a good distribution of both particle sizes. Within the tube bank region, there is almost a linear relationship of particle size to height. There is a larger amount of large particles at the bottom, and fewer large particles at the top of the tubes. Above the tube region, the fraction of large particles is higher than in the tube region. The top of the bed has the highest concentration of large particles.

One interesting observation is that in the region where tube bundles are present, 12 to 30 inches in height, the fraction of large particles at the wall dropped quite significantly, becoming as low as 43%. It was observed that there was significant particle downflow near the walls, and correspondingly little gas flow in this region. The observed segregation behavior could be due to the local gas velocity near the wall being lower than the minimum fluidization velocity of the large particles. If one considers only that zone, there is a clear trend indicating that the smaller particles dominate in the top of that section. In other words, there does appear to be some local segregation near the walls in the region where the tube banks are located.

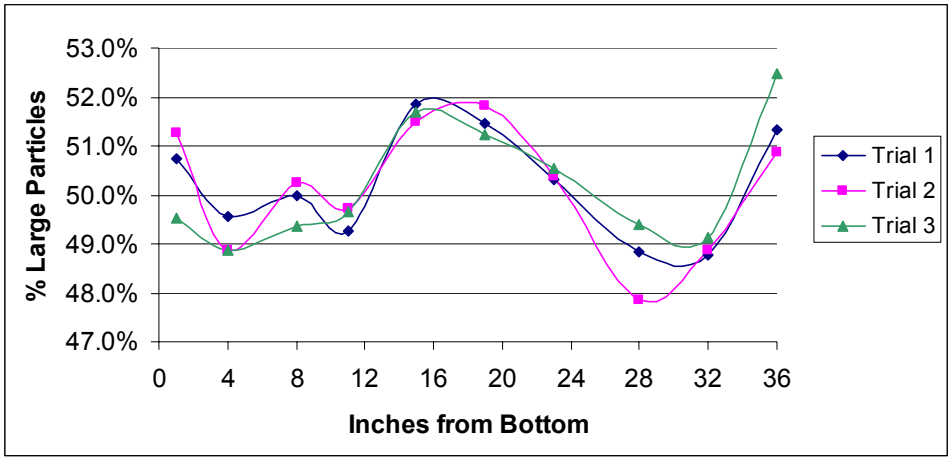

Figure 86. Fraction of large particles versus bed height when measured at the center of the bed.

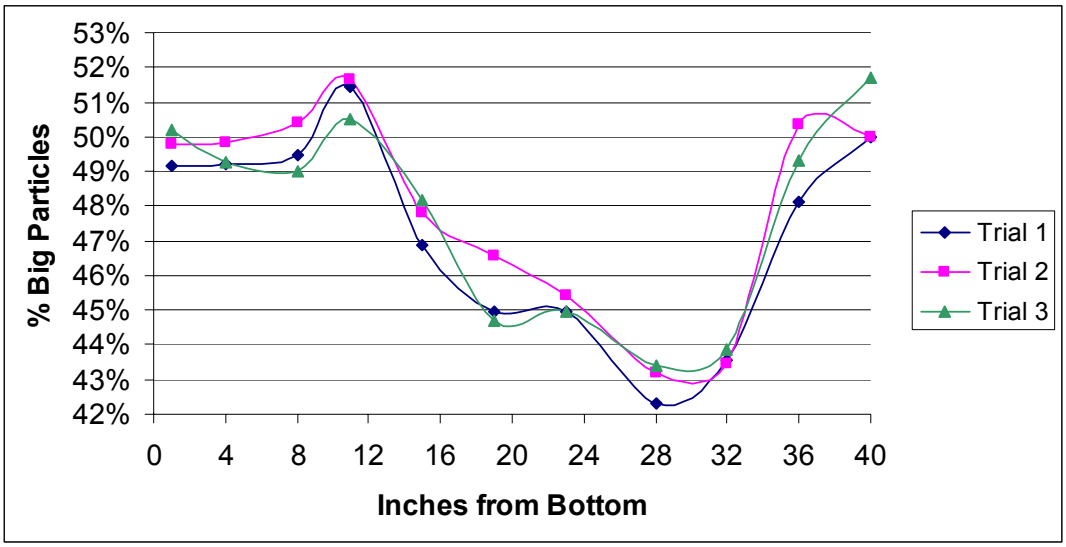

Figure 87. Fraction of large particles versus bed height when measured at the wall of the bed.

4.4.1.3 Heat Transfer Studies

To determine the heat transfer coefficient between the tubes and bed, several of the horizontal glass tubes in the tube bundles were replaced with copper tubes (Figure 88). A small cartridge heater with an internal thermocouple was placed into the various copper tubes, at different insertion depths within the tubes. Constant power was applied to the heater and the temperature of the internal thermocouple was measured. The local heat transfer coefficient at different locations could be calculated from the temperature difference and the surface area of the heated part of the tube.

Calculated heat transfer coefficients were generally 200 to 250 W/m^2-K. The average heat transfer coefficients in the middle tube of the 5-tube wide rows are shown in Figure 89. It is interesting to note that measured heat transfer is slightly less in the second heater bundle from the bottom (rows 5-8). The reason for this is unclear, but may be a consequence of a difference in gas and solids flow in that bundle.

The influence of particle size on heat transfer was determined by performing a series of experiments with particles having average sizes of 90, 200 and 625 microns. The results of these tests are presented in Table 10. The average heat transfer coefficient in the table is for the entire bed. The measured heat transfer coefficient decreased slightly as particle size increased. This is consistent with theory for tube-bed heat transfer in such systems.

Figure 88. Photo of tube bank region with copper tubes installed.

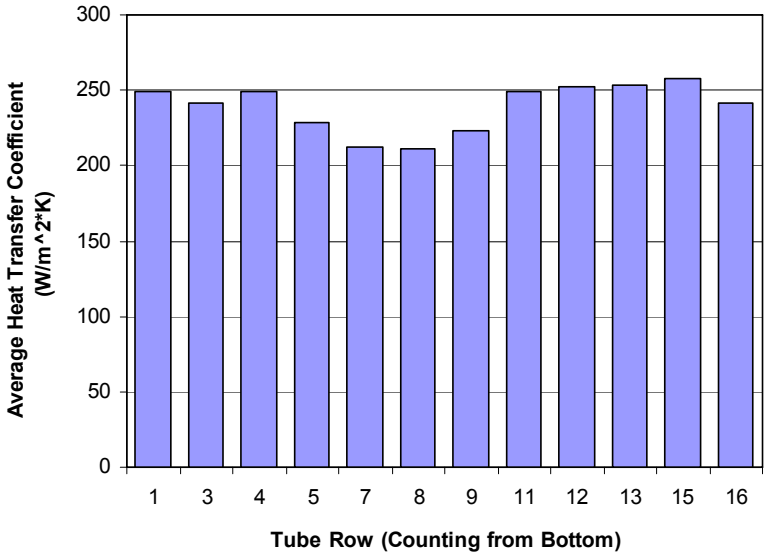

Figure 89. Measured heat transfer coefficients for the middle tube in 12 rows of the cold flow model. 200 micron particles, 1.07 ft/s fluidizing velocity.

TABLE 10. HEAT TRASFER VS. PARTICLE SIZE

Particle size (micron)	Average Heat Transfer Coefficient ($W/m^2 \cdot K$)
90	268
200	245
625	242

Heat transfer was also measured as a function of fluidizing velocity. A series of three experiments was performed in which 200 micron particles were fluidized with different gas velocities. The results are presented in Table 11. Theory suggests that heat transfer increases asymptotically with velocity. The results in Table 11 do not reflect this, though the variation in measured heat transfer is minor. It could be that local and solid flow patterns do not systematically change with increasing velocity.

TABLE 11. HEAT TRASFER VS. VELOCITY

Fluidizing velocity (ft/s)	Average Heat Transfer Coefficient ($W/m^2 \cdot K$)
0.54	257
1.07	245
1.57	258

4.4.2 Computational Modeling Results

Several computational models have been developed under this project to address different aspects of the steam reforming system. Results of these models are presented in the sections below.

4.4.2.1 Modeling of Carbon Conversion

The model described in Section 3.1 was used to predict the performance, notably the degree of carbon conversion, for two different theoretical steam reformers. One is a small-scale development unit processing roughly 0.2 tons of liquor per day, representative of the University of Utah steam reformer. The other is a full-scale system processing 100 tons of liquor per day, representative of the demonstration system that was built at Georgia-Pacific's Big Island mill. In the small-scale system, black liquor is injected 6 inches above the bottom of the reactor. In the full scale reactor, liquor is injected 18 inches above the bottom of the reactor. The same black liquor composition is used for both systems. The liquor chosen is a carbonate liquor since the full scale systems of the steam reforming technology have all been at carbonate-based mills.

Predicted performance – base cases. The base conditions for the analyses are reflective of normal operating conditions in the development-scale and full-scale systems. These are summarized in Table 12. For this preliminary analysis, the gasification reaction is assumed to be first order in carbon.

TABLE 12. BASE CASE OPERATING CONDITIONS

Parameter	Development Scale	Full Scale
Black liquor flow (kg/hr)	6.3	3,350
Black liquor solids (wt%)	42%	58%
Steam flow (kg/hr)	100	4,720
Freeboard pressure (atma)	1.07	1.29
System temperature (°C)	607	607
Bed diameter (m)	0.53	3.35
Bed height (m)	1.16	9.75

Under these conditions, and without any adjustments to the rate expression, the model predicts 99.0% carbon conversion for the development scale system and 97.4% carbon conversion for the full scale system. The corresponding organic carbon content of the solids are 0.9% and 2.4% by weight, respectively. This corresponds remarkably well with what has been observed in real systems, particularly for the small scale case. Reported carbon conversion efficiencies for development scale reformers are on the order of 99%. This indicates that the rate expressions that were calculated in earlier studies for black liquor char reasonably predict gasification rates for carbon on bed particles in a fluidized bed steam reformer.

The progression of the gas environment in the two systems is depicted in Figure 90. Clearly, the concentrations of the gases differ between the small and full scale systems. At the exit of the fluidized bed, the concentration of steam has dropped from 100% to roughly 50% in the full scale case, while the exit gas in the development scale reactor is still more than 90% steam. This difference in driving force between the two systems is exacerbated by the fact that the full scale system operates under higher pressure due to a combination of higher freeboard pressure and the much deeper bed and associated pressure drop. The maximum partial pressure of hydrogen in the full scale system, for example, is seven times that in the small scale system.

The change in gas composition over the height of the bed affects the gasification rate; as the product gases H_2 and CO are formed, the local gasification rate decreases. This is seen in Figure 91, where the local rates of gasification for the two systems are shown. There are several interesting features of this graph. First, the initial gasification rates of the two systems are the same. This is a consequence of the form of the rate equation (Eq. 4). The hydrogen and water vapor terms are lumped together with hydrogen as a numerator. At the bottom of the reactor, the gas is pure steam, so this term becomes zero. Secondly, the rates do decrease over the height of the reactor, and that decrease is much more significant for the full scale system. The rate at the top of the bed in the small scale system is 89% of that at the bottom. In the full scale system the rate at the top is only 40% of that at the bottom. The final feature of note is the sudden decrease in rate near the position where black liquor is injected (13% through the reactor in the full scale case). This is a consequence of the change in gas environment as elements, most notably carbon, are released during devolatilization. The notable jump in hydrogen concentration for the full scale system in Figure 90 is a result of carbon release and subsequent hydrogen formation by the water-gas shift reaction.

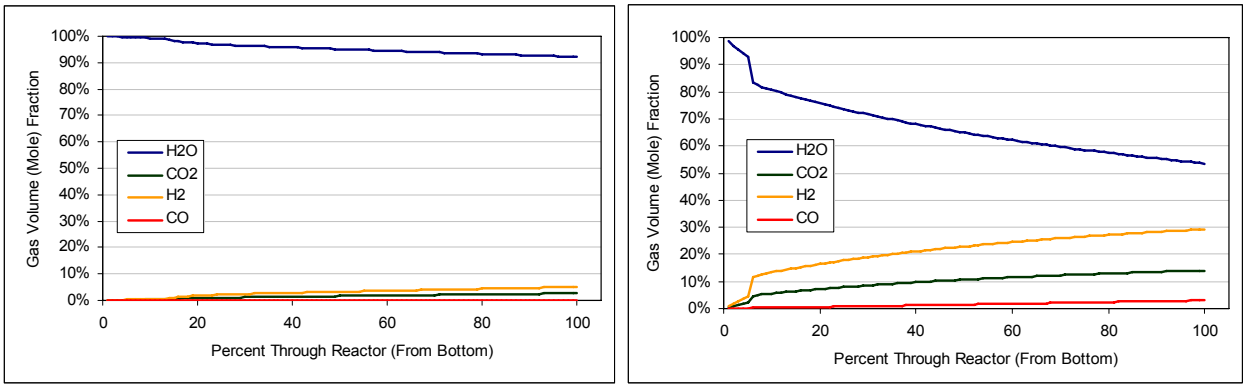

Figure 90. Gas compositions over the height of the bed for the small scale (left) and full scale (right) reactors. The ordering of the lines (top to bottom) in both cases is H_2O, H_2, CO_2, CO.

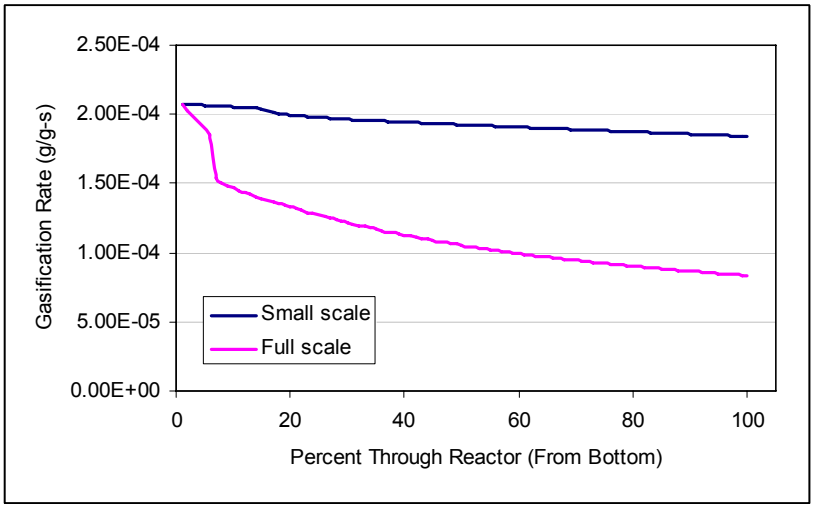

Figure 91. Local gasification rate as a function of position in the reactor for the small scale (top line) and full scale systems.

The difference in gasification rates resulted in the lower carbon conversion for the full scale system noted previously. Approximately 2.7 times more organic carbon remained unconverted on the particles in the full scale system than in the small scale system.

The model was used to predict how changing operating conditions affects performance of the full-scale simulated system.

Influence of black liquor flow on carbon conversion. Increasing liquor flow while holding all other operating variables and model parameters constant results in lower carbon conversion, as one would expect (Figure 92). The primary cause of the decrease is the decreased gasification rate resulting from more carbon being introduced into the gas and the resulting hydrogen and carbon monoxide increases. At half the base case flow rate, carbon conversion exceeds 99%.

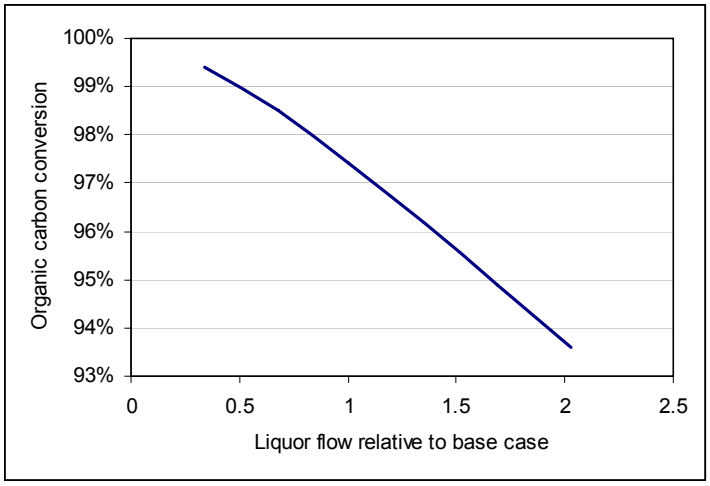

Figure 92. Carbon conversion versus liquor flow relative to the base case for the full scale system.

Influence of temperature on carbon conversion. Increasing the operating temperature of the system results in better carbon conversion (Figure 93). The trend is not linear, however. The gains in carbon conversion with increasing temperature are less than the loss in carbon conversion if the system is operated at a lower temperature. Below roughly 570°C conversion becomes significantly less.

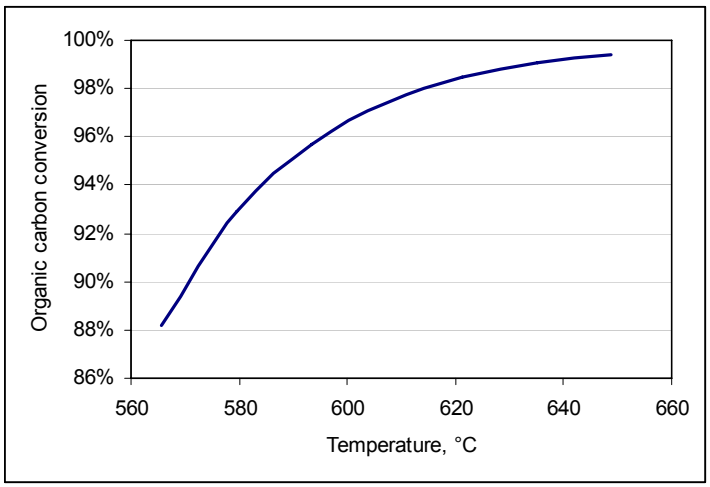

Figure 93. Carbon conversion versus system temperature.

Influence of steam flow rate on carbon conversion. Figure 94 shows the influence of steam flow rate on carbon conversion. Relative to the base case, doubling the steam flow rate has only marginal effect, increasing carbon conversion by approximately one percentage point. Significantly decreasing the steam flow rate does have a strong negative effect, however, since gas becomes enriched in species that hinder the gasification reactions.

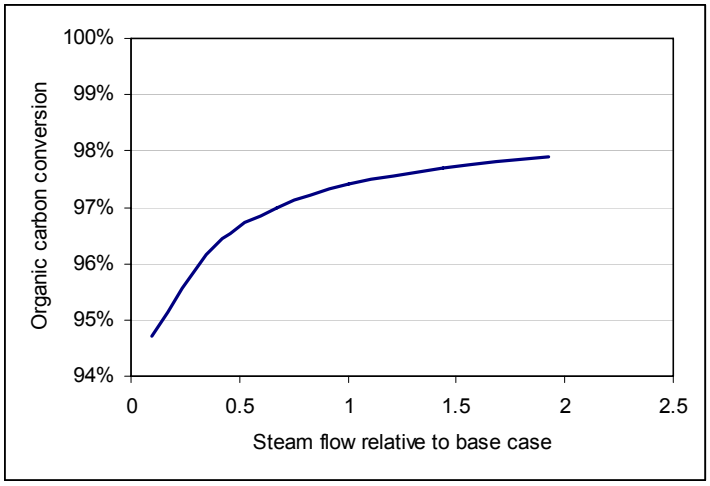

Figure 94. Carbon conversion versus system temperature.

Influence of black liquor solids content on conversion. Changing the solids content of the black liquor but holding the flow rate of dry solids constant has limited influence on carbon conversion. The trend is reverse of what might seem logical. As seen in Figure 95, increasing the solids content actually results in a decrease in carbon conversion because less steam that results from liquor drying is produced. The concentrations of the rate inhibiting gases are correspondingly higher. Changing the liquor solids concentration from the base case of 59% to 80% results in a decrease in carbon conversion from 97.4% to 97.0%. Correspondingly, decreasing the solids content to 40% increases conversion to 97.8%. Such small differences are not worth considering. In a real system, any decrease in carbon conversion that would result from an increase in solids content would be far outweighed by the decreased heating load that would result from not having to vaporize as much water.

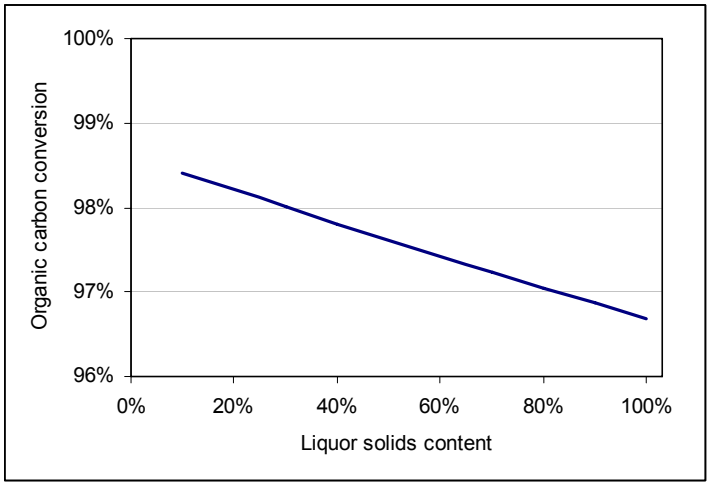

Figure 95. Carbon conversion versus liquor solids content.

Influence of model assumptions on conversion. To a large extent, carbon conversion was insensitive to assumptions made in the model. The times for drying and pyrolysis had little effect on overall conversion. Increasing drying and pyrolysis times from 0.2 and 0.3 seconds, respectively, to 1.0 and 5.0 seconds changed overall conversion by less than 0.1%. The additional steam created by drying the liquor is relatively small and would impact only a local section of the bed. The amount of material released during pyrolysis is small compared to carbon released by heterogeneous gasification.

The assumed reaction order does make a significant difference, particularly when small and large scale units are compared. Several researchers suggest that black liquor char conversion is first order in carbon [10,11,15]. However, gasification of bed solids appears to be less than first order in carbon [53]. It is unclear whether the specific chemical reaction is less than first order, or if conversion follows such behavior due to physical changes taking place within the particles. Changing the assumed reaction order only slightly, from 1.0 to 0.85, created a notable decrease in conversion and performance of the small and large scale systems deviated demonstrably. Instead of 99.0% and 97.4% carbon conversion for the small and large scale systems, conversions dropped to 98.3% and 87.9%, respectively. This is similar to differences that have been observed in practice. More investigation into the influence of reaction order is necessary.

4.4.2.2 Modeling of Gas Flow Within the Bed

Simulation of the Big Island steam reformer using the Reaction Engineering International model (Section 3.2) has been performed using the following process conditions:

- Black liquor solids: 8300 lb/hr
- Liquor solids mass fraction: 0.59
- Steam flow rate: 6850 lb/hr
- Pressure in the freeboard: 8.8 psig
- Solids removal rate: 2835 lb/hr
- Pulse combustor energy input: 7.84 MW

Figure 96 depicts the superficial gas velocity and the gas mass flow rate as functions of the reactor height (including the freeboard). A jump increase in both the gas mass flow rate and the superficial gas velocity near the bottom of the fluidized bed is due to the vaporization of black liquor water and pyrolysis of black liquor, after which, the gas mass flow rate increases gradually because of heterogeneous gasification of the bed material. Inside the tube bundles, decreases in the cross-sectional area lead to spikes in the gas velocity. In the freeboard, the gas mass flow rate remains constant, whilst the gas velocity in the freeboard changes because of the expansion of the freeboard and changes in the gas temperature. The velocity increases from approximately 0.4 to 0.8 m/s over the bed section.

The bubble properties predicted by the REI model are shown in Figure 97. Inside the tube bundles, bubble size is assumed to be the same as the tube pitch. In the open space between the tube banks and the confining cylindrical walls, the maximum bubble size is assumed to be 1/3 of the open space size. In the model calculations, an area-averaged bubble size is used. Also shown in the figure are the bubble sizes for a fluidized bed without any horizontal tubes; for this case, bubbles keep growing along the bed height. The bubble fraction is in the range of 0.15 to 0.45; spikes inside the tube bundles are due to increases in the superficial gas velocity.

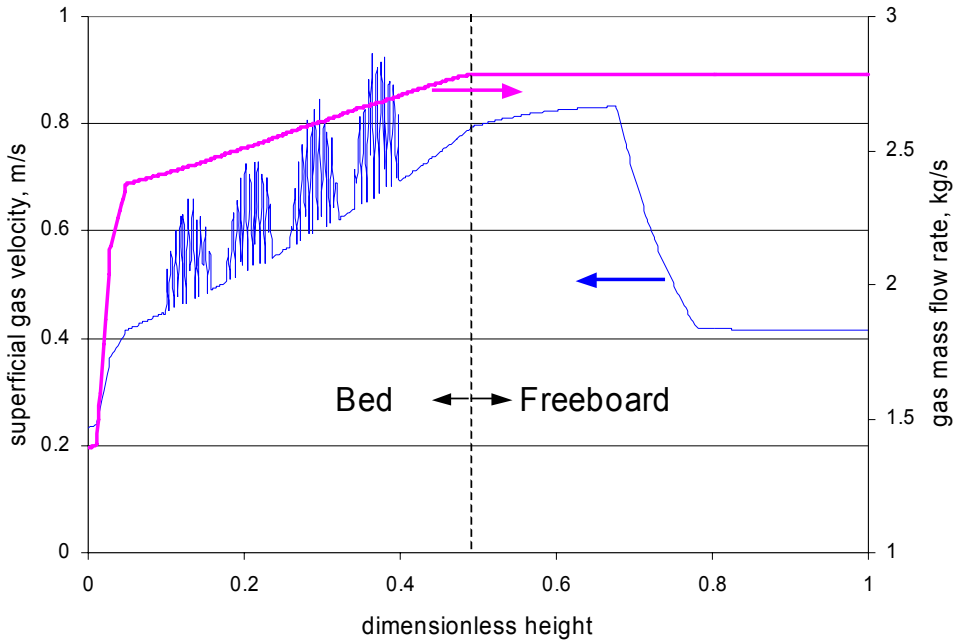

Figure 96. Gas velocity and gas mass flow rate as functions of reactor height.

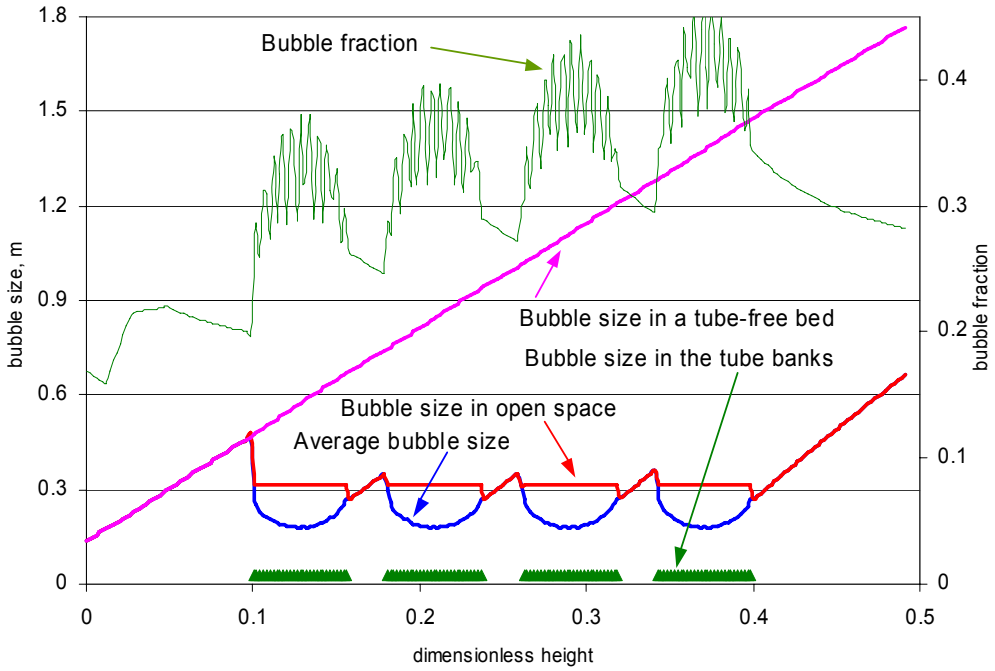

Figure 97. Variation of bubble properties with bed height.

4.4.2.3 Modeling of Jet Penetration Depth

There is concern that jet penetration of the black liquor injectors may be limited, leading to poor horizontal mixing in the bed. Jet penetration projections from available correlations can be used to assess the penetration depth of the feed. A literature survey has been carried out; several correlations for horizontal and vertical jets into a fluidized bed are summarized in Table 13. The predictions of jet penetration depth using different correlations are presented in Table 14 and Table 15. In Table 14, the feed stream was assumed to be in a liquid phase. The results indicate very limited penetration of the feed into the gasifier, ranging from 0.1 to 0.4 m for most of the correlations. For the correlation of Wen et al. [54], the predicted penetration depth is about 0.8 meters. The liquor at Big Island is fed at high temperature and pressure. A rough energy balance indicates that approximately 15% of the water in the liquor flashes as it is fed into the reactor. Since vaporization takes place during the injection of black liquor and some of the feed stream is in a gas phase, calculations were performed assuming all the feed stream was in the gas phase. Calculated penetration depths using various correlations are given in Table 15. It can be seen that jet gas velocity is unrealistically high, leading to much higher penetration depths, ranging from 0.5 to 6 meters.

TABLE 13 – JET PENETRATION CORRELATIONS

Vertical jet Yang and Keairns [55]	$\frac{L}{d_o} = 6.5\left[\left(\frac{\rho_f}{\rho_p - \rho_f}\right)\left(\frac{V_o^2}{g d_o}\right)^2\right]^{0.5}$
Merry [56]	$\frac{L}{d_o} = 5.2\left(\frac{\rho_f d_o}{\rho_p d_p}\right)^{0.3}\left[1.3\left(\frac{V_o^2}{g d_o}\right)^{0.2} - 1\right]$
Wen, et al. [54]	$\frac{L}{d_o} = 814.2\left(\frac{\rho_f d_o}{\rho_p d_p}\right)^{0.585}\left(\frac{\rho_f d_o V_o}{\mu}\right)^{-0.654}\left(\frac{V_o^2}{g d_o}\right)^{0.47}$
Zenz [57]	$0.0144\frac{L}{d_o} + 1.3 = 0.5\log(\rho_f V_o^2)$
Yang [58]	$\frac{L}{d_o} = 7.65\left[\frac{u_{cf,atm}}{u_{cf,p}}\left(\frac{\rho_f}{\rho_p - \rho_f}\right)\frac{V_o^2}{g d_o}\right]^{0.472}$
Horizontal jet Yates [59]	$\frac{L}{d_o} = 9.77\left[\frac{u_{cf,amb}}{u_{cf,p/T}}\left(\frac{\rho_f}{\rho_p - \rho_f}\right)\frac{V_o^2}{g d_o}\right]^{0.38}$
Merry [60]	$\frac{L}{d_o} + 4.5 = 5.25\left(\frac{\rho_f V_o^2}{(1-\varepsilon)\rho_p g d_p}\right)^{0.4}\left(\frac{\rho_f d_p}{\rho_p d_o}\right)^{0.2}$

TABLE 14 – JET PENETRATION DEPTH (FEED: LIQUID)

	Jet diameter, d_0, m	0.012	
	Number of jets	8	
	Stream density, kg/m^3	1400	
	Velocity, m/s	0.849	**Liquid**
		L/d_0	L, m
Vertical jet	Yang and Keairns [55]	20.48	0.24
	Merry [56]	11.81	0.14
	Wen, et al. [54]	68.85	0.81
	Zenz [57]	8.02	0.09
	Yang [58]	37.74	0.45
Horizontal Jet	Yates [59]	35.31	0.42
	Merry [60]	16.61	0.20

TABLE 15 – JET PENETRATION DEPTH (FEED: STEAM)

	Jet diameter, d_0, m	0.012	
	Number of jets	8	
	Stream density, kg/m^3	1.55	
	Velocity, m/s	666.8	**Steam**
		L/d_0	L, m
Vertical jet	Yang and Keairns [55]	331.67	3.93
	Merry [56]	45.56	0.54
	Wen, et al. [54]	95.80	1.13
	Zenz [57]	106.41	1.26
	Yang [58]	523.04	6.19
Horizontal Jet	Yates [59]	239.17	3.47
	Merry [60]	69.04	0.82

4.4.2.4 Heat Transfer Modeling

Reaction Engineering International used the heat transfer model described in Section 3.3 to estimate temperature profiles in the Big Island reformer. A first-order upwind finite-difference scheme has been used to discretize Equation 67. Along with Equations 58, 59 and 63, the discretized equation has been solved using the tri-diagonal matrix algorithm (TDMA). Solids flux and bed voidage inside the tube bundles under the gasifier normal operating conditions from the MFIX simulation have been provided by the National Energy Technology Laboratory.

Figure 98 shows solids flux within the pulse combustors, predicted from the MFIX simulation. It appears that particles pass through the tube bundles and move downward near the gasifier walls. Figure 99 shows bed voidage distribution from the MFIX simulation and the predicted particle temperature profile from Equation 67. It can be seen that bed voidage is relatively low below the tube bundles. The predicted particle temperature is fairly uniform with a higher temperature in the

top section. There are some locations with relatively higher particle temperature due to lower solids flux. A cross-section view of the predicted particle temperature is presented in Figure 100. Near the firing end of the pulse combustor tubes, the particle temperature is higher due to a higher flue gas temperature inside the tubes and lower solids flux.

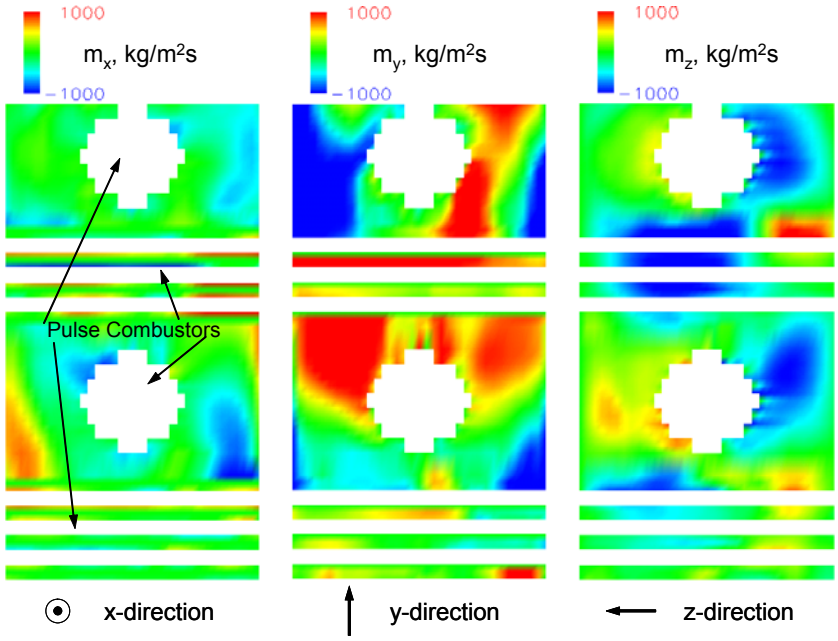

Figure 98. Solids flux inside the tube bundles (Side view across the centerline of the gasifier)

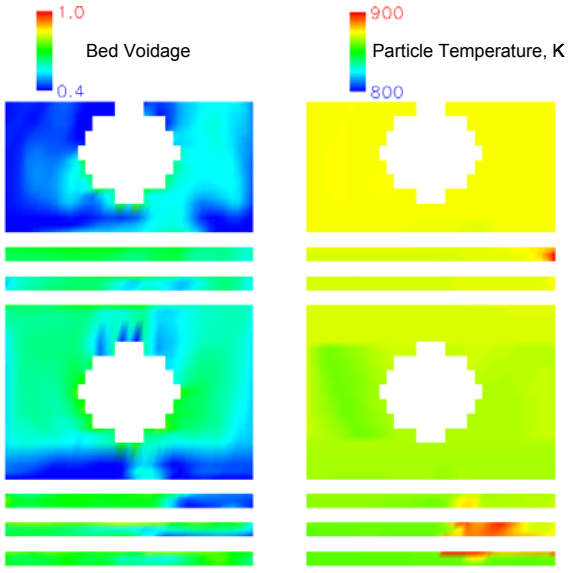

Figure 99. Bed voidage and predicted particle temperature (Side view across the centerline of the gasifier)

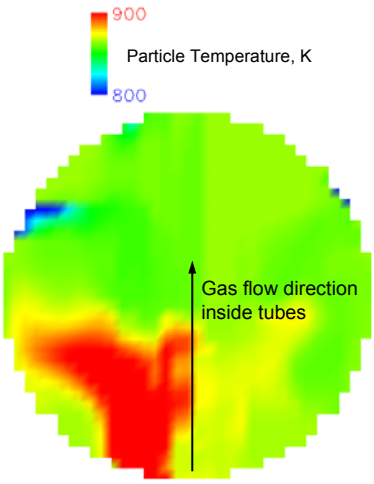

Figure 100. Predicted particle temperature (View across bottom pulse combustor)

The heat transfer model was used to predict surface temperatures of the tubes in the heater bundles in the Big Island reformer. The predictions were made using a combination of heat transfer modeling for the hot gases on the inside of the heater tubes and heat transfer from the tubes estimated using results of the MFIX simulations performed by the modeling group at DOE's National Energy Technology Laboratory.

An example of the predicted tube surface temperature is presented in Figure 101 and Figure 102, which show temperature profiles for four of the heater tubes: one on the outside plus the center tube of the row halfway up each of the bottom and top tube bundles. The bottom bundle tube temperatures are slightly less than the top bundle temperatures. Generally, the temperatures of the outside and center tubes within a level are predicted to follow the same profile. It should be noted that these predictions did not take into consideration the shield tubes around the hot end of the heater tubes.

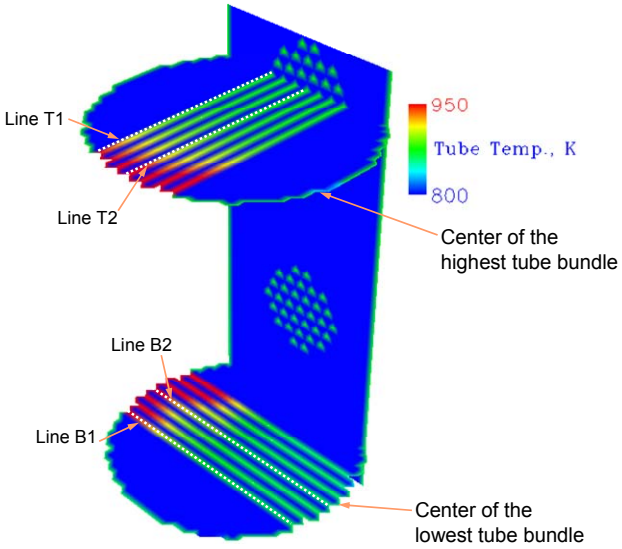

Figure 101. Cross section of the upper and lower tube bundle of a full scale reformer, indicating temperatures of the heater tubes.

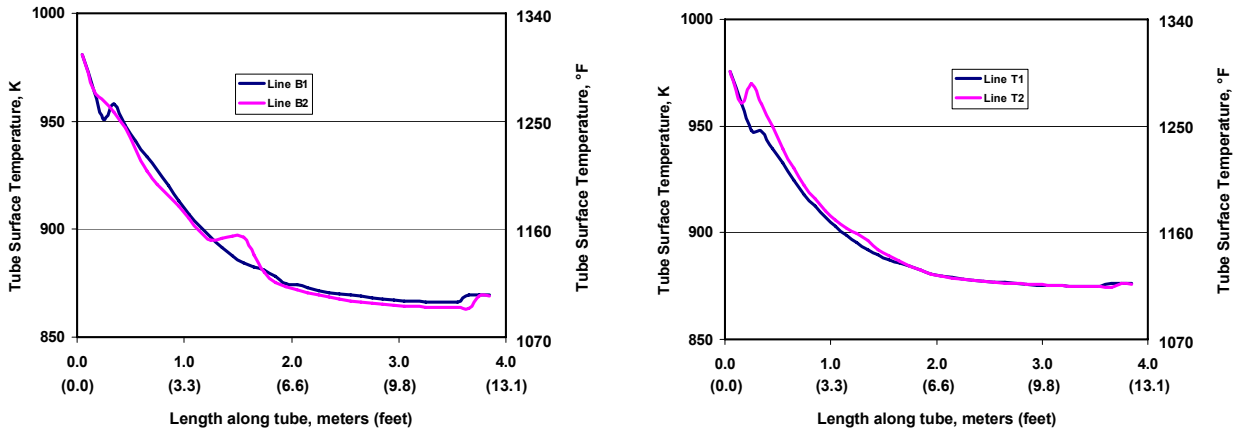

Figure 102. Predicted tube surface temperatures across the vertical center of the bottom (B, left) and top (T, right) tube bundles.

5. CONCLUSIONS

The University of Utah project "Investigation of Fuel Chemistry and Bed Performance in a Fluidized Bed Black Liquor Steam Reformer" produced a lot of new information regarding bed characteristics and performance, liquor conversion and corresponding quality of the product gas.

5.1 Research Tools

Many one-of-a-kind tools for studying fluidized bed black liquor steam reforming were constructed for this project. These are summarized below. Details about these systems are contained within this report and in its appendices.

Black liquor steam reformer. The University of Utah's gasification research system has a 10-inch fluidized bed that holds roughly 200 pounds of bed solids, has eighty electric heaters within the bed, and can simulate the behavior of a full-scale fluidized bed steam reformer. This system is useful for investigating syngas properties, carbon conversion rates and bed particle development under industrially-relevant conditions.

Bed agglomeration test system. A reactor specifically for investigation of bed agglomeration was constructed at Brigham Young University. The reactor is a 6 by 6-inch square nitrogen-fluidized bed containing sixteen cartridge heaters within the bed. Several thermocouples and pressure sensors allow one to follow the performance of the bed, and to identify the temperature at which the system begins to agglomerate. Agglomeration temperatures can be compared to bed material properties and compositions.

2-inch fluidized bed. A small, lab-scale fluidized bed at the University of Utah makes it possible to focus on mechanisms responsible for particle growth. Bed solids can be fluidized in nitrogen while black liquor is injected, thus coating the particles in a manner similar to that which occurs in a full-scale system. Particles grown under controlled conditions can be analyzed by electron microscopy to identify the structure of the growth, thus providing insight into the mechanisms responsible.

Single droplet reactor. A lab-scale reactor for heating small quantities of black liquor allows investigation of pyrolysis characteristics (volatiles yield and composition, swelling behavior), production of char and determination of char properties during conversion. A filter system can be appended to this reactor to allow capture of condensable hydrocarbons ("tars") formed during pyrolysis.

Cold flow model of Utah gasifier. A two-thirds scale Plexiglas cold flow model of the University of Utah steam reformer, including glass tubes representing the 80 horizontal heating tubes, allows visualization of gas and solids flow patterns. A unique system for measuring bubble frequency and average voidage within the tube banks has been developed. A system for measuring heat transfer between the "heater" tubes and the bed has also been developed.

5.2 Bed Particle Behavior

Particle size development. Several mechanisms contribute to growth and shrinkage of particles. Particle growth can occur by (1) liquor coating the particles and adding "shells" of material, (2) particle agglomeration, either by sintering or clustering ("droplet-induced agglomeration"), (3) particle sintering and (4) "clustering," in which several small particles are captured by a larger droplet of liquor and bound together by the liquor. Similarly, a number of mechanisms can be responsible for reductions in particles size: (1) fracturing, whereby a particle breaks into several relatively even sized particles, (2) attrition, where asperities on the particle surface are broken off and (3) cluster breaking, where the material holding the smaller particles together reacts away to the point where they are released. The overall development of the particle size distribution depends on the relative rates of these mechanisms which, in turn, depend on reactor design and operating conditions. Based on data gathered so far, it appears that liquor coating and attrition are the most significant mechanisms impacting particle size development.

Bed agglomeration. Bed agglomeration is a function of particle composition, particle size distribution, bed temperature and heater temperature. For a constant power feed to the heaters, the onset of agglomeration can be detected by an increase in the temperature difference between the heaters and the bed itself, as larger particles resulting from agglomeration decrease the efficiency of heat transfer. Pure sodium carbonate was found to begin agglomerating at roughly 520°C. Addition of just 2% potassium chloride decreased the agglomeration temperature by more than 50°C. SEM analysis indicates that bridges are formed between the edges of the particles. Interestingly, particles from a commercial steam reformer could be fluidized at 650°C without agglomerating. Apparently, the presence of organic carbon in the material helps minimize particle stickiness.

Tests with addition of titanate. Addition of titanium dioxide to kraft black liquor fed to a fluidized bed steam reformer allows the bed to be operated at higher temperature, without agglomeration, than normal bed particles created from black liquor inorganics during standard steam reforming. Carbon conversion is consequently very high. The titanium dioxide forms a complex with the sodium in the black liquor, which, when dissolved in water, forms sodium hydroxide. Preliminary full-scale tests indicate that these in-situ causticization reactions are effective under the conditions tested. It is recommended that any future testing with titanates use very round bed particles that fluidize well.

5.3 Product Gas Properties

The major non-steam species in the steam reformer's product gas are H_2, CO_2, CO and CH_4. Hydrogen is present in concentrations well in excess of 50%. Although CO is a primary product from the reforming process, very little is present in the product gas. The water-gas shift reaction, which converts CO to CO_2 and is typically very slow at steam reformer temperatures, is strongly catalyzed by alkali metals in the bed material so that the gas exiting the system is near equilibrium with regard to that reaction. Overall, the heating value of the product gas is in the range 10.5–12.0 MJ/Nm^3 (250-300 Btu/scf) on a dry nitrogen- and oxygen-free basis.

Black liquor steam reforming produces condensable hydrocarbons, or "tars." These tars comprise a wide array of mono- and polyaromatic compounds that may condense in or on downstream equipment. Tars from both the Utah reformer and commercial systems are similar, and over 100

compounds have been identified. The majority of these were un-, mono- and di-substituted, mostly methyl phenols.

The temperature at which the reformer is operated has a significant impact on the amount of tar in the product gas, with higher temperatures resulting in lower tar formation. This is likely due to enhanced thermal breakdown at higher temperatures, which converts otherwise condensable species into gas-phase species. Black liquor flow rate also significantly affects tar production. At otherwise similar conditions, higher black liquor flow rates result in more tars. Fluidizing steam temperature, fluidizing velocity, and addition of potassium hydroxide have no statistically significant influence on tar formation under conditions studied under this program. Addition of 15-20% air to the fluidizing gas appears to decrease tar formation somewhat under certain conditions, but additional study is necessary to verify this effect. The composition of the condensed tar does not vary significantly with changes in operating conditions.

5.4 Black Liquor Conversion

Conversion of black liquor in a low-temperature gasification system (operating below the melting point of the inorganic residue) occurs in three stages: (1) drying, which is nearly instantaneous, (2) pyrolysis (devolatilization), also a relatively rapid process during which volatile matter in the liquor is released (and tars are formed) and (3) heterogeneous reaction of components, primarily carbon, in the solid residue remaining after pyrolysis. The third step is by far the slowest, and determines the overall carbon conversion for a fluidized bed steam reformer. Many hours may be required to reach an acceptable degree of conversion.

When operating a small fluidized bed steam reformer with pure steam and no liquor injection, roughly 24 hours are required to steam reform all the carbon from bed material initially containing 17 percent carbon by weight. Previous studies indicate that the product gases of the steam reforming reaction, hydrogen and carbon monoxide, slow the rate of conversion. Adding 0.06 atm carbon monoxide to pure steam has only a slight effect on the rate of conversion. This is likely due to consumption of the CO by the water-gas shift reaction, thereby decreasing its actual concentration to almost zero. Any observed effect is probably a result of hydrogen produced by the water-gas shift reaction. Such CO conversion would not take place in an actual reformer since the gas would already be at equilibrium with regard to the water-gas shift reaction. The presence of 0.25 atm hydrogen does significantly slows the rate of carbon conversion, with the rate being approximately one-fifth that in a steam-only environment. The partial pressure of hydrogen in a commercial reformer processing black liquor is estimated to average more than 0.5 atm, so carbon conversion would be expected to be inhibited, resulting in solids with a higher carbon concentration.

Computational modeling confirms the observation above. In comparing small-scale and large-scale systems with equivalent solids residence times and liquor feed/bed volume ratios, the larger system, which does have a lower steam flow/bed volume ratio, has correspondingly higher concentrations of hydrogen and carbon monoxide. Because of the deep bed, the partial pressures are considerably higher than in a full-scale system. The depressed reaction rate relative to the small-scale system results in lower carbon conversion and higher bed carbon contents.

5.5 System Performance Modeling

Measurement of bubble voidage within the tube banks of an appropriately designed cold-flow model indicates that for particles corresponding to 300 microns in the Utah gasifier, bubbles flow through the tube bundles with no problem, and generally seem to prefer the center of the bundles to the walls of the reactor. This is particularly notable as one traverses a tube; at the ends, where the tubes touch the wall, bubble voidage is much lower, presumably due to downflow of solids along the walls. The propensity for bubbles to flow within the tube bundles decreases with particle size. For small particles (corresponding to 135 microns in gasifier) there is significant variation in bubble voidage within a given row of tubes (high near the center, low near the walls). For large particles (940 microns) the bubble voidage profile is nearly flat. Within the top bundle, variations in bubble voidage are smaller than for the lower three bundles. This could be due to downflow of the solids above that bundle.

Segregation of particles by size is limited, at least within the range of particle sizes and conditions tested. The range of velocities tested were all above the minimum fluidization velocity of all particles. It could be that segregation would be observed if larger particles or lower velocities were used.

Heat transfer between the heater tubes and bed material is very good, with heat transfer coefficients on the order of 200-250 $W/m^2 \cdot K$ based on cold-flow model measurements. Interestingly, the second tube bundle from the bottom displayed somewhat less efficient heat transfer than the other three. The reason for this is unclear. Variations in heat transfer with particle size and fluidizing velocity were negligible under the conditions studied.

Three-dimensional modeling of the Big Island steam reformer suggests that bubbles flow through the heater bundles, and that the bundles have a significant influence on solids flow. Overall, solids downflow appears to occur near the walls, but the bundles disrupt this pattern, causing the particles to shift sideways. The particles prefer to flow downwards in the open areas on the sides of the heater bundles.

As one would expect, the surface temperature of the heaters decreases as one goes from the firing end to the exhaust end. The modeling simulations suggest that the temperature drops from roughly 700°C (1300°F) to bed temperature. These simulations did not account for the shield tubes within the heater bundles, however, so the actual hot end temperature is likely less.

NOMENCLATURE

A	cross-sectional area of the bed, m^2
C	carbon concentration, kg/m^3 particles
C_p	specific heat, J/kg·K
d	diameter, m
$d_{b,d}$	daughter bubble diameter, m
d_b	bubble diameter, m
$d_{b,e}$	average daughter diameter, m
d_p	particle diameter, m
D_g	gas diffusivity, m^2/s
D_{O2}	oxygen diffusivity, m^2/s
f	phase fraction
g	gravitational acceleration, m/s^2
h	heat transfer coefficient, $W/m^2·K$
H	computational cell height, m
H_t	expanded bed height, m
$K_{wd,p}$	solids exchange coefficient between the wake phase and the dense phase, 1/s
m_{dev}	volatiles flow rate, kg/s
m_{out}	mass outflow rate of bed material, kg/s
m_p	mass flow rate of black liquor solids, kg/s
m_{vap}	volumetric evaporation rate, $kg/m^3·s$
Q_t	heat transferred from the pulse combustor, W/m^3
Q_{vap}	heat required for evaporation of water, W/m^3
R	universal gas constant, J/mol·K
$R_{i,b}$, $R_{i,w,g}$, $R_{i,e,g}$	homogeneous reaction rate in the bubble, wake and dense phases, $kmol/m^3·s$
$R_{i,w,s}$, $R_{i,e,s}$	heterogeneous reaction rate in the wake and dense phases, $kmol/m^3·s$
T	temperature, K unless otherwise noted
u_0	superficial gas velocity, m/s
u_b	bubble rise velocity, m/s
$u_{p,d}$	particle velocity in the dense phase, m/s
X	mass fraction
ε	bed voidage
λ_{vap}	latent heat of vaporization, J/kg
ρ_g	gas density, kg/m^3
ρ_p	carbon density, kg/m^3
ΔH`	heat of reaction, J/kmol

Subscripts

b	bubble phase
C	carbon
d	dense (emulsion) phase

g	gas
i	reaction index
K	potassium
mf	minimum fluidization
Na	sodium
p	particle
tf	throughflow
w	wake phase

REFERENCES

1. WHITTY, K., VERRILL, C.L., "A Historical Look at the Development of Alternative Black Liquor Recovery Technologies and the Evolution of Black Liquor Gasifier Designs," Proc. 2004 TAPPI Int'l Chemical Recovery Conf., 6-10 June 2004, Charleston, S.C. (2004).
2. MANSOUR, M., CHANDRAN, R., ROCKVAM, L., "The evolution of and advances in steam reforming of black liquor", *Proc. 2002 TAPPI Joint Engineering / Pulping Conference*, 8-12 September 2002, San Diego, CA (2002).
3. ROWBOTTOM, B., NEWPORT, D., CONNER, E., "Black liquor gasification at Norampac", *Proc. 2005 TAPPI Engineering, Pulping & Environmental Conf.*, 28-31 August 2005, Philadelphia, PA (2005).
4. WHITTY, K., NARANJO, M., RUBIANO, C., "Performance of a Small-Scale Fluidized Bed Black Liquor Steam Reformer", *Proc. 2006 TAPPI Engineering, Pulping and Environmental Conf.*, 5-8 November 2006, Atlanta, GA (2006).
5. NEEFT, J.P.A., KNOEF, H.A.M., ZIELKE, U., SJÖSTRÖM, K., HASLER, P., SIMELL, P.A., DORRINGTON, M.A., THOMAS, L., ABATZOGLOU, N., DEUTCH, S., GREIL, C., BUFFINGA, G.J., BRAGE, C., SUOMALAINEN, M. *Guideline for Sampling and Analysis of Tar and Particle in Biomass Producer Gases. IEA Bioenergy Task 33.* ECN Biomass Report ECN-C-02-090: United Kingdom, 2002.
6. KUNII, D., LEVENSPIEL, O., *Fluidization Engineering*, Butterworth-Heinemann Publ., Newton, MA (1991).
7. FREDERICK, J., HUPA, M., "Combustion properties of kraft black liquors," *DOE Report DOE/CE/40936-T1,* Washington, D.C. (1993).
8. FREDERICK, W.J., IISA, K., WÅG, K., REIS, V.V., BOONSONGSUP, L., FORSSÉN, M., HUPA, M., "Sodium and sulfur release and recapture during black liquor burning," *DOE Report DOE/CE/40936-T2*, Washington, D.C. (1995).
9. LI, J., VAN HEININGEN, A.R.P., "Reaction kinetics of gasification of black liquor char", *Can. J. Chem. Eng.* 67:693-697 (1989).
10. WHITTY, K., HUPA, M., FREDERICK, W.J., "Gasification of black liquor char with steam at elevated pressures", *J. Pulp Paper Sci.* 21(6):J214 J221 (1995).
11. LI, J., VAN HEININGEN, A.R.P., "Kinetics of CO_2 gasification of fast pyrolysis black liquor char", *Ind. Eng. Chem. Res.* 29(9):1776-1785 (1990).
12. LI, J., VAN HEININGEN, A.R.P., "Kinetics of gasification of black liquor char by steam", *Ind. Eng. Chem. Res.* 30(7):1594-1601 (1991).
13. VAN HEININGEN, A.R.P., ARPIAINEN, V., ALÉN, R., "Effect of liquor type and pyrolysis rate on the steam gasification reactivities of black liquors", *Pulp Paper Canada* 95(9):T358-363 (1994).
14. FREDERICK, W.J., HUPA, M., "Gasification of black liquor char with CO_2 at elevated pressures", *Tappi J.* 74(7):177-183 (1991).
15. FREDERICK, W.J. WÅG, K.J., HUPA, M., "Rate and mechanism of black liquor char gasification with CO_2 at elevated pressures", *Ind. Eng. Chem. Res.* 32(8):1747-1753 (1993).
16. WHITTY, K., BACKMAN, R., HUPA, M., "An empirical rate model for black liquor char gasification as a function of gas composition and pressure", *Proceedings: Advances in Forest Products Environmental and Process Engineering, 1993 Forest Products Symposium* / ed. C.L. Verrill et al. AIChE Symposium Series 90, pp. 73 84 (1994).
17. VAN HEININGEN, A.R.P., CONNOLLY, S., "Kraft black liquor gasification kinetics", *Presented at the Colloquium on Black Liquor Combustion and Gasification,* 13-16 May 2003, Park City, Utah (2003).

18. MANSOUR, M., CHANDRAN, R., ROCKVAM, L., "The evolution of and advances in steam reforming of black liquor", *Proc. 2002 TAPPI Joint Engineering / Pulping Conference*, 8-12 September 2002, San Diego, CA (2002).

19. WHITTY, K., NARANJO, M., RUBIANO, C., "Performance of a Small-Scale Fluidized Bed Black Liquor Steam Reformer", *Proc. 2006 TAPPI Engineering, Pulping and Environmental Conf.*, 5-8 November 2006, Atlanta, GA (2006).

20. DARTON, R.C., LANAUZE, R.D., DAVIDSON, J.F., HARRISON, D., "Bubble growth due to coalescence in fluidized beds," *Trans. Instn Chem. Engrs*. 55:274-280 (1977).

21. HULL, A.S., CHEN, Z., FRITZ, J.W., AGARWAL, P.K., "Influence of horizontal tube banks on the behavior of bubbling fluidized beds. I. Bubble hydrodynamics," *Powder Technology* 103:230-242 (1999).

22. YATES, J.G., RUIZ-MARTINEZ R.S., "Influence between horizontal tubes and gas bubbles in a fluidized bed," *Chem. Eng. Comm.* 62:67-78 (1987).

23. YATES, J.G., RUIZ-MARTINEZ, R.S., CHEESMAN, D.J., "Prediction of bubble size in a fluidized bed containing horizontal tubes," *Chem. Eng. Sci.* 45:1105-1115 (1990).

24. DAVIDSON, J.F., HARRISON, D., *Fluidized Particles*, Cambridge University Press, London (1963).

25. ROWE, P.N., YACONO, C.X.R., "The bubbling behavior of fine powders when fluidized," *Chem. Eng. Sci.* 31:1179-1192 (1976).

26. WERTHER, J., "Bubble growth in large diameter fluidized beds," in D.L. Keairns (ed) *Fluidization Technology*, Vol. 1, Hemisphere Pub., 215-235 (1976).

27. ROWE, P.N., PARTRIDGE, B.A., "An x-ray study of bubbles in fluidized beds," *Trans. Instn Chem. Engrs.* 43:157-175 (1965).

28. CHEN, Z., LIN, M., IGNOWSKI, J., KELLY, B., LINJEWILE, T.M., AGARWAL, P.K., "Methematical modeling of fluidized bed combustion. 4. N_2O and NOx emissions from the combustion of char," *Fuel* 80:1259-1272 (2001).

29. FREDERICK, W.J., "Combustion processes in black liquor recovery: Analysis and interpretation of combustion rate data and an engineering design model," *DOE Report DOE/CE/40637-T8 (DE90012712) (1990).*

30. DAYTON, D.C., FREDERICK, W.J., "The direct observation of alkali vapor release during biomass combustion and gasification. 2. Black liquor combustion at 1100°C," *Energy and Fuels* (1996).

31. VERRILL, C.L., WESSEL, R.A., "Sodlium loss during black liquor drying and devolatilization – application of modeling results to understanding laboratory data," *Proc. 1995 Int'l. Chem.. Recovery Conf.* Toronto, April 23-27, B89-B103 (1995).

32. JONES, W.P., LINDSTEDT, R.P., "Global reaction schemes for hydrocarbon combustion," *Combustion and Flame*, 73:233-249 (1988).

33. GUENTHER, C., SHAHNAM, M., SYAMLAL, M., LONGANBACH, J., CICERO, D., SMITH, P.V., "CFD modeling of a transport gasifier," *Proc. 19th Annual Pittsburgh Coal Conference*, Sept. 23-27 (2002).

34. SYAMLAL, M., BISSETT, L.A., "METC gasifier advanced simulation (MGAS) model," Technical Note, *NTIS Report No. DOE/METC-92/4108* (1992).

35. WEN, C.Y., CHEN, H., ONOZAKI, M., "User's manual for computer simulation and design of the moving bed coal gasifier," DOE/MC/16474-1390, NTIS/DE83009533 (1982).

36. GUNN, D.J., "Transfer of heat or mass to particles in fixed and fluidized beds," *Int. J. Heat Mass Transfer*, 21:467-476 (1978).

37. DESAI, P.R., WEN, C.Y., "Computer modeling of the MERC fixed bed gasifier," MERC/CR-78/3 (1978).

38. WESTBROOK, C.K., DRYER, F.L., "Simplified mechanisms for the oxidation of hydrocarbon fuels in flames," *Combustion Sci. Tech.*, 27:31-43 (1981).

39. PETERS, N., "Premixed burning in diffusion flames -- the flame zone model of Libby and Economos," *Int. J. Heat Mass Transfer*, 22:691-703 (1979).

40. HANBY V.I., Convective heat transfer in a gas-fired pulsating combustor, *ASME J. of Engr for Power*, 91, 48-52 (1969).

41. DOE, Pulse combustor design qualification test: A DOE assessment, DOE/NETL-2003/1190, July 2003.

42. ARPACI A.C., DEC J.E. AND KELLER J.O., Heat transfer in pulse combustor tailpipe, *Combustion Science and Technology*, 94, 131-146 (1993).

43. GLICKSMAN L.R., CHEN J.C., DECKER N. AND OZKAYNAK T. F., Chapter 6: Design of heat transfer surface, in *Atmospheric Fluidized-Bed Combustion: A Technical Source Book*, Final Report, by S-E. Tung and G.C. Williams, MIT, January 1987.

44. ANDEEN B.R. AND GLICKSMAN L.R., Heat Transfer Conference, ASME Paper 76-HT-67, 1976.

45. PIETSCH, W., Size Enlargement by Agglomeration. England: John Wiley & Sons Ltd, 1991.

46. NOHLGREN, I., "Recovery of kraft black liquor with direct causticization using titanates," Ph.D. Thesis, Luleå University of Technology, Luleå, Sweden (2002).

47. BUSTAMANTE, F., ENICK, R.M., KILLMEYER, R.P., HOWARD, B.H., ROTHENBURGER, K.S., CUGINI, A.V., MORREALE, B.D., CIOCCO, M.V., "Uncatalyzed and wall-catalyzed forward water-gas shift reaction kinetics", *AIChE J.* 51(5):1440-1454 (2005).

48. TINGEY, G.L., "Kinetics of the water-gas shift reaction. I. The reaction of carbon dioxide with hydrogen", *J. Phys. Chem.* 70(5):1406-1412 (1966).

49. MEIJER, R., SIBEIJN, M., VAN DILLEN, M.R.B., KAPTEIJN, F., MOULIJN, J.A., "Kinetics of the alkali-metal-carbonate-catalyzed gasification of carbon. 2. The water-gas shift reaction", *I&ECR* 30(8):1760-1770 (1991).

50. WHITTY, K., HUPA, M., FREDERICK, W.J., "Gasification of Black Liquor Char With Steam at Elevated Pressures," *Journal of Pulp and Paper Science* 21(6):J214-J221 (1995).

51. WHITTY, K., BACKMAN, R., HUPA, M., "An Empirical Rate Model for Black Liquor Char Gasification as a Function of Gas Composition and Pressure," *Proceedings: Advances in Forest Products Environmental and Process Engineering*, 1993 Forest Products Symposium / ed. C.L. Verrill et al. AIChE Symposium Series 90, pp. 73-84 (1994).

52. FREDERICK, W.J., HUPA, M., "Gasification of black liquor char with CO_2 at elevated pressures," *Tappi J.* 74(7):177-183 (1991).

53. WHITTY, K., NARANJO, M., RUBIANO, C., "Performance of a Small-Scale Fluidized Bed Black Liquor Steam Reformer", *Proc. 2006 TAPPI Engineering, Pulping and Environmental Conf.*, 5-8 November 2006, Atlanta, GA (2006).

54. WEN C.Y., HORIO M., KRISHNAN R., KHOSRAVI R. RENGARAJAN P., "Jetting phenomena and dead zone formation of fluidized bed distributors," *Proc. 2nd Pacific Chem. Eng. Conf.*, AIChE, New York (1977).

55. YANG W.C. KEAIRNS D.L., "Design and operating parameters for a fluidized bed agglomerating combustor/gasifier," Fluidization, Cambridge University Press, Cambridge (1978).

56. MERRY J.M.D., Penetration of vertical jets into fluidized beds, *AIChE J.* 21:507 (1975).

57. ZENZ F.A., "Bubble formation and grid design," *Inst. Chem. Eng. Symp. Ser.*, 30:136 (1968).

58. YANG W.C., "Jet penetration in a pressurized fluidized bed," *Ind. Eng. Chem. Fundam.* 20:297-300 (1981).

59. YATES J.G, "Effects of temperature and pressure on gas-solid fluidization," *Chem. Eng. Sci.*, 51:167-205 (1996).

60. MERRY J.M.D., "Penetration of a horizontal gas jet into a fluidized bed," *Trans. Instn Chem. Engrs*. 49:189-195 (1971).

Appendix A

Process and Instrumentation Diagrams for University of Utah's Fluidized Bed Gasification Test System

Appendix A-1: Steam Supply System

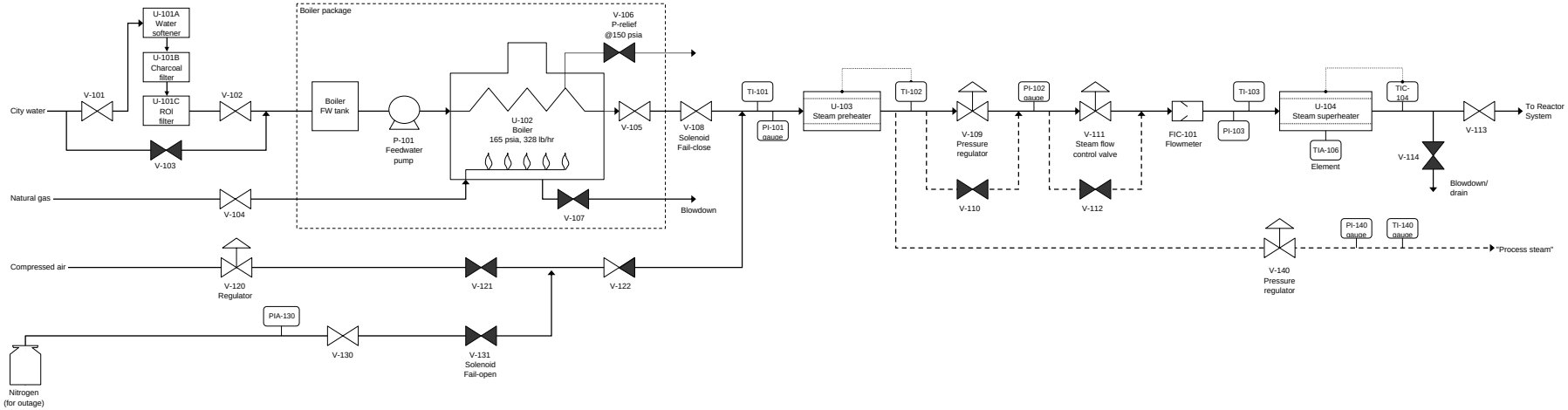

Num	Part	Specs
U-101	Water conditioner (softener)	Softener
U-102	Boiler	150 psi, 328 lb/hr, 398,000 Btu/hr
U-103	Preheater (shell heaters)	3.5" ID, 24" long, 240V, 1800W / half
U-104	Superheater	42 kW, 8 W/in2, 8" x 107"
P-101	Feedwater pump	150 psi, in boiler package
FIC-101	Steam flow meter	1/2", approx. 20-250 lb/hr, 0.8% acc.
V-101	Valve	1/4-turn ball valve
V-102	Valve	1/4-turn ball valve
V-103	Valve	1/4-turn ball valve
V-104	Valve	1/4-turn ball valve
V-105	Steam outlet valve	1/4-turn ball valve
V-106	Pressure relief valve	150 psi relief
V-107	Boiler blow-down valve	1/4-turn ball valve
V-108	Solenoid valve	Fail close
V-109	Steam pressure regulator	Adjustable manual
V-110	Bypass Valve	1/4-turn ball valve
V-111	Control valve	Control valve, 3-15 psi
V-112	Bypass Valve	1/4-turn ball valve
V-113	Valve	1/4-turn ball valve
V-114	Drain valve	1/4-turn ball valve
V-120	Regulator	Adjustable manual
V-121	Shutoff valve	1/4-turn ball valve
V-122	Check valve	Check valve
V-130	Shutoff valve	1/4-turn ball valve
V-131	Solenoid valve	Fail open
V-140	Steam pressure regulator	Adjustable manual

LEGEND

Non-traced lines

Traced lines

THE UNIVERSITY OF UTAH
Chemical & Fuels Engineering Department

Drawing Name:
1. Steam Supply System

Revised by
Whitty

Revision:
1.2 (09/04/03)

Appendix A-2: Black Liquor Supply System

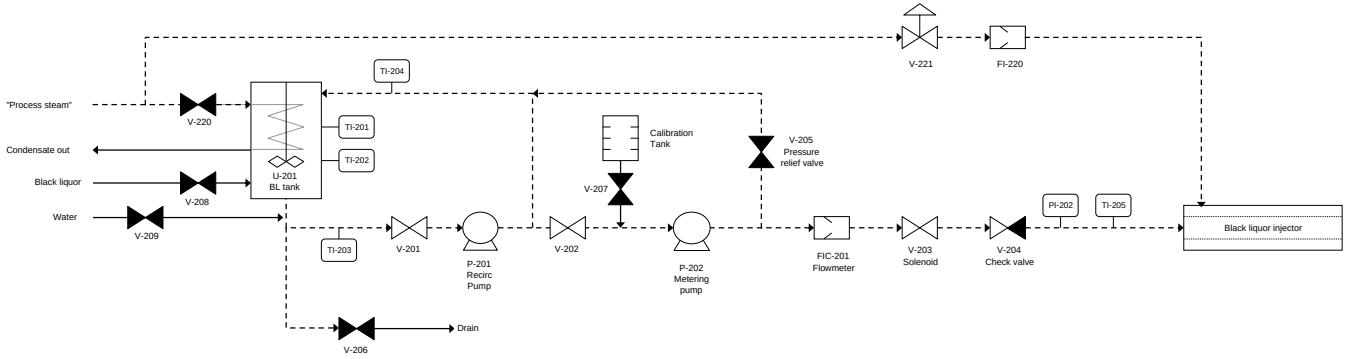

Num	Part	Specs
U-201	Black liquor tank	100 gal, steam jacketed, SS304
P-201	Black liquor recirc pump	Positive displacement, 200 gal/hr max
P-202	Black liquor metering pump	Variable speed, 100 psi, max 30 gal/hr
FIC-201	Black liquor flow meter	Gear drive meter
FIC-220	Steam flow meter	Heated variable area flow meter
V-201	Black liquor shutoff valve	1/4-turn ball valve
V-202	Metering shutoff valve	1/4-turn ball valve
V-203	Liquor shutoff solenoid	Fail-close
V-204	Check valve	Check valve, SS
V-205	Pressure release valve	150 psi release
V-206	Drain valve	1/4-turn ball valve
V-207	Calibration shutoff	1/4-turn ball valve
V-208	Black liquor loading valve	1/4-turn ball valve
V-209	Water shutoff	1/4-turn ball valve
V-220	Steam shutoff	1/4-turn ball valve
V-221	Steam regulator	Manual adjutable

LEGEND

Non-traced lines

Traced lines

THE UNIVERSITY OF UTAH
Chemical & Fuels Engineering Department

Drawing Name:
2. Black Liquor Supply System

Revised by
Whitty

Revision:
1.2 (09/04/03)

Appendix A-3: Reactor and Solids Handling System

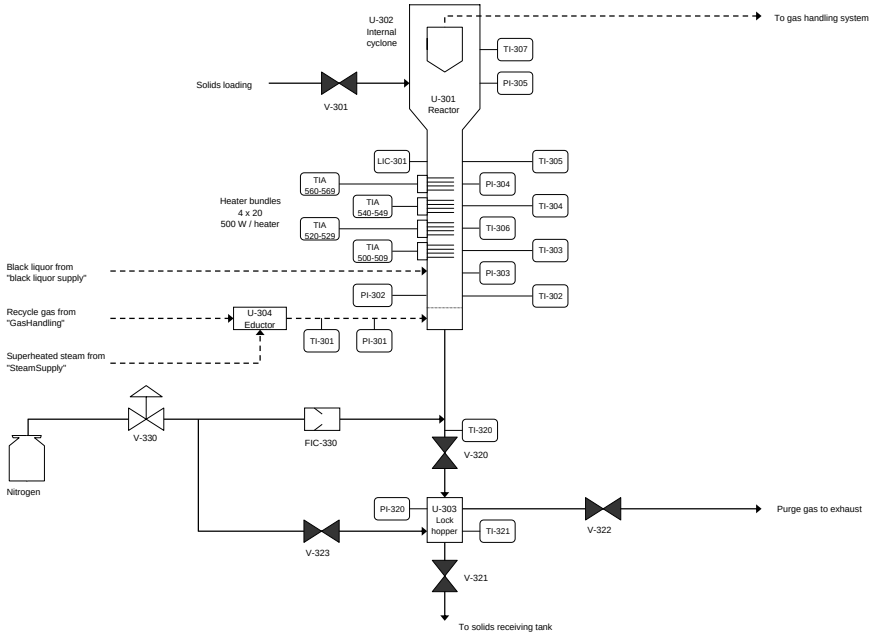

Num	Part	Specs
U-301	Reactor	10" bed ID, approx 18 ft total
U-302	Internal cyclone	"Lazy"
U-303	Lock hopper	2" SS pipe
U-304	High temperature eductor	1 1/2"
V-301	Solids loading valve	1/4-turn ball valve
V-320	Solids removal valve 1	Slide valve
V-321	Solids removal valve 2	Slide valve
V-322	Lock hopper pess release/exhaust valve	Solenoid, fail open
V-323	Lock hopper purge valve	1/4-turn ball valve
V-330	Nitrogen pressure regulator	Manual adjustable
FIC-330	Nitrogen purge flow controller	Mass flow controller

LEGEND

Non-traced lines

Traced lines

THE UNIVERSITY OF UTAH
Chemical & Fuels Engineering Department

Drawing Name:
3. Reactor System

Revised by
Whitty

Revision:
1.2 (09/04/03)

Appendix A-4: Product Gas Handling System

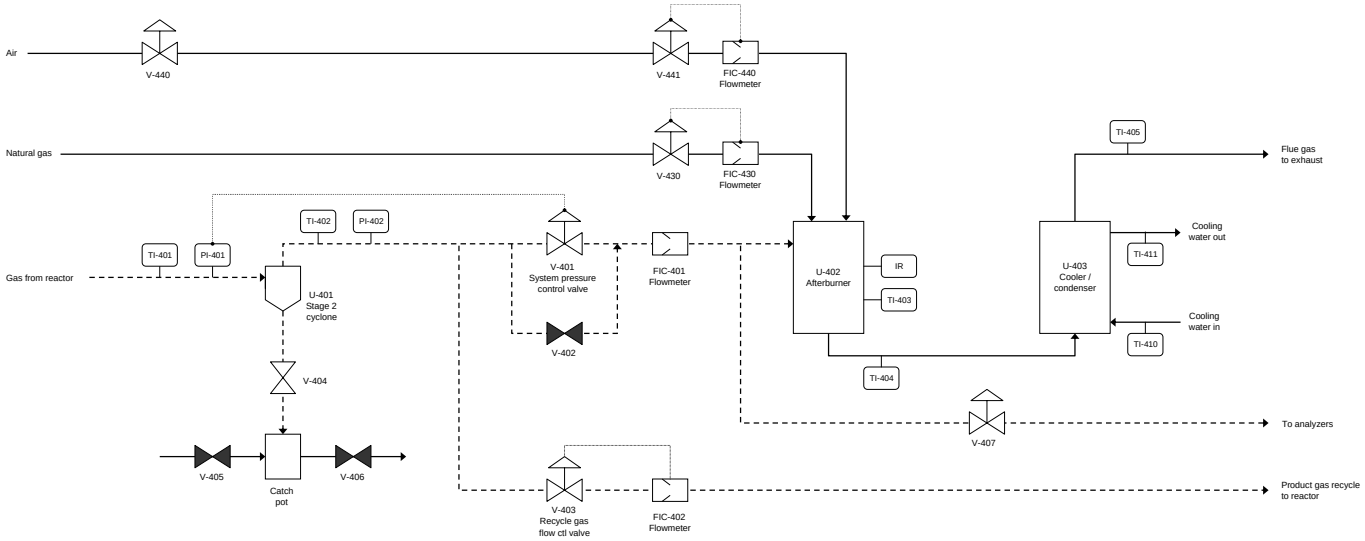

Num	Part	Specs
U-401	Cyclone	SS 304L
U-402	Afterburner	2000 F, 2 sec min res time
U-403	Condenser/cooler	SS 304
FIC-401	Product gas flowmeter	SS 304L
FIC-402	Recycle gas flowmeter	SS 304L
FIC-430	Natural gas flowmeter	Flow meter
FIC-440	Combustion air flowmeter	Flow meter
V-401	Pressure control valve	High temp
V-402	Bypass valve	1/4-turn ball valve
V-403	Recycle gas control valve	High temp
V-404	Cyclone catch pot isolation valve	1/4-turn ball valve
V-405	Catch pot purge valve	1/4-turn ball valve
V-406	Catch pot pressure release/exhaust valve	1/4-turn ball valve
V-407	Analyzer flow control valve	Adjustable + on/off
V-430	Natural gas flow control valve	Control valve
V-440	Combustion air pressure regulator	Manual adjustable
V-441	Combustion air flow control valve	Control valve

LEGEND

Non-traced lines

Traced lines

THE UNIVERSITY OF UTAH
Chemical & Fuels Engineering Department

Drawing Name:
4. Gas Handling System

Revised by
Whitty

Revision:
1.2 (09/04/03)

Appendix B

Select Design Drawings of the Reactor for University of Utah's Fluidized Bed Gasification Test System

ITEM NO.	QTY.	PART NO.	DWG. NO.	WEIGHT
1	1	Section 01	BLG-01	1092.84
2	1	Section 02	BLG-02	4724.13
3	1	Section 03	BLG-03	2646.00
4	1	Section 04	BLG-04	2829.17
5	1	Section 05	BLG-05	2463.36
6	1	Section 06	BLG-06	1322.06
7	1	Section 07	BLG-07	246.34

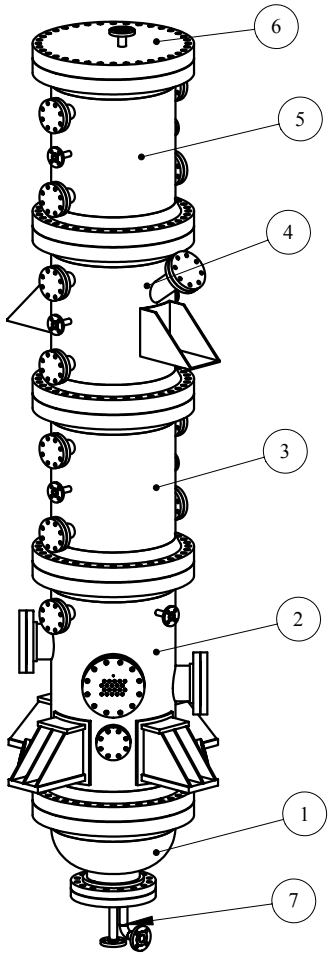

DATE	REVISION	MADE BY	CK'D BY
12/13/03		Ryan Okerlund	

University Combustion Research Center
870 South 500 West, Salt Lake City, UT 84101
(801) 238-6661

Black Liquor Gasifier

SIZE B | DWG. NO. BLG-00

SCALE 1:30 | CAD FILE: BLG-00 | SHEET 1 of 1

ITEM NO.	QTY.	PART NO.	DESCRIPTION	MATERIAL	WEIGHT
1	1	30inch 300lb Weld-Neck Flange	30" 300 lb Weld-Neck Flange	SA 105 Gr. B	620.88
2	1	30inch Cap	30" Sch. 40 Cap	516 Gr. 70	229.23
3	1	12inch Pipe	12" Sch. 40 Pipe	A53	22.19
4	1	12inch 300lb Slip-On Flange	12" 300 lb Slip-On Flange	SS 304L	112.16

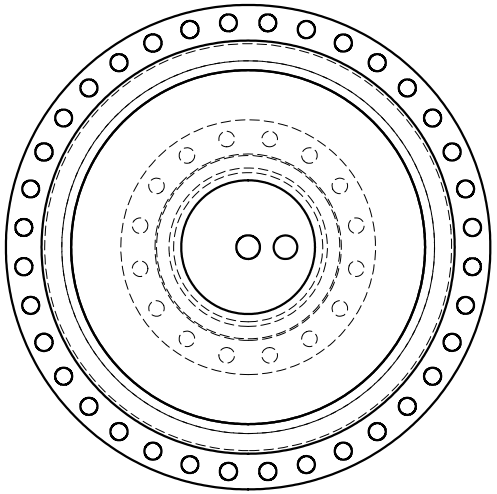

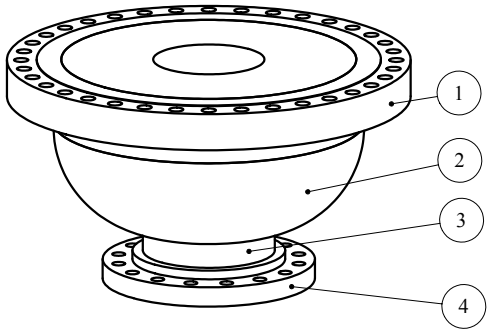

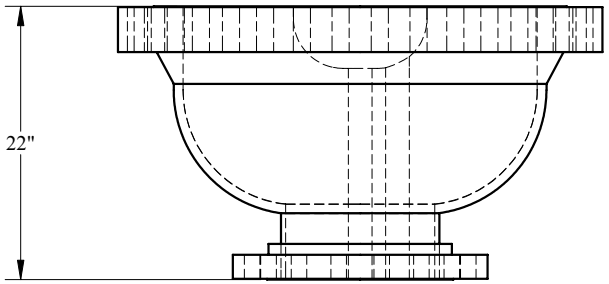

DATE	REVISION	MADE BY	CK'D BY
08/01/03		Ryan Okerlund	

University Combustion Research Center
870 South 500 West, Salt Lake City, UT 84101
(801) 238-6661

Section 01

SIZE B | DWG. NO. BLG-01

SCALE 1:12 | CAD FILE: BLG-01 | SHEET 1 of 2

ITEM NO.	QTY.	PART NO.	DWG. NO.	DESCRIPTION	MATERIAL	WEIGHT
1	1	Section 02 - Shell	BLG-02-1	30" Sch. 40 Pipe	516 Gr. 70	864.74
2	2	30inch 300lb Weld-Neck Flange		30" 300 lb Weld-Neck Flange	SA 105 Gr. B	620.88
3	5	Thermal Well Nozzle		8" Sch. 40 Pipe	SS 304L	15.01
4	5	8inch 300lb Slip-On Flange		8" 300 lb Slip-On Flange	SS 304L	53.65
5	2	Sample Port Nozzle		3" Sch. 40 Pipe	A53	3.19
6	2	Injection Port Nozzle		3" Sch. 40 Pipe	A53	4.76
7	4	3inch 300lb Slip-On Flange		3" 300 lb Slip-On Flange	A36	12.80
8	1	T&P Nozzle		1" Sch. 40 Pipe	A53	0.70
9	1	1inch 300lb Slip-On Flange		1" 300 lb Slip-On Flange	A36	3.02
10	4	Support Bracket	BLG-08	3/8" Plate	A36	161.99

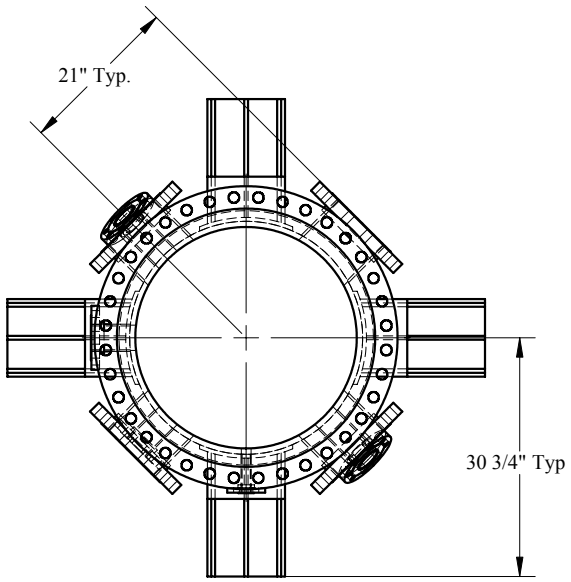

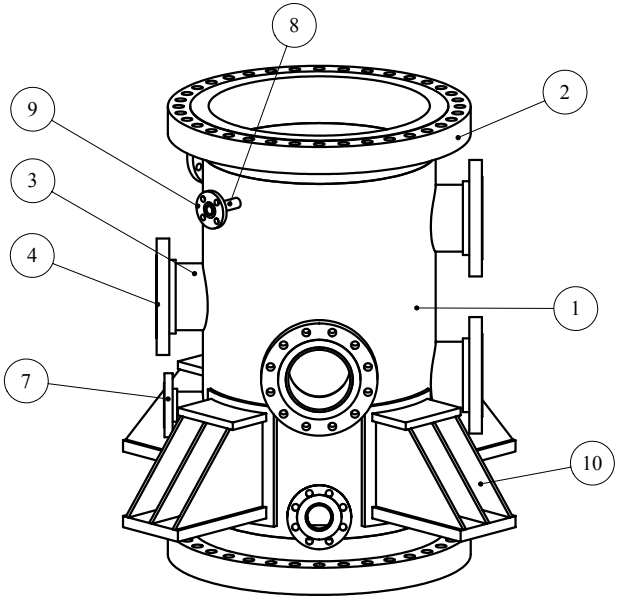

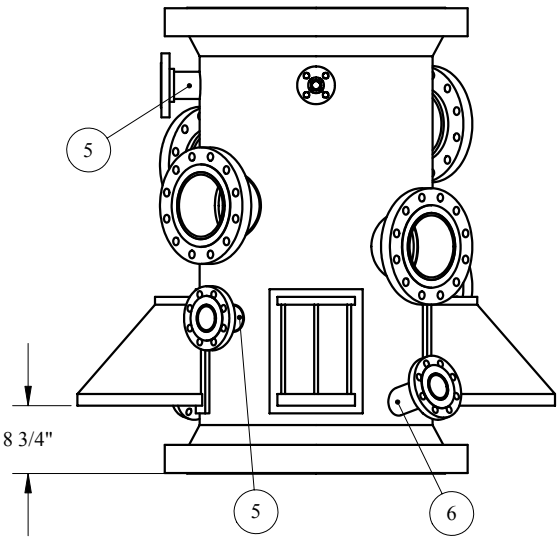

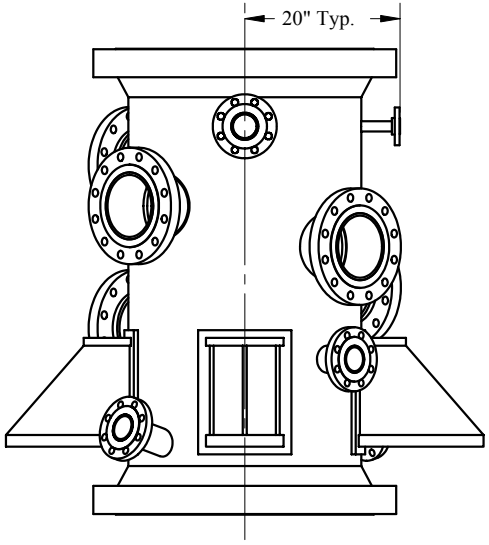

DATE	REVISION	MADE BY	CK'D BY
12/13/03		Ryan Okerlund	

University Combustion Research Center
870 South 500 West, Salt Lake City, UT 84101
(801) 238-6661

Section 02

SIZE B | DWG. NO. BLG-02

SCALE 1:16 | CAD FILE: BLG-02 | SHEET 1 of 2

ITEM NO.	QTY.	PART NO.	DWG. NO.	DESCRIPTION	MATERIAL	WEIGHT
1	1	Section 03 - Shell	BLG-03-1	30" Sch. 40 Pipe	516 Gr. 70	523.82
2	2	30inch 300lb Weld-Neck Flange		30" 300 lb Weld-Neck Flange	SA 105 Gr. B	620.88
3	4	Sample Port Nozzle		3" Sch. 40 Pipe	A53	3.19
4	4	3inch 300lb Slip-On Flange		3" 300 lb Slip-On Flange	A36	12.80
5	2	T&P Nozzle		1" Sch. 40 Pipe	A53	0.70
6	2	1inch 300lb Slip-On Flange		1" 300 lb Slip-On Flange	A36	3.02

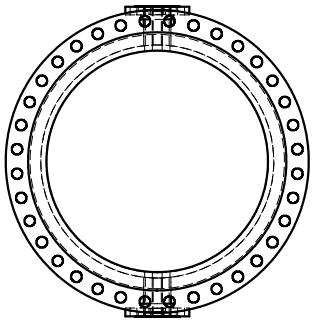

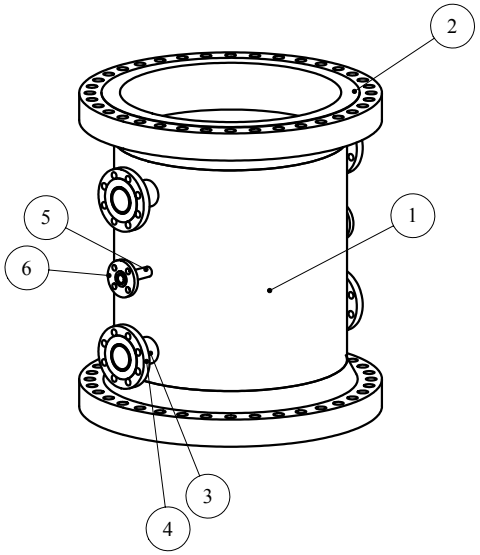

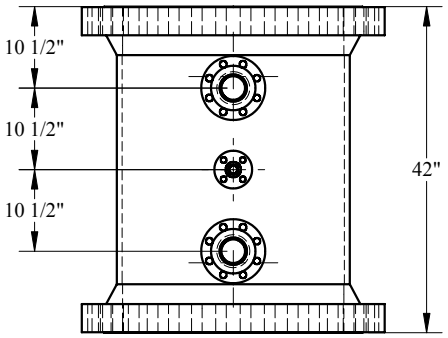

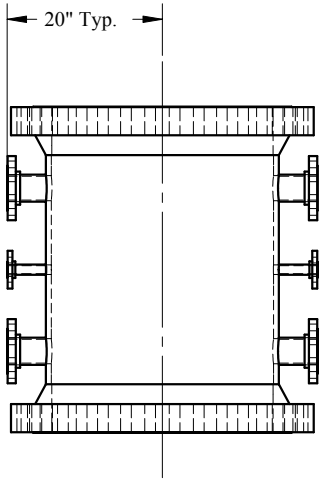

DATE	REVISION	MADE BY	CK'D BY
08/01/03		Ryan Okerlund	

University Combustion Research Center
870 South 500 West, Salt Lake City, UT 84101
(801) 238-6661

Section 3

SIZE B | DWG. NO. BLG-03

SCALE 1:16 | CAD FILE: BLG-03 | SHEET 1 of 2

ITEM NO.	QTY.	PART NO.	DWG. NO.	DESCRIPTION	MATERIAL	WEIGHT
1	1	Section 04 - Shell	BLG-04-1	30" Sch. 40 Pipe	516 Gr. 70	566.10
2	2	30inch 300lb Weld-Neck Flange		30" 300 lb Weld-Neck Flange	SA 105 Gr. B	620.88
3	4	Sample Port Nozzle		3" Sch. 40 Pipe	A53	3.19
4	1	Solids Port Nozzle		4" Sch. 40 Pipe	A53	10.62
5	4	3inch 300lb Slip-On Flange		3" 300 lb Slip-On Flange	A36	12.80
6	1	4inch 300lb Slip-On Flange		4" 300 lb Slip-On Flange	A36	20.92
7	2	T&P Nozzle		1" Sch. 40 Pipe	A53	0.70
8	2	1inch 300lb Slip-On Flange		1" 300 lb Slip-On Flange	A36	3.02
9	2	Support Bracket - Upper	BLG-08	3/8" Plate	A36	56.59

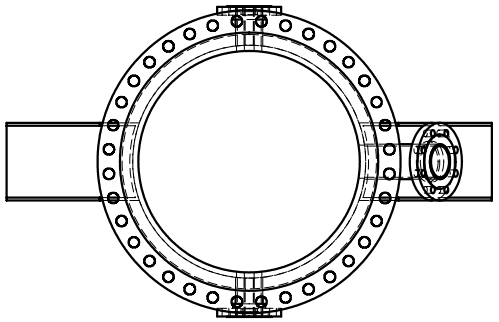

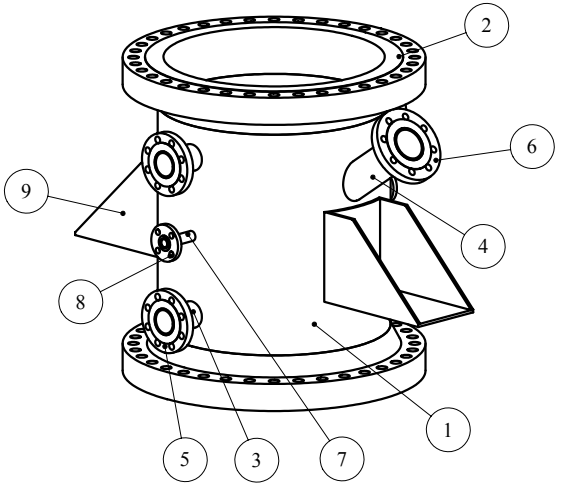

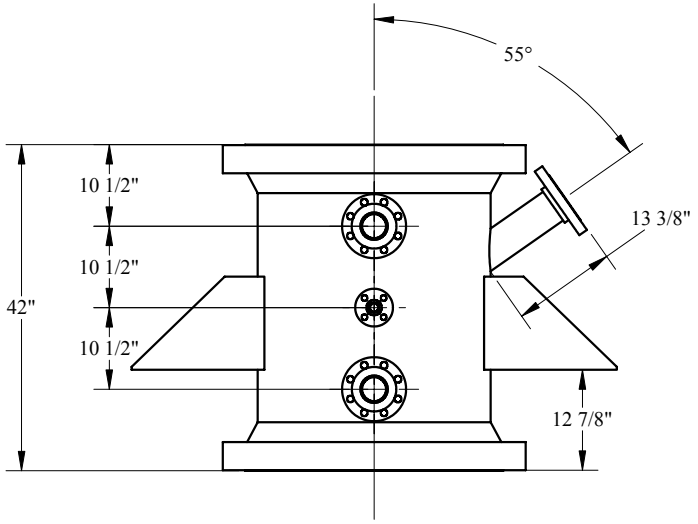

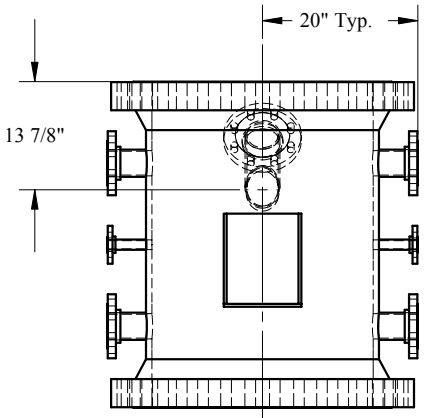

VIEW

DATE	REVISION	MADE BY	CK'D BY
08/01/03		Ryan Okerlund	

University Combustion Research Center
870 South 500 West, Salt Lake City, UT 84101
(801) 238-6661

Section 04

SIZE B | DWG. NO. BLG-04

SCALE 1:16 | CAD FILE: BLG-04 | SHEET 1 of 2

ITEM NO.	QTY.	PART NO.	DWG. NO.	DESCRIPTION	MATERIAL	WEIGHT
1	1	Section 05 - Shell	BLG-05-1	30" Sch. 40 Pipe	516 Gr. 70	523.82
2	2	30inch 300lb Weld-Neck Flange		30" 300 lb Weld-Neck Flange	SA 105 Gr. B	620.88
3	4	Sample Port Nozzle		3" Sch. 40 Pipe	A53	3.19
4	4	3inch 300lb Slip-On Flange		3" 300 lb Slip-On Flange	A36	12.80
5	2	T&P Nozzle		1" Sch. 40 Pipe	A53	0.70
6	2	1inch 300lb Slip-On Flange		1" 300 lb Slip-On Flange	A36	3.02

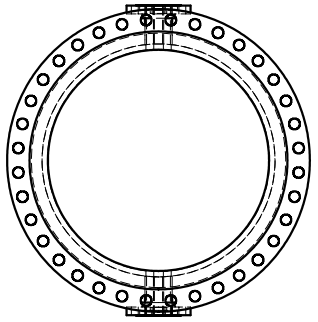

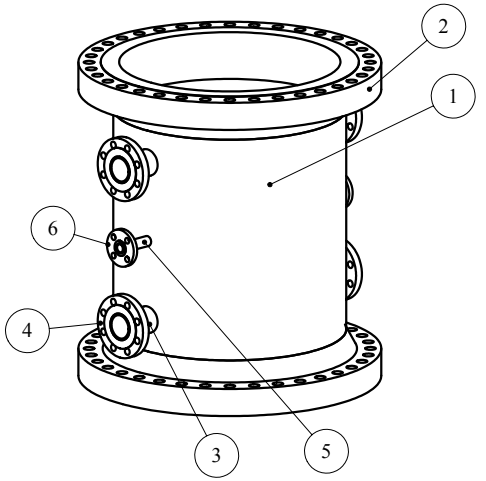

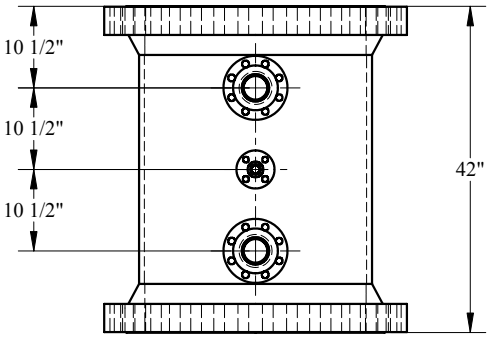

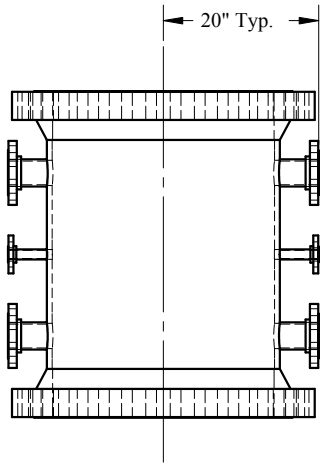

DATE	REVISION	MADE BY	CK'D BY
08/01/03		Ryan Okerlund	

University Combustion Research Center
870 South 500 West, Salt Lake City, UT 84101
(801) 238-6661

Section 05

SIZE B | DWG. NO. BLG-05

SCALE 1:16 | CAD FILE: BLG-05 | SHEET 1 of 2

ITEM NO.	QTY.	PART NO.	DESCRIPTION	MATERIAL	WEIGHT
1	1	Exit Flange	30" 300 lb Blind Flange	SS 304L	1195.28
2	1	Exit Pipe	1 1/2" Sch. 40 Pipe	SS 304L	4.34
3	2	1.5inch 300lb Slip-On Flange	1 1/2" 300 lb Slip-On Flange	SS 304L	6.04

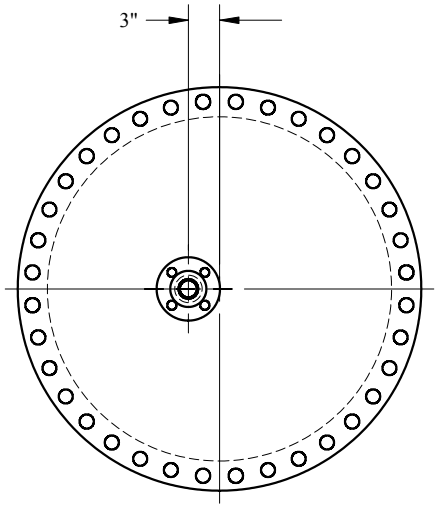

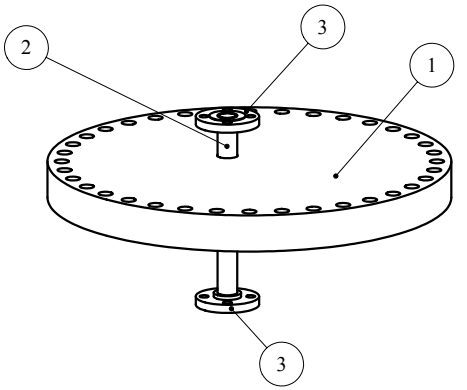

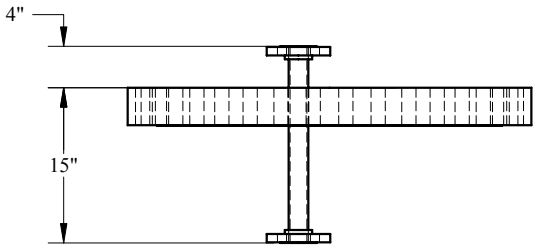

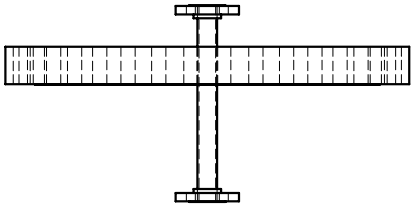

DATE	REVISION	MADE BY	CK'D BY
08/01/03		Ryan Okerlund	

University Combustion Research Center
870 South 500 West, Salt Lake City, UT 84101
(801) 238-6661

Section 06

SIZE B | DWG. NO. BLG-06

SCALE 1:8 | CAD FILE: BLG-06 | SHEET 1 of 2

ITEM NO.	QTY.	PART NO.	DWG. NO.	DESCRIPTION	MATERIAL	WEIGHT
1	1	Distributor Plate	BLG-07-1	1" Plate	321 Stainless	23.94
2	1	10inch Cap		10" Sch. 40 Cap	321 Stainless	18.31
3	1	12inch 300lb Blind Flange		12" 300 lb Blind Flange	SS 304L	171.80
4	1	Solids Pipe		1 1/2" Sch. 40 Pipe	321 Stainless	8.23
5	1	1.5inch 300lb Slip-On Flange		1 1/2" 300 lb Slip-On Flange	SS 304L	6.04
6	1	Steam Pipe 1		1 1/2" Sch. 40 Pipe	321 Stainless	6.17
7	1	Steam Pipe 2		1 1/2" Sch. 40 Pipe	321 Stainless	0.91
8	1	1.5inch Elbow		1 1/2" Sch. 40 Long-Radius Elbow	321 Stainless	0.81
9	1	1.5inch 600lb Slip-On Flange		1 1/2" 600 lb Slip-On Flange	SS 304L	6.61
10	1	Deflector Plate		1/4" Plate	321 Stainless	18.31
11	20	Distributor Nozzle	BLG-07-2	Distributor Nozzle	321 Stainless	0.13

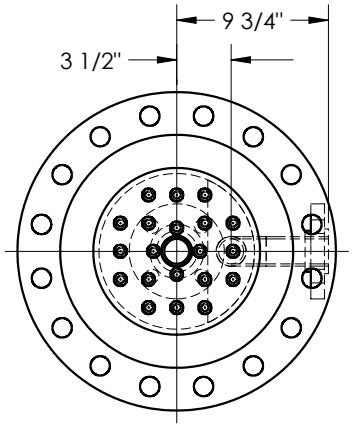

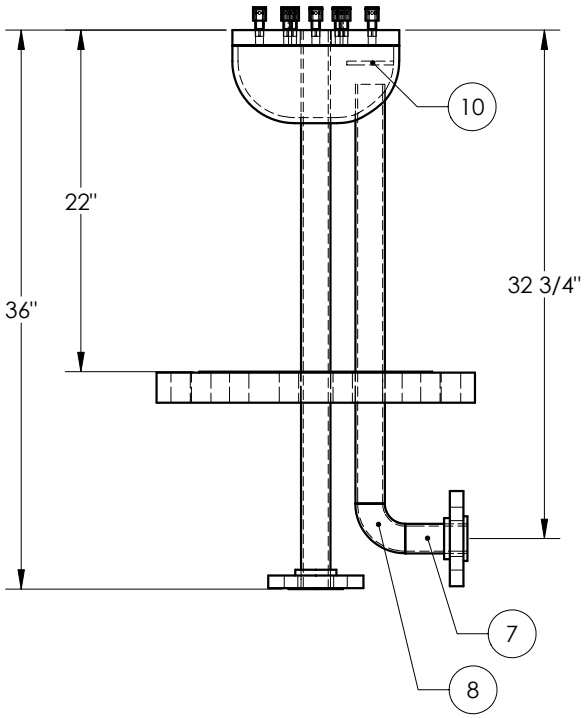

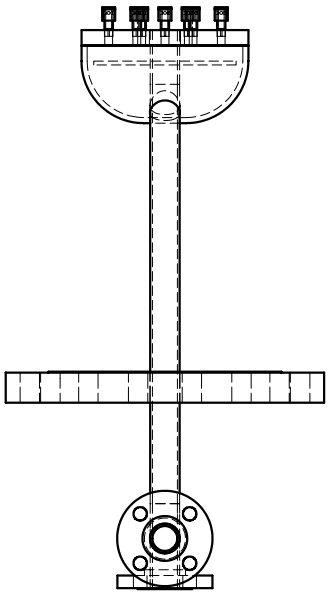

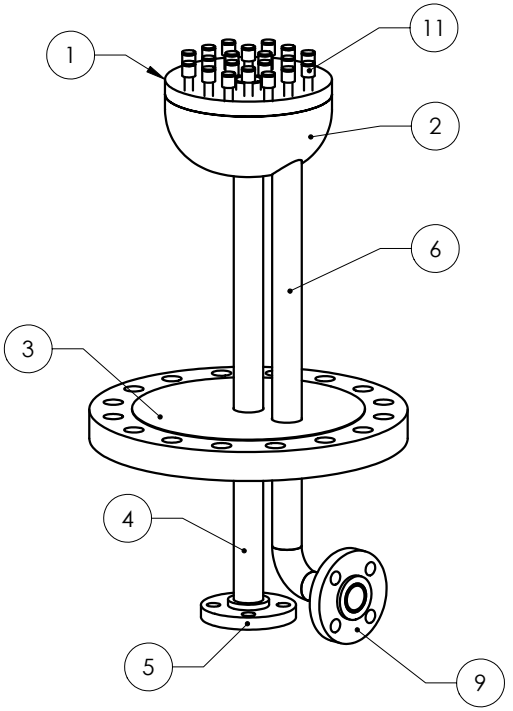

Fabricate 1

DATE	REVISION	MADE BY	CK'D BY
12/13/03		Ryan Okerlund	

University Combustion Research Center
870 South 500 West, Salt Lake City, UT 84101
(801) 238-6661

Section 7

SIZE B | DWG. NO. BLG-07

SCALE 1:8 | CAD FILE: BLG-07 | SHEET 1 of 1

Appendix C

Summary of Mass Balances of Tests with the University of Utah Fluidized Bed Steam Reformer

System Mass Balance Calculations

RUN NUMBER:	19	PURPOSE:	Tar sampling reproducibility	NOTES:	Reproducibility test.

Note: Standard conditions are 14.7 psia and 70°F

LIQUOR COMPOSITION (DRY)

C (carbon)	34.43	mass%
H (hydrogen)	3.00	mass%
O (oxygen)	41.45	mass%
S (sulfur)	0.10	mass%
Na (sodium)	18.70	mass%
K (potassium)	2.02	mass%
Cl (chlorine)	0.09	mass%
N (nitrogen)	0.21	mass%
Other (Si, Ca, Mg, etc)	0.00	mass%
TOTAL LIQUOR COMPOSITION	100.00	mass%

EST. INORGANIC SOLIDS COMPOSITION (100 lb basis)

	lb	wt%	% of BLS
C (carbon)	5.19	11.1%	15.1%
H (hydrogen)	0.00	0.0%	0.0%
O (oxygen)	20.75	44.4%	50.1%
S (sulfur)	0.01	0.0%	10.0%
Na (sodium)	18.70	40.0%	100.0%
K (potassium)	2.02	4.3%	100.0%
Cl (chlorine)	0.09	0.2%	100.0%
N (nitrogen)	0.00	0.0%	0.0%
Other (Si, Ca, Mg, etc)	0.00	0.0%	100.0%
TOTAL	46.76	100.0%	46.8%

Percent of BLS that is organic carbon:	29.2	wt%
Percent of tars that is organic carbon:	87.0	wt%

BLACK LIQUOR

19.6	lb/hr	
58%	solids	
11.37	lb/hr solids	
8.23	lb/hr water	

STEAM

31.8	lb/hr fluidizing	
1.5	lb/hr thru injector	

NITROGEN

12	slpm	
25	scfh	
1.8	lb/hr	

AIR

0	slpm	0.0%
0	scfh	
0.0	lb/hr	

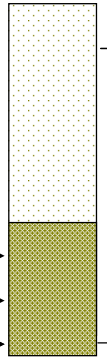

PRODUCT GAS

49.9	lb/hr		1072	scfh total gas flow
18.01	assumed MW (lb/lbmol)		308	scfh dry gas flow
52.5%	H2 (vol%)		2.77	lbmol/hr total gas
3.2%	CO (vol%)		0.80	lbmol/hr dry gas
23.9%	CO2 (vol%)		15.46	analyzed MW dry (lb/lbmol)
4.0%	CH4 (vol%)		17.28	analyzed MW wet (lb/lbmol)
8.4%	N2 (vol%)		47.9	corrected prod gas flow (lb/hr)
92.0%	Total		35.6	H2O flow in prod gas (lb/hr)

TARS

300	liters dry gas sampled	253	std liters dry gas sampled
468.3	grams water condensed	628	std liters steam condensed
17.7	grams tars recovered	29%	dry gas in product gas
25.0	minutes sampling time	31	scf sampled
12.5	psia dry gas meter pressure	7.0%	of total product gas
75	F dry gas meter temperature	1.3	lb/hr tar production rate

SOLIDS

5.5	lb/hr production rate	5.32	lb/hr inorganics
3.0%	organic carbon content		

TAR CONCENTRATION IN GAS

70 gram tar per scm dry gas	**20 g tar per scm wet gas**
4.4 lb tar per 1000 scf dry gas	**1.3 lb tar per 1000 scf wet gas**

TAR PRODUCTION RATE (APPROX)

0.118 lb tar per lb BLS	
35% of liquor organic C as tar C	

TOTAL BALANCE

IN	
Black liquor	19.6
Steam	33.3
Nitrogen	1.8
Air	0.0
TOTAL IN	**54.7**
OUT	
Product gas	47.9
Tars	1.3
Solids	5.5
TOTAL OUT	**54.7**
OUT - IN	0.0
CLOSURE	**100%**

CARBON (C) BALANCE

IN	
BL organic C	3.3
BL inorganics	0.6
TOTAL IN	**3.9**
OUT	
Dry product gas	3.0
Tars	1.2
Solids	0.8
TOTAL OUT	**4.9**
OUT - IN	1.0
CLOSURE	**125%**

HYDROGEN (H) BALANCE

IN	
Steam	3.7
BLS hydrogen	0.3
BL water	0.9
TOTAL IN	**5.0**
OUT	
Dry product gas	1.0
Steam	4.0
Tars	0.2
TOTAL OUT	**5.1**
OUT - IN	0.1
CLOSURE	**103%**

SODIUM BALANCE

IN	
Black liquor	2.1
TOTAL IN	**2.1**
OUT	
Solids	2.1
TOTAL OUT	**2.1**
OUT - IN	0.0
CLOSURE	**100%**

NITROGEN (N) BALANCE

IN	
Black liquor	0.0
Nitrogen gas	1.8
Air	0.0
TOTAL IN	**1.9**
OUT	
Dry product gas	1.9
TOTAL OUT	**1.9**
OUT - IN	0.0
CLOSURE	**100%**

System Mass Balance Calculations

RUN NUMBER:	19	PURPOSE:	Tar sampling reproducibility	NOTES:	Reproducibility test.

Note: Standard conditions are 14.7 psia and 70°F

LIQUOR COMPOSITION (DRY)

C (carbon)	34.43	mass%
H (hydrogen)	3.00	mass%
O (oxygen)	41.45	mass%
S (sulfur)	0.10	mass%
Na (sodium)	18.70	mass%
K (potassium)	2.02	mass%
Cl (chlorine)	0.09	mass%
N (nitrogen)	0.21	mass%
Other (Si, Ca, Mg, etc)	0.00	mass%
TOTAL LIQUOR COMPOSITION	100.00	mass%

EST. INORGANIC SOLIDS COMPOSITION (100 lb basis)

	lb	wt%	% of BLS
C (carbon)	5.19	11.1%	15.1%
H (hydrogen)	0.00	0.0%	0.0%
O (oxygen)	20.75	44.4%	50.1%
S (sulfur)	0.01	0.0%	10.0%
Na (sodium)	18.70	40.0%	100.0%
K (potassium)	2.02	4.3%	100.0%
Cl (chlorine)	0.09	0.2%	100.0%
N (nitrogen)	0.00	0.0%	0.0%
Other (Si, Ca, Mg, etc)	0.00	0.0%	100.0%
TOTAL	46.76	100.0%	46.8%

Percent of BLS that is organic carbon:	29.2	wt%
Percent of tars that is organic carbon:	87.0	wt%

BLACK LIQUOR

19.6	lb/hr
58%	solids
11.37	lb/hr solids
8.23	lb/hr water

STEAM

31.8	lb/hr fluidizing
1.5	lb/hr thru injector

NITROGEN

12	slpm
25	scfh
1.8	lb/hr

AIR

0	slpm	0.0%
0	scfh	
0.0	lb/hr	

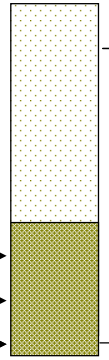

PRODUCT GAS

49.5	lb/hr	1064	scfh total gas flow
18.01	assumed MW (lb/lbmol)	272	scfh dry gas flow
52.5%	H2 (vol%)	2.75	lbmol/hr total gas
3.2%	CO (vol%)	0.70	lbmol/hr dry gas
23.9%	CO2 (vol%)	15.77	analyzed MW dry (lb/lbmol)
4.0%	CH4 (vol%)	17.44	analyzed MW wet (lb/lbmol)
9.5%	N2 (vol%)	47.9	corrected prod gas flow (lb/hr)
93.1%	Total	36.9	H2O flow in prod gas (lb/hr)

TARS

200	liters dry gas sampled	168	std liters dry gas sampled
365.9	grams water condensed	491	std liters steam condensed
13.1	grams tars recovered	26%	dry gas in product gas
30.0	minutes sampling time	23	scf sampled
12.5	psia dry gas meter pressure	4.4%	of total product gas
75	F dry gas meter temperature	1.3	lb/hr tar production rate

SOLIDS

5.5	lb/hr production rate	5.32	lb/hr inorganics
3.0%	organic carbon content		

TAR CONCENTRATION IN GAS

78 gram tar per scm dry gas	20 g tar per scm wet gas
4.9 lb tar per 1000 scf dry gas	1.2 lb tar per 1000 scf wet gas

TAR PRODUCTION RATE (APPROX)

0.116	lb tar per lb BLS
35%	of liquor organic C as tar C

TOTAL BALANCE

IN	
Black liquor	19.6
Steam	33.3
Nitrogen	1.8
Air	0.0
TOTAL IN	**54.7**
OUT	
Product gas	47.9
Tars	1.3
Solids	5.5
TOTAL OUT	**54.7**
OUT - IN	0.0
CLOSURE	**100%**

CARBON (C) BALANCE

IN	
BL organic C	3.3
BL inorganics	0.6
TOTAL IN	**3.9**
OUT	
Dry product gas	2.6
Tars	1.1
Solids	0.8
TOTAL OUT	**4.5**
OUT - IN	0.6
CLOSURE	**116%**

HYDROGEN (H) BALANCE

IN	
Steam	3.7
BLS hydrogen	0.3
BL water	0.9
TOTAL IN	**5.0**
OUT	
Dry product gas	0.9
Steam	4.1
Tars	0.2
TOTAL OUT	**5.2**
OUT - IN	0.2
CLOSURE	**103%**

SODIUM BALANCE

IN	
Black liquor	2.1
TOTAL IN	**2.1**
OUT	
Solids	2.1
TOTAL OUT	**2.1**
OUT - IN	0.0
CLOSURE	**100%**

NITROGEN (N) BALANCE

IN	
Black liquor	0.0
Nitrogen gas	1.8
Air	0.0
TOTAL IN	**1.9**
OUT	
Dry product gas	1.9
TOTAL OUT	**1.9**
OUT - IN	0.0
CLOSURE	**100%**

System Mass Balance Calculations

RUN NUMBER:	19	PURPOSE:	Tar sampling reproducibility	NOTES:	Reproducibility test.

Note: Standard conditions are 14.7 psia and 70°F

LIQUOR COMPOSITION (DRY)

C (carbon)	34.43	mass%
H (hydrogen)	3.00	mass%
O (oxygen)	41.45	mass%
S (sulfur)	0.10	mass%
Na (sodium)	18.70	mass%
K (potassium)	2.02	mass%
Cl (chlorine)	0.09	mass%
N (nitrogen)	0.21	mass%
Other (Si, Ca, Mg, etc)	0.00	mass%
TOTAL LIQUOR COMPOSITION	100.00	mass%

EST. INORGANIC SOLIDS COMPOSITION (100 lb basis)

	lb	wt%	% of BLS
C (carbon)	5.19	11.1%	15.1%
H (hydrogen)	0.00	0.0%	0.0%
O (oxygen)	20.75	44.4%	50.1%
S (sulfur)	0.01	0.0%	10.0%
Na (sodium)	18.70	40.0%	100.0%
K (potassium)	2.02	4.3%	100.0%
Cl (chlorine)	0.09	0.2%	100.0%
N (nitrogen)	0.00	0.0%	0.0%
Other (Si, Ca, Mg, etc)	0.00	0.0%	100.0%
TOTAL	46.76	100.0%	46.8%

Percent of BLS that is organic carbon:	29.2	wt%
Percent of tars that is organic carbon:	87.0	wt%

BLACK LIQUOR

19.6	lb/hr	
58%	solids	
11.37	lb/hr solids	
8.23	lb/hr water	

STEAM

31.8	lb/hr fluidizing	
1.5	lb/hr thru injector	

NITROGEN

12	slpm	
25	scfh	
1.8	lb/hr	

AIR

0	slpm	0.0%
0	scfh	
0.0	lb/hr	

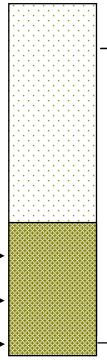

PRODUCT GAS

49.8	lb/hr		1070	scfh total gas flow
18.01	assumed MW (lb/lbmol)		301	scfh dry gas flow
52.5%	H2 (vol%)		2.76	lbmol/hr total gas
3.2%	CO (vol%)		0.78	lbmol/hr dry gas
23.9%	CO2 (vol%)		15.51	analyzed MW dry (lb/lbmol)
4.0%	CH4 (vol%)		17.31	analyzed MW wet (lb/lbmol)
8.6%	N2 (vol%)		47.9	corrected prod gas flow (lb/hr)
92.2%	Total		35.8	H2O flow in prod gas (lb/hr)

TARS

300	liters dry gas sampled	253	std liters dry gas sampled
481.4	grams water condensed	646	std liters steam condensed
18.6	grams tars recovered	28%	dry gas in product gas
27.0	minutes sampling time	32	scf sampled
12.5	psia dry gas meter pressure	6.6%	of total product gas
75	F dry gas meter temperature	1.4	lb/hr tar production rate

SOLIDS

5.5	lb/hr production rate	5.32	lb/hr inorganics
3.0%	organic carbon content		

TAR CONCENTRATION IN GAS

74 gram tar per scm dry gas	21 g tar per scm wet gas
4.6 lb tar per 1000 scf dry gas	1.3 lb tar per 1000 scf wet gas

TAR PRODUCTION RATE (APPROX)

0.122 lb tar per lb BLS	
36% of liquor organic C as tar C	

TOTAL BALANCE

IN	
Black liquor	19.6
Steam	33.3
Nitrogen	1.8
Air	0.0
TOTAL IN	**54.7**
OUT	
Product gas	47.9
Tars	1.4
Solids	5.5
TOTAL OUT	**54.7**
OUT - IN	0.0
CLOSURE	**100%**

CARBON (C) BALANCE

IN	
BL organic C	3.3
BL inorganics	0.6
TOTAL IN	**3.9**
OUT	
Dry product gas	2.9
Tars	1.2
Solids	0.8
TOTAL OUT	**4.9**
OUT - IN	0.9
CLOSURE	**124%**

HYDROGEN (H) BALANCE

IN	
Steam	3.7
BLS hydrogen	0.3
BL water	0.9
TOTAL IN	**5.0**
OUT	
Dry product gas	0.9
Steam	4.0
Tars	0.2
TOTAL OUT	**5.1**
OUT - IN	0.1
CLOSURE	**103%**

SODIUM BALANCE

IN	
Black liquor	2.1
TOTAL IN	**2.1**
OUT	
Solids	2.1
TOTAL OUT	**2.1**
OUT - IN	0.0
CLOSURE	**100%**

NITROGEN (N) BALANCE

IN	
Black liquor	0.0
Nitrogen gas	1.8
Air	0.0
TOTAL IN	**1.9**
OUT	
Dry product gas	1.9
TOTAL OUT	**1.9**
OUT - IN	0.0
CLOSURE	**100%**

System Mass Balance Calculations

RUN NUMBER:	19	PURPOSE:	Base for steam temp and air tar runs	NOTES:	Baseline conditions for run 19.

Note: Standard conditions are 14.7 psia and 70°F

LIQUOR COMPOSITION (DRY)

C (carbon)	34.43	mass%
H (hydrogen)	3.00	mass%
O (oxygen)	41.45	mass%
S (sulfur)	0.10	mass%
Na (sodium)	18.70	mass%
K (potassium)	2.02	mass%
Cl (chlorine)	0.09	mass%
N (nitrogen)	0.21	mass%
Other (Si, Ca, Mg, etc)	0.00	mass%
TOTAL LIQUOR COMPOSITION	100.00	mass%

EST. INORGANIC SOLIDS COMPOSITION (100 lb basis)

	lb	wt%	% of BLS
C (carbon)	5.19	11.1%	15.1%
H (hydrogen)	0.00	0.0%	0.0%
O (oxygen)	20.75	44.4%	50.1%
S (sulfur)	0.01	0.0%	10.0%
Na (sodium)	18.70	40.0%	100.0%
K (potassium)	2.02	4.3%	100.0%
Cl (chlorine)	0.09	0.2%	100.0%
N (nitrogen)	0.00	0.0%	0.0%
Other (Si, Ca, Mg, etc)	0.00	0.0%	100.0%
TOTAL	46.76	100.0%	46.8%

Percent of BLS that is organic carbon:	29.2	wt%
Percent of tars that is organic carbon:	87.0	wt%

BLACK LIQUOR

20.3	lb/hr
44%	solids
8.93	lb/hr solids
11.37	lb/hr water

STEAM

32.1	lb/hr fluidizing
1.5	lb/hr thru injector

NITROGEN

10	slpm
21	scfh
1.5	lb/hr

AIR

0	slpm	0.0%
0	scfh	
0.0	lb/hr	

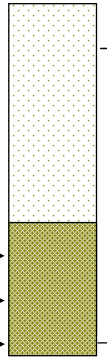

PRODUCT GAS

51.7	lb/hr	1110	scfh total gas flow
18.01	assumed MW (lb/lbmol)	239	scfh dry gas flow
52.3%	H2 (vol%)	2.87	lbmol/hr total gas
3.2%	CO (vol%)	0.62	lbmol/hr dry gas
23.7%	CO2 (vol%)	15.53	analyzed MW dry (lb/lbmol)
4.0%	CH4 (vol%)	17.48	analyzed MW wet (lb/lbmol)
9.0%	N2 (vol%)	50.1	corrected prod gas flow (lb/hr)
92.1%	Total	40.5	H2O flow in prod gas (lb/hr)

TARS

200	liters dry gas sampled	168	std liters dry gas sampled
456.8	grams water condensed	613	std liters steam condensed
11.2	grams tars recovered	22%	dry gas in product gas
29.0	minutes sampling time	28	scf sampled
12.5	psia dry gas meter pressure	5.1%	of total product gas
75	F dry gas meter temperature	1.0	lb/hr tar production rate

SOLIDS

4.3	lb/hr production rate	4.18	lb/hr inorganics
3.0%	organic carbon content		

TAR CONCENTRATION IN GAS

66 gram tar per scm dry gas	14 g tar per scm wet gas
4.1 lb tar per 1000 scf dry gas	0.9 lb tar per 1000 scf wet gas

TAR PRODUCTION RATE (APPROX)

0.111	lb tar per lb BLS
33%	of liquor organic C as tar C

TOTAL BALANCE

IN	
Black liquor	20.3
Steam	33.6
Nitrogen	1.5
Air	0.0
TOTAL IN	**55.4**
OUT	
Product gas	50.1
Tars	1.0
Solids	4.3
TOTAL OUT	**55.4**
OUT - IN	0.0
CLOSURE	**100%**

CARBON (C) BALANCE

IN	
BL organic C	2.6
BL inorganics	0.5
TOTAL IN	**3.1**
OUT	
Dry product gas	2.3
Tars	0.9
Solids	0.6
TOTAL OUT	**3.8**
OUT - IN	0.7
CLOSURE	**122%**

HYDROGEN (H) BALANCE

IN	
Steam	3.8
BLS hydrogen	0.3
BL water	1.3
TOTAL IN	**5.3**
OUT	
Dry product gas	0.8
Steam	4.5
Tars	0.1
TOTAL OUT	**5.4**
OUT - IN	0.1
CLOSURE	**102%**

SODIUM BALANCE

IN	
Black liquor	1.7
TOTAL IN	**1.7**
OUT	
Solids	1.7
TOTAL OUT	**1.7**
OUT - IN	0.0
CLOSURE	**100%**

NITROGEN (N) BALANCE

IN	
Black liquor	0.0
Nitrogen gas	1.5
Air	0.0
TOTAL IN	**1.6**
OUT	
Dry product gas	1.6
TOTAL OUT	**1.6**
OUT - IN	0.0
CLOSURE	**100%**

System Mass Balance Calculations

RUN NUMBER:	19	PURPOSE:	Test tars with low fluidizing steam T	NOTES:	Decreased temperature of fluidizing steam from normal 1120°F to 895°F as per request by TRI.

Note: Standard conditions are 14.7 psia and 70°F

LIQUOR COMPOSITION (DRY)

C (carbon)	34.43	mass%
H (hydrogen)	3.00	mass%
O (oxygen)	41.45	mass%
S (sulfur)	0.10	mass%
Na (sodium)	18.70	mass%
K (potassium)	2.02	mass%
Cl (chlorine)	0.09	mass%
N (nitrogen)	0.21	mass%
Other (Si, Ca, Mg, etc)	0.00	mass%
TOTAL LIQUOR COMPOSITION	100.00	mass%

EST. INORGANIC SOLIDS COMPOSITION (100 lb basis)

	lb	wt%	% of BLS
C (carbon)	5.19	11.1%	15.1%
H (hydrogen)	0.00	0.0%	0.0%
O (oxygen)	20.75	44.4%	50.1%
S (sulfur)	0.01	0.0%	10.0%
Na (sodium)	18.70	40.0%	100.0%
K (potassium)	2.02	4.3%	100.0%
Cl (chlorine)	0.09	0.2%	100.0%
N (nitrogen)	0.00	0.0%	0.0%
Other (Si, Ca, Mg, etc)	0.00	0.0%	100.0%
TOTAL	46.76	100.0%	46.8%

Percent of BLS that is organic carbon:	29.2	wt%
Percent of tars that is organic carbon:	87.0	wt%

BLACK LIQUOR

22.3	lb/hr	
44%	solids	
9.81	lb/hr solids	
12.49	lb/hr water	

STEAM

31.9	lb/hr fluidizing	
1.5	lb/hr thru injector	

NITROGEN

10	slpm	
21	scfh	
1.5	lb/hr	

AIR

0	slpm	0.0%
0	scfh	
0.0	lb/hr	

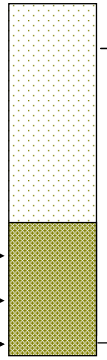

PRODUCT GAS

52.8	lb/hr		1134	scfh total gas flow
18.01	assumed MW (lb/lbmol)		232	scfh dry gas flow
52.3%	H2 (vol%)		2.93	lbmol/hr total gas
3.2%	CO (vol%)		0.60	lbmol/hr dry gas
23.7%	CO2 (vol%)		15.62	analyzed MW dry (lb/lbmol)
4.0%	CH4 (vol%)		17.52	analyzed MW wet (lb/lbmol)
9.3%	N2 (vol%)		51.4	corrected prod gas flow (lb/hr)
92.4%	Total		42.0	H2O flow in prod gas (lb/hr)

TARS

200	liters dry gas sampled		168	std liters dry gas sampled
488.7	grams water condensed		655	std liters steam condensed
13.3	grams tars recovered		20%	dry gas in product gas
30.0	minutes sampling time		29	scf sampled
12.5	psia dry gas meter pressure		5.1%	of total product gas
75	F dry gas meter temperature		1.1	lb/hr tar production rate

SOLIDS

4.7	lb/hr production rate	4.59	lb/hr inorganics
3.0%	organic carbon content		

TAR CONCENTRATION IN GAS

79 gram tar per scm dry gas	16 g tar per scm wet gas
4.9 lb tar per 1000 scf dry gas	1.0 lb tar per 1000 scf wet gas

TAR PRODUCTION RATE (APPROX)

0.117	lb tar per lb BLS
35%	of liquor organic C as tar C

TOTAL BALANCE

IN	
Black liquor	22.3
Steam	33.4
Nitrogen	1.5
Air	0.0
TOTAL IN	**57.2**
OUT	
Product gas	51.4
Tars	1.1
Solids	4.7
TOTAL OUT	**57.2**
OUT - IN	0.0
CLOSURE	**100%**

CARBON (C) BALANCE

IN	
BL organic C	2.9
BL inorganics	0.5
TOTAL IN	**3.4**
OUT	
Dry product gas	2.2
Tars	1.0
Solids	0.7
TOTAL OUT	**3.9**
OUT - IN	0.5
CLOSURE	**115%**

HYDROGEN (H) BALANCE

IN	
Steam	3.7
BLS hydrogen	0.3
BL water	1.4
TOTAL IN	**5.4**
OUT	
Dry product gas	0.7
Steam	4.7
Tars	0.1
TOTAL OUT	**5.6**
OUT - IN	0.1
CLOSURE	**103%**

SODIUM BALANCE

IN	
Black liquor	1.8
TOTAL IN	**1.8**
OUT	
Solids	1.8
TOTAL OUT	**1.8**
OUT - IN	0.0
CLOSURE	**100%**

NITROGEN (N) BALANCE

IN	
Black liquor	0.0
Nitrogen gas	1.5
Air	0.0
TOTAL IN	**1.6**
OUT	
Dry product gas	1.6
TOTAL OUT	**1.6**
OUT - IN	0.0
CLOSURE	**100%**

System Mass Balance Calculations

RUN NUMBER:	19	PURPOSE:	12 vol% air thru grid - tar testing	NOTES:	Fed air through grid by pre-mixing with steam.

Note: Standard conditions are 14.7 psia and 70°F

LIQUOR COMPOSITION (DRY)

C (carbon)	34.43	mass%
H (hydrogen)	3.00	mass%
O (oxygen)	41.45	mass%
S (sulfur)	0.10	mass%
Na (sodium)	18.70	mass%
K (potassium)	2.02	mass%
Cl (chlorine)	0.09	mass%
N (nitrogen)	0.21	mass%
Other (Si, Ca, Mg, etc)	0.00	mass%
TOTAL LIQUOR COMPOSITION	100.00	mass%

EST. INORGANIC SOLIDS COMPOSITION (100 lb basis)

	lb	wt%	% of BLS
C (carbon)	5.19	11.1%	15.1%
H (hydrogen)	0.00	0.0%	0.0%
O (oxygen)	20.75	44.4%	50.1%
S (sulfur)	0.01	0.0%	10.0%
Na (sodium)	18.70	40.0%	100.0%
K (potassium)	2.02	4.3%	100.0%
Cl (chlorine)	0.09	0.2%	100.0%
N (nitrogen)	0.00	0.0%	0.0%
Other (Si, Ca, Mg, etc)	0.00	0.0%	100.0%
TOTAL	46.76	100.0%	46.8%

Percent of BLS that is organic carbon:	29.2	wt%
Percent of tars that is organic carbon:	87.0	wt%

BLACK LIQUOR

21.7	lb/hr
44%	solids
9.55	lb/hr solids
12.15	lb/hr water

STEAM

27.4	lb/hr fluidizing
1.5	lb/hr thru injector

NITROGEN

10	slpm
21	scfh
1.5	lb/hr

AIR

38	slpm	12.0%
81	scfh	
6.0	lb/hr	

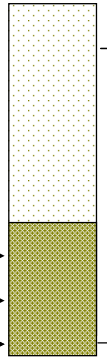

PRODUCT GAS

51.6	lb/hr	1108	scfh total gas flow
18.01	assumed MW (lb/lbmol)	291	scfh dry gas flow
35.9%	H2 (vol%)	2.86	lbmol/hr total gas
2.7%	CO (vol%)	0.75	lbmol/hr dry gas
21.1%	CO2 (vol%)	19.29	analyzed MW dry (lb/lbmol)
2.0%	CH4 (vol%)	18.35	analyzed MW wet (lb/lbmol)
29.3%	N2 (vol%)	52.5	corrected prod gas flow (lb/hr)
91.0%	Total	38.1	H2O flow in prod gas (lb/hr)

TARS

200	liters dry gas sampled	168	std liters dry gas sampled
353.6	grams water condensed	474	std liters steam condensed
9.4	grams tars recovered	26%	dry gas in product gas
30.0	minutes sampling time	23	scf sampled
12.5	psia dry gas meter pressure	4.1%	of total product gas
75	F dry gas meter temperature	1.0	lb/hr tar production rate

SOLIDS

4.6	lb/hr production rate	4.46	lb/hr inorganics
3.0%	organic carbon content		

TAR CONCENTRATION IN GAS

56 gram tar per scm dry gas	15 g tar per scm wet gas
3.5 lb tar per 1000 scf dry gas	0.9 lb tar per 1000 scf wet gas

TAR PRODUCTION RATE (APPROX)

0.106	lb tar per lb BLS
32%	of liquor organic C as tar C

TOTAL BALANCE

IN	
Black liquor	21.7
Steam	28.9
Nitrogen	1.5
Air	6.0
TOTAL IN	**58.1**
OUT	
Product gas	52.5
Tars	1.0
Solids	4.6
TOTAL OUT	**58.2**
OUT - IN	0.0
CLOSURE	**100%**

CARBON (C) BALANCE

IN	
BL organic C	2.8
BL inorganics	0.5
TOTAL IN	**3.3**
OUT	
Dry product gas	2.3
Tars	0.9
Solids	0.6
TOTAL OUT	**3.8**
OUT - IN	0.6
CLOSURE	**117%**

HYDROGEN (H) BALANCE

IN	
Steam	3.2
BLS hydrogen	0.3
BL water	1.4
TOTAL IN	**4.9**
OUT	
Dry product gas	0.6
Steam	4.3
Tars	0.1
TOTAL OUT	**5.0**
OUT - IN	0.1
CLOSURE	**102%**

SODIUM BALANCE

IN	
Black liquor	1.8
TOTAL IN	**1.8**
OUT	
Solids	1.8
TOTAL OUT	**1.8**
OUT - IN	0.0
CLOSURE	**100%**

NITROGEN (N) BALANCE

IN	
Black liquor	0.0
Nitrogen gas	1.5
Air	4.6
TOTAL IN	**6.2**
OUT	
Dry product gas	6.2
TOTAL OUT	**6.2**
OUT - IN	0.0
CLOSURE	**100%**

System Mass Balance Calculations

RUN NUMBER: 19

PURPOSE: "12%" air thru injector - tar testing

NOTES: Ran air through injector annulus. Flow rate of air is the same as when displacing 12% of air thru grid, but grid injection had 100% steam in this run.

Note: Standard conditions are 14.7 psia and 70°F

LIQUOR COMPOSITION (DRY)

C (carbon)	34.43	mass%
H (hydrogen)	3.00	mass%
O (oxygen)	41.45	mass%
S (sulfur)	0.10	mass%
Na (sodium)	18.70	mass%
K (potassium)	2.02	mass%
Cl (chlorine)	0.09	mass%
N (nitrogen)	0.21	mass%
Other (Si, Ca, Mg, etc)	0.00	mass%
TOTAL LIQUOR COMPOSITION	100.00	mass%

EST. INORGANIC SOLIDS COMPOSITION (100 lb basis)

	lb	wt%	% of BLS
C (carbon)	5.19	11.1%	15.1%
H (hydrogen)	0.00	0.0%	0.0%
O (oxygen)	20.75	44.4%	50.1%
S (sulfur)	0.01	0.0%	10.0%
Na (sodium)	18.70	40.0%	100.0%
K (potassium)	2.02	4.3%	100.0%
Cl (chlorine)	0.09	0.2%	100.0%
N (nitrogen)	0.00	0.0%	0.0%
Other (Si, Ca, Mg, etc)	0.00	0.0%	100.0%
TOTAL	46.76	100.0%	46.8%

Percent of BLS that is organic carbon:	29.2	wt%
Percent of tars that is organic carbon:	87.0	wt%

BLACK LIQUOR

23.1	lb/hr
42%	solids
9.70	lb/hr solids
13.40	lb/hr water

STEAM

31.7	lb/hr fluidizing
1.5	lb/hr thru injector

NITROGEN

10	slpm
21	scfh
1.5	lb/hr

AIR

38	slpm	10.6%
81	scfh	
6.0	lb/hr	

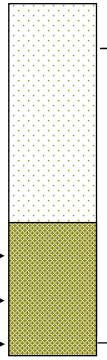

PRODUCT GAS

57.8	lb/hr	1241	scfh total gas flow
18.01	assumed MW (lb/lbmol)	319	scfh dry gas flow
37.0%	H2 (vol%)	3.21	lbmol/hr total gas
2.5%	CO (vol%)	0.82	lbmol/hr dry gas
21.1%	CO2 (vol%)	18.53	analyzed MW dry (lb/lbmol)
2.0%	CH4 (vol%)	18.15	analyzed MW wet (lb/lbmol)
26.7%	N2 (vol%)	58.2	corrected prod gas flow (lb/hr)
89.3%	Total	43.0	H2O flow in prod gas (lb/hr)

TARS

200	liters dry gas sampled	168	std liters dry gas sampled
363.9	grams water condensed	488	std liters steam condensed
8.1	grams tars recovered	26%	dry gas in product gas
27.0	minutes sampling time	23	scf sampled
12.5	psia dry gas meter pressure	4.1%	of total product gas
75	F dry gas meter temperature	1.0	lb/hr tar production rate

SOLIDS

4.7	lb/hr production rate	4.54	lb/hr inorganics
3.0%	organic carbon content		

TAR CONCENTRATION IN GAS

48 gram tar per scm dry gas	12 g tar per scm wet gas
3.0 lb tar per 1000 scf dry gas	0.8 lb tar per 1000 scf wet gas

TAR PRODUCTION RATE (APPROX)

0.099	lb tar per lb BLS
29%	of liquor organic C as tar C

TOTAL BALANCE

IN	
Black liquor	23.1
Steam	33.2
Nitrogen	1.5
Air	6.0
TOTAL IN	**63.8**
OUT	
Product gas	58.2
Tars	1.0
Solids	4.7
TOTAL OUT	**63.8**
OUT - IN	0.0
CLOSURE	**100%**

CARBON (C) BALANCE

IN	
BL organic C	2.8
BL inorganics	0.5
TOTAL IN	**3.3**
OUT	
Dry product gas	2.5
Tars	0.8
Solids	0.6
TOTAL OUT	**4.0**
OUT - IN	0.7
CLOSURE	**120%**

HYDROGEN (H) BALANCE

IN	
Steam	3.7
BLS hydrogen	0.3
BL water	1.5
TOTAL IN	**5.5**
OUT	
Dry product gas	0.7
Steam	4.8
Tars	0.1
TOTAL OUT	**5.6**
OUT - IN	0.1
CLOSURE	**102%**

SODIUM BALANCE

IN	
Black liquor	1.8
TOTAL IN	**1.8**
OUT	
Solids	1.8
TOTAL OUT	**1.8**
OUT - IN	0.0
CLOSURE	**100%**

NITROGEN (N) BALANCE

IN	
Black liquor	0.0
Nitrogen gas	1.5
Air	4.6
TOTAL IN	**6.2**
OUT	
Dry product gas	6.2
TOTAL OUT	**6.2**
OUT - IN	0.0
CLOSURE	**100%**

System Mass Balance Calculations

RUN NUMBER:	20	PURPOSE:	Baseline for more tar testing with air	NOTES:	Baseline for test 20. No air addition.

Note: Standard conditions are 14.7 psia and 70°F

LIQUOR COMPOSITION (DRY)

C (carbon)	34.43	mass%
H (hydrogen)	3.00	mass%
O (oxygen)	41.45	mass%
S (sulfur)	0.10	mass%
Na (sodium)	18.70	mass%
K (potassium)	2.02	mass%
Cl (chlorine)	0.09	mass%
N (nitrogen)	0.21	mass%
Other (Si, Ca, Mg, etc)	0.00	mass%
TOTAL LIQUOR COMPOSITION	100.00	mass%

EST. INORGANIC SOLIDS COMPOSITION (100 lb basis)

	lb	wt%	% of BLS
C (carbon)	5.19	11.1%	15.1%
H (hydrogen)	0.00	0.0%	0.0%
O (oxygen)	20.75	44.4%	50.1%
S (sulfur)	0.01	0.0%	10.0%
Na (sodium)	18.70	40.0%	100.0%
K (potassium)	2.02	4.3%	100.0%
Cl (chlorine)	0.09	0.2%	100.0%
N (nitrogen)	0.00	0.0%	0.0%
Other (Si, Ca, Mg, etc)	0.00	0.0%	100.0%
TOTAL	46.76	100.0%	46.8%

Percent of BLS that is organic carbon:	29.2	wt%
Percent of tars that is organic carbon:	87.0	wt%

BLACK LIQUOR

23.0	lb/hr
56%	solids
12.88	lb/hr solids
10.12	lb/hr water

STEAM

33.0	lb/hr fluidizing
1.5	lb/hr thru injector

NITROGEN

11	slpm
23	scfh
1.7	lb/hr

AIR

0	slpm	0.0%
0	scfh	
0.0	lb/hr	

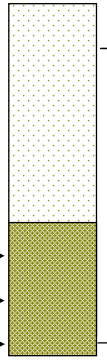

PRODUCT GAS

52.6	lb/hr	1131	scfh total gas flow
18.01	assumed MW (lb/lbmol)	255	scfh dry gas flow
53.0%	H2 (vol%)	2.92	lbmol/hr total gas
3.7%	CO (vol%)	0.66	lbmol/hr dry gas
24.3%	CO2 (vol%)	16.04	analyzed MW dry (lb/lbmol)
4.0%	CH4 (vol%)	17.57	analyzed MW wet (lb/lbmol)
9.3%	N2 (vol%)	51.3	corrected prod gas flow (lb/hr)
94.3%	Total	40.8	H2O flow in prod gas (lb/hr)

TARS

200	liters dry gas sampled	168	std liters dry gas sampled
431.7	grams water condensed	579	std liters steam condensed
17.4	grams tars recovered	23%	dry gas in product gas
26.0	minutes sampling time	26	scf sampled
12.5	psia dry gas meter pressure	5.4%	of total product gas
75	F dry gas meter temperature	1.6	lb/hr tar production rate

SOLIDS

6.2	lb/hr production rate	6.02	lb/hr inorganics
3.0%	organic carbon content		

TAR CONCENTRATION IN GAS

103 gram tar per scm dry gas	23 g tar per scm wet gas
6.4 lb tar per 1000 scf dry gas	1.5 lb tar per 1000 scf wet gas

TAR PRODUCTION RATE (APPROX)

0.128	lb tar per lb BLS
38%	of liquor organic C as tar C

TOTAL BALANCE

IN	
Black liquor	23.0
Steam	34.5
Nitrogen	1.7
Air	0.0
TOTAL IN	**59.2**
OUT	
Product gas	51.3
Tars	1.6
Solids	6.2
TOTAL OUT	**59.2**
OUT - IN	0.0
CLOSURE	**100%**

CARBON (C) BALANCE

IN	
BL organic C	3.8
BL inorganics	0.7
TOTAL IN	**4.4**
OUT	
Dry product gas	2.5
Tars	1.4
Solids	0.9
TOTAL OUT	**4.8**
OUT - IN	0.4
CLOSURE	**109%**

HYDROGEN (H) BALANCE

IN	
Steam	3.9
BLS hydrogen	0.4
BL water	1.1
TOTAL IN	**5.4**
OUT	
Dry product gas	0.8
Steam	4.6
Tars	0.2
TOTAL OUT	**5.6**
OUT - IN	0.2
CLOSURE	**104%**

SODIUM BALANCE

IN	
Black liquor	2.4
TOTAL IN	**2.4**
OUT	
Solids	2.4
TOTAL OUT	**2.4**
OUT - IN	0.0
CLOSURE	**100%**

NITROGEN (N) BALANCE

IN	
Black liquor	0.0
Nitrogen gas	1.7
Air	0.0
TOTAL IN	**1.7**
OUT	
Dry product gas	1.7
TOTAL OUT	**1.7**
OUT - IN	0.0
CLOSURE	**100%**

System Mass Balance Calculations

RUN NUMBER:	20	PURPOSE:	Tar testing with 18 vol% thru grid	NOTES:	Fed air through grid by pre-mixing with steam.

Note: Standard conditions are 14.7 psia and 70°F

LIQUOR COMPOSITION (DRY)

C (carbon)	34.43	mass%
H (hydrogen)	3.00	mass%
O (oxygen)	41.45	mass%
S (sulfur)	0.10	mass%
Na (sodium)	18.70	mass%
K (potassium)	2.02	mass%
Cl (chlorine)	0.09	mass%
N (nitrogen)	0.21	mass%
Other (Si, Ca, Mg, etc)	0.00	mass%
TOTAL LIQUOR COMPOSITION	100.00	mass%

EST. INORGANIC SOLIDS COMPOSITION (100 lb basis)

	lb	wt%	% of BLS
C (carbon)	5.19	11.1%	15.1%
H (hydrogen)	0.00	0.0%	0.0%
O (oxygen)	20.75	44.4%	50.1%
S (sulfur)	0.01	0.0%	10.0%
Na (sodium)	18.70	40.0%	100.0%
K (potassium)	2.02	4.3%	100.0%
Cl (chlorine)	0.09	0.2%	100.0%
N (nitrogen)	0.00	0.0%	0.0%
Other (Si, Ca, Mg, etc)	0.00	0.0%	100.0%
TOTAL	46.76	100.0%	46.8%

Percent of BLS that is organic carbon:	29.2	wt%
Percent of tars that is organic carbon:	87.0	wt%

BLACK LIQUOR

23.6	lb/hr
56%	solids
13.19	lb/hr solids
10.36	lb/hr water

STEAM

26.8	lb/hr fluidizing
1.5	lb/hr thru injector

NITROGEN

11	slpm
23	scfh
1.7	lb/hr

AIR

60	slpm	18.1%
127	scfh	
9.5	lb/hr	

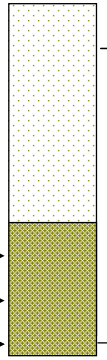

PRODUCT GAS

52.7	lb/hr	1132	scfh total gas flow
18.01	assumed MW (lb/lbmol)	346	scfh dry gas flow
30.6%	H2 (vol%)	2.92	lbmol/hr total gas
2.9%	CO (vol%)	0.89	lbmol/hr dry gas
20.5%	CO2 (vol%)	21.15	analyzed MW dry (lb/lbmol)
4.0%	CH4 (vol%)	18.97	analyzed MW wet (lb/lbmol)
35.9%	N2 (vol%)	55.5	corrected prod gas flow (lb/hr)
93.9%	Total	36.6	H2O flow in prod gas (lb/hr)

TARS

200	liters dry gas sampled	168	std liters dry gas sampled
285.5	grams water condensed	383	std liters steam condensed
9.5	grams tars recovered	31%	dry gas in product gas
28.0	minutes sampling time	19	scf sampled
12.5	psia dry gas meter pressure	3.7%	of total product gas
75	F dry gas meter temperature	1.2	lb/hr tar production rate

SOLIDS

6.4	lb/hr production rate	6.17	lb/hr inorganics
3.0%	organic carbon content		

TAR CONCENTRATION IN GAS

56 gram tar per scm dry gas	17 g tar per scm wet gas
3.5 lb tar per 1000 scf dry gas	1.1 lb tar per 1000 scf wet gas

TAR PRODUCTION RATE (APPROX)

0.092 lb tar per lb BLS	
27% of liquor organic C as tar C	

TOTAL BALANCE

IN	
Black liquor	23.6
Steam	28.3
Nitrogen	1.7
Air	9.5
TOTAL IN	**63.0**
OUT	
Product gas	55.5
Tars	1.2
Solids	6.4
TOTAL OUT	**63.1**
OUT - IN	0.0
CLOSURE	**100%**

CARBON (C) BALANCE

IN	
BL organic C	3.9
BL inorganics	0.7
TOTAL IN	**4.5**
OUT	
Dry product gas	2.9
Tars	1.1
Solids	0.9
TOTAL OUT	**4.9**
OUT - IN	0.3
CLOSURE	**107%**

HYDROGEN (H) BALANCE

IN	
Steam	3.2
BLS hydrogen	0.4
BL water	1.2
TOTAL IN	**4.7**
OUT	
Dry product gas	0.7
Steam	4.1
Tars	0.2
TOTAL OUT	**4.9**
OUT - IN	0.2
CLOSURE	**105%**

SODIUM BALANCE

IN	
Black liquor	2.5
TOTAL IN	**2.5**
OUT	
Solids	2.5
TOTAL OUT	**2.5**
OUT - IN	0.0
CLOSURE	**100%**

NITROGEN (N) BALANCE

IN	
Black liquor	0.0
Nitrogen gas	1.7
Air	7.3
TOTAL IN	**9.0**
OUT	
Dry product gas	9.0
TOTAL OUT	**9.0**
OUT - IN	0.0
CLOSURE	**100%**

System Mass Balance Calculations

RUN NUMBER:	20	PURPOSE:	Tar testing with "18%" thru injector	NOTES:	Ran air through injector annulus. Flow rate of air is the same as when displacing 18% of air thru grid, but grid injection had 100% steam in this run.

Note: Standard conditions are 14.7 psia and 70°F

LIQUOR COMPOSITION (DRY)

C (carbon)	34.43	mass%
H (hydrogen)	3.00	mass%
O (oxygen)	41.45	mass%
S (sulfur)	0.10	mass%
Na (sodium)	18.70	mass%
K (potassium)	2.02	mass%
Cl (chlorine)	0.09	mass%
N (nitrogen)	0.21	mass%
Other (Si, Ca, Mg, etc)	0.00	mass%
TOTAL LIQUOR COMPOSITION	100.00	mass%

EST. INORGANIC SOLIDS COMPOSITION (100 lb basis)

	lb	wt%	% of BLS
C (carbon)	5.19	11.1%	15.1%
H (hydrogen)	0.00	0.0%	0.0%
O (oxygen)	20.75	44.4%	50.1%
S (sulfur)	0.01	0.0%	10.0%
Na (sodium)	18.70	40.0%	100.0%
K (potassium)	2.02	4.3%	100.0%
Cl (chlorine)	0.09	0.2%	100.0%
N (nitrogen)	0.00	0.0%	0.0%
Other (Si, Ca, Mg, etc)	0.00	0.0%	100.0%
TOTAL	46.76	100.0%	46.8%

Percent of BLS that is organic carbon:	29.2	wt%
Percent of tars that is organic carbon:	87.0	wt%

BLACK LIQUOR

25.3	lb/hr
56%	solids
14.17	lb/hr solids
11.13	lb/hr water

STEAM

33.1	lb/hr fluidizing
1.5	lb/hr thru injector

NITROGEN

11	slpm
23	scfh
1.7	lb/hr

AIR

60	slpm	15.2%
127	scfh	
9.5	lb/hr	

PRODUCT GAS

62.7	lb/hr	1347	scfh total gas flow
18.01	assumed MW (lb/lbmol)	383	scfh dry gas flow
29.1%	H2 (vol%)	3.48	lbmol/hr total gas
2.7%	CO (vol%)	0.99	lbmol/hr dry gas
16.2%	CO2 (vol%)	18.19	analyzed MW dry (lb/lbmol)
4.0%	CH4 (vol%)	18.06	analyzed MW wet (lb/lbmol)
32.4%	N2 (vol%)	62.9	corrected prod gas flow (lb/hr)
84.4%	Total	44.8	H2O flow in prod gas (lb/hr)

TARS

200	liters dry gas sampled	168	std liters dry gas sampled
315.9	grams water condensed	424	std liters steam condensed
9.6	grams tars recovered	28%	dry gas in product gas
29.0	minutes sampling time	21	scf sampled
12.5	psia dry gas meter pressure	3.2%	of total product gas
75	F dry gas meter temperature	1.4	lb/hr tar production rate

SOLIDS

6.8	lb/hr production rate	6.62	lb/hr inorganics
3.0%	organic carbon content		

TAR CONCENTRATION IN GAS

57 gram tar per scm dry gas	16 g tar per scm wet gas
3.6 lb tar per 1000 scf dry gas	1.0 lb tar per 1000 scf wet gas

TAR PRODUCTION RATE (APPROX)

0.096	lb tar per lb BLS
29%	of liquor organic C as tar C

TOTAL BALANCE

IN	
Black liquor	25.3
Steam	34.6
Nitrogen	1.7
Air	9.5
TOTAL IN	**71.0**
OUT	
Product gas	62.9
Tars	1.4
Solids	6.8
TOTAL OUT	**71.1**
OUT - IN	0.0
CLOSURE	**100%**

CARBON (C) BALANCE

IN	
BL organic C	4.1
BL inorganics	0.7
TOTAL IN	**4.9**
OUT	
Dry product gas	2.7
Tars	1.2
Solids	0.9
TOTAL OUT	**4.8**
OUT - IN	0.0
CLOSURE	**99%**

HYDROGEN (H) BALANCE

IN	
Steam	3.9
BLS hydrogen	0.4
BL water	1.2
TOTAL IN	**5.5**
OUT	
Dry product gas	0.7
Steam	5.0
Tars	0.2
TOTAL OUT	**5.9**
OUT - IN	0.4
CLOSURE	**107%**

SODIUM BALANCE

IN	
Black liquor	2.6
TOTAL IN	**2.6**
OUT	
Solids	2.6
TOTAL OUT	**2.6**
OUT - IN	0.0
CLOSURE	**100%**

NITROGEN (N) BALANCE

IN	
Black liquor	0.0
Nitrogen gas	1.7
Air	7.3
TOTAL IN	**9.0**
OUT	
Dry product gas	9.0
TOTAL OUT	**9.0**
OUT - IN	0.0
CLOSURE	**100%**

System Mass Balance Calculations

RUN NUMBER:	20	PURPOSE:	Tar testing - Low BL flow (20%)	NOTES:	Set BL flow to 1/3 that of high case. Flow calcs in DCS integrate over longer time than time after flow switch.

Note: Standard conditions are 14.7 psia and 70°F

LIQUOR COMPOSITION (DRY)

C (carbon)	34.43	mass%
H (hydrogen)	3.00	mass%
O (oxygen)	41.45	mass%
S (sulfur)	0.10	mass%
Na (sodium)	18.70	mass%
K (potassium)	2.02	mass%
Cl (chlorine)	0.09	mass%
N (nitrogen)	0.21	mass%
Other (Si, Ca, Mg, etc)	0.00	mass%
TOTAL LIQUOR COMPOSITION	100.00	mass%

EST. INORGANIC SOLIDS COMPOSITION (100 lb basis)

	lb	wt%	% of BLS
C (carbon)	5.19	11.1%	15.1%
H (hydrogen)	0.00	0.0%	0.0%
O (oxygen)	20.75	44.4%	50.1%
S (sulfur)	0.01	0.0%	10.0%
Na (sodium)	18.70	40.0%	100.0%
K (potassium)	2.02	4.3%	100.0%
Cl (chlorine)	0.09	0.2%	100.0%
N (nitrogen)	0.00	0.0%	0.0%
Other (Si, Ca, Mg, etc)	0.00	0.0%	100.0%
TOTAL	46.76	100.0%	46.8%

Percent of BLS that is organic carbon:	29.2	wt%
Percent of tars that is organic carbon:	87.0	wt%

BLACK LIQUOR

12.7	lb/hr
56%	solids
7.09	lb/hr solids
5.57	lb/hr water

STEAM

33.0	lb/hr fluidizing
1.5	lb/hr thru injector

NITROGEN

12	slpm
25	scfh
1.8	lb/hr

AIR

0	slpm	0.0%
0	scfh	
0.0	lb/hr	

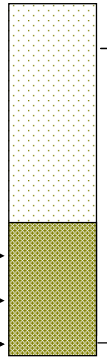

PRODUCT GAS

50.2	lb/hr	1079	scfh total gas flow
18.01	assumed MW (lb/lbmol)	232	scfh dry gas flow
24.1%	H2 (vol%)	2.79	lbmol/hr total gas
1.2%	CO (vol%)	0.60	lbmol/hr dry gas
8.9%	CO2 (vol%)	8.79	analyzed MW dry (lb/lbmol)
6.0%	CH4 (vol%)	16.03	analyzed MW wet (lb/lbmol)
11.0%	N2 (vol%)	44.7	corrected prod gas flow (lb/hr)
51.2%	Total	39.4	H2O flow in prod gas (lb/hr)

TARS

200	liters dry gas sampled	168	std liters dry gas sampled
457.6	grams water condensed	614	std liters steam condensed
10.3	grams tars recovered	22%	dry gas in product gas
29.0	minutes sampling time	28	scf sampled
12.5	psia dry gas meter pressure	5.3%	of total product gas
75	F dry gas meter temperature	0.9	lb/hr tar production rate

SOLIDS

3.4	lb/hr production rate	3.32	lb/hr inorganics
3.0%	organic carbon content		

TAR CONCENTRATION IN GAS

61 gram tar per scm dry gas	**13 g tar per scm wet gas**
3.8 lb tar per 1000 scf dry gas	**0.8 lb tar per 1000 scf wet gas**

TAR PRODUCTION RATE (APPROX)

0.125 lb tar per lb BLS	
37% of liquor organic C as tar C	

TOTAL BALANCE

IN	
Black liquor	12.7
Steam	34.5
Nitrogen	1.8
Air	0.0
TOTAL IN	**49.0**
OUT	
Product gas	44.7
Tars	0.9
Solids	3.4
TOTAL OUT	**49.0**
OUT - IN	0.0
CLOSURE	**100%**

CARBON (C) BALANCE

IN	
BL organic C	2.1
BL inorganics	0.4
TOTAL IN	**2.4**
OUT	
Dry product gas	1.2
Tars	0.8
Solids	0.5
TOTAL OUT	**2.4**
OUT - IN	0.0
CLOSURE	**98%**

HYDROGEN (H) BALANCE

IN	
Steam	3.9
BLS hydrogen	0.2
BL water	0.6
TOTAL IN	**4.7**
OUT	
Dry product gas	0.4
Steam	4.4
Tars	0.1
TOTAL OUT	**5.0**
OUT - IN	0.3
CLOSURE	**106%**

SODIUM BALANCE

IN	
Black liquor	1.3
TOTAL IN	**1.3**
OUT	
Solids	1.3
TOTAL OUT	**1.3**
OUT - IN	0.0
CLOSURE	**100%**

NITROGEN (N) BALANCE

IN	
Black liquor	0.0
Nitrogen gas	1.8
Air	0.0
TOTAL IN	**1.9**
OUT	
Dry product gas	1.9
TOTAL OUT	**1.9**
OUT - IN	0.0
CLOSURE	**100%**

System Mass Balance Calculations

RUN NUMBER:	20	PURPOSE:	Tar testing - Med BL flow (40%)	NOTES:	Set BL flow to 2/3 that of high case. Flow calcs in DCS integrate over longer time than time after flow switch.

Note: Standard conditions are 14.7 psia and 70°F

LIQUOR COMPOSITION (DRY)

C (carbon)	34.43	mass%
H (hydrogen)	3.00	mass%
O (oxygen)	41.45	mass%
S (sulfur)	0.10	mass%
Na (sodium)	18.70	mass%
K (potassium)	2.02	mass%
Cl (chlorine)	0.09	mass%
N (nitrogen)	0.21	mass%
Other (Si, Ca, Mg, etc)	0.00	mass%
TOTAL LIQUOR COMPOSITION	100.00	mass%

EST. INORGANIC SOLIDS COMPOSITION (100 lb basis)

	lb	wt%	% of BLS
C (carbon)	5.19	11.1%	15.1%
H (hydrogen)	0.00	0.0%	0.0%
O (oxygen)	20.75	44.4%	50.1%
S (sulfur)	0.01	0.0%	10.0%
Na (sodium)	18.70	40.0%	100.0%
K (potassium)	2.02	4.3%	100.0%
Cl (chlorine)	0.09	0.2%	100.0%
N (nitrogen)	0.00	0.0%	0.0%
Other (Si, Ca, Mg, etc)	0.00	0.0%	100.0%
TOTAL	46.76	100.0%	46.8%

Percent of BLS that is organic carbon:	29.2	wt%
Percent of tars that is organic carbon:	87.0	wt%

BLACK LIQUOR

25.3	lb/hr
56%	solids
14.19	lb/hr solids
11.15	lb/hr water

STEAM

33.0	lb/hr fluidizing
1.5	lb/hr thru injector

NITROGEN

12	slpm
25	scfh
1.8	lb/hr

AIR

0	slpm	0.0%
0	scfh	
0.0	lb/hr	

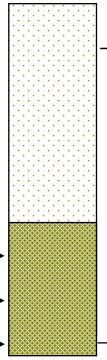

PRODUCT GAS

59.4	lb/hr	1277	scfh total gas flow
18.01	assumed MW (lb/lbmol)	284	scfh dry gas flow
25.9%	H2 (vol%)	3.30	lbmol/hr total gas
2.1%	CO (vol%)	0.73	lbmol/hr dry gas
10.1%	CO2 (vol%)	9.07	analyzed MW dry (lb/lbmol)
6.0%	CH4 (vol%)	16.03	analyzed MW wet (lb/lbmol)
9.1%	N2 (vol%)	52.9	corrected prod gas flow (lb/hr)
53.2%	Total	46.3	H2O flow in prod gas (lb/hr)

TARS

200	liters dry gas sampled	168	std liters dry gas sampled
440.3	grams water condensed	590	std liters steam condensed
18.3	grams tars recovered	22%	dry gas in product gas
26.0	minutes sampling time	27	scf sampled
12.5	psia dry gas meter pressure	4.8%	of total product gas
75	F dry gas meter temperature	1.9	lb/hr tar production rate

SOLIDS

6.8	lb/hr production rate	6.63	lb/hr inorganics
3.0%	organic carbon content		

TAR CONCENTRATION IN GAS

109 gram tar per scm dry gas	**24 g tar per scm wet gas**
6.8 lb tar per 1000 scf dry gas	**1.5 lb tar per 1000 scf wet gas**

TAR PRODUCTION RATE (APPROX)

0.136 lb tar per lb BLS	
40% of liquor organic C as tar C	

TOTAL BALANCE

IN	
Black liquor	25.3
Steam	34.5
Nitrogen	1.8
Air	0.0
TOTAL IN	**61.7**
OUT	
Product gas	52.9
Tars	1.9
Solids	6.8
TOTAL OUT	**61.7**
OUT - IN	0.0
CLOSURE	**100%**

CARBON (C) BALANCE

IN	
BL organic C	4.1
BL inorganics	0.7
TOTAL IN	**4.9**
OUT	
Dry product gas	1.6
Tars	1.7
Solids	0.9
TOTAL OUT	**4.2**
OUT - IN	-0.7
CLOSURE	**86%**

HYDROGEN (H) BALANCE

IN	
Steam	3.9
BLS hydrogen	0.4
BL water	1.2
TOTAL IN	**5.5**
OUT	
Dry product gas	0.6
Steam	5.2
Tars	0.3
TOTAL OUT	**6.0**
OUT - IN	0.5
CLOSURE	**108%**

SODIUM BALANCE

IN	
Black liquor	2.7
TOTAL IN	**2.7**
OUT	
Solids	2.7
TOTAL OUT	**2.7**
OUT - IN	0.0
CLOSURE	**100%**

NITROGEN (N) BALANCE

IN	
Black liquor	0.0
Nitrogen gas	1.8
Air	0.0
TOTAL IN	**1.9**
OUT	
Dry product gas	1.9
TOTAL OUT	**1.9**
OUT - IN	0.0
CLOSURE	**100%**

System Mass Balance Calculations

RUN NUMBER:	20	PURPOSE:	Tar testing - High BL flow (60%)	NOTES:	High flow rate of black liquor.

Note: Standard conditions are 14.7 psia and 70°F

LIQUOR COMPOSITION (DRY)

C (carbon)	34.43	mass%
H (hydrogen)	3.00	mass%
O (oxygen)	41.45	mass%
S (sulfur)	0.10	mass%
Na (sodium)	18.70	mass%
K (potassium)	2.02	mass%
Cl (chlorine)	0.09	mass%
N (nitrogen)	0.21	mass%
Other (Si, Ca, Mg, etc)	0.00	mass%
TOTAL LIQUOR COMPOSITION	100.00	mass%

EST. INORGANIC SOLIDS COMPOSITION (100 lb basis)

	lb	wt%	% of BLS
C (carbon)	5.19	11.1%	15.1%
H (hydrogen)	0.00	0.0%	0.0%
O (oxygen)	20.75	44.4%	50.1%
S (sulfur)	0.01	0.0%	10.0%
Na (sodium)	18.70	40.0%	100.0%
K (potassium)	2.02	4.3%	100.0%
Cl (chlorine)	0.09	0.2%	100.0%
N (nitrogen)	0.00	0.0%	0.0%
Other (Si, Ca, Mg, etc)	0.00	0.0%	100.0%
TOTAL	46.76	100.0%	46.8%

Percent of BLS that is organic carbon:	29.2	wt%
Percent of tars that is organic carbon:	87.0	wt%

BLACK LIQUOR

38.0	lb/hr
56%	solids
21.28	lb/hr solids
16.72	lb/hr water

STEAM

33.5	lb/hr fluidizing
1.5	lb/hr thru injector

NITROGEN

12	slpm
25	scfh
1.8	lb/hr

AIR

0	slpm	0.0%
0	scfh	
0.0	lb/hr	

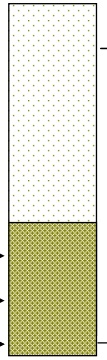

PRODUCT GAS

65.4	lb/hr	1405	scfh total gas flow
18.01	assumed MW (lb/lbmol)	319	scfh dry gas flow
45.5%	H2 (vol%)	3.63	lbmol/hr total gas
4.2%	CO (vol%)	0.82	lbmol/hr dry gas
18.8%	CO2 (vol%)	13.62	analyzed MW dry (lb/lbmol)
6.0%	CH4 (vol%)	17.02	analyzed MW wet (lb/lbmol)
8.2%	N2 (vol%)	61.8	corrected prod gas flow (lb/hr)
82.7%	Total	50.6	H2O flow in prod gas (lb/hr)

TARS

166	liters dry gas sampled	140	std liters dry gas sampled
355.4	grams water condensed	477	std liters steam condensed
19.6	grams tars recovered	23%	dry gas in product gas
29.0	minutes sampling time	22	scf sampled
12.5	psia dry gas meter pressure	3.2%	of total product gas
75	F dry gas meter temperature	2.8	lb/hr tar production rate

SOLIDS

10.3	lb/hr production rate	9.95	lb/hr inorganics
3.0%	organic carbon content		

TAR CONCENTRATION IN GAS

140	**gram tar per scm dry gas**
8.7	**lb tar per 1000 scf dry gas**
32	**g tar per scm wet gas**
2.0	**lb tar per 1000 scf wet gas**

TAR PRODUCTION RATE (APPROX)

0.131	**lb tar per lb BLS**
39%	**of liquor organic C as tar C**

TOTAL BALANCE

IN	
Black liquor	38.0
Steam	35.0
Nitrogen	1.8
Air	0.0
TOTAL IN	**74.8**
OUT	
Product gas	61.8
Tars	2.8
Solids	10.3
TOTAL OUT	**74.8**
OUT - IN	0.0
CLOSURE	**100%**

CARBON (C) BALANCE

IN	
BL organic C	6.2
BL inorganics	1.1
TOTAL IN	**7.3**
OUT	
Dry product gas	2.9
Tars	2.4
Solids	1.4
TOTAL OUT	**6.7**
OUT - IN	-0.6
CLOSURE	**92%**

HYDROGEN (H) BALANCE

IN	
Steam	3.9
BLS hydrogen	0.6
BL water	1.9
TOTAL IN	**6.4**
OUT	
Dry product gas	1.0
Steam	5.7
Tars	0.4
TOTAL OUT	**7.0**
OUT - IN	0.6
CLOSURE	**109%**

SODIUM BALANCE

IN	
Black liquor	4.0
TOTAL IN	**4.0**
OUT	
Solids	4.0
TOTAL OUT	**4.0**
OUT - IN	0.0
CLOSURE	**100%**

NITROGEN (N) BALANCE

IN	
Black liquor	0.0
Nitrogen gas	1.8
Air	0.0
TOTAL IN	**1.9**
OUT	
Dry product gas	1.9
TOTAL OUT	**1.9**
OUT - IN	0.0
CLOSURE	**100%**

System Mass Balance Calculations

RUN NUMBER: 21

PURPOSE: Tar sampling - Low bed temp (1050)

NOTES: Operating at very low bed temp. It's likely that the overall and C balances shouldn't balance since liquor conversion is very low at these temperatures.

Note: Standard conditions are 14.7 psia and 70°F

LIQUOR COMPOSITION (DRY)

C (carbon)	34.43	mass%
H (hydrogen)	3.00	mass%
O (oxygen)	41.45	mass%
S (sulfur)	0.10	mass%
Na (sodium)	18.70	mass%
K (potassium)	2.02	mass%
Cl (chlorine)	0.09	mass%
N (nitrogen)	0.21	mass%
Other (Si, Ca, Mg, etc)	0.00	mass%
TOTAL LIQUOR COMPOSITION	100.00	mass%

EST. INORGANIC SOLIDS COMPOSITION (100 lb basis)

	lb	wt%	% of BLS
C (carbon)	5.19	11.1%	15.1%
H (hydrogen)	0.00	0.0%	0.0%
O (oxygen)	20.75	44.4%	50.1%
S (sulfur)	0.01	0.0%	10.0%
Na (sodium)	18.70	40.0%	100.0%
K (potassium)	2.02	4.3%	100.0%
Cl (chlorine)	0.09	0.2%	100.0%
N (nitrogen)	0.00	0.0%	0.0%
Other (Si, Ca, Mg, etc)	0.00	0.0%	100.0%
TOTAL	46.76	100.0%	46.8%

Percent of BLS that is organic carbon:	29.2	wt%
Percent of tars that is organic carbon:	87.0	wt%

BLACK LIQUOR

14.7	lb/hr	
56%	solids	
8.23	lb/hr solids	
6.47	lb/hr water	

STEAM

33.5	lb/hr fluidizing	
1.5	lb/hr thru injector	

NITROGEN

12	slpm	
25	scfh	
1.8	lb/hr	

AIR

0	slpm	0.0%
0	scfh	
0.0	lb/hr	

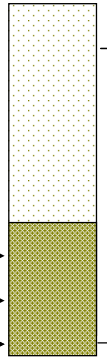

PRODUCT GAS

47.2	lb/hr		1014	scfh total gas flow
18.01	assumed MW (lb/lbmol)		176	scfh dry gas flow
40.4%	H2 (vol%)		2.62	lbmol/hr total gas
3.5%	CO (vol%)		0.45	lbmol/hr dry gas
19.9%	CO2 (vol%)		15.76	analyzed MW dry (lb/lbmol)
7.0%	CH4 (vol%)		17.62	analyzed MW wet (lb/lbmol)
14.6%	N2 (vol%)		46.2	corrected prod gas flow (lb/hr)
85.4%	Total		39.0	H2O flow in prod gas (lb/hr)

TARS

200	liters dry gas sampled		168	std liters dry gas sampled
598.8	grams water condensed		803	std liters steam condensed
21.3	grams tars recovered		17%	dry gas in product gas
32.0	minutes sampling time		34	scf sampled
12.5	psia dry gas meter pressure		6.3%	of total product gas
75	F dry gas meter temperature		1.4	lb/hr tar production rate

SOLIDS

4.0	lb/hr production rate	3.85	lb/hr inorganics
3.0%	organic carbon content		

TAR CONCENTRATION IN GAS

126 gram tar per scm dry gas	**22 g tar per scm wet gas**
7.9 lb tar per 1000 scf dry gas	**1.4 lb tar per 1000 scf wet gas**

TAR PRODUCTION RATE (APPROX)

0.169 lb tar per lb BLS	
50% of liquor organic C as tar C	

TOTAL BALANCE

IN	
Black liquor	14.7
Steam	35.0
Nitrogen	1.8
Air	0.0
TOTAL IN	**51.5**
OUT	
Product gas	46.2
Tars	1.4
Solids	4.0
TOTAL OUT	**51.5**
OUT - IN	0.0
CLOSURE	**100%**

CARBON (C) BALANCE

IN	
BL organic C	2.4
BL inorganics	0.4
TOTAL IN	**2.8**
OUT	
Dry product gas	1.7
Tars	1.2
Solids	0.5
TOTAL OUT	**3.4**
OUT - IN	0.6
CLOSURE	**120%**

HYDROGEN (H) BALANCE

IN	
Steam	3.9
BLS hydrogen	0.2
BL water	0.7
TOTAL IN	**4.9**
OUT	
Dry product gas	0.5
Steam	4.4
Tars	0.2
TOTAL OUT	**5.0**
OUT - IN	0.2
CLOSURE	**103%**

SODIUM BALANCE

IN	
Black liquor	1.5
TOTAL IN	**1.5**
OUT	
Solids	1.5
TOTAL OUT	**1.5**
OUT - IN	0.0
CLOSURE	**100%**

NITROGEN (N) BALANCE

IN	
Black liquor	0.0
Nitrogen gas	1.8
Air	0.0
TOTAL IN	**1.9**
OUT	
Dry product gas	1.9
TOTAL OUT	**1.9**
OUT - IN	0.0
CLOSURE	**100%**

System Mass Balance Calculations

RUN NUMBER: 21

PURPOSE: Tar sampling - baseline for T runs

NOTES: Baseline testing for Run 21.

Note: Standard conditions are 14.7 psia and 70°F

LIQUOR COMPOSITION (DRY)

C (carbon)	34.43	mass%
H (hydrogen)	3.00	mass%
O (oxygen)	41.45	mass%
S (sulfur)	0.10	mass%
Na (sodium)	18.70	mass%
K (potassium)	2.02	mass%
Cl (chlorine)	0.09	mass%
N (nitrogen)	0.21	mass%
Other (Si, Ca, Mg, etc)	0.00	mass%
TOTAL LIQUOR COMPOSITION	100.00	mass%

EST. INORGANIC SOLIDS COMPOSITION (100 lb basis)

	lb	wt%	% of BLS
C (carbon)	5.19	11.1%	15.1%
H (hydrogen)	0.00	0.0%	0.0%
O (oxygen)	20.75	44.4%	50.1%
S (sulfur)	0.01	0.0%	10.0%
Na (sodium)	18.70	40.0%	100.0%
K (potassium)	2.02	4.3%	100.0%
Cl (chlorine)	0.09	0.2%	100.0%
N (nitrogen)	0.00	0.0%	0.0%
Other (Si, Ca, Mg, etc)	0.00	0.0%	100.0%
TOTAL	46.76	100.0%	46.8%

Percent of BLS that is organic carbon:	29.2	wt%
Percent of tars that is organic carbon:	87.0	wt%

BLACK LIQUOR

14.7	lb/hr
56%	solids
8.23	lb/hr solids
6.47	lb/hr water

STEAM

33.5	lb/hr fluidizing
1.5	lb/hr thru injector

NITROGEN

12	slpm
25	scfh
1.8	lb/hr

AIR

0	slpm	0.0%
0	scfh	
0.0	lb/hr	

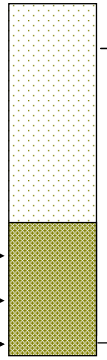

PRODUCT GAS

47.2	lb/hr	1014	scfh total gas flow
18.01	assumed MW (lb/lbmol)	196	scfh dry gas flow
49.8%	H2 (vol%)	2.62	lbmol/hr total gas
3.2%	CO (vol%)	0.51	lbmol/hr dry gas
23.8%	CO2 (vol%)	16.85	analyzed MW dry (lb/lbmol)
5.0%	CH4 (vol%)	17.79	analyzed MW wet (lb/lbmol)
13.1%	N2 (vol%)	46.6	corrected prod gas flow (lb/hr)
94.9%	Total	38.1	H2O flow in prod gas (lb/hr)

TARS

200	liters dry gas sampled	168	std liters dry gas sampled
525.2	grams water condensed	704	std liters steam condensed
13.4	grams tars recovered	19%	dry gas in product gas
30.0	minutes sampling time	31	scf sampled
12.5	psia dry gas meter pressure	6.1%	of total product gas
75	F dry gas meter temperature	1.0	lb/hr tar production rate

SOLIDS

4.0	lb/hr production rate	3.85	lb/hr inorganics
3.0%	organic carbon content		

TAR CONCENTRATION IN GAS

80 gram tar per scm dry gas	15 g tar per scm wet gas
5.0 lb tar per 1000 scf dry gas	1.0 lb tar per 1000 scf wet gas

TAR PRODUCTION RATE (APPROX)

0.118 lb tar per lb BLS	
35% of liquor organic C as tar C	

TOTAL BALANCE

IN	
Black liquor	14.7
Steam	35.0
Nitrogen	1.8
Air	0.0
TOTAL IN	**51.5**
OUT	
Product gas	46.6
Tars	1.0
Solids	4.0
TOTAL OUT	**51.5**
OUT - IN	0.0
CLOSURE	**100%**

CARBON (C) BALANCE

IN	
BL organic C	2.4
BL inorganics	0.4
TOTAL IN	**2.8**
OUT	
Dry product gas	1.9
Tars	0.8
Solids	0.5
TOTAL OUT	**3.3**
OUT - IN	0.5
CLOSURE	**118%**

HYDROGEN (H) BALANCE

IN	
Steam	3.9
BLS hydrogen	0.2
BL water	0.7
TOTAL IN	**4.9**
OUT	
Dry product gas	0.6
Steam	4.3
Tars	0.1
TOTAL OUT	**5.0**
OUT - IN	0.1
CLOSURE	**102%**

SODIUM BALANCE

IN	
Black liquor	1.5
TOTAL IN	**1.5**
OUT	
Solids	1.5
TOTAL OUT	**1.5**
OUT - IN	0.0
CLOSURE	**100%**

NITROGEN (N) BALANCE

IN	
Black liquor	0.0
Nitrogen gas	1.8
Air	0.0
TOTAL IN	**1.9**
OUT	
Dry product gas	1.9
TOTAL OUT	**1.9**
OUT - IN	0.0
CLOSURE	**100%**

System Mass Balance Calculations

RUN NUMBER: 21

PURPOSE: Tar sampling - High bed temp (1190)

NOTES: Methane concentration is a guess. This run seems screwy. % dry gas is very high, and C doesn't balance well. Wonder if there was an air leak.

Note: Standard conditions are 14.7 psia and 70°F

LIQUOR COMPOSITION (DRY)

C (carbon)	34.43	mass%
H (hydrogen)	3.00	mass%
O (oxygen)	41.45	mass%
S (sulfur)	0.10	mass%
Na (sodium)	18.70	mass%
K (potassium)	2.02	mass%
Cl (chlorine)	0.09	mass%
N (nitrogen)	0.21	mass%
Other (Si, Ca, Mg, etc)	0.00	mass%
TOTAL LIQUOR COMPOSITION	100.00	mass%

EST. INORGANIC SOLIDS COMPOSITION (100 lb basis)

	lb	wt%	% of BLS
C (carbon)	5.19	11.1%	15.1%
H (hydrogen)	0.00	0.0%	0.0%
O (oxygen)	20.75	44.4%	50.1%
S (sulfur)	0.01	0.0%	10.0%
Na (sodium)	18.70	40.0%	100.0%
K (potassium)	2.02	4.3%	100.0%
Cl (chlorine)	0.09	0.2%	100.0%
N (nitrogen)	0.00	0.0%	0.0%
Other (Si, Ca, Mg, etc)	0.00	0.0%	100.0%
TOTAL	46.76	100.0%	46.8%

Percent of BLS that is organic carbon:	29.2	wt%
Percent of tars that is organic carbon:	87.0	wt%

BLACK LIQUOR

14.7	lb/hr	
56%	solids	
8.23	lb/hr solids	
6.47	lb/hr water	

STEAM

33.5	lb/hr fluidizing	
1.5	lb/hr thru injector	

NITROGEN

12	slpm	
25	scfh	
1.8	lb/hr	

AIR

0	slpm	0.0%
0	scfh	
0.0	lb/hr	

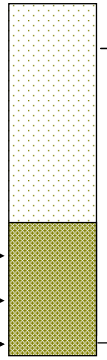

PRODUCT GAS

51.5	lb/hr		1106	scfh total gas flow
18.01	assumed MW (lb/lbmol)		347	scfh dry gas flow
59.7%	H2 (vol%)		2.86	lbmol/hr total gas
3.8%	CO (vol%)		0.90	lbmol/hr dry gas
18.0%	CO2 (vol%)		12.75	analyzed MW dry (lb/lbmol)
3.0%	CH4 (vol%)		16.36	analyzed MW wet (lb/lbmol)
7.4%	N2 (vol%)		46.8	corrected prod gas flow (lb/hr)
91.9%	Total		35.4	H2O flow in prod gas (lb/hr)

TARS

200	liters dry gas sampled		168	std liters dry gas sampled
275.5	grams water condensed		369	std liters steam condensed
6.1	grams tars recovered		31%	dry gas in product gas
29.0	minutes sampling time		19	scf sampled
12.5	psia dry gas meter pressure		3.6%	of total product gas
75	F dry gas meter temperature		0.8	lb/hr tar production rate

SOLIDS

4.0	lb/hr production rate	3.85	lb/hr inorganics
3.0%	organic carbon content		

TAR CONCENTRATION IN GAS

36 gram tar per scm dry gas	11 g tar per scm wet gas
2.3 lb tar per 1000 scf dry gas	0.7 lb tar per 1000 scf wet gas

TAR PRODUCTION RATE (APPROX)

0.095 lb tar per lb BLS	
28% of liquor organic C as tar C	

TOTAL BALANCE

IN	
Black liquor	14.7
Steam	35.0
Nitrogen	1.8
Air	0.0
TOTAL IN	**51.5**
OUT	
Product gas	46.8
Tars	0.8
Solids	4.0
TOTAL OUT	**51.5**
OUT - IN	0.0
CLOSURE	**100%**

CARBON (C) BALANCE

IN	
BL organic C	2.4
BL inorganics	0.4
TOTAL IN	**2.8**
OUT	
Dry product gas	2.7
Tars	0.7
Solids	0.5
TOTAL OUT	**3.9**
OUT - IN	1.1
CLOSURE	**137%**

HYDROGEN (H) BALANCE

IN	
Steam	3.9
BLS hydrogen	0.2
BL water	0.7
TOTAL IN	**4.9**
OUT	
Dry product gas	1.2
Steam	4.0
Tars	0.1
TOTAL OUT	**5.2**
OUT - IN	0.4
CLOSURE	**107%**

SODIUM BALANCE

IN	
Black liquor	1.5
TOTAL IN	**1.5**
OUT	
Solids	1.5
TOTAL OUT	**1.5**
OUT - IN	0.0
CLOSURE	**100%**

NITROGEN (N) BALANCE

IN	
Black liquor	0.0
Nitrogen gas	1.8
Air	0.0
TOTAL IN	**1.9**
OUT	
Dry product gas	1.9
TOTAL OUT	**1.9**
OUT - IN	0.0
CLOSURE	**100%**

System Mass Balance Calculations

RUN NUMBER: 23

PURPOSE: Test of KOH addition

NOTES: Conditions when feeding liquor containing 15% K/Na+K

Note: Standard conditions are 14.7 psia and 70°F

LIQUOR COMPOSITION (DRY)

C (carbon)	32.79	mass%
H (hydrogen)	2.94	mass%
O (oxygen)	40.83	mass%
S (sulfur)	0.10	mass%
Na (sodium)	21.13	mass%
K (potassium)	1.92	mass%
Cl (chlorine)	0.09	mass%
N (nitrogen)	0.20	mass%
Other (Si, Ca, Mg, etc)	0.00	mass%
TOTAL LIQUOR COMPOSITION	100.00	mass%

EST. INORGANIC SOLIDS COMPOSITION (100 lb basis)

	lb	wt%	% of BLS
C (carbon)	5.81	11.1%	17.7%
H (hydrogen)	0.00	0.0%	0.0%
O (oxygen)	23.22	44.5%	56.9%
S (sulfur)	0.01	0.0%	10.0%
Na (sodium)	21.13	40.5%	100.0%
K (potassium)	1.92	3.7%	100.0%
Cl (chlorine)	0.09	0.2%	100.0%
N (nitrogen)	0.00	0.0%	0.0%
Other (Si, Ca, Mg, etc)	0.00	0.0%	100.0%
TOTAL	52.18	100.0%	52.2%

Percent of BLS that is organic carbon:	27.0	wt%
Percent of tars that is organic carbon:	87.0	wt%

BLACK LIQUOR

18.8	lb/hr
54%	solids
10.15	lb/hr solids
8.65	lb/hr water

STEAM

33.0	lb/hr fluidizing
1.5	lb/hr thru injector

NITROGEN

12	slpm
25	scfh
1.8	lb/hr

AIR

0	slpm	0.0%
0	scfh	
0.0	lb/hr	

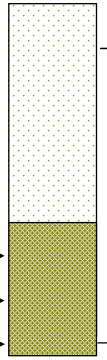

PRODUCT GAS

50.7	lb/hr	1090	scfh total gas flow
18.01	assumed MW (lb/lbmol)	263	scfh dry gas flow
46.0%	H2 (vol%)	2.82	lbmol/hr total gas
2.9%	CO (vol%)	0.68	lbmol/hr dry gas
21.4%	CO2 (vol%)	14.53	analyzed MW dry (lb/lbmol)
4.0%	CH4 (vol%)	17.17	analyzed MW wet (lb/lbmol)
9.7%	N2 (vol%)	48.4	corrected prod gas flow (lb/hr)
84.0%	Total	38.5	H2O flow in prod gas (lb/hr)

TARS

200	liters dry gas sampled	168	std liters dry gas sampled
394.1	grams water condensed	528	std liters steam condensed
13.7	grams tars recovered	24%	dry gas in product gas
30.0	minutes sampling time	25	scf sampled
12.5	psia dry gas meter pressure	4.5%	of total product gas
75	F dry gas meter temperature	1.3	lb/hr tar production rate

SOLIDS

5.5	lb/hr production rate	5.30	lb/hr inorganics
3.0%	organic carbon content		

TAR CONCENTRATION IN GAS

81 gram tar per scm dry gas	**20 g tar per scm wet gas**
5.1 lb tar per 1000 scf dry gas	**1.2 lb tar per 1000 scf wet gas**

TAR PRODUCTION RATE (APPROX)

0.132	**lb tar per lb BLS**
42%	**of liquor organic C as tar C**

TOTAL BALANCE

IN	
Black liquor	18.8
Steam	34.5
Nitrogen	1.8
Air	0.0
TOTAL IN	**55.1**
OUT	
Product gas	48.4
Tars	1.3
Solids	5.5
TOTAL OUT	**55.2**
OUT - IN	0.0
CLOSURE	**100%**

CARBON (C) BALANCE

IN	
BL organic C	2.7
BL inorganics	0.6
TOTAL IN	**3.3**
OUT	
Dry product gas	2.3
Tars	1.2
Solids	0.8
TOTAL OUT	**4.2**
OUT - IN	0.9
CLOSURE	**127%**

HYDROGEN (H) BALANCE

IN	
Steam	3.9
BLS hydrogen	0.3
BL water	1.0
TOTAL IN	**5.1**
OUT	
Dry product gas	0.7
Steam	4.3
Tars	0.2
TOTAL OUT	**5.2**
OUT - IN	0.1
CLOSURE	**102%**

SODIUM BALANCE

IN	
Black liquor	2.1
TOTAL IN	**2.1**
OUT	
Solids	2.1
TOTAL OUT	**2.1**
OUT - IN	0.0
CLOSURE	**100%**

NITROGEN (N) BALANCE

IN	
Black liquor	0.0
Nitrogen gas	1.8
Air	0.0
TOTAL IN	**1.9**
OUT	
Dry product gas	1.9
TOTAL OUT	**1.9**
OUT - IN	0.0
CLOSURE	**100%**

System Mass Balance Calculations

RUN NUMBER: 23

PURPOSE: Test of high fluidizing velocity

NOTES: Operating at ca. 1.45 ft/sec fluidizing velocity

Note: Standard conditions are 14.7 psia and 70°F

LIQUOR COMPOSITION (DRY)

C (carbon)	34.43	mass%
H (hydrogen)	3.00	mass%
O (oxygen)	41.45	mass%
S (sulfur)	0.10	mass%
Na (sodium)	18.70	mass%
K (potassium)	2.02	mass%
Cl (chlorine)	0.09	mass%
N (nitrogen)	0.21	mass%
Other (Si, Ca, Mg, etc)	0.00	mass%
TOTAL LIQUOR COMPOSITION	100.00	mass%

EST. INORGANIC SOLIDS COMPOSITION (100 lb basis)

	lb	wt%	% of BLS
C (carbon)	5.19	11.1%	15.1%
H (hydrogen)	0.00	0.0%	0.0%
O (oxygen)	20.75	44.4%	50.1%
S (sulfur)	0.01	0.0%	10.0%
Na (sodium)	18.70	40.0%	100.0%
K (potassium)	2.02	4.3%	100.0%
Cl (chlorine)	0.09	0.2%	100.0%
N (nitrogen)	0.00	0.0%	0.0%
Other (Si, Ca, Mg, etc)	0.00	0.0%	100.0%
TOTAL	46.76	100.0%	46.8%

Percent of BLS that is organic carbon:	29.2	wt%
Percent of tars that is organic carbon:	87.0	wt%

BLACK LIQUOR

18.6	lb/hr
54%	solids
10.02	lb/hr solids
8.53	lb/hr water

STEAM

50.0	lb/hr fluidizing
1.5	lb/hr thru injector

NITROGEN

12	slpm
25	scfh
1.8	lb/hr

AIR

0	slpm	0.0%
0	scfh	
0.0	lb/hr	

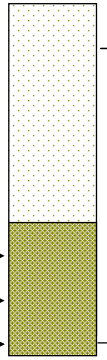

PRODUCT GAS

68.2	lb/hr	1465	scfh total gas flow
18.01	assumed MW (lb/lbmol)	281	scfh dry gas flow
46.8%	H2 (vol%)	3.79	lbmol/hr total gas
2.9%	CO (vol%)	0.73	lbmol/hr dry gas
21.4%	CO2 (vol%)	14.38	analyzed MW dry (lb/lbmol)
4.0%	CH4 (vol%)	17.32	analyzed MW wet (lb/lbmol)
9.2%	N2 (vol%)	65.6	corrected prod gas flow (lb/hr)
84.3%	Total	55.1	H2O flow in prod gas (lb/hr)

TARS

200	liters dry gas sampled	168	std liters dry gas sampled
530.2	grams water condensed	711	std liters steam condensed
14.8	grams tars recovered	19%	dry gas in product gas
32.0	minutes sampling time	31	scf sampled
12.5	psia dry gas meter pressure	4.0%	of total product gas
75	F dry gas meter temperature	1.5	lb/hr tar production rate

SOLIDS

4.8	lb/hr production rate	4.68	lb/hr inorganics
3.0%	organic carbon content		

TAR CONCENTRATION IN GAS

88 gram tar per scm dry gas	**17 g tar per scm wet gas**
5.5 lb tar per 1000 scf dry gas	**1.1 lb tar per 1000 scf wet gas**

TAR PRODUCTION RATE (APPROX)

0.154	**lb tar per lb BLS**
46%	**of liquor organic C as tar C**

TOTAL BALANCE

IN	
Black liquor	18.6
Steam	51.5
Nitrogen	1.8
Air	0.0
TOTAL IN	**71.9**
OUT	
Product gas	65.6
Tars	1.5
Solids	4.8
TOTAL OUT	**71.9**
OUT - IN	0.0
CLOSURE	**100%**

CARBON (C) BALANCE

IN	
BL organic C	2.9
BL inorganics	0.5
TOTAL IN	**3.4**
OUT	
Dry product gas	2.5
Tars	1.3
Solids	0.7
TOTAL OUT	**4.5**
OUT - IN	1.0
CLOSURE	**130%**

HYDROGEN (H) BALANCE

IN	
Steam	5.8
BLS hydrogen	0.3
BL water	1.0
TOTAL IN	**7.0**
OUT	
Dry product gas	0.8
Steam	6.2
Tars	0.2
TOTAL OUT	**7.2**
OUT - IN	0.2
CLOSURE	**102%**

SODIUM BALANCE

IN	
Black liquor	1.9
TOTAL IN	**1.9**
OUT	
Solids	1.9
TOTAL OUT	**1.9**
OUT - IN	0.0
CLOSURE	**100%**

NITROGEN (N) BALANCE

IN	
Black liquor	0.0
Nitrogen gas	1.8
Air	0.0
TOTAL IN	**1.9**
OUT	
Dry product gas	1.9
TOTAL OUT	**1.9**
OUT - IN	0.0
CLOSURE	**100%**

System Mass Balance Calculations

RUN NUMBER:	23	PURPOSE:	Low black liquor flow	NOTES:	Operating at 3 lb/hr BLS instead of standard 10

Note: Standard conditions are 14.7 psia and 70°F

LIQUOR COMPOSITION (DRY)

C (carbon)	34.43	mass%
H (hydrogen)	3.00	mass%
O (oxygen)	41.45	mass%
S (sulfur)	0.10	mass%
Na (sodium)	18.70	mass%
K (potassium)	2.02	mass%
Cl (chlorine)	0.09	mass%
N (nitrogen)	0.21	mass%
Other (Si, Ca, Mg, etc)	0.00	mass%
TOTAL LIQUOR COMPOSITION	100.00	mass%

EST. INORGANIC SOLIDS COMPOSITION (100 lb basis)

	lb	wt%	% of BLS
C (carbon)	5.19	11.1%	15.1%
H (hydrogen)	0.00	0.0%	0.0%
O (oxygen)	20.75	44.4%	50.1%
S (sulfur)	0.01	0.0%	10.0%
Na (sodium)	18.70	40.0%	100.0%
K (potassium)	2.02	4.3%	100.0%
Cl (chlorine)	0.09	0.2%	100.0%
N (nitrogen)	0.00	0.0%	0.0%
Other (Si, Ca, Mg, etc)	0.00	0.0%	100.0%
TOTAL	46.76	100.0%	46.8%

Percent of BLS that is organic carbon:	29.2	wt%
Percent of tars that is organic carbon:	87.0	wt%

BLACK LIQUOR

5.8	lb/hr
54%	solids
3.13	lb/hr solids
2.67	lb/hr water

STEAM

33.0	lb/hr fluidizing
1.5	lb/hr thru injector

NITROGEN

12	slpm
25	scfh
1.8	lb/hr

AIR

0	slpm	0.0%
0	scfh	
0.0	lb/hr	

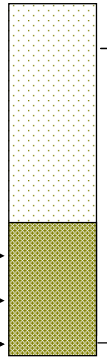

PRODUCT GAS

40.8	lb/hr	876	scfh total gas flow
18.01	assumed MW (lb/lbmol)	175	scfh dry gas flow
50.9%	H2 (vol%)	2.26	lbmol/hr total gas
2.0%	CO (vol%)	0.45	lbmol/hr dry gas
23.6%	CO2 (vol%)	16.70	analyzed MW dry (lb/lbmol)
4.0%	CH4 (vol%)	17.75	analyzed MW wet (lb/lbmol)
14.6%	N2 (vol%)	40.2	corrected prod gas flow (lb/hr)
95.1%	Total	32.6	H2O flow in prod gas (lb/hr)

TARS

200	liters dry gas sampled	168	std liters dry gas sampled
503.9	grams water condensed	676	std liters steam condensed
7.4	grams tars recovered	20%	dry gas in product gas
31.0	minutes sampling time	30	scf sampled
12.5	psia dry gas meter pressure	6.6%	of total product gas
75	F dry gas meter temperature	0.5	lb/hr tar production rate

SOLIDS

1.5	lb/hr production rate	1.46	lb/hr inorganics
3.0%	organic carbon content		

TAR CONCENTRATION IN GAS

44 gram tar per scm dry gas	9 g tar per scm wet gas
2.7 lb tar per 1000 scf dry gas	0.5 lb tar per 1000 scf wet gas

TAR PRODUCTION RATE (APPROX)

0.153 lb tar per lb BLS	
46% of liquor organic C as tar C	

TOTAL BALANCE

IN	
Black liquor	5.8
Steam	34.5
Nitrogen	1.8
Air	0.0
TOTAL IN	**42.1**
OUT	
Product gas	40.2
Tars	0.5
Solids	1.5
TOTAL OUT	**42.2**
OUT - IN	0.0
CLOSURE	**100%**

CARBON (C) BALANCE

IN	
BL organic C	0.9
BL inorganics	0.2
TOTAL IN	**1.1**
OUT	
Dry product gas	1.6
Tars	0.4
Solids	0.2
TOTAL OUT	**2.2**
OUT - IN	1.2
CLOSURE	**207%**

HYDROGEN (H) BALANCE

IN	
Steam	3.9
BLS hydrogen	0.1
BL water	0.3
TOTAL IN	**4.3**
OUT	
Dry product gas	0.5
Steam	3.7
Tars	0.1
TOTAL OUT	**4.3**
OUT - IN	0.0
CLOSURE	**100%**

SODIUM BALANCE

IN	
Black liquor	0.6
TOTAL IN	**0.6**
OUT	
Solids	0.6
TOTAL OUT	**0.6**
OUT - IN	0.0
CLOSURE	**100%**

NITROGEN (N) BALANCE

IN	
Black liquor	0.0
Nitrogen gas	1.8
Air	0.0
TOTAL IN	**1.8**
OUT	
Dry product gas	1.8
TOTAL OUT	**1.8**
OUT - IN	0.0
CLOSURE	**100%**

System Mass Balance Calculations

RUN NUMBER:	23	PURPOSE:	Basline for run 23	NOTES:	Base condtions

Note: Standard conditions are 14.7 psia and 70°F

LIQUOR COMPOSITION (DRY)

C (carbon)	34.43	mass%
H (hydrogen)	3.00	mass%
O (oxygen)	41.45	mass%
S (sulfur)	0.10	mass%
Na (sodium)	18.70	mass%
K (potassium)	2.02	mass%
Cl (chlorine)	0.09	mass%
N (nitrogen)	0.21	mass%
Other (Si, Ca, Mg, etc)	0.00	mass%
TOTAL LIQUOR COMPOSITION	100.00	mass%

EST. INORGANIC SOLIDS COMPOSITION (100 lb basis)

	lb	wt%	% of BLS
C (carbon)	5.19	11.1%	15.1%
H (hydrogen)	0.00	0.0%	0.0%
O (oxygen)	20.75	44.4%	50.1%
S (sulfur)	0.01	0.0%	10.0%
Na (sodium)	18.70	40.0%	100.0%
K (potassium)	2.02	4.3%	100.0%
Cl (chlorine)	0.09	0.2%	100.0%
N (nitrogen)	0.00	0.0%	0.0%
Other (Si, Ca, Mg, etc)	0.00	0.0%	100.0%
TOTAL	46.76	100.0%	46.8%

Percent of BLS that is organic carbon:	29.2	wt%
Percent of tars that is organic carbon:	87.0	wt%

BLACK LIQUOR

18.2	lb/hr	
54%	solids	
9.80	lb/hr solids	
8.35	lb/hr water	

STEAM

33.0	lb/hr fluidizing
1.5	lb/hr thru injector

NITROGEN

12	slpm	
25	scfh	
1.8	lb/hr	

AIR

0	slpm	0.0%
0	scfh	
0.0	lb/hr	

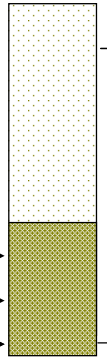

PRODUCT GAS

49.6	lb/hr	1066	scfh total gas flow
18.01	assumed MW (lb/lbmol)	239	scfh dry gas flow
47.4%	H2 (vol%)	2.76	lbmol/hr total gas
3.2%	CO (vol%)	0.62	lbmol/hr dry gas
23.6%	CO2 (vol%)	15.89	analyzed MW dry (lb/lbmol)
4.0%	CH4 (vol%)	17.54	analyzed MW wet (lb/lbmol)
10.7%	N2 (vol%)	48.3	corrected prod gas flow (lb/hr)
88.9%	Total	38.5	H2O flow in prod gas (lb/hr)

TARS

200	liters dry gas sampled	168	std liters dry gas sampled
434.3	grams water condensed	582	std liters steam condensed
16.6	grams tars recovered	22%	dry gas in product gas
32.0	minutes sampling time	27	scf sampled
12.5	psia dry gas meter pressure	4.7%	of total product gas
75	F dry gas meter temperature	1.5	lb/hr tar production rate

SOLIDS

4.7	lb/hr production rate	4.58	lb/hr inorganics
3.0%	organic carbon content		

TAR CONCENTRATION IN GAS

99 gram tar per scm dry gas	**22 g tar per scm wet gas**
6.2 lb tar per 1000 scf dry gas	**1.4 lb tar per 1000 scf wet gas**

TAR PRODUCTION RATE (APPROX)

0.150 lb tar per lb BLS	
45% of liquor organic C as tar C	

TOTAL BALANCE

IN	
Black liquor	18.2
Steam	34.5
Nitrogen	1.8
Air	0.0
TOTAL IN	**54.5**
OUT	
Product gas	48.3
Tars	1.5
Solids	4.7
TOTAL OUT	**54.5**
OUT - IN	0.0
CLOSURE	**100%**

CARBON (C) BALANCE

IN	
BL organic C	2.9
BL inorganics	0.5
TOTAL IN	**3.4**
OUT	
Dry product gas	2.3
Tars	1.3
Solids	0.7
TOTAL OUT	**4.2**
OUT - IN	0.8
CLOSURE	**125%**

HYDROGEN (H) BALANCE

IN	
Steam	3.9
BLS hydrogen	0.3
BL water	0.9
TOTAL IN	**5.1**
OUT	
Dry product gas	0.7
Steam	4.3
Tars	0.2
TOTAL OUT	**5.2**
OUT - IN	0.1
CLOSURE	**102%**

SODIUM BALANCE

IN	
Black liquor	1.8
TOTAL IN	**1.8**
OUT	
Solids	1.8
TOTAL OUT	**1.8**
OUT - IN	0.0
CLOSURE	**100%**

NITROGEN (N) BALANCE

IN	
Black liquor	0.0
Nitrogen gas	1.8
Air	0.0
TOTAL IN	**1.9**
OUT	
Dry product gas	1.9
TOTAL OUT	**1.9**
OUT - IN	0.0
CLOSURE	**100%**